

Parametric design of grid shell structures

A design method considering semi-rigid joints
and stiffness based connection design

July 2024

Friso van Spengler
MSc Thesis

octatube

TU Delft

Cover image: ©EvaBloem, photograph of C30 shell structure designed by Octatube

Parametric design of grid shell structures

A design method considering semi-rigid joints and stiffness based connection design

A thesis submitted to the Delft University of Technology in partial fulfilment of the requirements for the degree of

Master of Science in Building Engineering

Author: Friso van Spengler
July 2024

Faculty of Civil Engineering & Geosciences
Delft University of Technology

Graduation committee:	Dr. Florentia Kavoura	- TU Delft
	Dr. Robin Oval	- TU Delft
	Dr. ir. Pierre Hoogenboom	- TU Delft
	Ir. Peter van de Rotten	- Octatube



(This page is intentionally left blank)

Abstract

The characteristics of the joints play a considerable role in the stability of grid shells. Therefore, the connections are usually assumed to be rigid during the design phase. However, considering the semi-rigid behaviour of connections in the design could be beneficial. This leads to two major challenges. (1) The application of semi-rigid joints increases the indeterminacy of the structure. And (2) the current connection design strategy is not well-equipped for the integration of semi-rigid connections in the design. The following research questions is formulated: *How can a semi-rigid approach to steel connection design and considering the semi-rigidity of the joints, be combined in a parametric design strategy for grid shells?*

To answer this, three objectives have been formulated. Objective 1 focusses on the connection design, creating a design method for connection based on a pre-determined stiffness. Objective 2 focusses on the influence of joint stiffness on the structural behaviour of grid shells. Objective 3 is to design a grid shell, applying the results from objectives 1 and 2. Finally, the method is applied to a case study.

Results from objective 1 show that the load ratio can significantly influence the stiffness of connections. Also, design parameters, such as plate thickness and bolt spacing, can be adjusted to achieve different stiffness values. Combining these findings, a design space is generated to enable stiffness based connection design. Results from objective 2 show that the axial stiffness and the out-of-plane bending stiffness of the joints are relevant for the stability of the shell. Depending on the boundary conditions, shape and size of the shell, also in-plane stiffness parameters are relevant. For objective 3, a design workflow is proposed. A design space for the connections is combined with joint stiffness optimisation, resulting in the design of a grid shell with reversible connections. The application is checked with a case study of the C30 Shell. Complexities with increased size of the shell were managed by segmentation of the shell and clustering of the nodes. Resulting in a structure with 58% reversible joints.

The following conclusion is drawn: *A semi-rigid approach to connection design and the inclusion of semi-rigidity of the joints in the structural design of a grid shell can be combined in the design of a grid shell. This can be achieved by defining a relation between the connection design and the joint stiffness design. This way, a design space can be created that links the connection design to pre-determined stiffness requirements and load ratios in the structural design. Which allows for efficient design iterations and eliminates guesswork in the design of both the connection and the joint stiffness distribution of the shell.*

For effective application of this method it is important to be aware that the initial design largely determines the efficiency of the end result. The effectiveness of the stiffness optimisation, the segmentation of the shell, and the clustering of the joints all impact the result of the design significantly. Future research could be directed towards a better understanding of these aspects.

Acknowledgements

This report marks the final step towards completion of my Master of Science in Building Engineering at the Delft University of Technology. I would like to acknowledge everyone who has helped me during my studies and my graduation project.

Specifically, I would like to thank the members of my graduation committee for their guidance during my thesis. I am very grateful to Florentia Kavoura for her willingness to chair the committee. Her help and feedback, especially regarding the design of the connections, has contributed greatly to the project. I am also thankful to Robin Oval for his feedback and guidance during my project. His expertise on special structures and his input during our conversations have been invaluable for the completion of my thesis. Furthermore, I would like to thank Pierre Hoogenboom for his feedback and interesting perspectives during our meetings. Last but not least, I would like to express my gratitude to Peter van de Rotten, as my supervisor from Octatube, for his comments and observations that sent my research in the right direction. I would like to thank Peter and everyone at Octatube for the opportunity to perform my graduation with the company.

My gratitude goes towards my family and friends that have supported me throughout my studies. I look back on this time with great memories.

Most importantly, my greatest thanks go to my parents for their love and support during my studies and before. Because of them, I can be where I am today. It is invaluable to have felt their support and trust at every step I took.

Friso van Spengler
Delft, July 2024

Summary

Grid shells are lightweight double-curved structures, constructed from a grid of structural members that are joined together in the nodes. The characteristics of the joints play a considerable role in the structural behaviour of grid shells. The design of the connections is usually done with a forward design method, assuming rigid joints during the design of the shell. However, considering the semi-rigid behaviour of connections during the design phase could benefit the design efficiency.

Considering the semi-rigidity of the connections, leads to two major challenges. (1) The application of semi-rigid joints increases the indeterminacy of the structure. And (2) the current approach towards connection design is not well-equipped for early integration of the joint design into the structural analysis. Therefore, the following research questions has been formulated:

How can a semi-rigid approach to steel connection design and considering the semi-rigidity of the joints, be combined in a parametric design strategy for grid shells?

To answer this question, three objectives have been formulated. Objective 1 and objective 2 make up the research phase of the project. Objective 1 is directed towards the connection design and creating a design method for connection based on a pre-determined stiffness. In objective 2, research is focussed on the influence of different joint stiffness parameters on the structural behaviour of a grid shell. Objective 3 focusses on the design of a grid shell, applying the results from the research phase. Also, a case study is performed to research the application of the results from objective 3. The case study will research the C30 Shell, which is designed and constructed by Octatube. (*Octatube, 2020*)

In preparation for the research, a literature study is performed to investigate the current practice of the design of connections for grid shells and to understand the design principles of grid shells. Because codes and guidelines are mostly focussed on regular steel connections in frame structures, general rules for design of grid shell connections are not available. Available research is focussed on testing of specific connection designs. Studies on the design of grid shells show that stiffness of the joints is an important factor in the structural design of the shells, especially in non-rigid frames, such as quadrangular grids. Still, knowledge on the effects of the stiffness parameters in the connections is scarce and connections are often assumed rigid in the design of grid shells.

For objective 1, research is performed on a basic connection design, consisting of a central node with rectangular hollow sections connected to each side. The connections are realised with a bolted endplate. An investigation of the effect of the loads on the stiffness shows that load ratios can significantly increase or decrease the rotational stiffness of a connection. Also, the effect of different design components on the stiffness of the connection is studied. The dimensions of the node, the thickness of the plates and bolt dimensions can be applied to alter the stiffness of a connection. Combining these findings, a design diagram has been constructed that can aid in the design of a steel connection for grid shells, based on pre-determined stiffness requirements.

For objective 2, a parametric study is performed on a grid shell model. The importance of the different stiffness parameters of the joints depends on the design of the grid shell. The axial stiffness and the out-of-plane bending stiffness are relevant for the stability of all grid shells. For grid shells with free edges, the parameters that ensure in-plane stability of the frame (in-plane shear and in-plane bending stiffness) also become relevant. In addition, the size and shape of the shell can influence the importance of the joint stiffness parameters.

In the design phase of the project, the outcomes from the research are applied to the design of a grid shell with semi-rigid joints. A design workflow is proposed for the integration of joint stiffness optimisation and the design of connections. The connection design is based on the stiffness determined in the optimisation. The design showed a quick convergence in the iterations through joint stiffness and load ratios. The subsequent stiffness analysis showed that the estimates of the stiffness based on the design diagrams were accurate. Some inconsistencies in the results can be attributed to unpredictability of the stiffness for very small load ratios ($M_y/N = 0,03 \text{ m}$). In practice these peaks in the stiffness diagrams should be approached cautiously.

The design method is applied to a case study of the C30 shell, constructed by Octatube. This is a grid shell with a quadrangular grid diagonally oriented towards the boundaries. To deal with the greater size of the structure the shell was segmented into parts and the nodes connecting these parts were clustered based on their location in the structure. The segmentation created the possibility to include rigid joints in the structure that provide in-plane stiffness to the structure, ensuring that only out-of-plane bending stiffness would have to be regarded in the design. The clustering of the joints reduced the number of unique connections, which reduced the computational effort required for the design. The design resulted in a construction with 113 joints of which 65 are reversible. The mass of the joints is approximately 11% of the mass of the structural members. Some attention points can be drawn from the design. The joint stiffness optimisation plays an important role in the effectiveness of the design method. Also, the efficiency of the design results depends heavily on the clustering of the joints. Clustering the joints based on load conditions might render better results than clustering based on geometry.

Based on the performed research and design, the following conclusion can be drawn:

A semi-rigid approach to connection design and the inclusion of semi-rigidity of the joints in the structural design of a grid shell can be combined in the design of a grid shell. This can be achieved by defining a relation between the connection design and the joint stiffness design. This way, a design space can be created that links the connection design to pre-determined stiffness requirements and load ratios in the structural design. Which allows for efficient design iterations and eliminates guesswork in the design of both the connection and the joint stiffness distribution of the shell.

For effective application of this method it is important to consider several aspects in the design. The initial design largely determines the efficiency of the end result. Therefore, it is important to have a good understanding of the structure. The effectiveness of the stiffness optimisation, the segmentation of the shell, and the clustering of the joints all impact the result of the design significantly.

Future research could be directed towards the inclusion of axial load in the calculation of grid shell connections and the determination of axial stiffness of the joints. In addition, understanding of the interaction between different joints with various stiffness values could be further developed. And the definition of a relation between the load ratios and the stiffness of grid shell connections could improve the efficiency of grid shell connections.

Table of Contents

1 Introduction.....	3
1.1 Problem statement.....	3
1.2 Terminology	4
1.3 Research question	4
1.4 Objectives.....	4
1.5 Methodology	5
2 Literature study.....	7
2.1 Introduction to grid shells	7
2.2 The design of grid shells.....	11
2.3 Design of grid shell connections	19
2.4 Joint stiffness optimisation	22
2.5 Constructability and sustainability.....	28
3 Connection design	29
3.1 Connection model and analysis.....	29
3.2 Base connection design.....	31
3.3 Influence of load interaction on connection stiffness	33
3.4 Stiffness ranges.....	37
3.5 Conclusion	41
4 Joint stiffness influence.....	43
4.1 Parametric model.....	43
4.2 Influence of stiffness parameters	46
4.3 Load ratio in the nodes	52
4.4 Discussion and conclusion.....	55
5 Design of a grid shell	57
5.1 Design workflow	57
5.2 Design example.....	59

6 Case study: C30 Shell.....	75
6.1 C30 Shell design.....	75
6.2 Case study design	77
6.3 Additional fictional load combination.....	86
7 Discussion.....	89
7.1 Connection design	89
7.2 Joint stiffness in grid shell structures.....	90
7.3 Design of a grid shell with semi-rigid joints	91
8 Conclusion and recommendations.....	95
8.1 Conclusion	95
8.2 Recommendations.....	96
Bibliography.....	98
Appendix A. Influence of load ratio M_y/N on initial rotational stiffness.....	102
Appendix B: Grasshopper script.....	115
Appendix C: Results Parameter study joint stiffness influence.....	118
Appendix D: Connection design diagrams	126
Appendix E: Design Iterations	133
Appendix F: Stiffness analysis	138
Appendix G: Nodal forces (RFEM Output).....	198

1 Introduction

1.1 Problem statement

Grid shells are lightweight single-layer structures with a double-curved surface composed of structural members that are joined together in the nodes of the structure. The characteristics of these joints play a considerable role in the structural behaviour of grid shells. Due to the complex calculation procedure, joints are often assumed to be fully rigid in the structural design phase. It can, however, be beneficial to consider the actual behaviour of the joints by implementing the mechanical characteristics of the semi-rigid behaviour of the joints. This implementation could reduce the structural weight of the connections and provide benefits in terms of production and installation of the structure, for example, by realising bolted connections instead of welded connections.

The consideration of the semi-rigidity of the connections during the design of a grid shell knows two major challenges. The first is that the effect of joint stiffness on the structural performance of a grid shell is complex and influenced by many aspects. The structural design of single-layer structures is already a highly iterative process. The inclusion of semi-rigid joint would lead to a further increase in the indeterminacy of the structure. Therefore, the inclusion of finite joint stiffness in the early stages of the structural design would increase the complexity of this time-consuming process. Secondly, the current approach towards connection design is not well-equipped for the integration of joint stiffness in the global structural analysis. In the traditional forward design methods, based on the assumption of rigid or pinned joints, member design and connection design are separate tasks. Which is inconvenient when the structural performance of both member design and connection design are closely related and interdependent. For a feasible application of semi-rigid joints in grid shell structural the approach to connection design should be adapted to allow for design based on specific requirements.

This thesis builds upon the previous thesis written by *Fiori Isufi (2021)*. *Isufi (2021)* focussed on the out-of-plane rotational stiffness of joints in grid shell roof structures over existing buildings. It was found that a structure could be designed consisting of semi-rigid joints, which reduced structural weight in the connections of the structure. For the design of this structure *Isufi* designed several connections with varying stiffness values. Moving forward from this work questions remain regarding the influence of semi-rigid joints on grid shell structures. Also, the connection design was still performed with a forward method. Further steps could be made in adapting the connection design strategy. For this reason this research is investigating the design of connections based on pre-determined characteristics and the influence of the consideration of semi-rigidity of the connections on the structural performance of grid shells in order to define a design strategy for grid shells with semi-rigid joints.

1.2 Terminology

Shell structures

Shell structures are related to plate structures, being defined by their middle plane, thickness, and material properties. In shell structures the middle plane is curved, allowing for out-of-plane loads to be carried by in-plane membrane forces. This creates structurally efficient and economic structures. (Blaauwendraad & Hoefakker, 2014)

Grid shell

To create a grid shell the surface of a shell structure is fragmented into bars, creating a transparent structure. The efficiency of grid shells, therefore, also depends on the way the structural elements are connected in the nodes (Schober, 2015).

Connection and joint

A connection is the set of elements that make up the design for the fastening of the structural elements at the nodes. The wording ‘joint’ refers to the zone of interaction between connected members. Here the connection and the characteristics of the connected members are all considered. (Jaspart & Weynand, 2016)

The definitions are illustrated for a beam-column connection in figure 1.1.

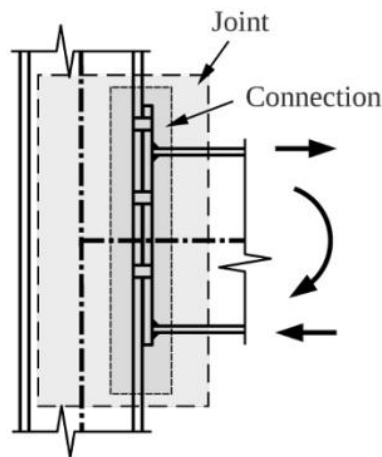


Figure 1.1: The difference in definition between a joint and a connection (Jaspart & Weynand, 2016)

1.3 Research question

To address the problem statement the following research question has been formulated:

How can a semi-rigid approach to steel connection design and taking into account the semi-rigidity of the joints be combined in a parametric design strategy for grid shells?

The goal is to advise on a design approach that would clearly define the process of including finite joint stiffness during the structural design phase.

1.4 Objectives

Three objectives have been formulated to help answer the research question. The first two objectives relate to the challenges mentioned in the problem statement. Objective 1 focusses on the design strategy for steel connections in grid shells and objective 2 focusses on the influence

of considering the actual joint stiffness on the structural performance of a grid shell. The third objective relates to the integration of the results of objectives 1 and 2. The aim of objective 3 is to define a design approach for grid shells with semi-rigid joints. A case study is performed to verify the results of objective 3. The specific objectives and their corresponding research questions are listed below:

Objective 1: Adapt the forward design method for steel connections to make it suitable for the integration into structural design of structures with finite joint stiffness.

- How does the interaction of loads influence the stiffness of a bolted steel connection?
- How do different design parameters influence the stiffness of a bolted steel connection?
- How can a steel connection be designed based on a pre-determined stiffness?

Objective 2: Optimisation of the joint stiffness in grid shell design.

- How do different joint stiffness parameters influence the structural capacity of a grid shell?
- How does the joint stiffness influence the ratio between the loads on the joints?
- What are the challenges for the implementation of semi-rigid joints in the design and optimisation of a grid shell?

Objective 3: Integrate the results from objectives 1 and 2 to determine a design strategy for grid shells with semi-rigid joints.

- Can the optimisation of joint stiffness and the design strategy for steel connections lead to a feasible design for grid shells with semi-rigid nodes?

Case study: Application of the design method in practice.

- How do constructability and sustainability considerations influence the design of a grid shell with semi-rigid steel connections?

1.5 Methodology

To achieve the objectives the project is divided into different phases, which are explained below. Figure 1.2 shows an overview of the different stages of the project.

Phase 1. Preparation

First, a literature study is executed to develop a sufficient understanding of the subject and to determine what relevant knowledge is currently available. In the literature study, the state-of-the-art of shell structures and grid shell design is studied. More in depth research on the influence of joint stiffness on grid shell structures is performed and the current standings of connection design are discussed. Also, the possible benefits of the research with regard to constructability and sustainability are investigated. The literature study is presented in chapter 2.

The second aspect of this phase is the set-up of the parametric model in preparation for the research. Using Grasshopper (*Mode Lab, 2014*), a parametric model of a grid shell is constructed. The design of this model is done based on learnings from the literature study regarding shape, grid and boundary conditions. Together with the parametric model, a connection model is designed. The connection is designed and analysed using FEM models in IDEA StatiCa software (*IDEA StatiCa, n.d.-a*). This model allows for a parameter study on the components of the connection.

Phase 2. Research

In the research phase, the focus lies on the first two objectives of this thesis. Work is done on objective 1 and objective 2 simultaneously.

For objective 1, a parameter study is performed for the connection design. The study focusses on the loads on the connection as well as on the specific design parameters. The parameter study aims to determine the relation between different design parameters and the structural performance of the connection. With the results from the parameter study, an attempt is made to define a strategy for the connection design which allows for the integration of the connection design in the early stages of the structural analysis of a grid shell. The research is presented in chapter 3.

For objective 2 the relation between the different stiffness parameters and the load-bearing capacity of the grid shell is researched with a parameter study on the parametric model. Also the influence of the joint stiffness on the load distribution is investigated. With the results from the research an attempt is made to define the challenges for the inclusion of finite joint stiffness in the structural design of grid shells. Further information about relevant parameters and the optimisation approach is given in chapter 4.

Phase 3. Design

In the design phase, the focus is on the integration of the structural design and the connection design. For objective 3 the results from the research phase are reviewed and used in a design of a grid shell structure, which is presented in chapter 5. The results of the three objectives are applied to a case study of the C30 shell that was designed and constructed by Octatube. The case study is presented in chapter 6.

Phase 4. Discussion

The results from phases 2 and 3 are reviewed and discussed. Based on the discussion an answer to the research question is formulated. The conclusion is drawn and recommendations resulting from the research are given. Specific reflections on the performed structural design and optimisation are also directed to the safety margins in the structural design and how they are influenced by the design approach.

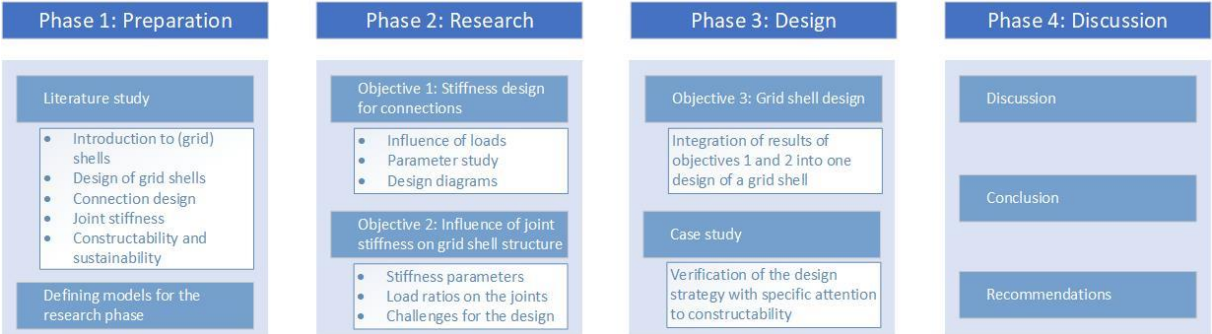


Figure 1.2: Structure of the research

2 Literature study

The literature study provides background information for a better understanding of the research performed in this thesis. Relevant available literature is reviewed to be able to determine adequate starting points and considerations for the research. The literature study consists of five parts. In section 2.1 an introduction on shell structures and grid shells is given. Section 2.2 explains the design process of a grid shell. Then in section 2.3, the approach to connection design in grid shells is elaborated. The importance of joint stiffness and possibilities for optimisation is discussed in section 2.4. And section 2.5 provides some insights into constructability and sustainability considerations that are relevant in the design of grid shells.

2.1 Introduction to grid shells

This section introduces shell structures and the specific characteristics of grid shells, to provide some background information and a basic understanding of the subject. The section discusses the characteristics of shells and grid shells in section 2.1.1, gives a brief overview of historic developments in section 2.1.2 and discusses the load transfer in shell structures in section 2.1.3.

2.1.1 What are grid shells?

Shell structures

Grid shells form a category of shell structures. Therefore, a basic understanding of shell structures is required for a study on grid shells. Shell structures are lightweight structures that derive their strength and stability from the double curvature of their surface. Shell structures are usually very slender as to avoid bending and only transfer loads as compressive stresses, tension, and tangential shear. Still, a shell should be sufficiently thick to avoid buckling. Figure 2.1 shows an example of a concrete continuous shell structure. (*Schueller, 1983*)



Figure 2.1: Thin concrete shell covering a service station near Deitingen by Heinz Isler (Photo: Eugen Brühwiler)

The structural behaviour of a shell depends on the shape of its surface. Shell geometry is described by the curvature of the surface and the thickness. An important indication of the load transfer in a shell is the Gaussian curvature of the surface. The Gaussian curvature is the product of the two principal curvatures, see figure 2.2. A surface is classified as synclastic if both principal curvatures have the same sign, resulting in the Gaussian curvature being greater than zero. When the principal curvatures are of opposite sign, the Gaussian curvature is smaller than zero and the surface is classified as anticlastic. If one of the principal curvatures is zero, the surface is mono-clastic or single-curved.

A second method of classification is by the developability of the surface, which influences to what extent a shell requires stiff boundaries. A surface is developable if the surface can be flattened without tearing or stretching the surface, thus more easily deformed. Anti- and synclastic surfaces are non-developable whereas mono-clastic surfaces are developable. (Blaauwendraad & Hoefakker, 2014)

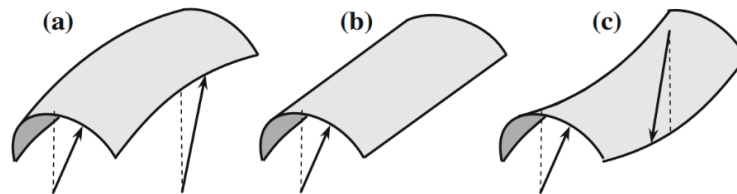


Figure 2.2: Surface classification based on Gaussian curvature. (a) synclastic, (b) monoclastic, (c) anticlastic. (Blaauwendraad & Hoefakker, 2014)

Grid shells

For the design of a grid shell, the surface of a continuous shell is fragmented into bars, creating a grid. The result is a double-curved transparent structure (Schober, 2015). Grid shells are defined by Octatube (2023) as a “lightweight structure, composed of discrete members following a curved free-form shape”. Stating that the shape of the grid shells ensures that large spans can be achieved with relatively little material. The surface of grid shells is usually composed of a repeating pattern of structural members, creating a homogenous appearance. Figure 2.3 shows an example of a grid shell structure constructed by Octatube.



Figure 2.3: C30 Shell grid shell structure © Octatube, 2022

Grid shells are versatile structures with different means of transferring loads. This can be illustrated with an attempt to classify the structure based on load transfer mechanisms.

The principles of arches and shell domes can be derived from hanging chains that are inverted to create compressive structures. Therefore, although they do not adjust to the loading conditions, shells are sometimes classified as form-active structures (Crielaard & Terwel, 2020; Venuti & Bruno, 2018; Octatube, 2023). Also, because of the ability to transfer loads as forces within the surface, shell structures can be classified as surface-active structures (Coenders, 2008). Out-of-plane loads are transferred as compressive loads and membrane forces ensure equilibrium in the structure, resulting in tensile forces and shear forces. In the case of grid shells, those membrane forces are taken care of by members in tension or compression, showing characteristics of a vector-active structure (Crielaard & Terwel, 2020). Finally, concentrated loads and boundary conditions can lead to local bending in grid shells. Therefore, structural members also have to be able to behave according to cross-section-active principles (Octatube, 2023).

The description above cannot clearly define a shell structure. In general, the classification of the structural behaviour of a true shell or grid shell is determined by the ability to activate membrane action within the surface of the shell.

A distinction can be made between two types of grid shells. The difference is best visible in the method of construction of the shells. Bending-active grid shells are constructed as a flat grid on the ground and are then ‘pushed’ in place and fixed at the boundaries, resulting in a prestressed structure. Discrete grid shells are constructed by connecting the members in their final shape, until completion the shell relies on temporary supports.

Common choices for the material of grid shells include steel, timber or FRP structures. Grid shells made from flexible material like timber are usually constructed as bending-active grid shells. Steel grid shells are mostly discrete grid shells constructed by connecting prefabricated members on-site by welding or bolting (Malek et al., 2014). In this thesis, the focus is exclusively on discrete grid shells with steel members.

2.1.2 Historic developments

The reason for the construction of shell structures throughout history is elegantly described by Gohnert (2022); “The emergence of shell structures is undoubtedly the result of a practical need for a wide-open space, without being inhibited by column supports. Shells are able to span over enormous spaces, and therefore are ideal for places of large gatherings”. Gohnert also remarks that of the structures that have survived since ancient times, a remarkably large majority are domes or arches.

Shell structures find their origin in early dome structures. The earliest structures using dome principles are corbelled domes constructed first around the thirteenth century BC. Continuous concrete domes first emerge during the Roman period. Of this, the most famous is the dome of the Pantheon in Rome (constructed 123 AD), figure 2.4a. This dome structure relies on thickness and hoop forces for structural stability and cannot yet be described as a lightweight structure. Nevertheless, it was the largest spanning concrete dome until the 20th century. Another impressive early dome is the brick dome of the Hagia Sophia in Istanbul (537 AD), figure 2.4b. This dome applies compression ribs transferring the load to heavy buttresses supporting four corners underneath the dome. The dome of the Santa Maria Del Fiore in Florence (1434 AD) can be considered the first modern dome. Here, a limestone and a timber tension ring are used to resist lateral thrust forces resulting from the weight of the dome. (Schueller, 1983)

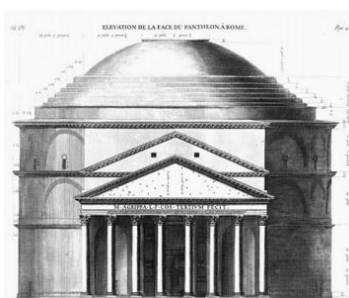


Figure 2.4: Historic dome structures, (a) Pantheon and (b) Hagia Sophia (Gohnert, 2022)

In the 19th century, the industrial revolution created a new application for large-span structures. In this period, iron and steel were used for the first time to create these large spans (Schlaich, 2011). In combination with the need for transparency, this eventually resulted in the construction of the first double-curved grid shell by Vladimir Shukhov in 1897 (Venuti & Bruno, 2018), see figure 2.5. This grid shell covered a large steel-rolling workshop that required daylight and open space.

In the second half of the 20th century, new advances in material technology of structural steel and glass led to the next steps in the design of highly transparent steel grid shells (Schlaich, 2011). Nowadays, grid shells are often chosen for a design because of their architectural qualities.



Figure 2.5: Vyksa grid shell by Vladimir Shukhov (Beckh & Barthel, 2009)

2.1.3 Load transfer in grid shells

Shell theory

The structural theory that describes the ability of shell structures to transfer out-of-plane loads as in-plane forces is called membrane theory. This ability is created by the curvature of the shell and allows for achieving large spans requiring a low structural thickness. When membrane behaviour is activated, equilibrium is ensured between the loads on the surface and the stresses within the membrane. A two-dimensional visualisation of membrane forces as a result of a distributed load is shown in figure 2.6. (Blaauwendraad & Hoefakker, 2013)

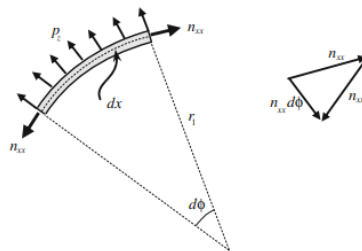


Figure 2.6: Equilibrium forces in a section of a two-dimensional membrane (Blaauwendraad & Hoefakker, 2014)

However, membrane theory does not hold in every situation. In the case of concentrated loads, incompatible boundary conditions or abrupt geometric changes the requirements for equilibrium cannot be satisfied by the membrane solution. At locations where membrane theory cannot guarantee equilibrium, local bending moments compensate for these shortcomings. These local bending moments do not inhibit the ability of the shell to show membrane behaviour as long as they remain local. The theory of these bending moments is called bending theory. (Van der Linden, 2015)

The combination of membrane theory and bending theory for shells is defined as shell theory and it describes the structural behaviour of the structure. Shell theory is the superposition of membrane action and bending action, as shown in figure 2.7. (Van der Linden, 2015).

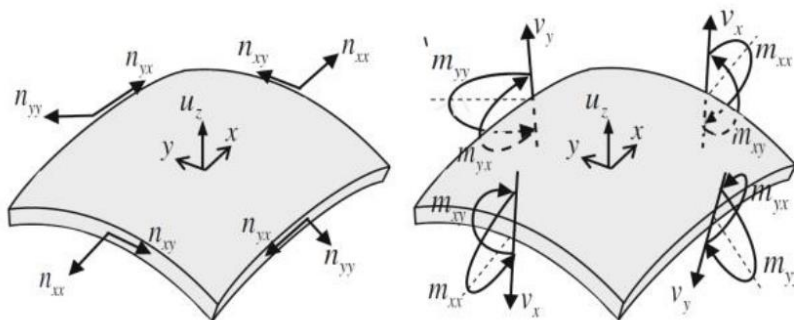


Figure 2.7: Shell theory: Membrane action (a) and bending action (b) (Blaauwendraad & Hoefakker, 2014)

Shell theory for grid shells

Grid shells differ from shell structures in the sense that they do not have a continuous surface, but a grid of discrete members. Therefore, a grid shell contains a limited number of load paths, whereas continuous shells have infinite load paths. To activate membrane behaviour, the structure needs to be able to transfer in-plane shear forces (Van der Linden, 2015). This can be ensured by diagonal members, bracing or stiffness of the joints.

The bending behaviour in grid shells corresponds to the bending behaviour in shells. Where local disturbances cannot be satisfied by membrane theory, local bending in the structural elements have to ensure the stability of the structure.

For stability, grid shells depend heavily on the characteristics of the nodes. This creates requirements for the nodes in grid shells that are different from requirements for joints in regular steel frame structures. These requirements can be subdivided into in-plane and out-of-plane requirements. Depending on the design of the grid and the boundary conditions grid shell joints need to be able to fulfil several or all of the requirements listed below. Figure 2.8 shows the three translational and rotational directions for which deformation can be resisted in a grid shell joint.

In-plane requirements:

- Transfer of axial forces
- Transfer of in-plane shear forces
- Transfer of in-plane bending moments

Out-of-plane requirements

- Transfer of out-of-plane bending moments
- Transfer of out-of-plane shear forces
- Transfer of torsional moments

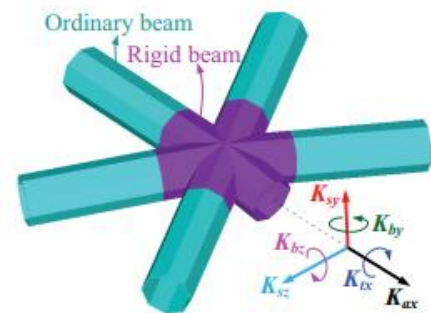


Figure 2.8: Degrees of freedom in a grid shell joint (Li & Taniguchi, 2020)

2.2 The design of grid shells

This section describes the design process of a grid shell structure. In section 2.2.1 the design of the surface is discussed. Section 2.2.2 gives some insight into the available methods for structural analysis of a grid shell. And section 2.2.3 dives deeper into the more specific considerations of grid shell design and their influence on the efficiency of the structure.

2.2.1 Grid shell geometry

In order to benefit from the full potential of efficient shell structures, it is important to determine the shape or geometry of the structure. The ideal structural shape depends on the loading conditions, design of the grid and characteristics of the connections. Also, it is important to consider that the ideal shape of the shell is different for every load combination.

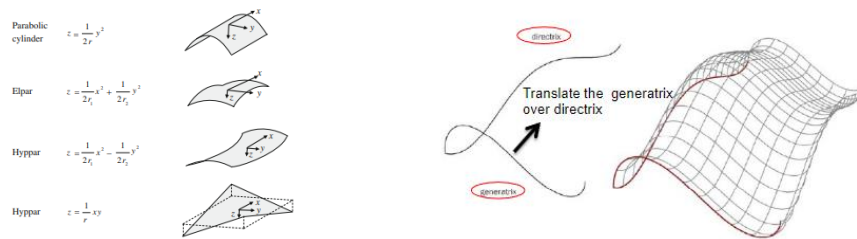
Another characteristic of grid shell design is that the structural design and architectural design are often identical. Therefore, the definition of the shape is not only a result of structural considerations. Architectural design might also influence the shape of the structure, which affects the structural efficiency of the structure.

The geometry of the surface can be mathematically defined by equations and translation or rotation of curves, through form-finding approaches and by free-form shape design.

Mathematical geometries

Shell geometries can be defined by analytic functions. This method is often chosen because the known geometry allows for more convenient analytic calculations of the structure and because analytic shells provide better possibilities for efficient fabrication (*Adriaenssens et al., 2014*). Mathematical geometries can be described by relatively simple functions. Examples of this are cylindrical surfaces, elliptic paraboloids, and hyperbolic paraboloids, shown in figure 2.9.

Other examples of mathematical geometries are surfaces of translation, where one curve (generatrix) is translated along another curve (directrix), or surfaces of revolution, where a surface is created by the revolution of a curve around an axis. Figure 2.10 shows the generation of a translational surface, by sliding one curve along another. Shapes produced by these methods have favourable possibilities for the generation of a grid composed of flat quadrangular elements.



Form-finding

Form-finding is a general term that can represent different design processes with different goals. In the design of grid shells, two major form-finding approaches can be defined. These are ‘statics-aware’ form-finding and ‘fabrication-aware’ form-finding. Statics-aware form-finding relates to structural optimisation and aims to find the optimal mechanical performance by ensuring compression-dominant behaviour. Fabrication-aware form-finding strives for optimisation of the fabricability of the structure, designing the shape and grid of the shell to achieve planar cladding and torsion-free joints. This paragraph describes statics-aware form-finding of the grid shell shape. Fabrication-aware form-finding is discussed in the paragraph on grid generation.

Statics-aware form-finding is a process of geometrical optimisation to determine a shape that achieves equilibrium within the structure for specific loading conditions. Form-finding provides the opportunity to achieve structurally and geometrically feasible surface forms in the case of loading and boundary conditions that do not result in an optimal shape (*Schober, 2015*).

Form-finding finds its origin in physical “hanging chain” models. A cable under load deforms into the funicular shape due to its inability to resist bending moments. When inverted the shape of the cable is the geometry in which a shell is in pure compression. Among the engineers who famously applied these principles in their designs are Frei Otto and Antoni Gaudí. A hanging chain model of the Multihalle by Frei Otto is shown in figure 2.11. With the development of computers and computer software, physical modelling has been replaced by computational form-finding methods. This allowed for a greater variety of form-finding methods. Some well-known methods are the Force Density Method, Dynamic Relaxation and Particle-Spring Systems, which can be closely compared to the physical hanging chain models (*Coenders, 2008*).

Form-finding methods can accurately determine the optimal shape of a structure for a certain loading condition. However, structures need to resist many different load combinations. It is, therefore, important to be aware that the optimised shape belongs to a specific load combination. A shape should be found that is structurally efficient for all loading conditions and the construction must be able to resist bending moments when deviations from the ideal load conditions occur.



Figure 2.11: Hanging chain model of the Multihalle by Frei Otto (Adriaenssens et al., 2014)

Free-form shapes geometries

Free-form shells are generally shaped without structural performance or the regularity of mathematical shapes in mind. They are often shaped using digital design software, in which the shapes are described by high-order polynomials (Adriaenssens et al., 2014). The mathematics and software behind originate from the car-manufacturing industry, driven by the need for free-flowing shapes that cannot easily be described by standard surfaces like cylinders, spheres, cones and translational or rotational surfaces. Examples of algorithms used in practice are Beziér Curves and B-Spline or NURBS surfaces (Pottmann et al., 2007).

Grid generation

Besides the design of the shape, the grid is an important aspect of grid shell design. For the design of the grid, both structural and fabrication characteristics have to be considered. Fabrication-aware design of grid shells conflicts with the statics-aware approach described previously. Statics-aware form-finding may lead to shapes that cannot be covered by a convenient grid.

Generally, the objective of grid generation methods is to design a grid over a surface that consists of flat triangles or quadrangles with a size that realises a balance between structural weight and a satisfactory approximation of the surface curvature (Schober, 2015).

When a smooth surface with rotated vertices is required, a triangulated grid might be the best option. However, triangular grids have a higher node valence, and it is not possible to create torsion-free nodes. Therefore, quadrangular meshes are sometimes preferred. Especially in the case of translational or rotational surfaces a quadrangular mesh is a good solution. The process of translation of a sectioned curve along another sectioned curve automatically results in a quadrangular mesh with flat planes. (Pottmann et al., 2007)

In the case of complex free-form shapes, there are methods available for unstructured grid generation. These grids have a non-regular joint distribution, unequal member lengths and planes that are not restricted by shape. Due to the irregularity, these methods are not often applied in practice. Figure 2.12 shows different grids from different generative techniques. (Coenders, 2008)

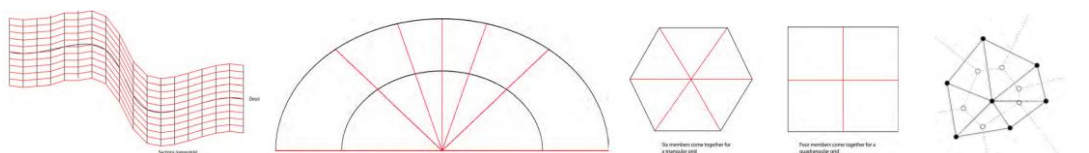


Figure 2.12: Different grids as a result of generation. (a) Translated grid (b) Grid by scaling or rotation (c) Grid from triangles or squares (d) unstructured grid (Coenders, 2008)

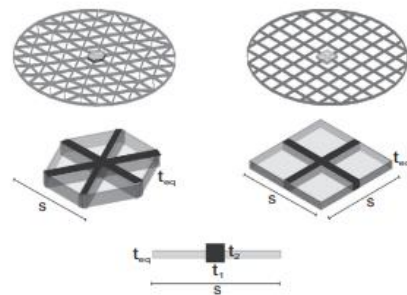
2.2.2 Structural analysis of grid shells

Analytical methods

Due to the non-linear interaction between the components and the indeterminacy of the structure of a grid shell, it is impossible to find an analytical expression that exactly describes the structural behaviour of the grid shell. However, attempts have been made at approximation of the behaviour of the structure.

The most often applied method of approximation is to define an equivalent continuous shell, for which the analytical solution is known. These approaches are called equivalent continuum methods. There are multiple approaches to determining the equivalent thickness of a continuous shell for a grid shell. To illustrate the method the derivation of the equivalent thickness based on the equivalent volume approach is shown in figure 2.13 and equation 2.1. Other more complex approaches have been proposed. (Malek, 2012)

$$\begin{aligned} V_c &= V_g \\ t_{eq} s^2 &= 2 * s t_1 t_2 \\ t_{eq} &= \frac{2 t_1 t_2}{s} \end{aligned} \quad (2.1)$$



Where:

V_c = The continuous volume

V_g = The volume of grid shell members

t_{eq} = is the equivalent thickness of the continuous shell

Figure 2.13: Equivalent volume analogy for grid shells

In Malek et al. (2014) different equivalent continuum approaches are compared to numerical results for different designs of spherical grid shells. Here is shown that based on a grid shell design an equivalent continuum can be selected that could help verify a numerical model of a grid shell.

It is, however, important to consider that equivalent continuum methods are not equipped to include all failure modes present in grid shell structures. Particularly, nodal snap-through buckling cannot be neglected in the analysis of a grid shell, especially in combination with non-rigid joints. Another issue with the use of this method is that also for continuous shells the analytical solution for the buckling load is only available for certain standard shapes.

Numerical methods

Because of the limitations of analytical methods, grid shells are usually analysed with numerical finite element methods. In a finite element analysis, the structure is divided into elements for which interaction equations are defined to satisfy equilibrium, compatibility, and constitutive relations. To include elastic boundaries or finite joint stiffness, spring elements can be modelled to account for connective effects. Many structural software programs provide the possibility to perform finite element analyses for structures.

When performing a finite element analysis it is important to consider the type of analysis that is performed. The most important distinction is between linear and non-linear methods. For linear analysis, a Linear Buckling Analysis (LBA) can be used to analyse a structure. This method assumes linear behaviour and ends at the point of buckling. LBA is mostly suitable for estimating the critical or buckling load of the structure as well as the imperfection pattern. (Rust, 2015)

In non-linear analysis several types of non-linearity can be accounted for. This includes geometric non-linearities, that account for the deformation of the structure in the previous load

step, and material non-linearities, that account for non-linear material properties. In materially non-linear analysis the structure can be analysed beyond the yield point of the structural material. Lastly, there is the option to include imperfections in the analysis of the structure. (Rust, 2015)

2.2.3 What are the important design considerations in grid shells?

Stability and failure mechanisms

Because of the slenderness of grid shell structures, stability is a critical issue in their design. Possible buckling modes are member buckling, local snap-through buckling of nodes, global buckling, and combinations of these. Snap-through instability and global buckling are generally decisive in the design of grid shells (Bulenda & Knippers, 2001).

The difference between snap-through instability and general buckling can be illustrated by a frame of two inclined members connected at the top as shown in figure 2.14. The strength of the frame is derived from the angle between the structural members. At a certain point, the deformation of the structure becomes large enough to cause the structure to snap into a new equilibrium. Snap-through occurs when the load at which this happens is lower than the Euler buckling load of the structural members. In the case of a grid shell the dynamic energy that is released upon snap-through can cause progressive collapse of the rest of the structure (Lopez et al., 2007). Figure 2.15 shows the difference between local and global buckling in a shell structure.

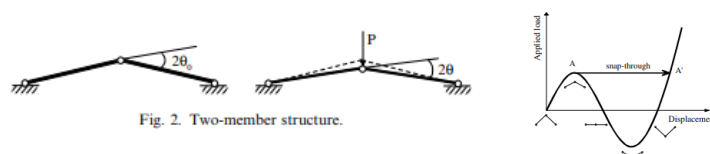


Figure 2.14: Snap-through instability of a two-member frame (Lopez et al., 2007)

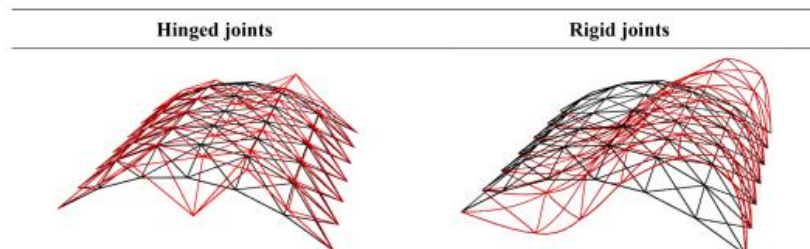


Figure 2.15: Local buckling and global buckling of a cylindrical shell (Tomei, 2023)

The susceptibility to buckling is influenced by several factors. These factors are the curvature or rise-to-span ratio, the grid topology, boundary conditions and the stiffness of the joints (Bruno & Venuti, 2018). Each factor is described below.

Rise to span ratio

The rise-to-span ratio determines the height and the slope of the structure. This influences the structural behaviour of the grid shell. Depending on the design methodology, the rise-to-span ratio is a result of a chosen curvature or vice versa.

In general, it can be concluded that a shell with a larger rise-to-span ratio has a higher critical load and can, therefore, resist higher loads than its equivalent with a lower height. This effect is seen under different conditions in works from Bulenda & Knippers (2001), Li & Taniguchi (2020) and Feng et al. (2012). Tomei (2023) shows that, although member length might increase, the required structural weight for grid shells with a higher rise-to-span ratio is lower than that for a grid shell with lower height under the same loading conditions. The reason for this is that the bending resistance of a slender beam is generally lower than its axial resistance. In the case of a high rise-to-span ratio, the beam realises a more compression-dominant load transfer. When the

height decreases the arch increasingly tends to behave like a beam, which is loaded in bending and therefore requires a greater thickness. In shells, this changes analogously from shell behaviour to plate behaviour.

Grid topology

Grid topology refers to the mesh on the surface of the shell. This includes the mesh pattern, spacing of the elements or mesh size and the orientation of the grid towards the edges. Figure 2.17 shows several options for the mesh pattern in a shell. The design of grid patterns is not limited to the ones shown below. In theory, infinitely many grid designs can be developed. The generation of the grid has been briefly discussed in section 2.2.1.

From a structural perspective, the triangular grid is often regarded as the most efficient topology. This is because the diagonals create the ability transfer loads in any direction within the surface, without bar deflection. Therefore, the triangular grid has the inherent property of activating membrane action. Non-rigid grids, like the quadrangular grid, need to be braced by extra members or boundary conditions to produce effective shell structures (Schober, 2015).

Venuti (2021) provides an explanation for the differences between triangular and quadrangular grids. Triangular grid shells behave as isotropic structures, having the same properties in every direction. Quadrangular grid shells do not possess these isotropic properties and can only achieve such high stiffness when the grid orientation aligns with the direction of principal stresses of load case. The behaviour of quadrangular grids is described as orthotropic.

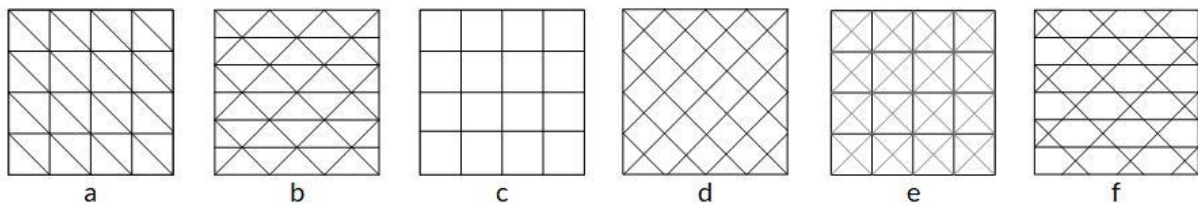


Figure 2.17: Grid patterns: a. triangular b. triangular c. quadrangular d. quadrangular e. braced quadrangular f. Kagome

The size of the mesh also plays a role in the structural behaviour of grid shells. In the case of a triangular grid, the load bearing capacity of the structure increases with an increase in structural density (Li & Taniguchi, 2020). This is also found for Kagome and quadrangular grid shells (Mesnil et al., 2017). However, Mesnil et al. did find a difference resulting from an increase of the grid density between Kagome and quadrangular grid shells. For Kagome grid shells, structural efficiency reaches a constant level when mesh sizes tend to zero, which does not happen for rectangular grid shells, where load bearing capacity keeps increasing with increasing grid density. This implies the isotropic tendencies of Kagome grid shells and the orthotropic behaviour of rectangular grid shells. This could be caused by the fact that isotropic shells possess the ability to activate shell behaviour and thus find a constant efficiency for high grid densities, this is not the case for orthotropic grids.

Malek et al. (2014) provide insights in the application of grid topologies for different rise-to-span ratios as a design help. They conclude that the structural advantages of a triangular grid are particularly beneficial in the case of a high rise-to-span ratio. This effect lessens in shallower shells. In the case of a shallow quadrangular shell, it is more effective to increase the grid density than to change the topology to a triangular grid.

Boundary conditions

Boundary conditions also play a vital role in the stability of grid shells. The way the structure is connected to the supports and the location of the supports on the structure greatly influences the strength and deformation of the structure. Usually, grid shells are assumed to be supported by pinned supports, either at corners or along the edges of the structure. The sensitivity of a shell to buckling is influenced by the support conditions. The lower the number of restrained sides the higher the required structural weight (Tomei et al., 2023). Crielaard & Terwel (2020) also mention that for an efficient structural performance a shell needs to be 'locked in' by stiff edges. This is because a flexible boundary allows for larger deformations, which significantly affects the load bearing behaviour of a form-resistant structure.

The effects of elastic boundaries on the performance of grid shells are investigated by Venuti & Bruno (2018). They point out that in practice most grid shells have one or more free edges, for example, due to required openings in the structure. The stiffness of the elastic boundary significantly influences the load bearing capacity of the shell. Particularly in the case of non-rigid grid patterns a low stiffness boundary leads to a decrease in load bearing capacity. The reduction of load bearing capacity with reducing boundary stiffness can for a part be explained by the horizontal displacement of the boundary structure, as illustrated in figure 2.18. Due to the horizontal displacement, the rise-to-span ratio of the shell decreases, reducing the structural efficiency of the shell.

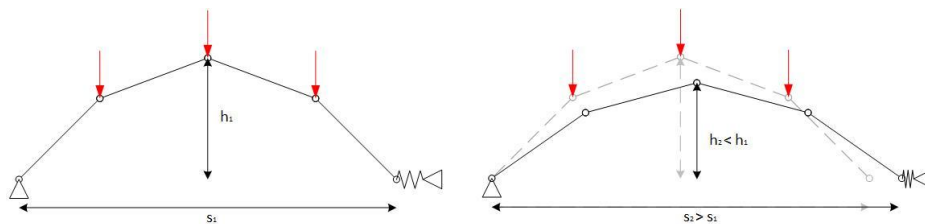


Figure 2.18: Horizontal displacement of the support at the elastic boundary

Not only the stiffness of the support but also the orientation between the structural members and the boundary can influence the efficiency of the shell. Although the grid orientation does not show a great influence on ultimate load bearing behaviour, it can significantly influence deformations in the structure. The grid orientation towards elastic boundaries seems to have a greater influence on non-rigid grids than on rigid grids (Venuti, 2021). This can be expected as orthotropic shells are highly dependent on shear stiffness and are influenced by the direction of the loads and structural members.

Joint stiffness

Stiffness of the joints is another factor in grid shell stability. The economic efficiency of transparent shells depends largely on the way the grid members are joined in the nodes. In practice the analysis of grid shells is usually performed with the nodes assumed to be either ideally pinned or fully rigid. However, for accurate analysis of a grid shell structure it is important to consider the actual stiffness of the joints (Schober, 2015).

It has been conclusively established that an increase of joint stiffness has a positive effect on the load carrying capacity of grid shells, independent of the shape or grid design of the shell. Numerical research consistently shows this effect (Wang et al., 2016), (Ye & Lu, 2020) and (Tomei, 2023). In the case of joints with a finite stiffness, it has been shown that an increase of joint stiffness can particularly benefit the efficiency of grid shells with a non-rigid grid topology or free and elastic boundaries (Tomei, 2023), (Isufi, 2021), (Venuti & Bruno, 2018). Schober (2015) states that this is because those grid shells are dependent on joint stiffness for rigidity.

Wang *et al.* (2016) find that at a certain value of joint stiffness the governing failure mode of a grid shell changes from global buckling to local snap-through buckling. The lower the joint stiffness the higher the susceptibility to local buckling. This can be explained through the figure 2.14. Joint rigidity changes this curve because it reduces deformation. In figure 2.19, it is shown that for rigid joints the mechanism for snap-through instability completely disappears (Lopez *et al.*, 2007). Tomei (2023) shows this mechanism in a grid shell structure in figure 2.15, with the buckling shape for hinged and rigid joints besides each other.

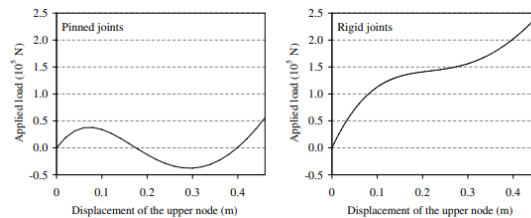


Figure 2.19: Joint rigidity can eliminate the risk of snap-through failure in grid shells (Lopez *et al.*, 2007)

Non-structural considerations

Grid shells are interesting structures in the sense that the architectural and structural design coincide. This results in the fact that architectural choices and non-structural limitations have a major influence on the structural design and vice versa.

Several non-structural constraints that contribute to decision making in the designs of grid shells are restrictions to the height, the grid spacing, the panel shapes and load carrying capacity of support structures. An example of this is the grid shell that covers the Great Court of The British Museum in London, see figure 2.20. Here the shell height was constrained to prevent obstructing the view of the central dome and triangulated panels were used to achieve a smoothness of the surface that could not have been achieved with quadrangular panels (Malek, 2012). In addition, the boundary of the shell had to be selected so that no horizontal thrust would have been exerted on the existing structure on other locations than the corners (Williams, 2001).

Another example is the Dutch Maritime Museum, see figure 2.20. The height of the shell could not exceed the existing building and the supporting courtyard facades could only carry vertical loading. Therefore, horizontal loads had to be transferred to the corners of the structure. Also, the grid of shell is based on navigational patterns and not on structural considerations (Adriaenssens *et al.*, 2010). Isufi (2021) discusses the C30 grid shell (see figure 2.3) constructed by Octatube over an existing courtyard in The Hague, where the issue of limitations of the supporting structure was solved by letting horizontal ties take up the horizontal forces generated at the base of the shell.

Furthermore, cost and manufacturing constraints also play a role in the design of the grid. Although triangular grids have favourable structural characteristics, these have some disadvantages in terms of joint design and constructability. Also, as most cladding material is produced in rectangular planes a quadrangular mesh would most likely result in the least amount of waste when cutting the panels. (Pottmann *et al.*, 2015)



Figure 2.20: Dutch Maritime Museum (left, ©photo-daylight.com) and British Museum (right, ©2024 Foster + Partners)

2.3 Design of grid shell connections

2.3.1 Connection types in grid shells

For the design of steel connections, both research and guidelines are mostly focused on frames. In the Eurocode (*EC3 part 1-8, 2011*), no specific design regulations for connections in grid shells are specified. The lack of general design guidelines for grid shell connections is also reflected in the available literature on the use of semi-rigid connections in grid shells. Research either focuses on the theoretical effect of joint stiffness on the behaviour of a shell, as is discussed in section 2.4, or it researches the properties of a specific connection design to test its structural behaviour for application in a structure. These are often experimental studies that test a joint and occasionally a scale model of a grid shell. This results in useful knowledge on the researched connection type but does not provide insights into the opportunities for optimisation of the joint design.

In general, a connection can be realised by either welding or bolting. With welding it is easier to realise a continuous connection, but bolting provides advantages in terms of easy assembly and disassembly.

For grid shells, a main distinction can be made between two types of connectors. The first type is the splice connector in which the connecting surface is along the length of the members. Members are connected by welding or by bolts loaded in shear. The second type is the end-face connector, for which the connection surface is orthogonal to the member axis. Here members are connected by welding or with bolts loaded in tension (*Stephan et al., 2004*). Figure 2.21 shows several types of splice connectors and figure 2.22 shows different types of end-face connectors.

Joints fabricated using additive design methods are another specific type of connection. These joints are often designed using topology optimisation and are produced with additive manufacturing methods, creating highly optimised joint designs. This way, it is possible to create lightweight nodes with a high structural performance (*Zuo et al., 2023*) and reduced stress concentrations (*Seifi et al., 2018*). However, design of the nodes comes at a higher cost and increased computational complexity compared to regular joints (*van der Linden, 2015*). Figure 2.23 shows a few examples of these connections. This thesis does not pay further attention to this type of connection.

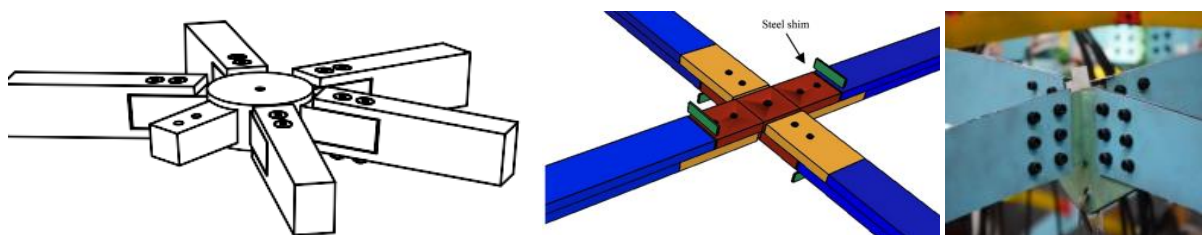


Figure 2.21: Splice connections in grid shells (from left to right: *Stephan et al. (2004)*, *Feng et al. (2015)*, *Ge et al. (2020)*)

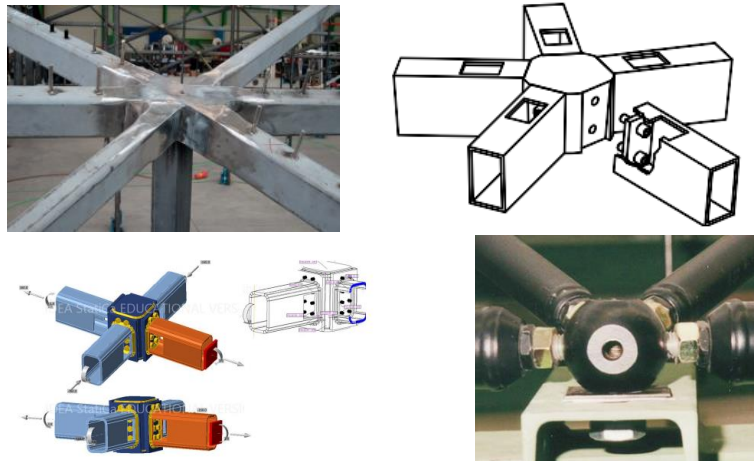


Figure 2.22: End-face connections in grid shells (From top left to bottom right: Schober (2015), Stephan et al. (2004), Isufi (2021), Lopez et al. (2007))

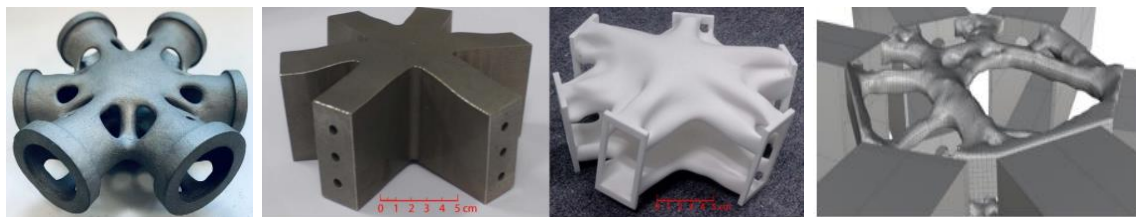


Figure 2.23: Joints optimised and produced with additive design methods (From left to right: Zuo et al. (2023), Seifi et al. (2018), Van der Linden (2015))

2.3.2 Connection design in the structural analysis

Although joints play a key role in structural performance, joints in grid shells are assumed either pinned or rigid in the first stages of the design (Ma et al., 2016). The use of semi-rigid joints is faced with similar challenges in both the design of steel frames and the design of grid shells.

During the design of steel structures joints are initially assumed to be either pinned or rigid. The structure is designed based on these assumptions. However, it has been recognised that considering the actual stiffness of the joints in the structural analysis can lead to a more economical design. Semi-rigid joints result in a more efficient distribution of forces and moments in the structure as opposed to the assumption of pinned joints, realising a more lightweight structure. In general, semi-rigid connections can be realised with less effort and material use than connections that are required to perform as rigid connections. However, including finite joint stiffness in the structural analysis of a structure increases the complexity, resulting in the fact that in practice often the traditional method is still applied. (Jaspart & Weynand, 2016)

Especially in the case of space structures, such as grid shells, the application of a semi-rigid approach to the connection design might prove to be complex. The interdependency of all structural elements and the adaptation of semi-rigid joints early in the structural calculation might lead to an iterative process which requires high computational capacity. Therefore, in grid shell structures, it is also common practice to initially consider the joints to be either pinned or rigid.

As mentioned, the current approach for the structural design of connections is not well equipped for the implementation of optimised semi-rigid connections. In this approach, the member design and the connection design are separated and often not performed by the same person. This separation becomes troublesome when semi-rigid joints are assumed, as in that case the design of the connections becomes an integral part of the rest of the structural design process. The

traditional approach in structural design generally follows the following steps: (*Jaspart & Weynand, 2016*)

1. Modelling of the structure, with the assumption of either pinned or rigid joints
2. Initial estimation of the size of structural members
3. Structural analysis of the design for the various load combinations
4. Design checks for Ultimate limit state (ULS) and serviceability limit state (SLS)
5. Iteration of member design
6. Design of the connections to resist resulting forces and moment, confirming the earlier assumption of pinned or rigid joints

For the practical application of semi-rigid connections, three different aspects need to be known. These are the moment-rotation characteristics of the joint, the matrix formulations of the structure and the design method (*Çelik & Şakar, 2022*). The first aspect is discussed in section 2.3.3 and the second aspect relates to the frame analysis method, which leaves the third aspect considering integration of the connection into the structural design.

Yin et al. (2022a) recognise the possible advantages of implementing semi-rigid joints in the design of steel frames. They define the traditional approach as described above as a ‘forward approach’ and determine two challenges for the application of semi-rigid connections in practice. The first is establishing an accurate joint model, which has, at least for frames, been widely researched. The second challenge is the integration of the connection design with the member design. To address this second challenge, a new design approach for the application of semi-rigid connections is proposed. The requirements for the joints are determined in a structural analysis. Based on the required rotational stiffness and moment resistance, the joint details can be obtained quickly. This avoids the complexity of the iterative character of joint design in steel frames, where a change in stiffness values also influences the load distribution throughout the design. (*Yin et al., 2022a*)

Isufi (2021) performed a connection design to achieve different stiffness values for grid shell joints in her thesis. Based on the classification defined by *Fan et al. (2011)* stiffness values for the joints were determined to range from rigid to pinned with several semi-rigid joints in between. Still this approach involved the design of the connections first, followed by an assessment of the stiffness performance. Determination of the design based on the stiffness requirements could be the following step in developing a connections design strategy that is applicable in combination with joint stiffness optimisation for grid shells.

2.3.3 Calculation of connections for grid shells

For the analysis of steel structures, where the actual behaviour of the joint is considered, the determination of the moment-rotation curve is the most common method for describing the rotational behaviour of a joint. To determine the moment-rotation behaviour of a joint the rotational behaviour of a connection should be determined. There is a wide variety of models to obtain the moment-rotation curve of a connection, these models can be analytical, empirical, experimental, informational, mechanical, and numerical. (*Diaz et al., 2011*)

For the calculation of steel connections in structural frames, mechanical methods are most commonly used, with the component method being the most popular among these methods (*Diaz et al., 2011*). In the component method, the stiffness and strength contributions of all separate components of a connection are combined to determine the overall moment-rotation behaviour of the connection. In figure 2.24 the component method is visualised for a beam-column connection.

The component method is well-documented for beam-column connections in steel frames and included in the Eurocode (*EC3 part 1-8, 2011*). However, these guidelines are not directly applicable to grid shell connections. Therefore, the use of numerical methods is better equipped for analysis in those cases. With finite element methods, the behaviour of a connection can be modelled. For the design of connections component-based finite element methods (CBFEM) are a convenient solution. These methods use the advantages of the regular component method and integrate them into finite element methods (*Broeders, 2021*). The advantage of component based methods is that the individual contribution of the components to the behaviour of the connection can be evaluated. Therefore, this calculation method provides possibilities for parametrisation of the design. Allowing for a more straightforward optimisation process.

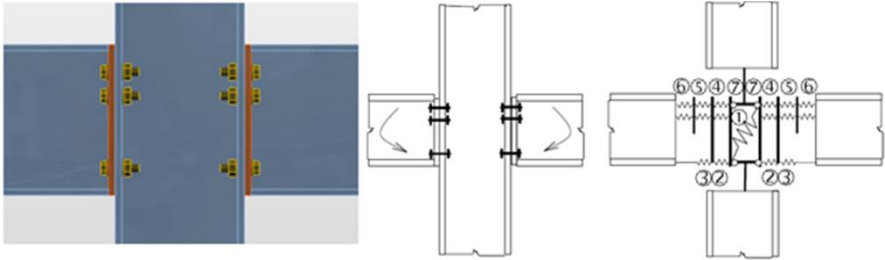


Figure 2.24: Component method. © IDEA StatiCa 2009-2024

2.4 Joint stiffness optimisation

In this section the effects of joints stiffness optimisation on the structural behaviour of a grid shell are investigated further. Section 2.4.1 gives an introduction into joint stiffness in structural analysis, Section 2.4.2 investigates the influence of several stiffness parameters on the structural behaviour of a grid shell and section 2.4.3 described some approach to joint stiffness optimisation in literature.

2.4.1 How is the joint stiffness defined?

Joint stiffness refers to the flexibility of the connection between structural members. In structural design and analysis, there are three possible classifications of the joint stiffness. These are defined in Eurocode 3 *Design of steel structures – Part 1-8 Design of joints (EC3 part 1-8,2011)*, section 5.2.2 as pinned, rigid and semi-rigid. Pinned or hinged joints should be able to transmit internal forces, without generating a significant moment in the connection. Rigid joints have sufficient rotational stiffness to ensure continuous connection between the joined structural members. Whether joints are considered to be rigid or pinned has a significant influence on the load distribution in a structure. This is illustrated by the frame in figure 2.25. If a connection does not satisfy the criteria for either pinned or rigid connections it is considered to be semi-rigid.

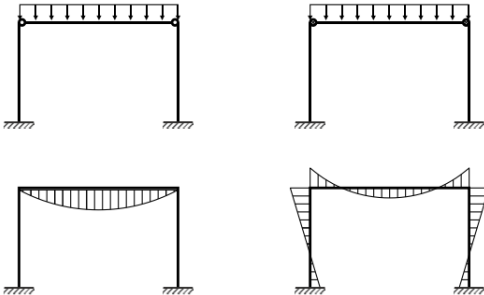


Figure 2.25: Load distribution structural frame for pinned (left) and rigid connections (right) (Jaspart & Weynand, 2016)

Joint stiffness is not merely the result of the connection design but a combination of the stiffness of connecting elements and the stiffness of the structural members. The behaviour of the joint can be described by the initial rotational stiffness of the joint and the moment capacity. The relation between the applied bending moment and the rotation of the joint can be visualised with a moment rotation curve, see figure 2.26a. In the research and design in this project the aim is to stay within the elastic range of the joints. According to *EC3 part 1-8 5.1.2 (3)* the initial rotational stiffness ($S_{j,ini}$) can be used when the acting bending moment ($M_{j,Ed}$) does not exceed 2/3 of the moment capacity ($M_{j,Rd}$). In that case a linear stiffness model can be chosen for the connections as shown in figure 2.26b.

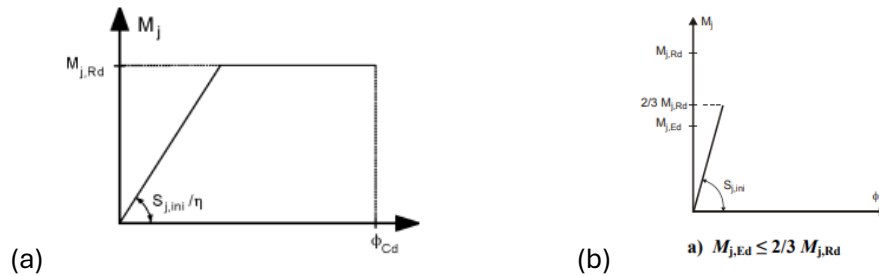


Figure 2.26: (a) Bi-linear moment rotation curve of a joint (*EC3 part 1-8 fig 5.2*)
 (b) Initial rotational stiffness to be used in elastic calculation (*EC3 part 1-8 fig 5.1*)

The Eurocode (*EC3 part 1-8, 2011*) provides a classification system for joints in steel frames, which is based on the initial stiffness ($S_{j,ini}$) and the moment capacity ($M_{j,Rd}$). However, the classification system as presented in *EC3 part 1-8 section 5.2* is not applicable to grid shell structures. Depending on the structural characteristics the same joint may be classified differently in different structures. *Fan et al. (2011)* propose a classification system for joints in grid shell structures. The method is illustrated below with a derivation of the rigid stiffness boundary of a joint in a frame consisting of two members (Figure 2.27). This method can be expanded to classify joints in larger structures. Parametric investigation of the structure leads to the diagram in figure 2.28 which shows the stiffness boundaries.

Rigid joint:
$$M_{zr} = \frac{4EI}{L} (\theta_0 - \theta) + \frac{6EI}{L} \cos \theta (\sin \theta_0 - \sin \theta)$$

Actual joint stiffness:
$$M_{zs} = k * 2(\theta - \theta_0)''$$

For Rigid boundary:
$$M_{zr} = M_{zs}$$

Considering small deformations this gives:
$$k = \frac{2EI}{L} + \frac{3EI}{L} * \cos \theta$$

With $\cos(0)=1$ this gives the rigid boundary:
$$k = \frac{5EI}{L} \rightarrow \alpha = \frac{k}{EI/L} = 5$$

Where k is the joint stiffness and L is the length of the members

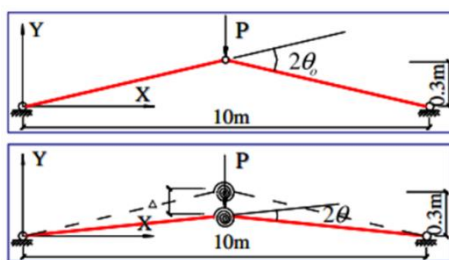


Figure 2.27: Two member frame structure (*Fan et al., 2011*)
 stiffness

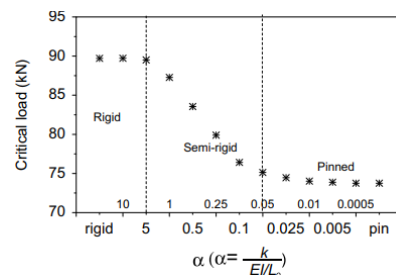


Figure 2.28: Classification boundaries for joint based on parametric analysis (*Fan et al., 2011*)

As mentioned in section 2.1.3, grid shell joints have both in-plane and out-of-plane requirements. Standard connections in frames are generally designed to resist shear and bending in one direction, most often loaded in the strong axis of the cross-section as is the case for the top beam in figure 2.21. However, in grid shells the connections are responsible for the stiffness of the frame in two directions. Out-of-plane loads have to be resisted, but the connections also play a role in providing shear stiffness of the frame. Figure 2.29 visualises how the in-plane rotational stiffness of the connections can be responsible for the in-plane shear stiffness of the frame or grid.

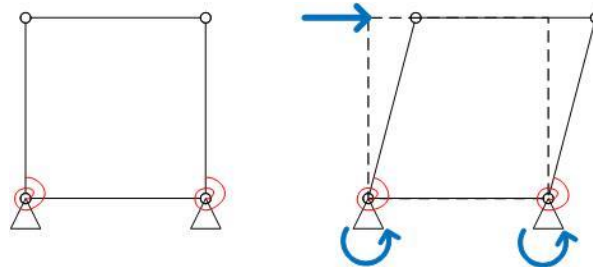


Figure 2.29: In-plane shear deformation of a square grid cell is resisted by in-plane rotational stiffness of the connections.

2.4.2 The influence of joint stiffness on the behaviour of grid shells

In this section, the influence of joint stiffness on the behaviour of grid shells, which has been briefly discussed in section 2.2.3, is described in further detail. Figure 2.8 (Section 2.1.3) shows the different degrees of freedom for which a grid shell joints should be able to provide stiffness. The separate stiffness values of the joints are not much represented in literature.

Although not making a distinction between in-plane and out-of-plane stiffness *Li & Taniguchi (2020)* evaluated the influence of the different stiffness parameters. In a numerical study, the effect of joint stiffness on the load bearing capacity of a triangular grid shell was studied. The effect of bending stiffness (k_{by} , k_{bz}), axial stiffness (k_{ax}), torsional stiffness (k_{tx}) and shear stiffness (k_{sy} , k_{sz}) of the joints on the structural behaviour are considered separately. Figure 2.30 shows the results of the effect of varying the stiffness on the critical load of the grid shell.

As expected, the reduction of bending stiffness leads to a decrease in the load bearing capacity of the structure. Remarkable is that the same seems to apply for the axial stiffness. Torsional stiffness seems to have only a slight effect on the load bearing behaviour of grid shells. The shear stiffness shows interesting behaviour in the sense that for low stiffness the load bearing capacity of the shell is greatly influenced by the shear stiffness of the joints. However, already for relatively low values of shear stiffness the connections are rigid in shear and increasing the shear stiffness does not benefit the load bearing capacity of the shell any further.

The indication that torsional stiffness of the joints does not significantly affect load bearing capacity of triangular grid shells is confirmed in a study by *Ma et al. (2013)*.

Venuti & Bruno (2018) studied a half dome with a quadrangular grid in both unbraced and fully braced conditions with varying boundary stiffness. Although joints were considered fully rigid the variation between unbraced and braced situations can provide some insights into the effect of the shear stiffness of the frame on load bearing capacity of the shell. The research indicates that a shell without bracing has a significantly lower load factor than a shell with some bracing, the correlation between increasing bracing and increasing load factor was reduced after minimal shear stiffness was achieved. This could further reinforce the suggestion that a grid shell structure requires a minimal degree of shear stiffness, but that an optimisation of shear stiffness would not be beneficial.

The in-plane rotational stiffness of the joints and, therefore, the in-plane shear stiffness of the frame is also explicitly mentioned in papers by *Feng et al. (2012)* and *Wang et al. (2016)*. In both these projects elliptic paraboloid domes with a braced quadrangular grid are researched. Feng et al. compare a shell with fully rigid joints to a shell with in-plane pinned joints and out-of-plane rigid joints and find a minor reduction in load-bearing capacity between the two structures. Evaluation of the result from Wang et al. shows that also, in that case, a significant reduction of in-plane joint stiffness only leads to a small reduction in load-bearing capacity.

The study by *Feng et al. (2012)* did however highlight that, although load-bearing capacity is not particularly influenced, the deformation of the shell is more significantly influenced by the reduction of in-plane stiffness of the joints.

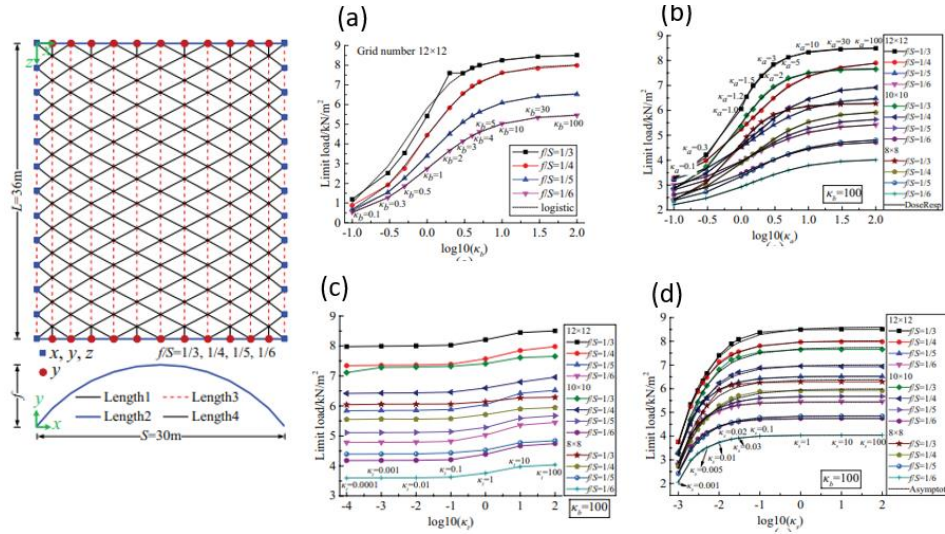


Figure 2.30: Effect of joint stiffness on load bearing capacity for a triangular grid shell (Li & Taniguchi, 2020).
(a) Bending stiffness (b) Axial stiffness (c) Torsional stiffness (d) Shear stiffness

Ge et al. (2020) researched a quadrangular elliptic paraboloid shell supported only in the corners, see figure 2.31. In this paper, both in- and out-of-plane rotational stiffness is considered. The in-plane rotational stiffness of the connection (about v-axis) shows a major influence for relatively low joint stiffness, then when some in-plane stiffness is achieved the load factor remains constant. The out-of-plane stiffness shows a different result, increasing the out-of-plane stiffness of the joint increased the load factor of the shell to the point where the joint stiffness already exceeded the member stiffness significantly. This research also suggests the importance of out-of-plane rotational stiffness over in-plane rotational stiffness. However, in this case, the result could have been affected by the very limited in-plane rotational stiffness of the member, which is displayed in figure 2.28.



Figure 2.31: Grid shell and connection investigated by Ge et al. (2020)

In the reviewed research, some trends can be discovered for the different stiffness parameters. However, it is not possible to draw any definite conclusions based on the presented knowledge. The effect of the different stiffness parameters on the performance of the grid shell structure should be determined in a parametric study before decisions can be made on the implementation or exclusion of parameters in the optimisation of joint stiffness.

The research at least suggests that out-of-plane rotational stiffness and axial stiffness play a significant role in structural performance and could, therefore, be important parameters in the optimisation of joint stiffness. In-plane bending stiffness, shear stiffness and torsional stiffness shows a less significant impact, but this can be highly case-specific and inquiries into the effects should be made during a parametric study. A possible example of this could be that unsupported edges in combination with reduced in-plane rotational stiffness can significantly influence deformations, resulting in the in-plane rotational stiffness being an important stiffness parameter.

2.4.3 Optimisation approaches to optimise joint stiffness in grid shells

A small number of studies researching the optimisation of joint stiffness have been performed. They are described in this section. In work from *Grande et al. (2020)*, *Tomei (2023)* and *Isufi (2021)*, two general approaches can be identified.

Grande et al. and *Tomei* perform their research on a similar grid shell with a rigid grid, which shape is determined through hanging model form-finding, shown in figure 2.32. *Tomei* also considers different boundary conditions. Both studies apply an optimisation strategy that can be described as the ‘pinned-rigid’ approach. During the optimisation process the percentage of rigid joints in the structure is varied, remaining joints are assumed pinned, as shown in figure 2.33. For each step a member sizing optimisation is performed. Both studies show a considerable reduction in required structural weight when a part of the joints are designed rigid when compared to a structure with only pinned joints.

Tomei and *Isufi* both perform a joint stiffness optimisation according to a semi-rigid approach. In these cases, all joints are assigned the same stiffness. This stiffness value is then reduced, creating a reduction in structural weight. *Tomei* performs this optimisation for the same structure as shown in figure 2.32. *Isufi* performs the optimisation for both a triangular and a quadrangular grid shell that is shown in figure 2.34. Both *Tomei* and *Isufi* found that optimisation of joint stiffness can reduce structural weight in grid shell design. However, the case of a fully constrained grid shell with a rigid grid turns out to be an exception. In these rigid grid shells, joint stiffness has a less significant effect on structural performance and pinned joints already provide sufficient stability.

A difference should be noted between the optimisations by *Tomei* and *Grande et al.* and the one performed by *Isufi*. The starting point in a triangular structure is pinned joints, where weight reduction is a result of member size reduction at higher joint stiffness. In the quadrangular structure, the starting point is rigid joints and optimisation leads to weight reduction in the joint design.

The existence of both the pinned-rigid approach and the semi-rigid approach can suggest the possible benefits of varying the stiffness values of joints between different finite values.

Ye and Lu (2020) developed an algorithm that performs both a member sizing optimisation as well as a joint stiffness optimisation in a dome structure. The results of the optimisation are shown below in figure 2.35. The optimal dome has a significant reduction in steel use for the connection while steel use for the members and load bearing capacity of the dome remains the same for both the optimised dome and the dome with rigid connections. Optimising the joint

stiffness of a grid shell might be beneficial. However, in this approach the result is seemingly random, where a new optimisation might lead to a different result and where it is not clear why the result is as shown. For practical application of joint stiffness optimisation, a certain degree of uniformity and predictability is required.

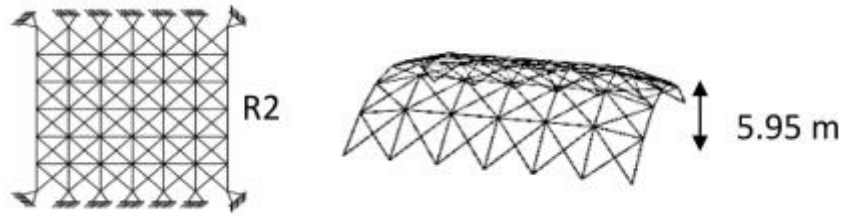


Figure 2.32: Grid shell as investigated by Tomei (2023) and Grande et al. (2019)

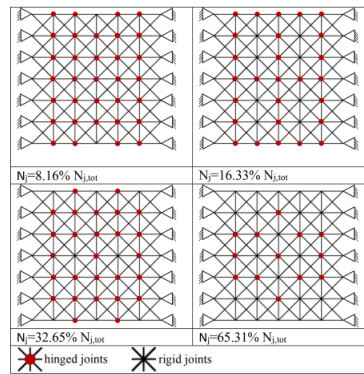


Figure 2.33: Joint stiffness distribution in pinned-rigid joints approach (Tomei, 2023)

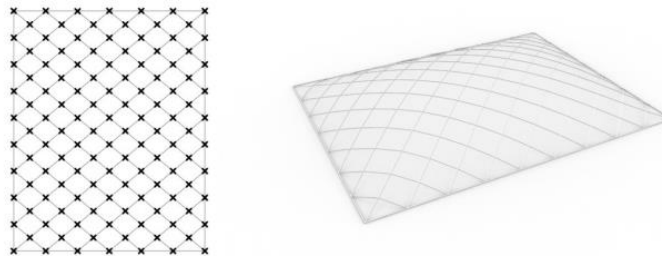


Figure 2.34: Grid shell as investigated by Isufi (2021)

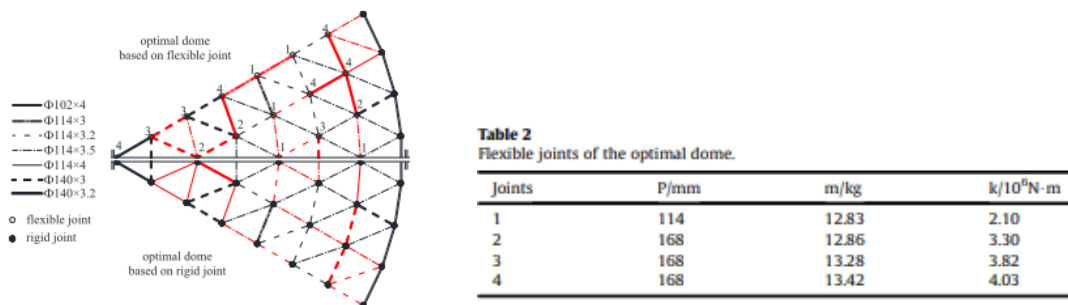


Figure 2.35: Result of the grid shell optimisation (Ye and Lu, 2020)

2.5 Constructability and sustainability

As mentioned before, there are several considerations on constructability and sustainability that can influence design choices for grid shells. The joint stiffness optimisation and connection design could actually have several advantages for the constructability and sustainability of grid shells when compared to current approaches to grid shell design.

Constructability refers to the production and installation of grid shells. Production complexity can for example be influenced by the regularity of the structural elements and the size of the elements. The installation considers the assembly of the grid shell and is influenced by element size and the method of connecting the elements. Also transport restrictions can influence the constructability of a grid shell. Finally, cost also plays a role in the possibilities for the realisation of a structure.

The sustainability of grid shells is also influenced by several factors. All can be more or less captured in numbers with embodied carbon or emissions as a result of the construction of a grid shell. Some aspects to consider for the sustainability of a grid shell are transport needs, material use and structural weight, and the opportunities for reuse or disassembly of the structure.

The connection method of the structural elements plays an important role in these considerations. Bolted connections are reversible and are, therefore, better for the reuse of a structure than welded connections. Overall, the reuse of structural elements outperforms the recycling of structural material in terms of sustainability (Yeung *et al.*, 2016). The reuse of structural elements is proven to be a feasible solution by application in projects over time. However, many challenges remain including disassembly and availability of stock (Brütting *et al.* 2019). Researching the application of semi-rigid connections opens possibilities for wider use of reversible bolted connections and can, therefore, aid in solving one of these challenges.

The connection design also greatly influences installation methods. Welded joints are generally prefabricated and bolted joints can be connected on site. This influences element size and transport requirements. In general, the aim should be to minimise the emission of transport by reducing the amount of required transport movements. In addition, constructability is complicated when the element size is bigger than restricted for regular trucks. The application of semi-rigid joints provides a larger possibility for the application of bolted joints in grid shells. But it also influences erection speed.

Furthermore, as mentioned before, the grid design can influence sustainability and constructability. Despite structural disadvantages, a quadrangular mesh has several advantages over triangular meshes. Because they consist of fewer structural members quad shells are generally more lightweight structures and square panels generate less cutting waste for the glazing (Mesnil *et al.*, 2017). In terms of constructability, it is impossible to achieve torsion-free beam connections in triangular grids (Pottmann *et al.*, 2015 and Schober, 2015) which complicates the fabrication of the connections.

Lastly, the regularity of structural elements affects the constructability. Clustering of joints and elements can reduce the variety of structural elements. Koronaki *et al.* (2023) research this and provide methods to cluster joints to reduce differences. Clustering can be performed based on geometrical characteristics but could also be applied for clustering based on joint stiffness.

3 Connection design

In this chapter, research is focused on answering the questions related to objective 1. The goal of the objective is the development of an adapted design strategy for steel connections, improving the possibilities for the implementation of semi-rigid connections in grid shell design. The research questions are:

- How does the interaction of loads influence the stiffness of a bolted steel connection?
- How do different design parameters influence the stiffness of a bolted steel connection?
- How can a steel connection be designed based on a pre-determined stiffness?

3.1 Connection model and analysis

A specific connection design is selected for the research. This connection is described in section 3.1.1. Section 3.1.2 discusses some background information on the analysis method for the connection.

3.1.1 Connection model

A basic example of the type of connection that is considered during the research is displayed in figure 3.1.

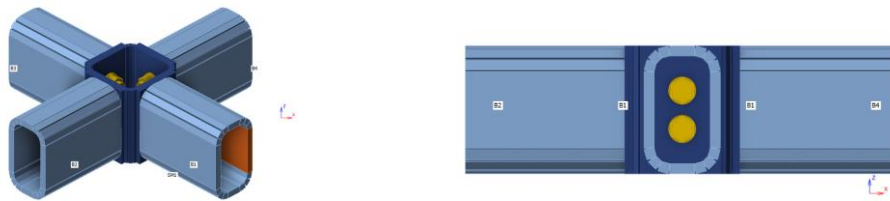


Figure 3.1. Connection design for the research

The connection is an end-face connection with a central box. The box is a square hollow section, which forms the central node of the joints. The elements are connected to the node using an endplate that is welded to the end of the profile. Bolts connect the endplate to the centre box. The strength and stiffness of the base connection can be increased by adjusting the design parameters, which is discussed in section 3.2.

The design principles of the connection are inspired by different example connections. Figure 3.2a shows the connection as researched by *Isufi (2021)*, which serves as the main inspiration for the connection design. The connection shows design operations like the addition of cap plate stiffeners and extra bolt rows that can increase the stiffness. Figure 3.2b shows a connection realised by Octatube for the construction of The Bubble in Eindhoven (2013). This picture shows the fastening of a bolt in the connection that is based on similar principles.



Figure 3.2: Connection examples. (a) Connection from work by Isufi (2021). (b) Mock-up connection for The Bubble

3.1.2 Connection analysis and CBFEM

Connections are analysed with the Component Based Finite Element Method (CBFEM), which is mentioned in section 2.3.3 in the literature study. The method combines FEM software with the in the Eurocode regulated component method based on *prEN 1993-1-8:2021*. The CBFEM will be applied using IDEA StatiCa software (*IDEA StatiCa, n.d.-a*).

In the structural model, the node is defined as a dimensionless point. In the analysis of the connection, it is important to design a joint model that represents the actual behaviour. In the CBFEM, the ends of the members that are connected to the nodes are included in the analysis. Forces and moments are applied to the end of the included member. The location of the node in the model is important to consider. IDEA StatiCa provides the option to select the location of the load effect at either the centre of the node, in the bolts, or at the end of the element. Figure 3.3 shows how the chosen location can affect the loads on components in the connection. Depending on the selection of the location of the load effect, bending moments throughout the joint are adjusted with a counter moment, ensuring that the desired load distribution is achieved. (*IDEA StatiCa, n.d.-b*)

Steel plates in the connection (webs, flanges, endplates, stiffeners) are modelled using meshed shell elements. Fastening components (bolts and welds) are modelled with special FEM components. Equivalent elastoplastic shell elements are implemented to simulate a welded connection between plates. Bolts have different characteristics as they only resist loads in tension, shear and bearing. The bolts are modelled with nonlinear spring elements, combined with rigid body elements and gap elements. Lastly, contact stresses at location where plates meet are simulated with a penalty stiffness that prevents one mesh from penetrating into another. (*IDEA StatiCa, n.d.-b*)

The components of the connection are modelled according to an elastic-plastic material model with a nominal yielding plateau according to NEN EN 1993-1-5 section C.6. Material is assumed to be elastic until the design yield stress is reached (*IDEA StatiCa, n.d.-c*). The type of analysis that is performed depends on the cross-section profile. For open sections, the performed analysis is geometrically linear and materially nonlinear. In case of hollow sections, geometrical nonlinearities can be considered. In this project, a geometrical and material nonlinear analysis (GMNA) is performed.

Three performance parameters of the connection are determined during the analysis. These are the strength, stiffness, and rotation capacity. For the strength analysis, nonlinear elastic-plastic analysis is used to perform strain checks of the plates and code checks for the components. (*IDEA StatiCa, n.d.-b*)

In this thesis, the stiffness analysis is important. The stiffness is analysed separately for the connection of each member to the node. The loads defined in the model are applied simultaneously in the analysis. A moment-rotation or load-deformation diagram is generated by applying the loads in proportional increments. The load steps depend on the applied load and the member resistance. The maximum load is determined by multiplying the applied load by a factor α . The definition of α is given in equation 3.1. The maximum loads are divided into 12 load steps. For each step the rotation (φ) in the joint is analysed for generation of the M- φ -diagram.

$$\alpha = \min \left(\frac{N_R}{N} ; \frac{M_{y,R}}{M_y} ; \frac{M_{z,R}}{M_z} \right) \quad (3.1)$$

In eq. 3.1, N_R , $M_{y,R}$ and $M_{z,R}$ refer to the load and moment resistance of the structural members.

This research focuses on the elastic capacity of the connection and, therefore, uses the initial rotational stiffness of the connection. The initial stiffness is determined as the secant stiffness at the point where 2/3 of the joint moment capacity is reached ($2/3M_{j,Rd}$). The bending moment capacity is set at the 5% equivalent strain limit. To ensure elastic behaviour of the connections, the acting bending moment is not allowed to exceed the value of $2/3M_{j,Rd}$ according to NEN EN 1991-1-3 section 5.1.2, as discussed in chapter 2 section 4.1 of this report.

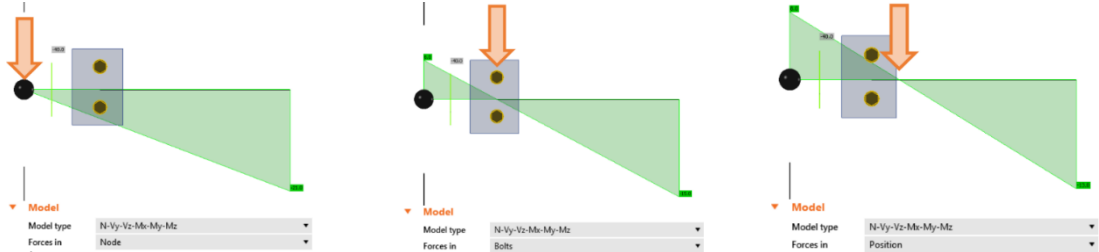


Figure 3.3. The location of the load effect influences the load on the connection components. (IDEA StatiCa, n.d.-b)

3.2 Base connection design

In this section, the approach for the design of a connection is discussed. Section 3.2.1 discusses the design of a base connection determined by the cross-section of the structural elements. In section 3.2.2, the parameters for changing of the stiffness of a connection are described.

3.2.1 Design based on cross-section

The profiles selected for the structural elements dictate the base dimensions for the connection. The cross-sections of the structural elements follow from the structural design. Therefore, the cross-section size is fixed for the connection design. The dimensions of the cross-section provide constraints for the base design of the connection.

The dimensions of the endplate and the centre box are determined by the height and width of the steel profile. The minimum dimensions of the endplate depend on the method of welding. In the case of butt welds, the minimal dimensions of the endplate are the height and width of the cross-section. For the centre box, the web of the square hollow section should be sufficiently wide to fit the endplate. Therefore, a cross-section has to be selected where the width of the web is at least equal to the width of the endplate. The width of the web can be determined by subtracting two times the outside radius of the corners from the width of the element. The length of the centre box should at least match the height of the endplate.

The placement of the bolts is determined by the size of the endplate and dimensions of the steel profile. If bolts fit inside the cross-section the maximal spacing is dictated by the height of the endplate. Minimum spacing and edge distances are given in NEN EN 1993-1-8 section 3.5 table 3.3 (EC3 part 1-8, 2011).

Base connection

The connection is designed based on an assumed structural cross-section RHS100x60x8. This cross-section has been used in the design in the work of Isufi (2021) and is similar to the dimensions realised in the design in chapter 5. This leads to the dimensions for the connection in figure 3.1 that are listed in table 3.1.

Endplate	height	100 mm
	width	60 mm
Centre box web	Length	100 mm
	Web	60 mm

Table 3.1. Minimal dimension elements based on RHS100x60x8

This gives the following dimensions for a minimal design of the base connection.

- End plate: 100x60x5 mm
- Centre box: SHS80x80x5 (Web = 80 – 2*r_o = 60 mm)
- Bolts: M12 8.8 (Spacing is 30 mm, centred around the middle of the endplate)

3.2.2 Design parameters

With the base connection as a starting point, different parameters can be identified that influence the stiffness performance of the connection. These parameters can be divided into two categories. The first group are direct parameters that can be easily adjusted without altering the connection and can, therefore, realise a range of stiffness that can be achieved for the connection design. The second group consists of larger adjustments to the connection design that increase the rigidity, after which the direct stiffness parameters can be adjusted to create a new stiffness range. The two categories of parameters are elaborated below. The influence of the parameters on the performance of the connection will be further evaluated in section 3.4.

Direct stiffness parameters

Four direct stiffness parameters can be identified. Figure 3.5 visualises how the parameters influence the stiffness of the connection. The parameters are listed below:

1. Bolt spacing: Changing the spacing of the bolts leads to changes in the lever arm of the acting bending moment. An increase in bolt spacing will lead to a decrease in loading on the bolts, which will, therefore, increase the stiffness of the connection.
2. Bolt type: The selected bolt type gives the diameter and material properties of the bolts. These can both have an influence on the strain of the bolts and with that the stiffness of the connection.
3. Centre box dimensions: An increase in the thickness of the stiffening box will likely increase the stiffness of the connection. However, when a larger cross-section is selected the increase in span of the web of the profile could lead to a decrease in stiffness. These two factors play a role in the selection for the cross-section.
4. Endplate thickness: An increase in the thickness of the end-plate would decrease deformation in the end-plate, increasing the stiffness of the connection.

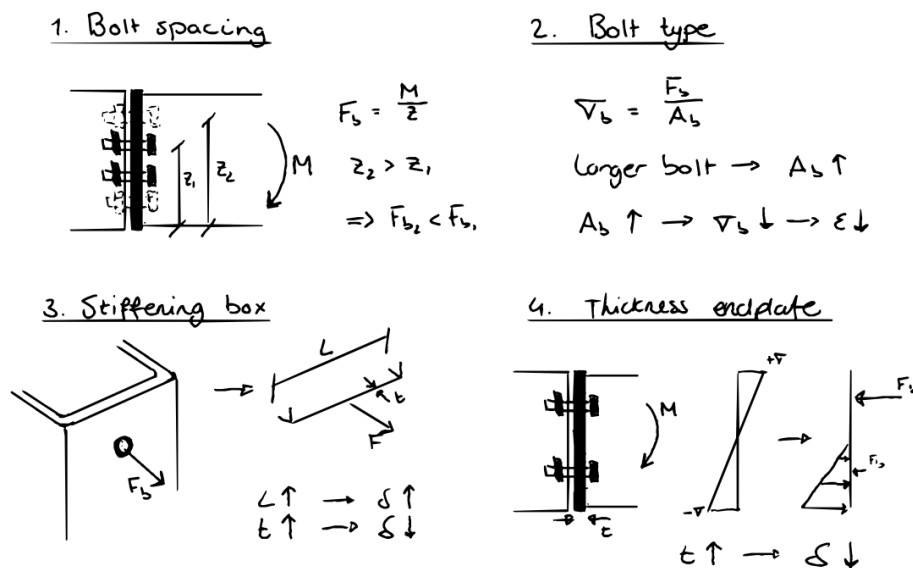


Figure 3.5 Effect of stiffness parameters on the stiffness of the connection.

Stiffness range parameters

Multiple design actions can be performed to increase the stiffness of the connections. It is also possible to combine these operations to further increase the stiffness. Examples are given below:

1. Addition of capping plates: Cap plates welded to the top and bottom of the connection would act as stiffeners for the cross-section, which would reduce deformations in the connection. However, for reasons of constructability of the connection, the addition of caps would require openings in the beam to be able to fasten the bolts.
2. Addition of a bolt row outside the profile: Adding an extra bolt row would increase the lever arm carrying the bending moment as well as increase the number of bolts that carry the loads on the connection. Therefore, this would increase the stiffness. As mentioned, the addition of a bolt row could be combined with the addition of capping plates.
3. Considering prestressed bolts could be an option if a specific connection allows for their installation. Prestressed bolts are expected to significantly increase the joint stiffness by realising compression in the connection. However, in this connection design installation could prove complex because it is difficult to reach both ends of the bolts during installation. Accessibility is governing for the application of prestressed bolts.

3.3 Influence of load interaction on connection stiffness

In the Eurocode (NEN EN 1993-1-8 Design of steel connections (*EC3 part 1-8, 2011*)) the focus is on connections of steel frames, connections in these frames are mostly loaded in bending moments and shear force. Bending moments are expected to cause rotation in the connections. Therefore, in the code, the stiffness of the connection is determined solely based on acting bending moments. However, connections in grid shell are also loaded by axial forces. Axial loads can significantly influence the rotation of the connection. In this chapter, the effect of the ratio between loading in different directions on a grid shell connection is investigated.

The assumption that different loads on the connection influence the stiffness of the connection means that, in the case of including semi-rigid stiffness in the structural analysis, the design steps away from the standard calculation of joint stiffness as prescribed in the Eurocode. Therefore, parametric research is performed below. Also, it is important to consider that only the initial rotational stiffness ($S_{j,ini}$) of the connections is considered. For the determination of the initial stiffness, the magnitude of the loading is not of influence. Because the loading is applied in increments to construct the complete moment-rotation diagram, only the ratio between the loads affects the calculation of the initial rotational stiffness. The magnitude of the loads does not influence the initial stiffness and only helps to determine whether the capacity of the joint is reached under the applied loading conditions.

Stiffness influence M/N

In this paragraph the influence of the load ratio on the stiffness of the connection is investigated. Figure 3.6 shows the influence on the Initial rotational stiffness in y-direction ($S_{j,ini,y}$) for the base connection. Figure 3.7 shows a similar image for the stiffness in z-direction ($S_{j,ini,z}$). Data points are retrieved by calculating $S_{j,ini}$ for various M/N-ratios. Variation of the M/N-ratio is realised by varying the value of the bending moment (M_y or M_z [kNm]) for a fixed value of axial force ($N = -2$ kN).

The figures show an increase in $S_{j,ini}$ for small M/N-ratios, the M/N-ratio is small when the magnitude of the axial force is high compared to the magnitude of the bending moment. When M/N-ratio increases, in this case due to an increase in bending moment, $S_{j,ini}$ approaches a stable value.

Figure 3.8 presents an explanation for the behaviour seen in figures 3.6 and 3.7. Figure 3.8a shows stresses in the cross-section in the case that the value of axial force is considerably larger than the value of the bending moment, resulting in the entire cross-section being in compression. Figure 3.8b shows the stresses in the cross-section for large load ratios. In this case part of the cross-section will experience tensile stresses. Based on the assumption that compression stabilises the connection by pressing the components together and, therefore, restricting rotation, this explains the increase in $S_{j,ini}$ for small M/N -ratios. Also, the stabilisation of the stiffness value for large M/N -ratios can be explained. In the case of a compressive axial load, never more than half the cross-section will be in tension.

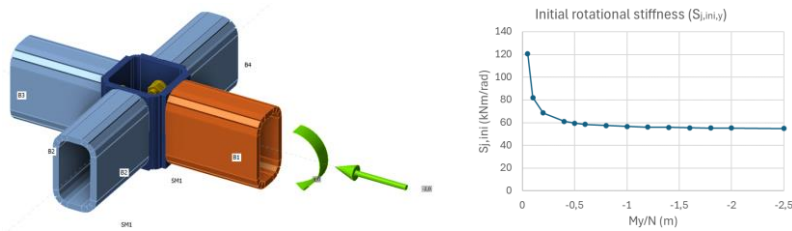


Figure 3.6: Influence of the M_y/N -ratio on the initial rotational stiffness ($S_{j,ini,y}$) of the connection

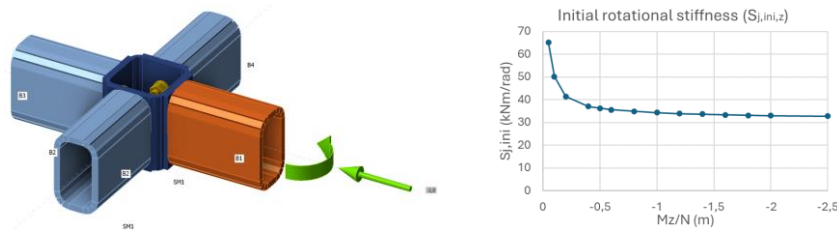


Figure 3.7: Influence of the M_z/N -ratio on the initial rotational stiffness ($S_{j,ini,z}$) of the connection

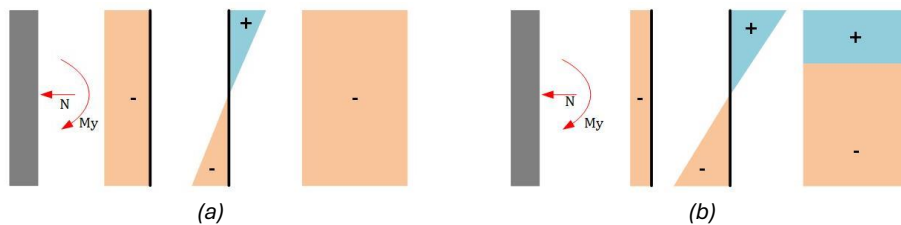


Figure 3.8: (a) Stresses in the cross-section for a low M/N -ratio. (b) Stresses in the cross-section for high M/N -ratio

Figure 3.9a shows a similar diagram as shown in figures 3.6 and 3.7 for the case of a tensile axial force. Now $S_{j,ini}$ clearly decreases for small M/N -ratios. Analogous to the explanation of figure 3.8, the decrease in $S_{j,ini}$ can be explained by the decrease in the size of the area in compression when the tensile axial force is large compared to the magnitude of the bending moment. This is shown in figure 3.9b. Therefore, this is a scenario that requires specific attention in case it occurs in a grid shell with semi-rigid connections.

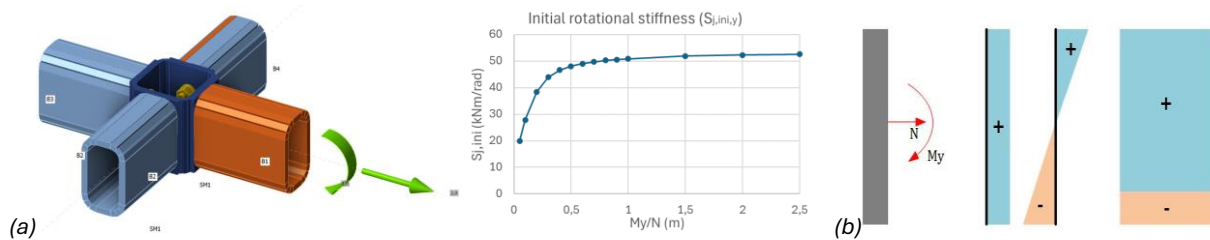


Figure 3.9: (a) Influence of the ratio M_y/N on the initial rotational stiffness in case of tensile axial force. (b) Stresses in the cross-section in the case of a tensile axial force

Not only the ratio between the bending moment and axial force can influence $S_{j,ini}$. Figure 3.10a shows $S_{j,ini,y}$ when a bending moment around the z-axis (M_z) is also applied to the connection of the results in figure 3.6. Figure 3.10 shows that the presence of a bending moment in y-direction can stiffen the connection for rotations around the y-axis. Figure 3.10b shows how a bending moment around the z-axis can increase the compression in the cross-section, increasing the stiffness. This is only the case when stress caused by M_z is smaller than stress as a result of M_y . Figure 3.11 shows a similar diagram for the case where a shear force in z-direction is present in the cross-section. It shows only a minor influence on the rotational stiffness of the connection.

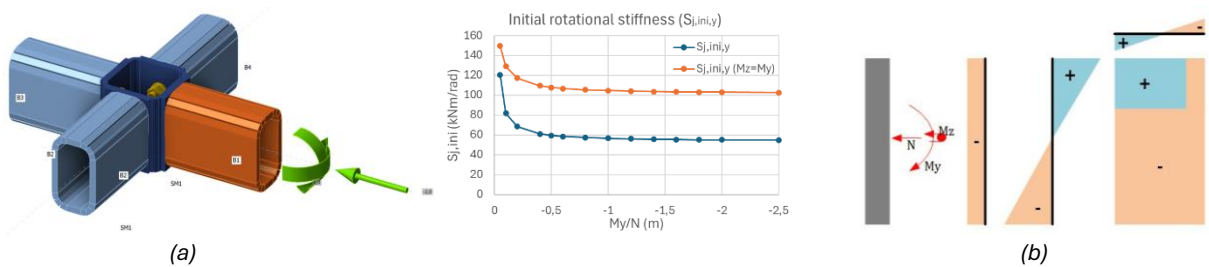


Figure 3.10: (a) The influence of an applied M_z on the initial rotational stiffness for different M_y/N ratios. (b) The influence of a bending moment around the z-axis on the stresses in the cross-section.

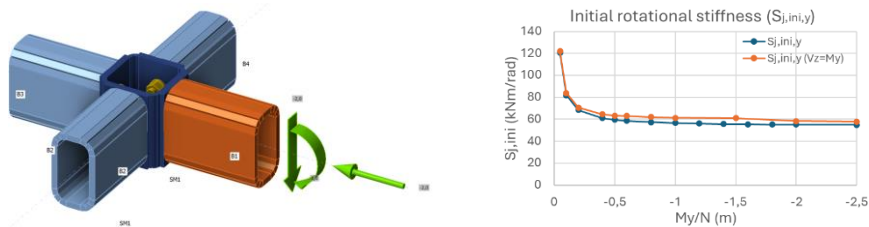


Figure 3.11. The influence of an applied V_z on the initial rotational stiffness for different M_y/N ratios.

In general, it can be concluded that compression stabilises a connection because it restricts the movement of the different components. The opposite happens in case of tension.

Peak in stiffness for small load ratios

For small load ratios, a greater area of the cross section is in compression. Therefore, the connection has a higher initial stiffness. However, further research into the lower range of the load ratios reveals an unexpected result. When the initial stiffness is calculated for load ratios with very small bending moments ($M_y/N \approx -0,02$ m), a peak occurs in the stiffness values. For ratios lower than the peak value ($-0,02$ m $<$ M_y/N $<$ 0 m), the stiffness seems to decrease. The results, showing the peak in the stiffness, are shown in figure 3.12. This peak cannot be explained through the mechanical behaviour of the connection.

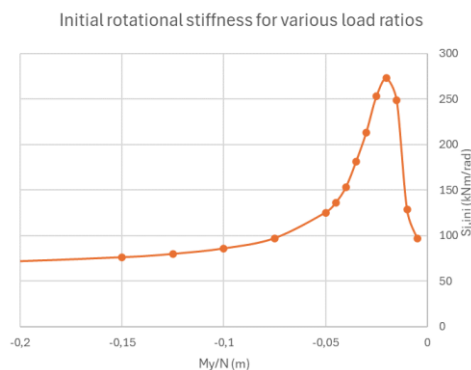


Figure 3.12. Peak in the initial rotational stiffness for small load ratios

A separate study has been performed to determine the cause of the peak. The goal of the study is to define which values of the results are reliable. The full investigation is included in appendix A. The conclusion of the study is summarized in this section.

Parametric investigation shows that the peak in the results is not caused by inconsistencies in the input of data into the model. Varying the axial load instead of the bending moment, the beam length, the design rigidity, and the magnitude of the loading do not influence the location of the peak that occurs. The height of the cross-section does influence the location of the peak. This can be expected according to the assumption that compression increases the stiffness, because a higher cross-section would require a larger load ratio for the cross-section to be fully in compression.

The results of the stiffness analysis for very low load ratios are most likely unreliable. The applied calculation method as described in section 3.1.2 is not equipped to determine the stiffness for these load configurations. Rotations in the connection are simply too small to accurately calculate the stiffness or the moment-rotation relation. However, the question remains up to which load ratio the results are reliable.

A hand calculation is performed to give a reference for the stiffness of the connection. This calculation is based in the component method for connections of open sections as specified in NEN EN 1993-1-8 (*EC3 part 1-8, 2011*). In the calculation of the stiffness values at the peak it is assumed that the connection is only subjected to compressive forces. The difference in the compression between the top and bottom of the cross-section causes the rotation in the connection. This results in the exclusion of tensile stiffness components from the calculation of the stiffness. Based on this assumption, a stiffness of 739 kNm/rad is calculated at the peak value, this is almost three times as high as the stiffness of calculated with the CBFEM calculation (250 kNm/rad). This is an indication that the increase in stiffness for small bending moments with high axial load could be valid. Additionally, results from the design phase of the project support the assumption that the tensile elements of the connection do not influence the stiffness at load ratios around the peak in stiffness.

When the entirety of the research presented in appendix A is reviewed it can be said that the increase in stiffness for lower load ratios could be representative of the actual behaviour of the connection. However, it cannot be determined with any certainty, up to which values the results from the stiffness analysis are reliable. They, therefore, have to be approached cautiously when applied in the design of a structure. When using the stiffness analysis for the design of connections, special attention must be directed to the reliability of the results. This will be specifically mentioned in the design phase of this thesis in chapter 5 and chapter 6.

3.4 Stiffness ranges

This section will focus on determining the ranges of rotational stiffness that can be achieved for the defined base connection by adjusting the stiffness parameters. As seen in section 3.3, the load interaction will influence the achievable stiffness ranges of a connection. Therefore, the determined stiffness ranges are specific to one load configuration. In section 3.4.1 and 3.4.2 an example of the determination of stiffness ranges will be demonstrated for a connection subjected to an out-of-plane bending moment and a compressive normal force. The loading on the connection is given below. In section 3.4.3 the range will be extended for more M_y/N -ratios.

- Compressive axial force: $N = -2 \text{ kN}$
- Bending moment: $M_y = 0.2 \text{ kNm}$
- Load ratio: $M_y/N = -0.1 \text{ m}$

The goal of the stiffness ranges for the different design action is to be able to quickly design the connection based on the requirements resulting from the structural optimisation. The methodology for this will be elaborated further in Chapter 5.

Base connection

First a base value is determined for the base connection as defined in section 3.2. The minimal initial rotational stiffness for the given load ratio is given below. In this case the connection operates well within the elastic range, strength capacity is not an issue.

$$S_{j,ini,y} = 85,6 \text{ kNm/rad}$$

3.4.1 Direct stiffness parameters

Bolt spacing

Table 3.3 shows the increase in rotational stiffness of the base connection as a consequence of increasing the bolt spacing from 30 mm to 50 mm. The bolt spacing has a significant impact on the rotational stiffness of the connection, without extra cost or material requirements.

	Bolt spacing (mm)	$S_{j,ini,y}$ (kNm/rad)
Base connection	30	85,6
1	40	98,1
2	50	109,8

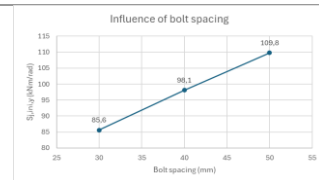


Table 3.3: Effect of bolt spacing on the rotational stiffness of the base connection for $M_y/N = -0,1 \text{ m}$

Bolt type

Table 3.4 shows that the bolt type has a minimal impact on the rotational stiffness of the connection in this case. This is probably because the bolts are not governing in the current configuration. Changing the bolt type might have a greater impact on the stiffness when the bolts are the limiting factor in the performance of the connection.

	Bolt spacing (mm)	$S_{j,ini,y}$ (kNm/rad)
Base connection	M12 8.8	85,6
1	M12 10.9	85,7

Table 3.4: Effect of bolt diameter on the rotational stiffness of the base connection for $M_y/N = -0,1 \text{ m}$

Centre box

Table 3.5 shows that strengthening of the centre box has a significant impact on the performance of the connection. However, attention should be paid to the requirement that the web of the centre box should be equal to or wider than the width of the end-plate. This results in the fact that the only possible option in this case is to move the step to a centre box with SHS90/90/6.3, which performs better than the base connection.

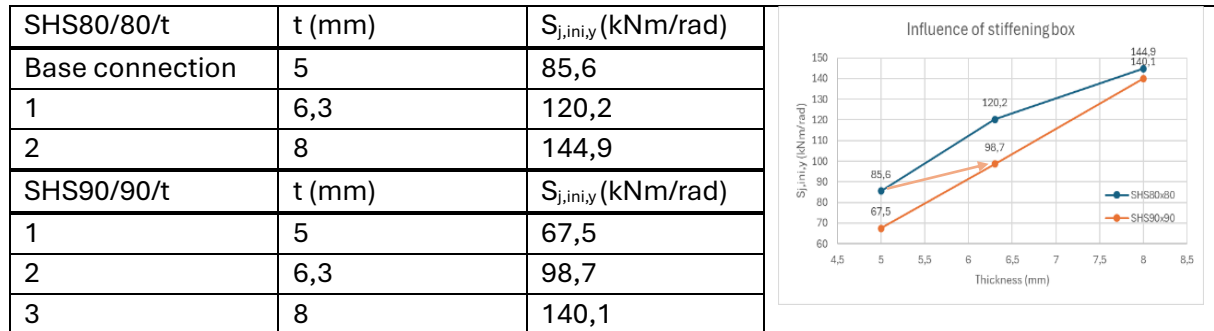


Table 3.5: Effect of stiffening box cross-section on the rotational stiffness of the base connection for $M_y/N = -0,1$ m

Endplate thickness

Table 3.6 shows that the thickness of the endplate seems to have only a minor effect on the stiffness of the connection. However, this again has to do with the governing elements in the connection.

To verify this the thickness of the end-plate has also been increased for the connection with the centre box SHS90/90/8. An endplate with a thickness of 8 mm here results in a stiffness of 163,5 kNm/rad, which is a considerable improvement compared to the same connection with an endplate thickness of 5 mm (140,1 kNm/rad).

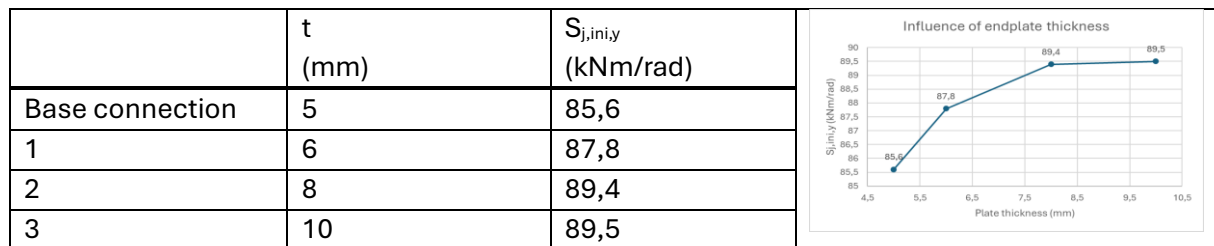


Table 3.6: Effect of endplate thickness on the rotational stiffness of the base connection for $M_y/N = -0,1$ m

Maximum connection

Based on the previous results a design for the base connection can be defined that realises a maximal stiffness, without making any major changes to the design of the connection. The characteristics of the maximal connection are:

- Bolt spacing: 50 mm
- Bolt type: M12 8.8
- Centre box: SHS90x90x6,3
- Endplate: 8 mm

This gives an initial rotational stiffness of: 137 kNm/rad

Which result in the stiffness range for the base connection for a load ratio $M_y/N = -0.1$ m:

85 kNm/rad – 137 kNm/rad

3.4.2 Stiffness range operations

Section 3.4.1 discussed parameters that could change the stiffness of the connection within a certain stiffness range. This section will give examples of design operations that adapt the connection so that a new stiffness range can be defined.

Addition of cap plates

Stiffeners are added to the top and bottom of the centre box of the connection defined in section 3.2. For constructability, openings must be added in the web of the structural elements. The new connection is depicted in figure 3.15.

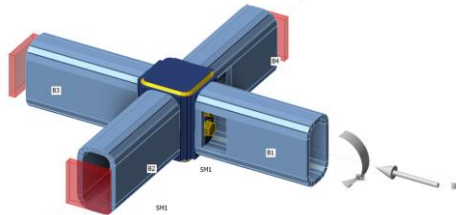


Figure 3.15: Base connection with caps

- Base connection:
 - o Caps: $t = 5 \text{ mm}$
 - o Openings: $60 \times 40 \text{ mm}$, offset = 30 mm
 - o Base stiffness: $175,2 \text{ kNm/rad}$

To determine the maximum stiffness value of the new range, the cap plates are also added to the maximum connection as defined in the previous section. Also, the thickness of the caps can be increased to adjust the stiffness. This results in the stiffness values as presented in table 3.7.

	Cap thickness (mm)	$S_{j,ini,y}$ (kNm/rad)
Base + caps	5	175,2
Max + caps (t = 5 mm)	5	350,6
Max + caps (t = 8 mm)	8	378,2

Table 3.7: Influence of thickness of cap plates on the stiffness of the maximum connection

This results in a new stiffness range for the base connection with stiffener cap plates added to the top and bottom of the centre box of the connection for a load ratio $M_y/N = -0.1 \text{ m}$:

$$175 \text{ kNm/rad} - 378 \text{ kNm/rad}$$

Addition of an extra bolt row

The same procedure can be followed by adding an extra bolt row to the connection. This leads to the stiffness range mentioned below. As the range falls fully within the stiffness range of the connection with cap plates, it can be concluded that adding stiffeners is more efficient than adding a bolt row.

$$211 \text{ kNm/rad} - 290 \text{ kNm/rad}$$

Cap plates and a bolt row

The addition of stiffening cap plates and an extra bolt row can, however, be combined to create a new stiffness range. This connection is shown in figure 3.16. The new stiffness range for the base connection with stiffener cap plates and an added bolt row for a load ratio $M_y/N = -0.1 \text{ m}$:

$$419 \text{ kNm/rad} - 766 \text{ kNm/rad}$$

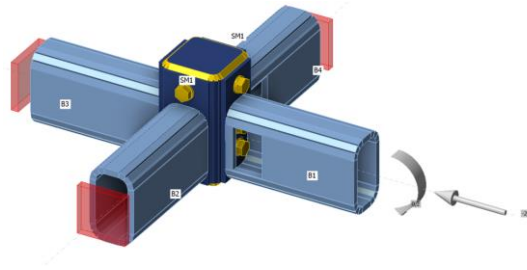


Figure 3.16: Base connection with cap plates and an extra bolt row

3.4.3 Stiffness range chart

The method presented in section 3.4.2 can be combined with the load interaction diagrams as presented in section 3.4.1 figure 3.6. This would result in the chart presented in figure 3.17. On it, multiple areas can be seen each representing a stiffness range of either the base connection (Blue lines), the base connection with cap plates (Orange lines) and the base connection with cap plates and an extra bolt row (Green lines).

The intention of the graph is to serve as a design aid for connection based on a pre-determined stiffness requirement. Based on the design of the grid shell the required stiffness and occurring bending moment and axial force should be known. Based on these values a location in the graph can be selected. Based on this location a connection design could be generated.

As an example, the result of the structural analysis and optimisation could be as follows:

- Required rotational stiffness: $S_{j,ini,y} = 150 \text{ kNm/rad}$
- Axial force: $N = -2 \text{ kN}$
- Bending moment: $M_y = 1 \text{ kNm}$

This would give a load ratio of $1/-2 = -0,5 \text{ m}$. Together with the required stiffness this would relate to the orange area in the compressive zone of the chart. Therefore, the design of the base connection including cap plates should be selected. Then the direct stiffness parameters should be chosen so that a stiffness of approximately 150 kNm/rad is achieved.

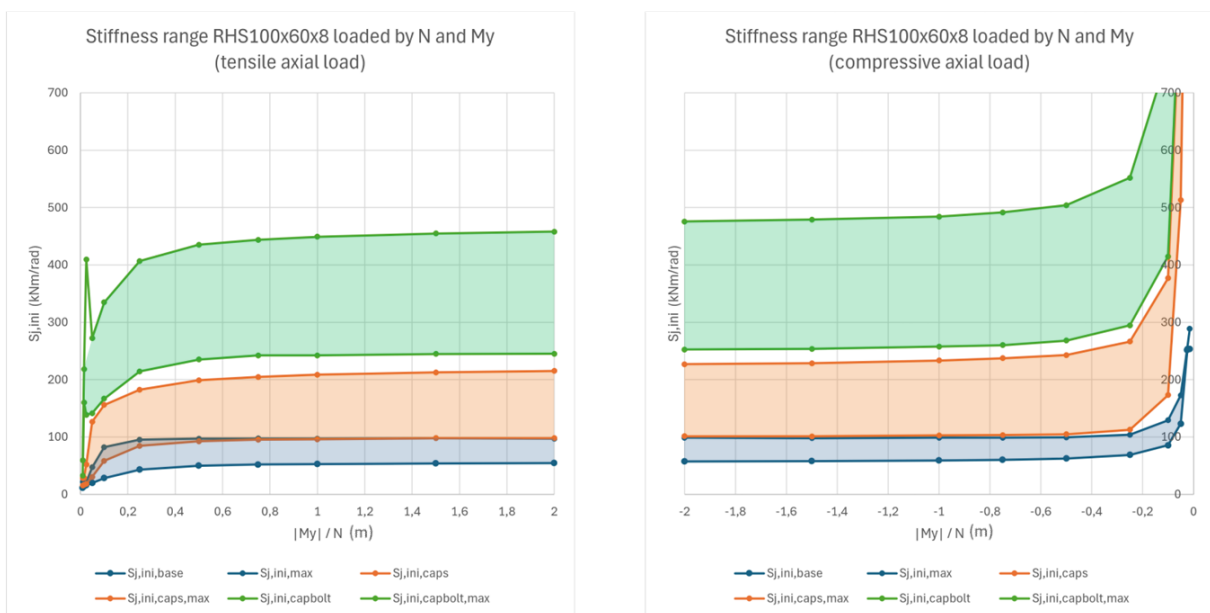


Figure 3.17: Stiffness range diagram

3.5 Conclusion

- *How does the interaction of loads influence the stiffness of a bolted steel connection?*

Generally, stiffness of steel connections is calculated according to the Eurocode. This is often preferable because common connections are mostly loaded in bending and shear. However, connections in grid shell structures are loaded mostly by axial force and bending moment. A compressive axial load on a connection can increase the rotational stiffness of the connection. Therefore, the application of the Eurocode can be conservative when the stiffness of grid shell connections is calculated.

When the value of the bending moment on a connection is large compared to the magnitude of the axial force, the ratio between the loads has only a small influence on the rotational stiffness of the connection. However, when the axial load is relatively large compared to the bending moment, the results show a significant influence of the load ratio on the initial rotational stiffness. In the case of a compressive axial load, the stiffness increases and with a tensile axial load the stiffness decreases. Inclusion of a bending moment around the z-axis (M_z) could also increase the rotational stiffness around the y-axis. Shear force shows to have only a small influence on the connection stiffness.

It is important to note that considering the increase in stiffness for small load ratios (M_y/N) is not included in the Eurocodes. Also, the software used for the stiffness calculation does not result in reliable results for very small load ratios and it is not clear up to which ratios the results are reliable. For these reasons, it is difficult to prove the safety of a determined stiffness value. This should be considered in the design and will be discussed in chapter 5 and chapter 6 of this thesis.

- *How do different design parameters influence the stiffness of a bolted steel connection?*

The stiffness of the base connection can be adjusted by different design parameters. Two categories of design parameters can be identified. The first category contains direct parameters that are easy to adjust to create a range of stiffness that can be achieved. The second category contains larger design operations that increase the rigidity of the design to create a new stiffness range. Both categories and the effect of stiffness parameters are listed below.

Direct stiffness parameters:

1. Bolt spacing: Increasing the spacing between the bolts can lead to a considerable increase in rotational stiffness. Changing the bolt spacing does not increase the weight, cost, or constructability of a connection. The bolt spacing should be adjusted first.
2. Centre box profile: The cross-section of the centre box has a significant effect on the joint stiffness. Increasing the size of the cross-section should involve increasing the thickness. When only the cross-section size is increased, stiffness will be reduced.
3. Endplate thickness: Increasing the thickness of the endplate can influence the stiffness of the connection. However, the thickness of the centre box will likely be governing. Therefore, the thickness of the endplate should be increased when the thickness of the centre box profile is larger than the thickness of the endplate.
4. Bolt type: Changing the diameter or strength of the bolts only influences the stiffness of the connection when the bolts in tension are governing in the design.

Design operations:

1. **Stiffeners:** Adding stiffeners to the top and bottom of the centre box greatly increases the stiffness of the connection, because it reduces the deformation of the centre box. A disadvantage of the stiffeners is that openings in the structural elements will be required in order to fasten the bolts.
2. **Bolt row:** The addition of a bolt row can increase the stiffness of a connection. However, the effect is only limited when stiffeners are not yet applied. Therefore, a bolt row should be added when stiffeners do not yet yield a sufficient stiffness.
3. **Prestressed bolts:** By increasing the compression in a connection, prestressed bolts could significantly increase the stiffness of a connection. However, in the researched connection design the application of prestressed bolts is not possible, because only one side of the bolt can be accessed.

It should be noted that the discussed parameters do not provide an exhaustive list. Depending on the design of the connection, more direct parameters as well as design operations exist that can increase the stiffness of the connection.

- *How can a steel connection be designed based on a pre-determined stiffness?*

A design for a connection could be selected based on requirements that result from a structural analysis of a grid shell that considers finite joint stiffness. This connection can be selected based on a design diagram in which the connection design is linked to initial stiffness of the connections and the ratio of the loads that could act on the connection. For each connection that needs to be designed, information resulting from the structural analysis should include the required stiffness of the connection, the acting loads on the connection and the ratio between the forces.

The stiffness range chart can be constructed with the methodology described below:

1. Determine a base design for the connection
2. Determine stiffness limits for the base connection
3. Perform steps 1 and 2 for adjusted connection designs with a different stiffness range.
4. Calculate the stiffness for upper and lower limit of the connection design for different load ratios.
5. Plot the design diagrams

Once a location in the graph has been identified for the connection design. The design can be chosen based on the corresponding stiffness range. Within the stiffness range the stiffness can be adjusted by varying the direct stiffness parameters.

4 Joint stiffness influence

This chapter focusses on the achievement of objective 2. The goal is to research the influence of semi-rigid joints on the performance of a grid shell structure. Questions to be answered in this chapter are:

- How do the joint stiffness parameters influence the structural capacity of a grid shell?
- How does the joint stiffness influence the ratio between the loads on the joints?
- What are the challenges for implementation of semi-rigid joints in the design and optimisation of a grid shell?

4.1 Parametric model

The research is performed on a model that is constructed in Grasshopper for Rhino (*Mode Lab, 2014*). First, section 4.1.1 describes the geometrical definition of the model. Then, in section 4.1.2, the structural analysis of the model is discussed. In section 4.1.3, a verification of the calculation methods is presented. The modelling script is included in Appendix B.

4.1.1 Geometry

An example of the grid shell model is displayed in figure 4.1. The shape definition and the different parameters are explained below.

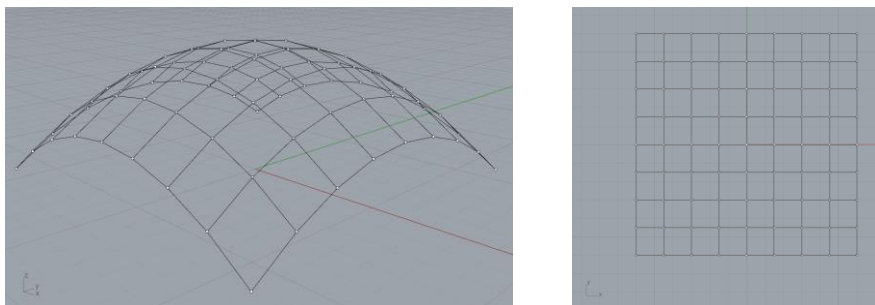


Figure 4.1: Example of a grid shell created with the parametric model

Shape: The geometry of the structure is defined through the function displayed in equation 4.1, which determines the z-coordinate of points with a known x and y location. This way an elliptic paraboloid geometry above a rectangular plan is created. The equation generates a shape with all z-coordinates in the negative range. Therefore, the model moves the structure upwards until the corner points have a z-coordinate of zero.

$$z = -\frac{x^2}{a^2} - \frac{y^2}{b^2} \quad (4.1)$$

Dimensions: The dimensions are defined through the parameters that can be adjusted in the model. Parameters L_x and L_y determine the size of the grid projection on a flat surface as shown in figure 4.1, this way they determine the span of the shell.

The height of the shell is determined by the parameters a and b . As a result of this the height of the shell is not a direct parameter. But it is given by equation 4.2.

$$h = \frac{(\frac{L_x}{2})^2}{a^2} + \frac{(\frac{L_y}{2})^2}{b^2} \quad (4.2)$$

Grid: The model defines a quadrangular grid that is orthogonal towards the edges. The grid parameter determines the spacing of the grid or the grid density. This is regulated by the number of segments the sides are divided in. Division X and Division Y determine this, the grid spacing resulting from these parameters can be calculated with equations 3.3 and 3.4.

$$S_x = \frac{L_x}{\text{Division } X} \quad (3.3)$$

$$S_y = \frac{L_y}{\text{Division } Y} \quad (3.4)$$

Boundary conditions: The remaining design parameter is the selected support condition of the structure. In a drop-down menu, three different options can be selected. The first option is a shell that is perfectly pinned along the edges (FC), the second option is a partially constrained shell that is fully pin-supported in the corners and horizontally constrained along the edges (PC) and the last option is a shell supported in the corners with free edges (CC). Figure 4.3 shows the three variations.

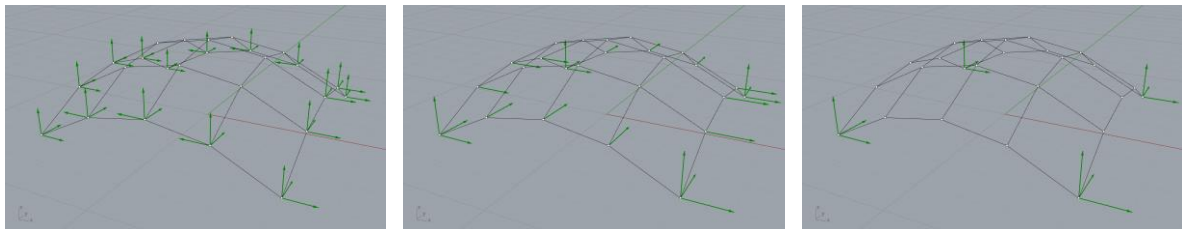


Figure 4.3: Boundary conditions for Fully Constrained (FC), Partially Constrained (PC) and Corner Constrained (CC)

4.1.2 Structural analysis

Material and cross-sections: As mentioned before, this research focusses on steel grid shell structures. The steel grade used in the research is S355. Profiles are rectangular hollow sections. In this chapter, the research is performed on a structure with RHS100x60x8 profiles. Cross-sections are defined centred along the line segments of the shell model. This results in the orientation of the elements as shown in figure 4.4a.

Joint stiffness: In the model, stiffness values of the six degrees of freedom of the joints can be specified separately. The direction of the joint stiffness is linked to the local coordinates of the beam the joint connects, as shown in Figure 4.4b. The assigned stiffness here is the connection stiffness, a visualisation of the modelling is shown in figure 4.4c. Also, the moment capacity of the connection cannot be specified, resulting in a linear elastic joint stiffness model.

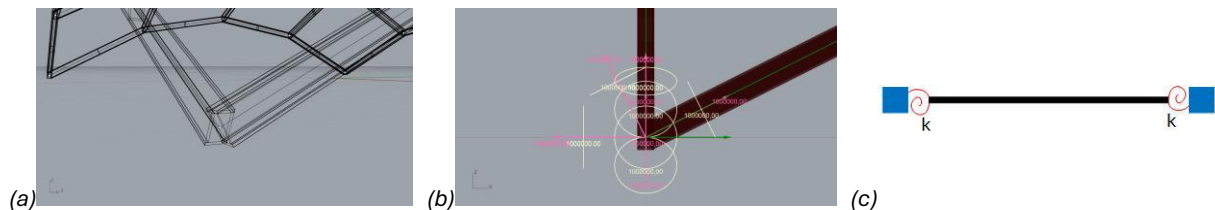


Figure 4.4: Orientation of the structural elements and nodal connections

Loads: Loads are defined as line loads on the beam elements. Surface loads on the shell are translated to beam loads. For each surface, the total load is uniformly distributed over the structural elements that enclose it. Three load cases can be considered in the structural model. These are the self-weight of the structural material and surface cladding (LC1), symmetric snow load (LC2) and asymmetric wind load (LC3). These load cases are applied in section 4.3. In section 4.2, a unit load of 1 kN/m is applied to all the beams. As visualised in figure 4.5.

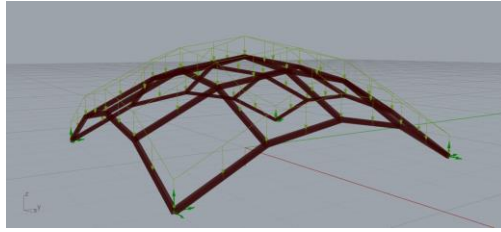


Figure 4.5: Structural model subjected to a unit load of 1 kN/m on the beams

The load cases are defined as follows:

LC 1: Deadload $g = 10 \text{ m/s}^2$

- Structural self-weight: $G_{\text{steel}} = 78,5 \text{ kN/m}^3$
- Deadload glass cladding: $G_{\text{glass}} = 25 \text{ kN/m}^3$
 $t_{\text{glass}} = 18 \text{ mm (3x6mm)}$
 $25 * 0,018 = 0,45 \text{ kN/m}^2$

LC 2: Snow load As defined in NEN EN 1991-1-3 (EC1 part 1-3, 2019)

$$S = m_u * C_e * C_t * S_k = 0,56 \text{ kN/m}^2$$

- $S_k = 0,7 \text{ kN/m}^2$
- $\text{Alpha} < 30 \rightarrow M_u = 0,8$
- $C_e * C_t = 1$

LC 3: Wind load As defined in NEN EN 1991-1-4 (EC1 part 1-4, 2011)

$$P_A = C_s C_d * C_p * q_p(z_e) = +0,55 \text{ kN/m}^2$$

$$P_A = C_s C_d * C_p * q_p(z_e) = -0,79 \text{ kN/m}^2$$

$$P_C = C_s C_d * C_p * q_p(z_e) = 0 \text{ kN/m}^2$$

- $C_s C_d = 1$
- Zone 2
- Rural $\rightarrow q_p = 0,79 \text{ kN/m}^2$
- $z_e = 8 \text{ m}$
- $h/d = 0$
- $f/d = 0,4 \rightarrow$
 - $C_{p,A} = 0,7$
 - $C_{p,B} = -1,0$
 - $C_{p,C} = 0$

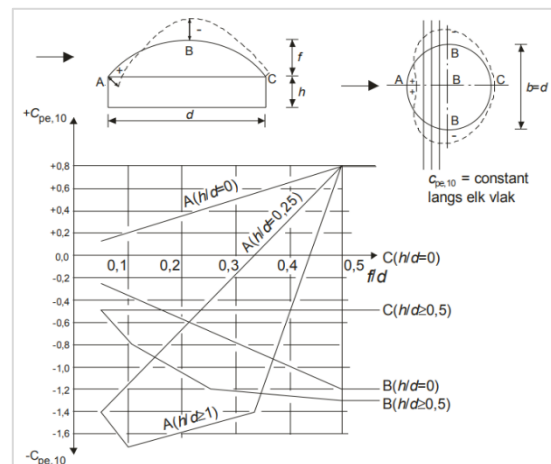


Figure 4.6: Pressure coefficients

Analysis type: The structural verification is performed using second order theory for small deflections. The method corresponds to the implementation of a linear buckling analysis (LBA) as was mentioned in section 2.2.2. In this method, normal forces are calculated which contribute to the second order deformations of a deformed structure. This gives a linear approximation of the nonlinear structural behaviour. As was mentioned in section 2.2.2, an LBA is not accurate when loads exceed the buckling resistance. Therefore, results that are generated for configurations that relate to a buckling load factor below 1 are not reliable and will not be allowed in the design of a grid shell.

The structural analysis is done with the Karamba3D plug-in for Grasshopper (Preisinger, 2013). For detailed calculations and verification of the model, calculations are performed in RFEM software. Three design criteria are regarded for the design of a grid shell in this report. These are

the buckling load factor, utilisation for axial stress and maximum deformation. The boundary conditions for the evaluation of the shell are as follows.

- Buckling resistance: Buckling load factor (BLfac) ≥ 10
- Axial stress utilisation: $UC_{\sigma} \leq 1.0$
- Global deformation: $u \leq L/250$

4.1.3 Verification with RFEM

For verification of the structural model in Grasshopper and for detailed calculation, Karamba3D provides the option to load the model into RFEM calculation software. A first assessment of the displacement results is performed on the models displayed in figure 4.7. The structure is subject to a unit load of 1kN/m in z-direction. Finite rotational stiffnesses are defined, $k_{by} = 347$ kNm/rad and $k_{bz} = 158$ kNm/rad.

In Grasshopper/Karamba, this results in a displacement of 49,5 mm. In RFEM, the calculated displacement is 49,7 mm. This is a difference of 0.4%, with the analysis in RFEM being slightly more conservative. Therefore, the results in both calculations are assumed to be reliable. This method of verification will also be performed in the final design stages of the project.

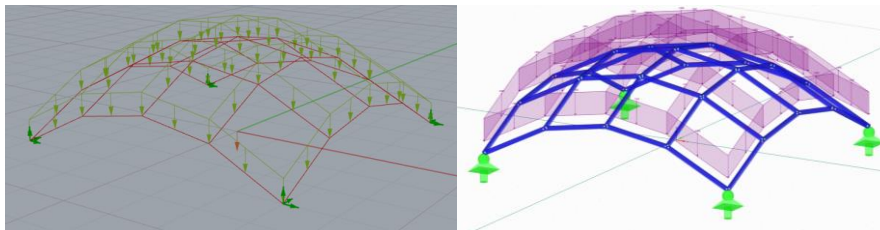


Figure 4.7: Structural model in Grasshopper compared to the model in RFEM5

4.2 Influence of stiffness parameters

4.2.1 Parameters and objectives

The first part of the research is focussed on the influence of the different stiffness parameters on the performance of the shell. The stiffness of the connections has been varied separately for the six degrees of freedom. The assessment is performed for the three boundary variations FC, PC and CC. For each of these variations, data is collected on buckling load, displacement, and axial stress utilisation of the elements in the structure. The six stiffness parameters are listed below.

- | | | |
|-------------------------------------|----------|-----------|
| - Axial stiffness | k_a | (kN/m) |
| - In-plane shear stiffness | k_{sy} | (kN/m) |
| - Out-of-plane shear stiffness | k_{sz} | (kN/m) |
| - Torsional stiffness | k_t | (kNm/rad) |
| - Out-of-plane rotational stiffness | k_{by} | (kNm/rad) |
| - In-plane rotational stiffness | k_{bz} | (kNm/rad) |

The assessment has been performed on a simple shell structure to be able to understand the structural behaviour. The shell has span of 6 m and a height of 2 meters. Over the span the shell is segmented into four parts. The model is equal to the structure in section 4.1.3 shown in figure 4.7. In this section, a load in negative z-direction (downward) of 1 kN/m on all elements is considered.

4.2.2 Results

Influence of stiffness parameters

Figure 4.8 shows the results of the research for the axial stiffness as an example. The columns in the figure show the diagrams for the three design criteria and the rows correspond to the three different models with varying support conditions. Each diagram has the stiffness of the connection along the x-axis. The stiffness is divided by the stiffness of the members (EA for translational stiffness and EI/L for rotational stiffness) to eliminate the effect of the cross-section choice on the results. Along the y-axes of the diagrams, the corresponding design objective is presented with the scale of the axis, adjusted to show the results as clear as possible. For the buckling load factor and the displacement, a global value for the shell is presented. Results for utilisation are presented per member. Due to symmetry, results for elements 0, 1, 4, 5, 8 and 9 represent all elements in the structure. In the case of the FC-shell, the edge beams (elements 0 and 1) are excluded from the results as they act as simply supported beams between the supports and do not contribute to the structural performance of the shell. Data points are retrieved by varying the researched stiffness parameter while the other five parameters stay constant and are assumed rigid.

Appendix C.1 shows the complete results for all the different stiffness parameters for each set of support conditions.

Axial stiffness (k_a): Figure 4.8 shows a significant influence of the axial stiffness on the structural performance of all three shells. The maximum displacement and utilisation of the elements reduce with an increase in stiffness.

The buckling resistance increases for lower stiffness values. This phenomenon is likely caused by redistribution of forces. For low axial stiffness, forces are redirected in such a way that the structure is less susceptible to buckling. When the stiffness exceeds $k/EA = 0,1 \text{ m}^{-1}$, the shell is not sensitive to further increase of the axial stiffness and a rigid connection can be assumed.

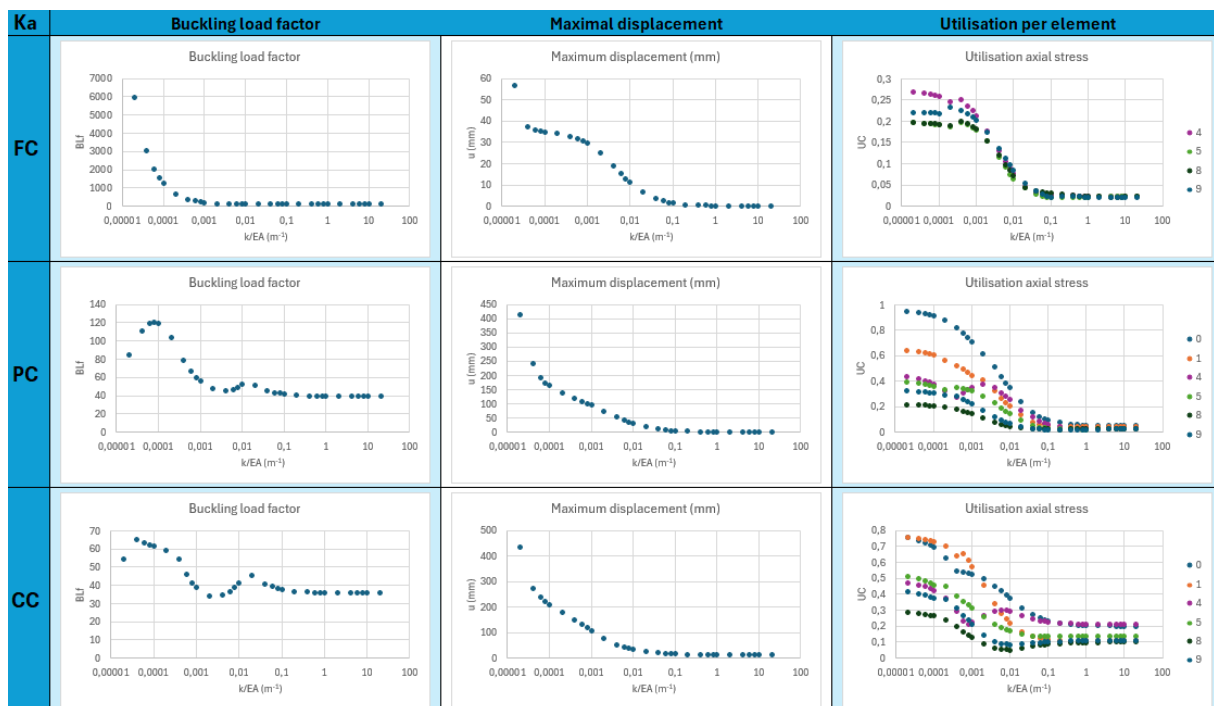


Figure 4.8: Influence of the axial stiffness of the joints on the buckling load factor, displacement, and stress utilisation for the different shell designs (FC, PC and CC)

In-plane shear stiffness (k_{sy}): Results for the buckling load factor for all three shells are presented in figure 4.9. For all three shells, the buckling load factor is influenced up to a certain extend by the in-plane shear stiffness of the joints. For low stiffness values ($k_{sy}/EA < 0,004 \text{ m}^{-1}$) the shell quickly loses buckling resistance. For stiffness values that exceed $k_{sy}/EA = 0,004 \text{ m}^{-1}$, the buckling load factor has reached rigid capacity and is not influenced any further by the in-plane shear stiffness. A notable difference is the considerably higher buckling capacity of the FC-shell compared to the PC- and CC-shells. This is discussed further on, in the section describing the differences between the support conditions.

In case of the displacement and stress utilisation, the FC- and PC-shell are not affected by a change of in-plane shear stiffness. The CC-shell is impacted by changes of in-plane shear stiffness. For the CC-shell, the rigid boundary for in-plane shear stiffness is at approximately $k_{sy}/EA = 0,02 \text{ m}^{-1}$. The diagram with the utilisation of the CC-shell shows the curves of different elements crossing. This is due to the redistribution of forces as a result of increased in-plane stiffness, which allows for a more even distribution of stresses between the inner elements and the edge elements. Figure 4.10 shows this for a low stiffness for in-plane shear ($k/EA=0,0002 \text{ m}^{-1}$), where the middle beams (elements 8 and 9) experience higher stresses, and for a more rigid joint ($k/EA = 1,0 \text{ m}^{-1}$), where element towards the edges of the structure can resist shear forces. This reduces the loads on the centre beams and reduces deformation of the shell.

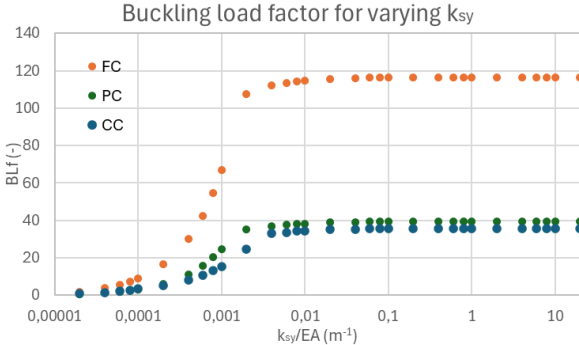


Figure 4.9: Buckling capacity of the shell for varying in-plane shear stiffness

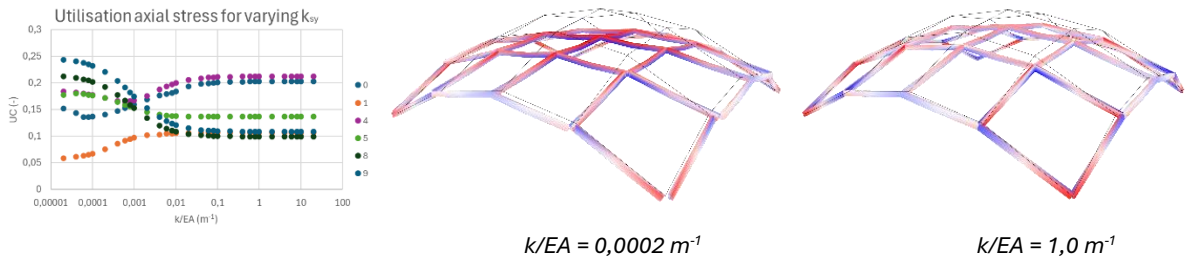


Figure 4.10: Changes in load distribution for changing in-plane shear stiffness in CC-shell (red shading indicates compressive axial stress utilisation and blue shading indicates tensile axial stress utilisation)

Out-of-plane shear stiffness (k_{sz}): For all three shells, the buckling load factor is influenced by the out-of-plane shear stiffness in a similar way as by the in-plane shear stiffness. For low stiffness values ($k_{sz}/EA < 0,002 \text{ m}^{-1}$) the shell quickly loses buckling resistance. For stiffness values that exceed $k_{sz}/EA = 0,002 \text{ m}^{-1}$, the buckling load factor has reached rigid capacity and is not influenced by further increase of the out-of-plane shear stiffness.

The displacement and utilisation show similar behaviour for all boundary conditions. For $k_{sz}/EA < 0,002 \text{ m}^{-1}$, displacement and utilisation increase significantly. When k_{sz}/EA exceeds $0,002 \text{ m}^{-1}$ displacement and utilisation of the elements are no longer influenced by the out-of-plane shear stiffness of the nodes. Figure 4.11 shows the steep increase in global deformation for low values of out-of-plane shear stiffness of the nodes.

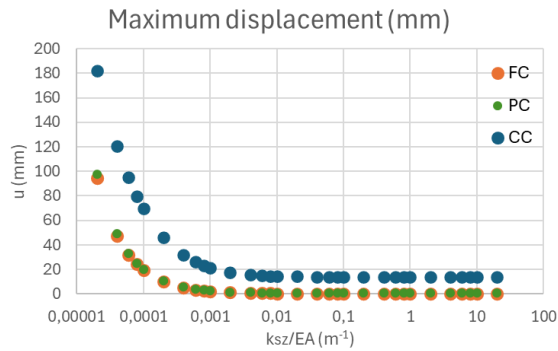


Figure 4.11: Maximum displacement of the shell structure for varying out-of-plane shear stiffness of the joints

Torsional stiffness (k_t): The torsional stiffness of the joints shows only minimal impact on the structural performance of the three shell configurations. None of the shells depends on torsional joint stiffness for the stability of the structure. In case the buckling load is governing for the design, a small increase in buckling load could however be realised by considering the torsional stiffness in the design phase.

Out-of-plane bending stiffness (k_{by}): The out-of-plane bending stiffness shows a significant influence on the structural performance of all three shell configurations. Both the PC- and CC-shell lose stability in the absence of the out-of-plane bending stiffness and the FC-shell shows a reduction in buckling resistance, as shown in figure 4.12. Also the displacement and the utilisation of the elements are affected by a change in joint stiffness in all models.

For the PC- and CC-shell, the displacement shows an interesting pattern. For low stiffness values, the displacement increases with an increasing stiffness. Then at $K_{by} \cdot L/EI = 0,02 \text{ rad}^{-1}$ the displacement reaches a peak value. This peak coincides with the point where the buckling load diagram crosses the value for $BLfac = 1$, thus, before the peak values correspond to a buckled shell and are not reliable. Figure 4.13 shows the deformed shape at the displacement peak and the deformed shape for a slightly higher stiffness. It clearly shows the buckled shape in the first point.

The utilisation for the FC- and PC-shell show a minimum in utilisation for certain elements at approximately $k_{by} \cdot L/EI = 4 \text{ rad}^{-1}$. This is caused by the change in stress distribution that is a result of the change in joint stiffness. For pinned joints, the moment in the midspan of the beam is at a maximum and there is no moment in the nodes. This changes with increasing joint stiffness. Figure 4.14 shows the utilisation for the FC-shell compared to the moments in the node and in the beam of element 9 of the FC-shell for changing joint stiffness. The location of the maximum moment changes. Therefore, the location of maximum utilisation also changes, causing the minimum in the diagram. Figure 4.14 also shows the moment distribution in the shell for pinned joints and rigid joints, which shows the difference in location of maximum bending moments.

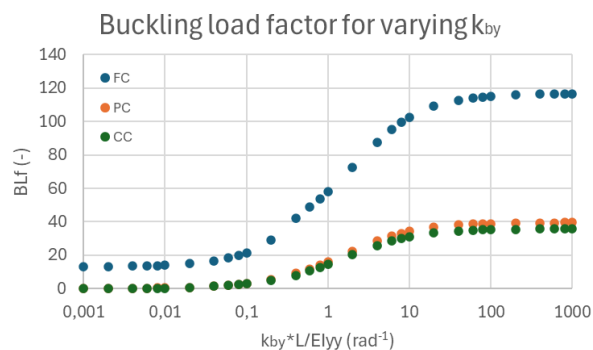


Figure 4.12: Buckling capacity of the shell for varying out-of-plane bending stiffness

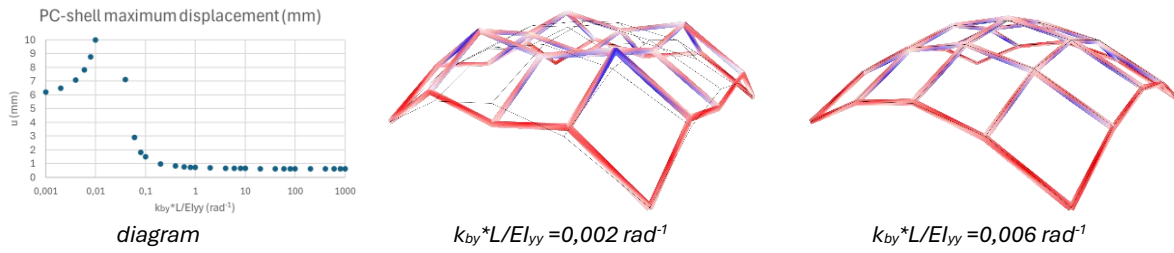


Figure 4.13: Change in bending moments at the node and at midspan of element 9 in the shell (red shading indicates compressive axial stress utilisation and blue shading indicates tensile axial stress utilisation)

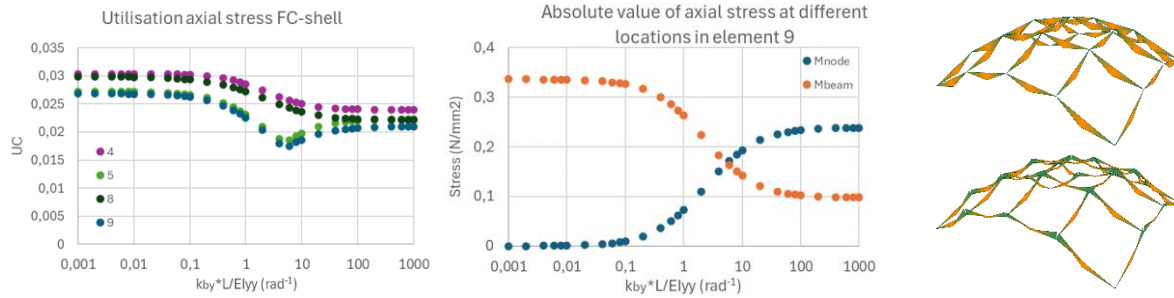


Figure 4.14: Change in bending moments at the node and at midspan of element 9 in the shell

In-plane bending stiffness (k_{bz}): For all three shells, configuration the in-plane bending stiffness of the joints influences the buckling load. However, without in-plane bending stiffness the CC-shell loses stability, while the other two shells remain stable and only experience a reduced buckling load factor, as shown in figure 4.15. This is also reflected in the results for the displacement and utilisation. The FC- and PC-shell are not affected by a reduction in in-plane bending stiffness, while CC-shell does experience an increase in displacement and utilisation with reducing in-plane bending stiffness.

Similar to the in-plane shear stiffness the CC-shell shows crossing of curves in the diagram with the utilisation of elements. Again, the CC-shell depends on the in-plane stiffness of the nodes, because of the lack of support conditions along the edges. Figure 4.16 shows how an increase in bending stiffness can reduce the deformation of the CC-shell significantly.

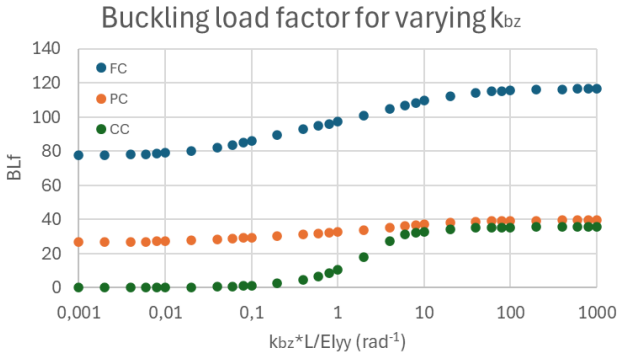


Figure 4.15: Buckling capacity of the shells for varying in-plane bending stiffness

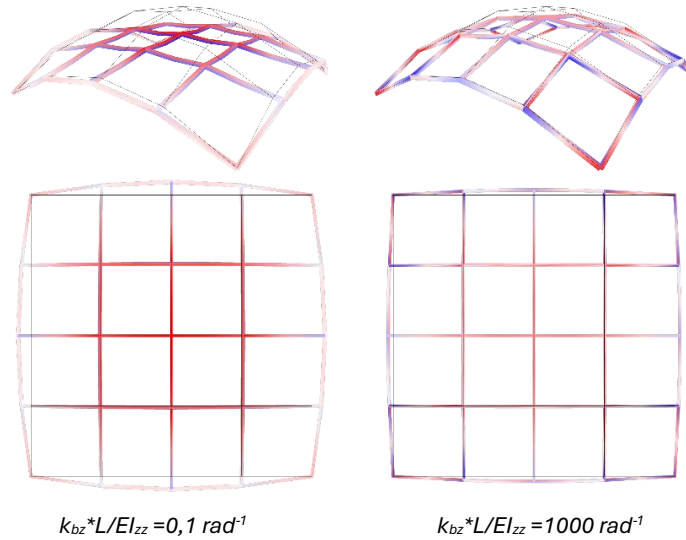


Figure 4.16: Changes in force distribution for the CC-shell for different values of in-plane bending stiffness (red shading indicates compressive axial stress utilisation and blue shading indicates tensile axial stress utilisation)

Effect of support conditions: Besides the effects of the separate stiffness parameters, some general differences between the three shell configurations can be discovered.

As can be seen in figures 4.9, 4.12 and 4.15, the FC-shell has a significantly higher buckling capacity than the PC- and CC-shells. This is as expected as the pinned boundaries of the FC-shell stabilise the shell. However, it is interesting that the capacity of the PC-shell is comparable to the capacity of the CC-shell whilst experiencing significantly lower displacement and utilisation. Figure 4.17 shows the utilisation for varying out-of-plane bending stiffness for both the FC-shell and the PC-shell. It can be seen that the difference in utilisation in the shells is solely caused by elements 0 and 1 in the PC-shell. These are the edge elements. This could indicate that it is the buckling of the edge elements that reduces the capacity of the PC-shell compared to the capacity of the FC shell.

The second general aspect that can be derived from the results is that while all three shells depend on axial stiffness and out-of-plane bending stiffness for stability, only the CC-shell is significantly impacted by in-plane stiffness of the connection. This is as expected, in the FC- and PC-shell the boundary conditions provide the lateral stability along the edges. The infinite stiffness of the edges can fully take the horizontal forces in the nodes. Therefore, these shells do not rely on in-plane shear or bending stiffness of the nodes.

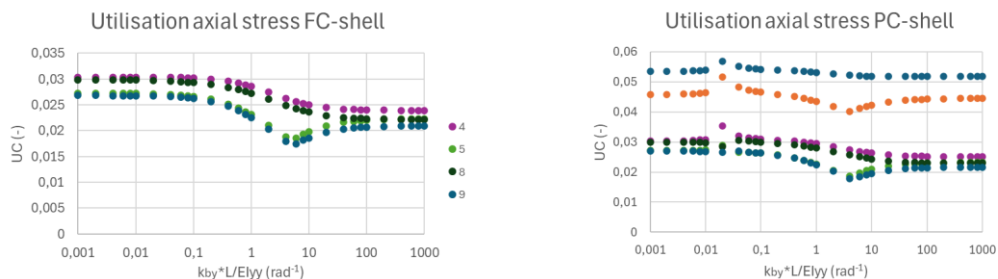


Figure 4.17: Utilisation for varying k_{by} for FC-shell and PC-shell

Effect of shell dimensions: To finalise this section, a small assessment of results for a larger version of the shell has been performed. The results for all stiffness parameters are shown in appendix C.2. This assessment has been performed on a shell with a span of 18 m with a height of 8 m. The sides are divided into twelve segments. Creating beams of approximately equal length as in the small shell. As the cross-section of the structural elements has not been adjusted, the

results indeed show a lower capacity of the larger shell. Nevertheless, the results seem to be mostly comparable to the results of the small shell.

One interesting result for the larger shell should be noted. The in-plane stiffness of the connections of the FC-shell and PC-shell becomes more important for the larger shell. This is shown for the in-plane bending stiffness in figure 4.18. It can be seen that the buckling capacity of the larger shell decreases to a greater extent with decreasing in-plane bending stiffness than the buckling capacity of the small shell. This can be explained by two aspects. The first is that by increasing the size of the shell the boundaries make up a smaller part of the total structure. The number of supports grows linearly, while the number of joints increases quadratically. Therefore, this reduces their stabilising effect, which then has to be ensured by in-plane stiffness of the joints. A second cause could be that a larger shell with more segments better approximates the funicular form than the small shell. This would reduce the importance of the out-of-plane bending stiffness for stability of the shell, which results in increased significance of the in-plane bending stiffness for stability of the shell.

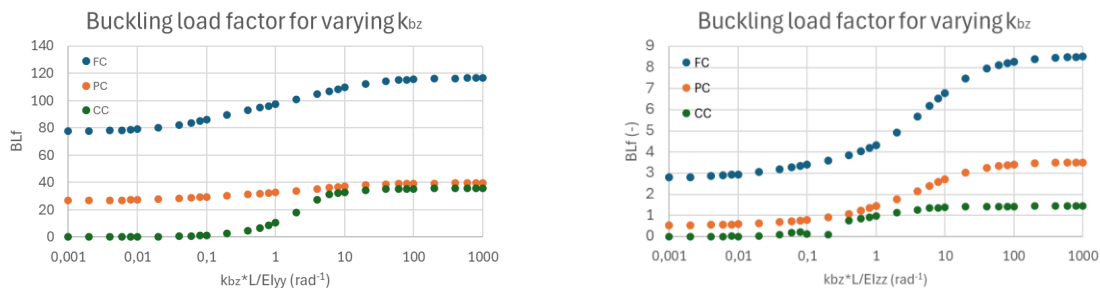


Figure 4.18: Buckling capacity for in-plane bending stiffness; small shell compared to big shell

For the remainder of the research and the design, the focus lies on the Partially constrained shell. The fully constrained shell does not show a loss of stability in case of the small shell and is, therefore, not interesting for a design optimisation with semi-rigid connections. And the corner constrained shell has more relevant parameters, therefore, leading to a design that would be to complex and time-consuming for the goals of this project.

4.3 Load ratio in the nodes

In chapter three, results showed the influence of the load ratio on the stiffness of the connections. Therefore, it is important to investigate the occurring load ratios in the actual structure to be able to identify the actual stiffness of the joints.

4.3.1 Parameters and objectives

In this section, research is performed on a similar shell as in section 4.2. The occurring out-of-plane bending moment and normal forces in the structure is determined for different values of out-of-plane bending stiffness. Torsional and in-plane bending stiffness are set to pinned conditions as to avoid torsional and in-plane bending moments in the structure. Shear stiffness values are set to values that correspond to the rigid state $k/EA = 0,01 \text{ m}^{-1}$. Axial stiffness is set to rigid. Therefore, the effect of axial stiffness on the load ratios is not evaluated. As mentioned, the research in this section is performed on the PC-shell.

For this part of the research the following load combinations are considered.

Self-weight + snow load:	$ULS1 = 1,2 * LC1 + 1,5 * LC2$
Self-weight + wind load:	$ULS2 = 1,2 * LC1 + 1,5 * LC3$
Self-weight (favourable) + wind load:	$ULS3 = 0,9 * LC1 + 1,5 * LC3$

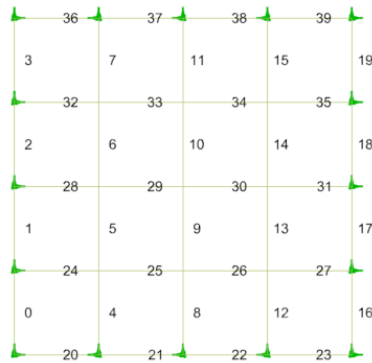


Figure 4.19: Numbered elements in the grid shell. The green arrows indicate support conditions and the orientation of the local x-axis of the elements aligned with them.

4.3.2 Results

For each of the load combinations, the value for M_y/N has been recorded for the range of out-of-plane bending stiffness for all the joints. Figure 4.19 shows the numbering of the elements that are referenced in the results.

Figure 4.20 shows the results for ULS1. Because of the symmetry in the structure and loading, results for elements 0, 1, 4, 5, 8 and 9 can represent results for all elements. Both the M_y/N -ratios at the start ($x = 0$) and end ($x = 1$) of the elements are reported. The x-coordinate refers to the local x-axis of the elements along the global x- or y-axis as shown in figure 4.19.

The node at $x=0$ for elements 0, 4 and 8 can be seen to have an M_y/N -ratio that is equal to zero. This is caused by the pinned support at these locations and the absence of torsional stiffness in the joints. This combination does not allow for out-of-plane bending moments to be generated at these points. Also, it can be seen that M_y/N -ratios of connections at opposite sides of the same node (0 ($x=1$) and 1 ($x=0$), 4 ($x=1$) and 5 ($x=0$), and 8 ($x=1$) and 9 ($x=0$)) have similar M_y/N -ratios. Regarding the influence of the out-of-plane bending stiffness of the joints on the loads on the structural elements, the diagram shows an increase in M_y/N -ratio for an increased joint stiffness. This is due to an increase in bending moment in the nodes as expected according to figure 4.14. However, load ratios in this load combination are still relatively low, with a maximum of $M_y/N = 0,06$ m at the top of the structure (element 9 at $x=1$). The low load ratios indicate that the structure performs as a compressive shell structure under the ULS1 load conditions.

Furthermore, a difference can be seen between the load ratios of the elements in the middle of the structure and the edge elements. Due to higher normal forces in the edge beams of the structure, as shown in figure 4.21, these elements experience lower load ratios than the beams in the middle of the structure.

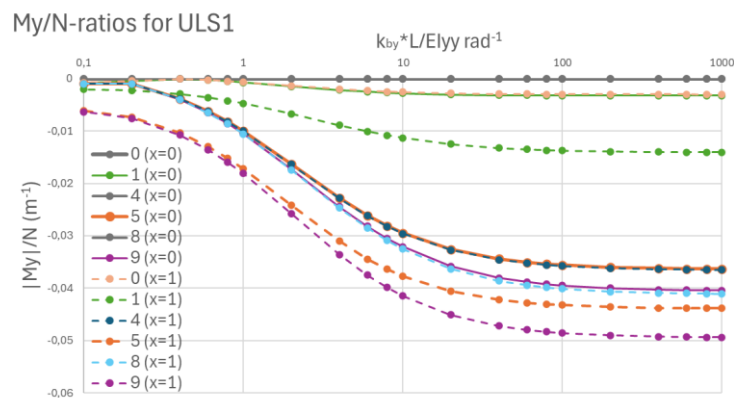
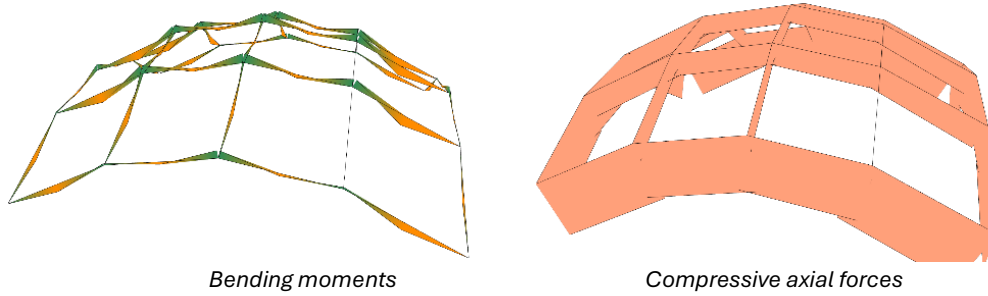


Figure 4.20: $|M_y|/N$ -ratio for nodes in ULS1



Bending moments Compressive axial forces
 Figure 4.21: Bending moment and axial forces in the grid shell for ULS 1

Figure 4.22 shows the results for ULS2. ULS 2 cancels out the symmetry in the direction of the wind loading. Therefore, to keep the results clear, only the results for the middle beams (elements 16, 17, 18 and 19) are presented. The results for other elements show a similar pattern.

Again, the nodes at the supports experience no bending moment (16 (x=0) and 19 (x=1)). The load ratios in ULS 2 show to be significantly higher than the load ratios under ULS 1. Load ratios in the considered beam reach up to $M_y/N = -1,4$ m. This is caused by the structural behaviour that is shown in figure 4.23. The bending moments are taken up mostly by the elements perpendicular to the direction of the wind load, while axial loads are taken by the elements orthogonal to the wind. Contrary to what might be expected, under this load combination the load ratios decrease for an increase in bending stiffness of the joints. This is caused by a redistribution of the normal forces in the structure. Although the bending moment does actually increase slightly with increasing joint stiffness, the axial forces in the same beams also increase because a greater part of the load is taken by beam parallel to the loading direction instead of the elements orthogonal to the loading.

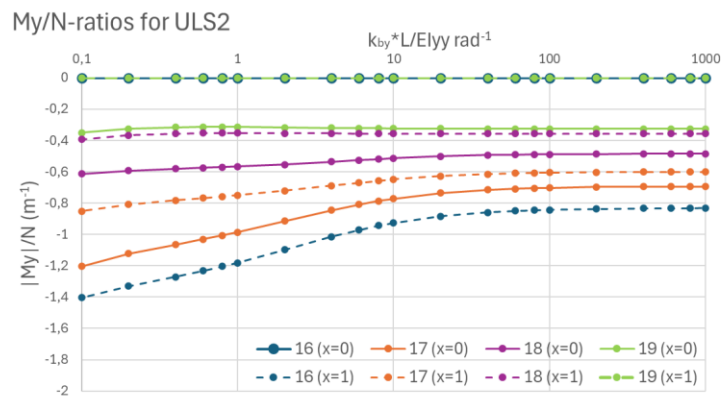
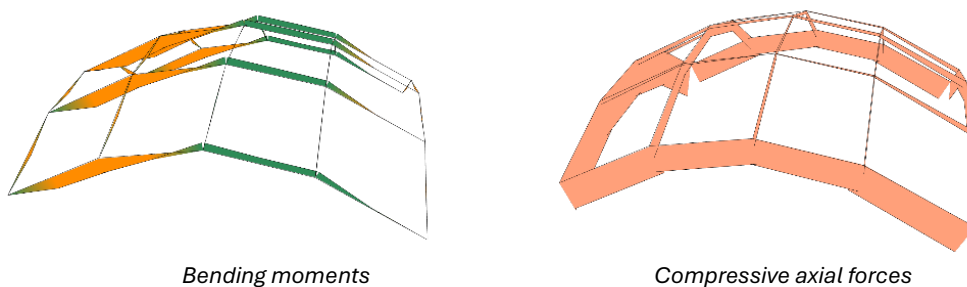


Figure 4.22: $|M_y|/N$ -ratios for ULS2



Bending moments Compressive axial forces
 Figure 4.23: Bending moment and axial forces in the grid shell for ULS 2

The results for ULS3 are presented in Figure 4.24. Again, the results for elements 16, 17, 18 and 19 are presented. The results show positive values for the M_y/N -ratios, indicating that tension occurs in the elements. In figure 4.25, these tensile forces are shown in blue. The load ratios of the elements are slightly influenced by the stiffness of the joints. The results for element 19 ($x=0$), however, show a large increase in load ratio for an increase in stiffness. In this case, an increase in bending stiffness slightly decreases the tensile force in the connection. This, results in an axial load that is close to zero, which greatly increases the load ratio on the connection.

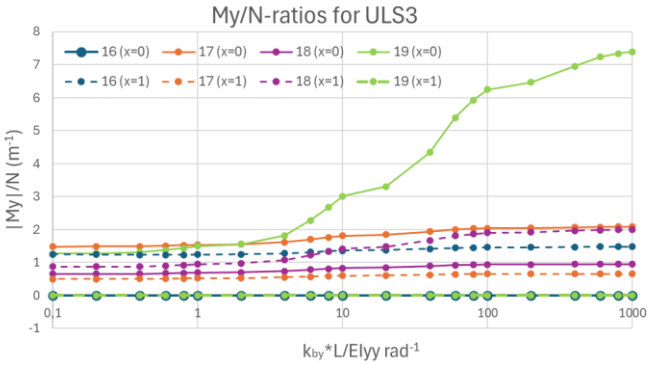
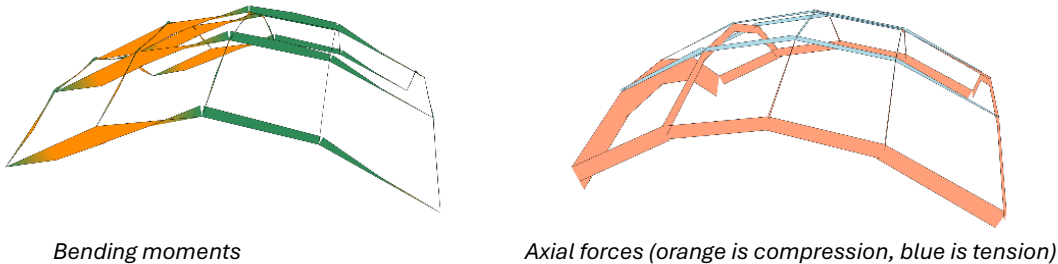


Figure 4.24: $|M_y|/N$ -ratios for ULS3



Bending moments

Axial forces (orange is compression, blue is tension)

Figure 4.25: Bending moment, axial forces, and axial stresses in the grid shell for ULS 3

4.4 Discussion and conclusion

- How do different joint stiffness parameters influence the structural capacity of a grid shell?

The research in section 4.2 shows the influence of the different stiffness parameters on the structural performance of the grid shell structure as defined in section 4.1.

Results show that axial stiffness and out-of-plane bending stiffness play an important role in the structural performance of the researched grid shell, regardless of the boundary conditions. For the shell that is only supported in the corners, also the in-plane shear stiffness and in-plane bending stiffness are seen to play an important role in the stability of the shell. This shows that the in-plane stability of the grid shell can be ensured by either boundary conditions or stiffness of the joints. Also, the structural capacity of the fully supported shell is considerably higher than the capacity of the less rigid shells. The vertical supports along the edges ensure a high rigidity of for this shell. Lastly, the research gives some insight into the effect of increasing the size of the grid shell model. With increasing size of the shell, the stabilising effect of the boundary conditions decreases. This results in an increase in relevance of in-plane stiffness parameters for a larger shell (FC and PC) when compared to a smaller shell. Additionally, the increased importance of in-plane parameters can be caused by the better approximation of the funicular shape of the larger shell. This reduces the importance of out-of-plane bending stiffness, increasing the relative importance of the in-plane bending stiffness.

- How does the joint stiffness influence the loads in the joints?

The importance of the ratio of the loads on the joints has been shown in chapter 3. From section 4.3, it can be concluded that the load ratio on the nodes is influenced by the stiffness of the joints. In different load combinations, different load ratios occur for different joints. Therefore, different stiffness values will be obtained for the same connection under different load combinations. This is important to realise during the design of a grid shell with semi-rigid joints. The design method has to account for the stiffness of the connection in all load combinations.

- What are the challenges for implementation of semi-rigid joints in the design and optimisation of a grid shell?

Design of a grid shell with semi-rigid joints poses several challenges that can be deduced from the learnings of chapter 3 and chapter 4. The challenges are listed below:

- **Iterative design**

In chapter 3, it has been shown that the stiffness of the connection depends on the ratio of the loads action on the joint. However, chapter 4 has shown that the ratio of the loads on the joint depends on the stiffness of the connections. Therefore, the design of both grid shell and connections requires an iterative process to arrive at a feasible design that satisfies both connections and structural analysis of the structure.

- **Load combinations**

The stiffness of the connections depends on the loads acting on the joints. These loads differ in the different load combinations. Therefore, the stiffness of the joints is different in every load combination. As a result it becomes complex to point out a governing load combination. Both the magnitude of the loads as well as the resulting stiffness of the connection design have an impact on the which load combination is governing.

- **Optimisation**

The results of chapter 4 do not yet give a clear indication as to what could be optimised for to achieve an efficient design. Optimisation of the joint stiffness is required to some degree to determine an initial stiffness design. Different optimisation objectives can be defined. The optimisation could be linked to structural weight of the connections, to the constructability or to a combination of objectives.

- **Scaling**

When designing a larger shell compared to a small shell the complexity of the design increases. This is caused not only by the increasing importance of in-plane stiffness of the joints for larger shell but also by the increasing number of connections that all experience different load ratios. In the design of the connection in this thesis, the in-plane bending stiffness of the connections is not included. Therefore, other methods should be applied to increase stability of the shell.

5 Design of a grid shell

This chapter focusses on the achievement of objective 3. An attempt is made at integrating the results of chapters 3 and 4. The goal is to define a methodology for the design of a grid shell structure with semi-rigid connections. In section 5.1, a design strategy is proposed. Section 5.2 applies the proposed strategy to the shell structure presented in chapter 4.

5.1 Design workflow

Figure 5.1 shows a proposal for the design workflow of a grid shell with semi-rigid joints. The different parts of the design are elaborated below.

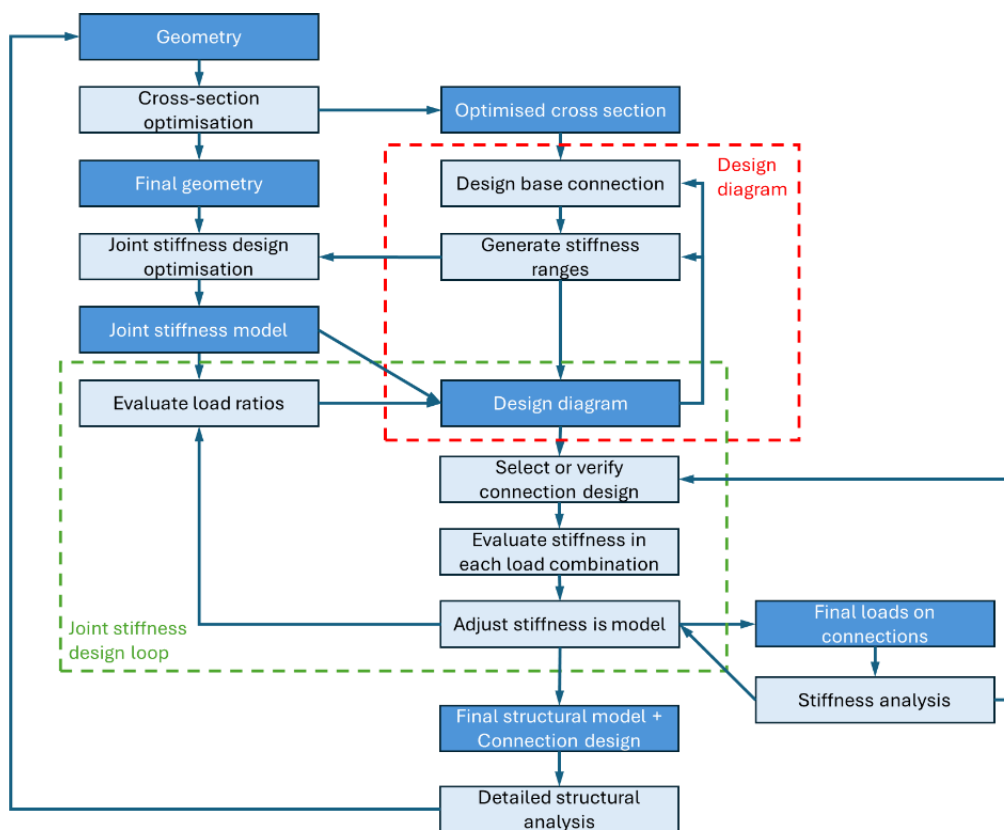


Figure 5.1. Design workflow

Geometry design and cross-section optimisation

The starting point for the design is the geometry of the structure. Specifics on shape, grid, boundary conditions, material and loads must be defined. Based on this structure, a sizing optimisation can be performed to determine the appropriate cross-sections for the structural elements. The objective of the optimisation is to minimise the mass of the structure. The optimisation should be performed with rigid joints to ensure the application of semi-rigid joints does not result in concessions on material use for the structural members.

With the selection of a cross-section for the beams in the structure, a final global geometry is defined. Based on the cross-section and the geometry, the connection design and joint stiffness design can be performed.

Connection design

The first step towards a connection design is to design the base connection based on the structural elements as described in section 3.2.1. From this base connection, a design specific version of the design diagram as shown in figure 3.17 is drafted.

When the diagram is defined, a check is performed to verify if the initial stiffness can be achieved with the current design range of the connection. If not, the connection design or the design operations should be reviewed to create an updated design range.

Initial stiffness design

As established in chapter 3, the design of a semi-rigid connection based on a pre-determined stiffness requires two aspects from the global structural analysis. These are the stiffness that is assigned to the connections in the model and the load ratio that results from the specific configuration. Therefore, an initial estimate for the required joint stiffness is necessary.

An optimisation is performed. The objective of the optimisation is to determine a distribution of joint stiffness throughout the structure that will lead to the design of lightweight and simple connections. This is done by optimising towards the design criteria, while applying penalty constraints for stiffness values that lead to complex and heavy connections. The joint stiffness optimisation is performed using Galapagos for Grasshopper. Galapagos is an evolutionary solver created by David Rutten (*Rutten, 2011*), which is an integrated plug-in in Grasshopper. Evolutionary solvers are able to find optimal solution for problems with multiple variables (genes). In the first step, a random selection of genomes (a specific combination of variables) is produced after which the best performing genomes are selected and used in the next step. Figure 5.2 visualises the optimisation process of an evolutionary solver. This algorithm is appropriate for the current optimisation problem as it is able to handle a fitness landscape with local minima, which can be expected in the problem. Further details regarding the optimisation are presented in section 5.2. It is important to note that the loads on the joints differ in the different load combinations. Therefore, the stiffness values must be estimated separately for each load combination and load ratios that are collected are specific to a certain load combination.

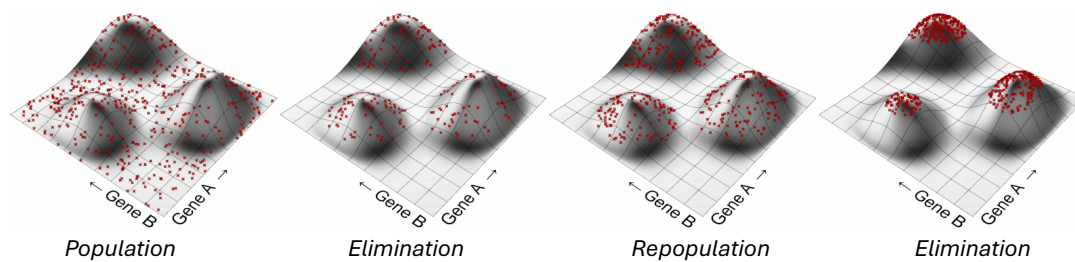


Figure 5.2: Optimisation algorithm in evolutionary solvers (Rutten, 2011)

Stiffness design iteration

The next step is the design loop in which the parametric model of the shell and the design diagram are used to iterate towards a design for the shell. The inputs for the design loop are the connection stiffness, the load ratios on the connections and the design diagram. In the first iteration, a connection design must be selected based on the required stiffness and the resulting load ratios. For each node, a connection should be selected that is sufficiently stiff in each load combination. With the selected connection and the design diagram the new stiffness of the connections can be estimated. This stiffness can then be adjusted in the structural model.

In following iterations the stiffness of the connections should be estimated based on updated load ratios. The estimate can be made with the help of the same design diagrams. If necessary, adjustments must be made in the design choice for the connections.

This step must be repeated until changes in the stiffness and load ratios become negligible. Then, the design loop is concluded with a final adjustment of the stiffness of the connections in the structural model. The iterations and the decision on a final design is further clarified with examples in section 5.2.

Stiffness analysis

When the joint stiffness design is successfully converged to a result, the stiffness of the connection must be verified. Up to this point, the stiffness values have been determined based on the design diagram. To verify if the stiffness values are accurate, a stiffness analysis on the specific connection designs under the corresponding loading is performed.

If the results from the stiffness analysis approximate the estimated values to a satisfactory point, the final stiffness values can be inserted in the structural model. If unexpected deviations from the estimates occur, the cause of this deviation should be investigated. Also, it should be checked if the acting bending moment is smaller than $2/3 M_{j,Rd}$, to verify if the connection indeed performs in the elastic stiffness range. If necessary, an extra iteration of the stiffness design should be performed.

Detailed structural analysis

Once the stiffness design is completed, the final structural model and the design of the connections can be subjected to the detailed structural analysis.

For the grid shell structure, this requires loading the model into finite element software that is capable of calculation on grid shell structure with finite joint stiffness. Here the structure should be checked for buckling, stress utilisation and deformation.

The detailed analysis of the connection includes the stress strain analysis. Here should be verified that the components of the connections are equipped to resist the applied loads in strength.

5.2 Design example

The design to explain the workflow as presented in section 5.1 is performed on a grid shell that is similar to the subject of the research in chapter 4.

Starting point: Geometry

The parameters that determine the design of the shell are presented in table 5.1.

Parameter	Value	Unit
Lx	6	m
Ly	6	m
Division x	4	-
Division y	4	-
a	3	-
b	3	-

Table 5.1. Design parameters

The shape of the shell is determined by equation 4.1, which results in equation 5.1. The height of the shell is calculated with equation 4.2, resulting in equation 5.2.

$$z = -\frac{x^2}{a^2} - \frac{y^2}{b^2} = -\frac{x^2}{3^2} - \frac{y^2}{3^2} \quad (5.1)$$

$$h = \frac{(\frac{Lx}{2})^2}{a^2} + \frac{(\frac{Ly}{2})^2}{b^2} = \frac{(\frac{6}{2})^2}{3^2} + \frac{(\frac{6}{2})^2}{3^2} = 1 + 1 = 2 \text{ m} \quad (5.2)$$

Each side is divided into four segments (Division $x = \text{Division } y = 4$). This results in a spacing of the grid of 1,5 m if it were projected on a flat plane. In combination with the shape, this results in two member lengths in the structure (1,52 m and 1,68 m).

The boundary conditions correspond to the partially constrained (PC) shell as described in chapter 4. In the corners it is constrained for translation in three directions and points along the edges laterally constrained perpendicular to the corresponding edge.

The resulting geometry is presented in figure 5.3.

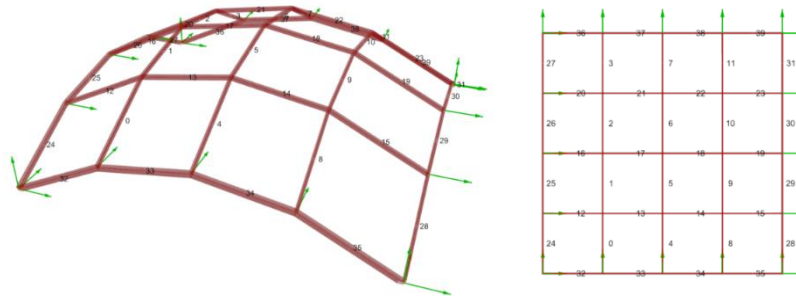


Figure 5.3. Structural geometry of the grid shell design

For the structural analysis the selected material is S355 steel.

The stiffness of the joints is defined in table 5.2. For the shear stiffness, a value is selected that represents a rigid joint for translational deformation ($k_s > 0,01EA \text{ m}^{-1}$). To avoid in-plane bending moment and torsional moment in the structure the joints are assumed pinned for in-plane bending and torsional stiffness. The out-of-plane bending stiffness is determined during the design. Results from chapter 4 show that the axial stiffness can significantly influence the structural performance of a grid shell. However, it is not possible to determine the initial axial stiffness. Therefore, the axial stiffness must be estimated. In compression, the axial stiffness can be assumed to be relatively high as there is relatively little capacity for deformation. Also, a rigid axial stiffness has shown to be governing in case buckling is the governing design criterium. Therefore, under compressive load combinations the axial stiffness is assumed to behave rigid at a value of $k_a \gg 0,1EA \text{ m}^{-1}$. For other load combinations, for example wind loading, the value for the axial stiffness is chosen close to the rigid boundary at $k_a \approx 0,1EA \text{ m}^{-1}$.

Parameter	Stiffness	Unit
k_a	Per LC	kN/m
K_{sy}	20000	kN/m
K_{sz}	20000	kN/m
K_t	0.1	kNm/rad
K_{by}	Variable	kNm/rad
K_{bz}	0.1	kNm/rad

Table 5.2. Joint stiffness

Loads are defined as surface loads on the shell. The surface loads on the shell are translated to beam loads. For each surface, the total load is uniformly distributed over the structural elements that enclose it. Load cases are defined according to the load cases listed below. The resulting loads that are inserted into the structural model are presented in table 5.3.

LC 1: Deadload $g = 10 \text{ m/s}^2$

- Structural self-weight: $G_{\text{steel}} = 7850 \text{ kg/m}^3$
- Deadload glass cladding: $G_{\text{glass}} = 25 \text{ kN/m}^3$, $t_{\text{glass}} = 18 \text{ mm (3x6mm)}$
 $G * t = 25 * 0,018 = 0,45 \text{ kN/m}^2$

LC 2: Snow load As defined in NEN EN 1991-1-3 (EC1 part 1-3, 2019)

$$S = m_u * C_e * C_t * S_k = 0,56 \text{ kN/m}^2$$

- $S_k = 0,7 \text{ kN/m}^2$
- $\text{Alpha} < 30 \rightarrow m_u = 0,8$
- $C_e * C_t = 1$

LC 3: Wind load As defined in NEN EN 1991-1-4 (EC1 part 1-4, 2019)

$$P_A = C_s C_d * C_p * q_p(z_e) = +0,42 \text{ kN/m}^2$$

$$P_A = C_s C_d * C_p * q_p(z_e) = -0,60 \text{ kN/m}^2$$

$$P_C = C_s C_d * C_p * q_p(z_e) = 0 \text{ kN/m}^2$$

- $C_s C_d = 1$
- Zone 2, Rural, $z_e = 2\text{m} \rightarrow q_p = 0,6 \text{ kN/m}^2$
- $h/d = 0, f/d = 0,4 \rightarrow C_{p,A} = 0,7$
- $C_{p,B} = -1,0$
- $C_{p,C} = 0$

LC1 Self-weight	Structural steel	In software ($g = 10\text{m/s}^2$)
	Glass cladding	0,45 kN/m ²
LC2 Snow load	Symmetric	0,56 kN/m ²
LC3 Wind load	P _A	0,42 kN/m ²
	P _B	-0,6 kN/m ²
	P _C	0 kN/m ²

Table 5.3: Load cases

For strength verification of the structure, the following load combinations are investigated

$$ULS1 = 1,2 * LC1 + 1,5 * LC2$$

$$ULS2 = 1,2 * LC1 + 1,5 * LC3$$

$$ULS3 = 0,9 * LC1 + 1,5 * LC3$$

Serviceability limit state load combinations are not considered. Therefore, deformations do not provide a hard criterium in the design. However, if deformations in the ULS load combinations satisfy the deformation limit ($u < L/250 = 6000/250 = 24 \text{ mm}$), then the deformation can be assumed fulfil the requirements.

Selection of a cross-section

Based on the defined geometry an optimisation is performed to determine the optimal cross-sections for the structural elements. As is established in chapter 4, the edge beams in this shell configuration play an important role in the stability of the structure. Therefore, in the design a distinction is made between beams in the middle of the structure and the edge beams. The optimisation results in two selected steel profiles. The optimisation is performed with rigid joints ($k_a = 100000 \text{ kN/m}$ and $k_{by} = 100000 \text{ kNm/rad}$).

The objective of the optimisation is to minimise the mass of the structure. Penalty functions are included to create boundaries $BLfac \geq 10$. As the buckling load factor for ULS1 is expected to be governing for the design other criteria are left out of the optimisation in this case. While a Buckling load factor smaller than 10 is not allowed, the value of the penalty function is

gradually increased to shape the fitness landscape in order to improve the efficiency of the evolutionary solver.

General objective:

$$\begin{aligned} \min_{C_i} \quad & Mass \\ \text{s.t.} \quad & BLfac \geq 10 \\ & u \leq u_{max} \\ & \sigma_{Ed} \leq \sigma_{Rd} \end{aligned}$$

Variables:

- C₁ = Cross-section Edge beams
- C₂ = Cross-section Beams

Penalty model:

$$\begin{aligned} \min_{C_i} \quad & p(BLfac) \\ p = \begin{cases} 0, & BLfac \geq 10 \\ 20, & 9 \leq BLfac < 10 \\ 50, & 8 \leq BLfac < 9 \\ 100, & 7 \leq BLfac < 8 \\ 500, & BLfac < 7 \end{cases} \end{aligned}$$

Unconstrained optimisation solver:

$$\min_{C_i} \quad Mass + p(BLfac)$$

The optimisation returned the following cross-sections:

- C₁ = RHS100x50x3
- C₂ = RHS80x40x3

Table 5.4 shows the checks for the different load combinations with these cross-sections. These design checks show that the buckling load factor for ULS 1 is indeed the governing design objective. This justifies the exclusion of the other objectives from the optimisation function. Figure 5.4 shows the buckling shape of the first buckling modes of the structure under the different load combinations. In all three load combinations a global buckling shape is found.

ULS1		ULS2		ULS3	
BLfac	11,8	BLfac	44,9	BLfac	68,4
UC	0,11	UC	0,09	UC	0,08
u	2,74 mm	u	4,64 mm	u	3,53 mm

Table 5.4: Design checks after cross-section optimisation

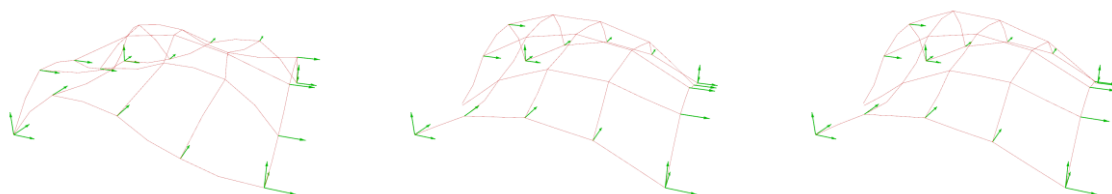


Figure 5.4: First buckling mode shapes for ULS1, ULS2 and ULS3

Connection design

The design consists of two different cross-sections. This results in the design of two different base connections. The first connection, shown in figure 5.5, connects four RHS80x40x3 elements to the central node. The second connection, shown in figure 5.6 connects two RHS100x50x3 edge beams and on RHS80x40x3 beam to the centre box. Table 5.5 lists the design parameters of the base connection.

Connection 1		Connection 2	
Cross-section	RHS80x40x3	Cross-section	RHS100x50x3
Centre box	SHS60x60x3 (L=90 mm)	Centre box	SHS70x70x5 (L = 100 mm)
Endplate	80x40x6	Endplate	100x50x6
Bolts	M12 8.8 (s=30 mm)	Bolts	M12 8.8 (s=30 mm)

Table 5.5: Connection design parameters for the base connections

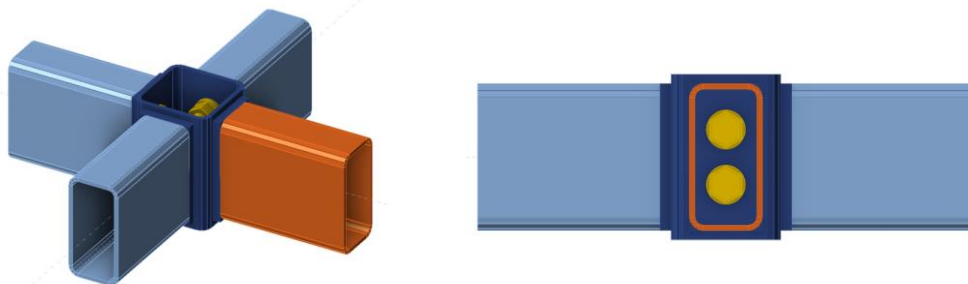


Figure 5.5: Base connection 1 (RHS80x40x3)

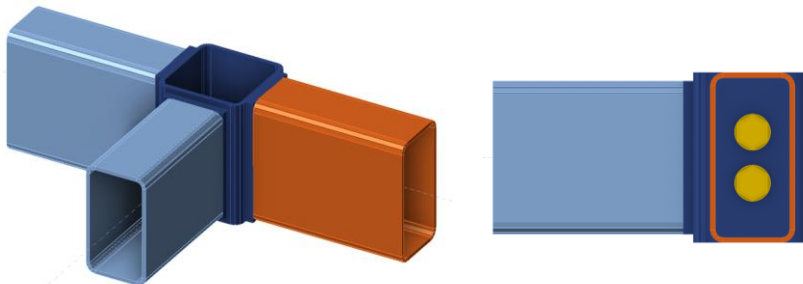


Figure 5.6: Base connection 2 (RHS100x50x3)

To be able to generate the design diagrams, it is necessary to determine the stiffness ranges of the two connections. Different design parameters are adjusted to create these ranges. Table 5.6 shows the design adjustments to create the stiffness range of the connections. For reference, the mass of the specific connections is included in the table.

Connection 1	Design changes	Mass (kg)	Connection 2	Design changes	Mass (kg)
1. Base	See table 5.5	1,47	1. Base	See table 5.5	2,00
2. Spaced	$S_{bolts} = 40 \text{ mm}$	1,47	2. Spaced	$S_{bolts} = 50 \text{ mm}$	2,0
3. SHS70	Centre box: SHS70x5	1,89	3. SHS80	Centre box: SHS80x6.3	2,42
4. SHS80	Centre box: SHS80x8	2,57	4. SHS90	Centre box: SHS90x8	3,01
5. Max	Endplate: 80x40x10	2,97	5. Max	Endplate: 100x50x10	3,48
Design operations	Stiffening caps ($t = t_{cb}$)	1,64 – 3,77	Design operations	Stiffening caps ($t = t_{cb}$)	2,38 – 4,50
	Extra bolt rows				

Table 5.6: Design adjustments to create stiffness range for connections 1 and 2

Initial stiffness design an evaluation of load ratios

Next, the initial design for the stiffness of the connections can be defined. Figure 5.10 shows the six different joints that occur in the structure, the joints are grouped based on symmetry of the structure. The division leads to 6 joints with 12 separate connections, as seen in figure 5.11. These connections are named a to l in the design of the structure.

As a result of the boundary conditions and the absence of torsional stiffness in the connections of the edge beams, connections a, e and i do not experience bending moments. Therefore, these connections do not require any rotational stiffness and can be excluded from the stiffness design optimisation.

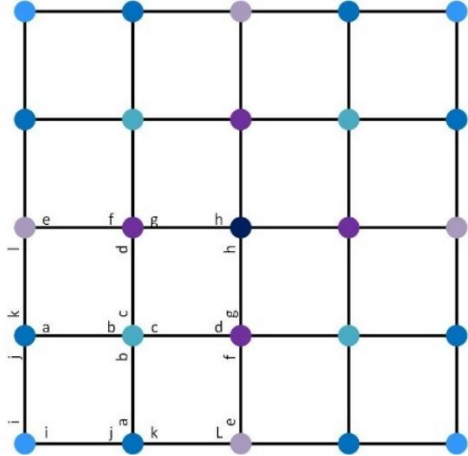
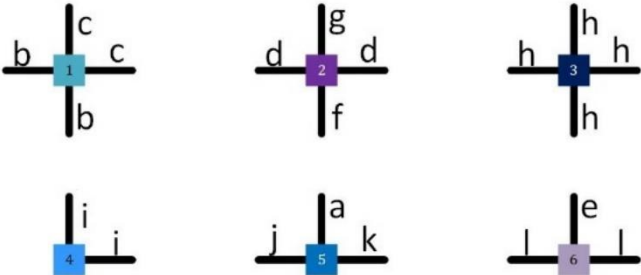


Figure 5.10: Locations of the different joints in the structure



5.11: Connections in the structure as found in the different joints

To reduce the computational effort required for the optimisation, the connections are clustered by their location in the structure. Connections b and c can be expected to require similar stiffness based on their location opposite of the same joint, as has been shown in section 4.3. The same clustering is applied for connections d, f and g and connections j, k and l.

As the buckling load is expected to be governing for the joint stiffness design, the buckling load factor functions as the governing design constraint in the optimisation. Penalty functions are defined to incentivise reduction of stiffness for the joints. The limit values for the penalty functions are based on the design diagrams. For ULS1, stiffness values for small $|M_y|/N$ -ratios are used, for ULS2 and 3 the stiffness values for large $|M_y|/N$ -ratios determine the limits in the penalty functions. This way the joint design optimisation is linked to the weight and constructability of the connections.

The optimisation strategy is described on the next page. The results of the optimisation for the different load combinations are listed in table 5.7.

General objective:

$$\begin{aligned} \min_{k_x} \quad & Mass \\ \text{s.t.} \quad & BLfac \geq 10 \\ & u \leq u_{max} \\ & \sigma_{Ed} \leq \sigma_{Rd} \end{aligned}$$

Variables k_x :

- k_{bc} = stiffness of connections b and c
- k_{dfg} = stiffness of connections d, f and g
- k_h = stiffness of connections h
- k_{jkl} = stiffness of connections j,k and l

Constrained optimisation function:

$$\begin{aligned} \min_{k_x} \quad & p_1(k_{bc}) + p_1(k_{dfg}) + \frac{p_1(k_h)}{2} + p_2(k_{jkl}) \\ \text{s.t.} \quad & BLfac = 10 \end{aligned}$$

Penalty functions on mass and joint complexity:

- o For ULS1:

$$p_{1,ULS1}(k) = \begin{cases} 0, & k \leq 100 \\ 0.5, & 100 < k \leq 300 \\ 1, & 300 < k \leq 1000 \\ 2, & k \geq 1000 \end{cases}$$

$$p_{2,ULS1}(k) = \begin{cases} 0, & k \leq 250 \\ 0.5, & 250 < k \leq 1000 \\ 1, & 1000 < k \leq 3000 \\ 2, & k \geq 3000 \end{cases}$$

- o For ULS2 and 3:

$$p_{1,ULS2,3}(k) = \begin{cases} 0, & k \leq 30 \\ 0.5, & 30 < k \leq 140 \\ 1, & 140 < k \leq 250 \\ 2, & k \geq 250 \end{cases}$$

$$p_{2,ULS2,3}(k) = \begin{cases} 0, & k \leq 30 \\ 0.5, & 30 < k \leq 120 \\ 1, & 120 < k \leq 375 \\ 2, & k \geq 375 \end{cases}$$

Unconstrained optimisation solver:

$$\min_{k_x} |BLfac - 10| + p_1(k_{bc}) + p_1(k_{dfg}) + \frac{p_1(k_h)}{2} + p_2(k_{jkl})$$

ULS1		ULS2		ULS3	
K_{bc} (kNm/rad)	641	K_{bc} (kNm/rad)	30	K_{bc} (kNm/rad)	17
K_{dfg} (kNm/rad)	90	K_{dfg} (kNm/rad)	30	K_{dfg} (kNm/rad)	20
K_h (kNm/rad)	30	K_h (kNm/rad)	30	K_h (kNm/rad)	1
K_{jkl} (kNm/rad)	2140	K_{jkl} (kNm/rad)	210	K_{jkl} (kNm/rad)	108
BLfac	10,00	BLfac	10,01	BLfac	10,01
UC	0,11	UC	0,11	UC	0,10
u (mm)	3,10	u (mm)	10,61	u (mm)	14,29

Table 5.7: Initial stiffness estimate based on the optimisation

With the first estimate of the joint stiffness, an initial distribution of the loads in the structure is determined. Table 5.8 presents the initial load ratios on the connections. For ULS2 and 3 the loading is not symmetric in one direction. Therefore, there are different load ratios acting on the connection designs in different parts of the structure. The load ratio that is governing the selection of the connection design must be selected. If both load ratios have the same sign, the minimum value is governing (as for both compressive and tensile load ratios stiffness reduces for a reducing load ratio). If the load ratios are of opposite sign, the tensile load ratio ($|M_y|/N > 0$) is governing over the compressive load ratio ($|M_y|/N < 0$). The governing load ratio for each connection in each load combination is shaded in table 5.8. The full table of load results for the initial estimate as well as all following iterations is included in appendix E.

$ M_y /N$ (m)	ULS1	ULS2		ULS3	
			1	2	1
a	0,00	0,00	0,00	0,00	0,00
b	-0,03	-1,15	-0,14	0,29	0,24
c	-0,03	-0,51	-0,16	0,43	0,18
d	-0,02	-0,48	-0,38	0,20	0,23
e	0,00	0,00	0,00	0,00	0,00
f	-0,02	-0,40	-0,09	0,71	-0,72
g	-0,02	-0,27	-0,11	2,36	2,67
h	0,00	-0,18	-0,16	0,03	0,04
i	0,00	0,00	0,00	0,00	0,00
j	0,00	-0,24	-0,09	-0,50	-0,19
k	-0,01	-0,29	-0,09	-0,66	-0,21
l	-0,01	-0,13	-0,12	-0,33	-0,29

Table 5.8: Initial load ratio on the connections

Joint stiffness design

With the design diagrams (figures 5.7, 5.8 and 5.9), the initial estimate of the joint stiffness (table 5.7) and the resulting load ratios (table 5.8), the design of the connections can be selected. For each of the load combinations, a connection is selected. From these connections, one design is selected that should achieve a sufficiently high stiffness in all load combinations. The selected designs are presented in table 5.9, the governing design for each connection is shaded.

The example of connection b is used to explain the selection of a connection design. This example includes an extra loop through the design diagram as shown in the red dashed rectangle in figure 5.1. Figure 5.12 shows the selected location of the initial stiffness and the load ratio for connection in ULS1. Because no connection design was close enough for an efficient choice an extra design is added to the diagram with a centre box SHS80x80x6.3. This creates the red line in the new diagram on the right. This is the selected connection design for connection b.

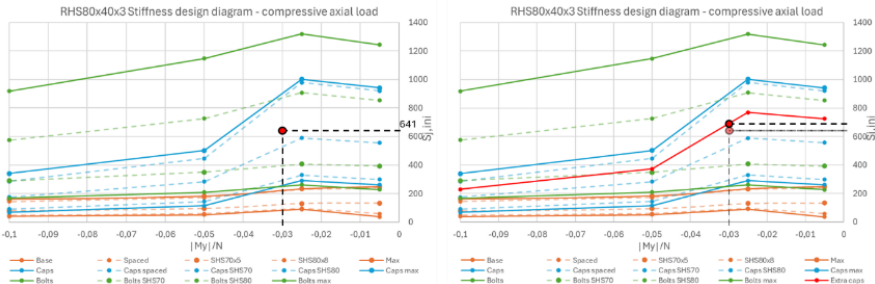


Figure 5.12: Stiffness and load ratio of the initial design (left) and the selection of a design and making a stiffness estimate (right) for connection b in ULS 1

	ULS1	ULS2	ULS3
a	Base	Base	Base
b	Extra caps	Base	Base
c	Extra caps	Base	Base
d	Base	Base	Base
e	Base	Base	Base
f	Base	Base	Base
g	Base	Base	Base
h	Base	Base	Base
i	Base	Base	Base
j	Caps SHS80	Caps SHS80	SHS80/Caps spaced
k	Caps SHS80	Caps SHS80	SHS80/Caps spaced
l	Caps SHS80	Caps SHS80	SHS80/Caps spaced

Table 5.9: Selection of connection designs based on the design diagrams, stiffness and load ratios.

After the selection of the connection designs, the first iteration is concluded with a new estimate of the stiffness of the connections. This is done with the load ratio on the connections and the design diagram of the selected connection. Table 5.10 shows the result of the first iteration. With the structural verification presented in table 5.11. Figure 5.13 shows the first buckling modes of the different load combinations, which remain similar to figure 5.4.

	ULS1			ULS2			ULS3		
	M /N	Design	S _{j,ini}	M /N	Design	S _{j,ini}	M /N	Design	S _{j,ini}
a	0,00	Base	1	0,00	Base	1	0,00	Base	1
b	-0,03	Extra caps	690	-1,15	Extra caps	154	0,24	Extra caps	161
c	-0,03	Extra caps	690	-0,51	Extra caps	160	0,18	Extra caps	116
d	-0,02	Base	82	-0,48	Base	32	0,20	Base	24
e	0,00	Base	1	0,00	Base	1	0,00	Base	1
f	-0,02	Base	82	-0,40	Base	32	0,71	Base	28
g	-0,02	Base	82	-0,27	Base	34	2,36	Base	29
h	0,00	Base	82	-0,18	Base	35	0,03	Base	12
i	0,00	Base	1	0,00	Base	1	0,00	Base	1
j	0,00	Caps SHS80	2050	-0,24	Caps SHS80	285	-0,50	Caps SHS80	253
k	-0,01	Caps SHS80	2050	-0,29	Caps SHS80	275	-0,66	Caps SHS80	250
l	-0,01	Caps SHS80	2050	-0,13	Caps SHS80	400	-0,33	Caps SHS80	273

Table 5.10: New stiffness design to conclude iteration 1 ($[M/N] = m$; $[S_{j,ini}] = kNm/rad$)

ULS1		ULS2		ULS3	
BLfac	10,04	BLfac	20,62	BLfac	28,52
UC	0,11	UC	0,10	UC	0,09
U (mm)	3,19	U (mm)	8,78	U (mm)	8,40

Table 5.11: Design criteria satisfied for the selected connections

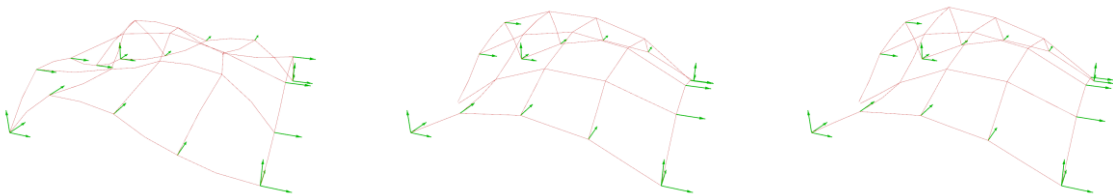


Figure 5.13: First buckling mode of the structure in different load combinations for the updated stiffness design

Following iterations are slightly different from the first iteration. After the first iteration, a connection design is selected, which is only changed when necessary. Therefore, the only task in

iteration 2 and further is to determine a new stiffness estimate, based on the updated load ratios and the selected connection design in the design diagram.

Table 5.12 shows the second iteration and table 5.13 shows the third iteration. It can be seen that the difference in stiffness from iteration 2 to iteration 3 is already small, with only minor changes in the stiffness for connections j, k and l for ULS 2 and 3. Therefore, iteration three is the final iteration and the design loop can be concluded. Table 5.14 shows the design checks for the final stiffness design. Figure 5.14 shows the first buckling modes, no large changes are visible.

		ULS1		ULS2			ULS3		
	Design	M /N	S _{j,ini}	M /N-1	M /N-2	S _{j,ini}	M /N-1	M /N-2	S _{j,ini}
a	Base	0,00	1	0,00	0,00	1	0,00	0,00	1
b	Extra caps	-0,03	690	-1,95	-0,29	153	0,61	0,34	134
c	Extra caps	-0,03	690	-1,17	-0,33	155	0,78	0,29	131
d	Base	-0,02	82	-0,46	-0,31	32	0,12	0,13	23
e	Base	0,00	1	0,00	0,00	1	0,00	0,00	1
f	Base	-0,02	82	-0,38	-0,08	33	0,47	-0,75	27
g	Base	-0,02	82	-0,24	-0,10	34	1,42	0,87	28
h	Base	-0,01	82	-0,19	-0,17	35	0,18	0,23	25
i	Base	0,00	1	0,00	0,00	1	0,00	0,00	1
j	Caps SHS80	-0,01	2050	-0,20	-0,06	331	-0,44	-0,14	259
k	Caps SHS80	-0,01	2050	-0,23	-0,07	302	-0,56	-0,16	250
l	Caps SHS80	-0,01	2050	-0,13	-0,12	400	-0,30	-0,27	277

Table 5.12: New stiffness design after iteration 2 ($[M/N] = m$; $[S_{j,ini}] = kNm/rad$)

		ULS1		ULS2			ULS3		
	Design	M /N	S _{j,ini}	M /N-1	M /N-2	S _{j,ini}	M /N-1	M /N-2	S _{j,ini}
a	Base	0,00	1	0,00	0,00	1	0,00	0,00	1
b	Extra caps	-0,03	690	-1,91	-0,27	153	0,62	0,34	134
c	Extra caps	-0,03	690	-1,11	-0,31	155	0,80	0,29	131
d	Base	-0,02	82	-0,45	-0,31	32	0,11	0,13	23
e	Base	0,00	1	0,00	0,00	1	0,00	0,00	1
f	Base	-0,02	82	-0,37	-0,08	33	0,45	-0,70	27
g	Base	-0,02	82	-0,24	-0,09	34	1,38	0,93	28
h	Base	-0,01	82	-0,18	-0,16	36	0,31	0,41	25
i	Base	0,00	1	0,00	0,00	1	0,00	0,00	1
j	Caps SHS80	-0,01	2050	-0,21	-0,06	320	-0,43	-0,14	260
k	Caps SHS80	-0,01	2050	-0,24	-0,07	292	-0,55	-0,16	255
l	Caps SHS80	-0,01	2050	-0,13	-0,12	400	-0,29	-0,27	277

Table 5.13: New stiffness design after iteration 3 / Final iteration ($[M/N] = m$; $[S_{j,ini}] = kNm/rad$)

ULS1		ULS2		ULS3	
BLfac	10,04	BLfac	20,62	BLfac	28,52
UC	0,11	UC	0,10	UC	0,09
U (mm)	3,19	U (mm)	8,78	U (mm)	8,40

Table 5.14: The design criteria after the final iteration

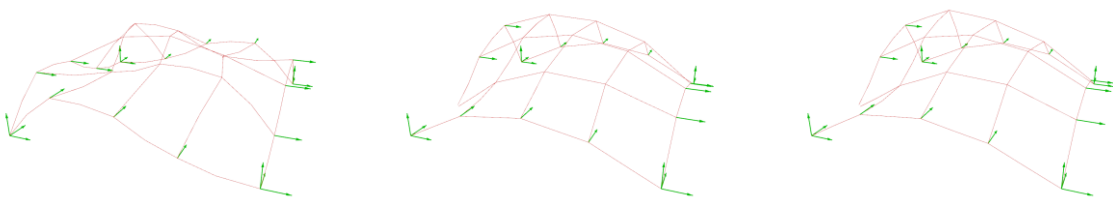


Figure 5.14: First buckling mode of the structure in different load combinations for the final design

Stiffness analysis

After the completion of the design loop, the stiffness analysis of the connection in IDEA StatiCa is performed. For each connection, five load combinations are defined (ULS1, ULS2-1, ULS2-2, ULS3-1 and ULS3-2). The double load combination for ULS 2 and 3 is the results of the symmetric joint design and asymmetric loading conditions. The results of the stiffness analysis are presented in table 5.15, the load values in table 5.15 can be retrieved from the table of the final design in appendix E. The full report of the stiffness analysis is included in appendix F.

Here, two important things should be considered. Firstly, the stiffness analysis in IDEA StatiCa does not run for an input axial load $N \leq 1$ kN. To work around this, load cases with axial loads that are smaller than 1 kN are multiplied, realising an axial load that is larger than 1 kN. For example, the loads on connection b in ULS 2 will be $N = -0,29 * 4 = -1,16$ kN and $M = -0,15 * 4 = -0,6$ kNm. When the ratio between the bending moment and the axial load remains the same, this has no influence on the calculated initial stiffness. The second point of attention is that for load ratios that are between $|M_y|/N = -0,03$ and $|M_y|/N = 0$ the load ratio should be increased to $-0,03$. This is done by increasing the bending moment. For example, the load on connection b in ULS 1 will be $N = -5,84$ kN and $M = -5,84 * 0,03 = 0,18$ kNm. This results in a conservative calculation for the initial stiffness that can be used in the structural model.

The results of the stiffness analysis in table 5.15 show that the estimates of the connections stiffness in the design loop are accurate for ULS 2 and ULS 3. For ULS 1, the stiffness analysis shows somewhat larger deviations, especially for connections j, k and l. This is likely caused by a low number of data points in the design diagrams. The stiffness values around the peak are unpredictable when too few data points are defined.

	ULS1			ULS2					ULS3				
	M	N	S _{j,ini}	M-1	N-1	M-2	N-2	S _{j,ini}	M-1	N-1	M-2	N-2	S _{j,ini}
a	0,00	-6,66	1	0,00	-0,54	0,00	-0,76	1	0,00	0,20	0,00	-0,02	1
b	0,15	-5,84	743,7	-0,29	-0,15	0,10	-0,37	151,2	-0,30	0,49	0,09	0,27	135,5
c	0,15	-5,85	744,5	-0,29	-0,26	0,10	-0,33	153,4	-0,30	0,38	0,09	0,32	135,5
d	0,09	-5,58	76,4	0,06	-0,14	0,06	-0,21	31,8	0,05	0,47	0,05	0,40	23,4
e	0,00	-5,64	1	0,00	-0,68	0,00	-0,97	1	0,00	-0,05	0,00	-0,34	1
f	0,11	-4,79	76,9	-0,11	-0,29	0,05	-0,59	33,6	-0,11	0,24	0,04	-0,05	26,6
g	0,11	-4,91	76,2	-0,11	-0,46	0,05	-0,50	34,7	-0,11	0,08	0,04	0,04	27,9
h	0,03	-4,63	76,9	0,07	-0,35	0,07	-0,38	34,5	0,05	0,17	0,05	0,13	25,8
i	0,00	-14,91	1	0,00	-3,35	0,00	-3,27	1	0,00	-1,62	0,00	-1,55	1
j	-0,07	-14,48	2301,5	-0,65	-3,12	0,19	-3,05	298,9	-0,63	-1,45	0,20	-1,38	257,2
k	-0,07	-13,36	2301,4	-0,65	-2,70	0,19	-2,80	286,8	-0,63	-1,15	0,20	-1,25	250,5
l	0,16	-13,22	2332,8	0,33	-2,62	0,33	-2,73	376,8	0,32	-1,10	0,32	-1,20	275,4

Table 5.15: Results stiffness analysis ($[M] = \text{kNm}$; $[N] = \text{kN}$; $[S_{j,ini}] = \text{kNm/rad}$)

As mentioned, an additional check should be performed during the stiffness analysis. By ensuring that the acting bending moment is smaller than the elastic limit of the connection the assumption of linear elastic stiffness behaviour for the joint is verified. The results in table 5.16 show that in this case all connections perform in the elastic range.

	M _{Ed} (kNm)			2/3 * M _{j,Rd} (kNm)			Check
	ULS1	ULS2	ULS3	ULS1	ULS2	ULS3	
a	-	-	-	-	-	-	-
b	0,16	0,29	0,30	1,58	2,04	1,88	OK
c	0,16	0,29	0,30	1,58	2,06	1,88	OK
d	0,10	0,06	0,05	0,67	0,59	0,49	OK

e	-	-	-	-	-	-	-
f	0,12	0,11	0,11	0,67	0,59	0,56	OK
g	0,12	0,11	0,11	0,67	0,60	0,57	OK
h	0,04	0,06	0,05	0,67	0,61	0,55	OK
i	-	-	-	-	-	-	-
j	-0,07	0,65	0,64	2,25	3,01	2,89	OK
k	-0,06	0,65	0,64	2,27	3,07	2,84	OK
l	0,16	0,33	0,32	2,27	3,35	3,01	OK

Table 5.16: Stiffness design check $M_{Ed} < 2/3 M_{j,Rd}$

Final geometry and connection design

The design of the grid shell results in the final design of the shell as shown in figure 5.15. The final designs for the connections are shown in figure 5.16. In the final design four different connection designs are applied, the locations of the connections are indicated with the colours. All connections are reversible, with 36% (9 out of 25) being simple connections and 68% (16 out of 25) requiring stiffening caps. The total mass of the connections is 75 kg, which is approximately 20% of the mass of the structural elements.

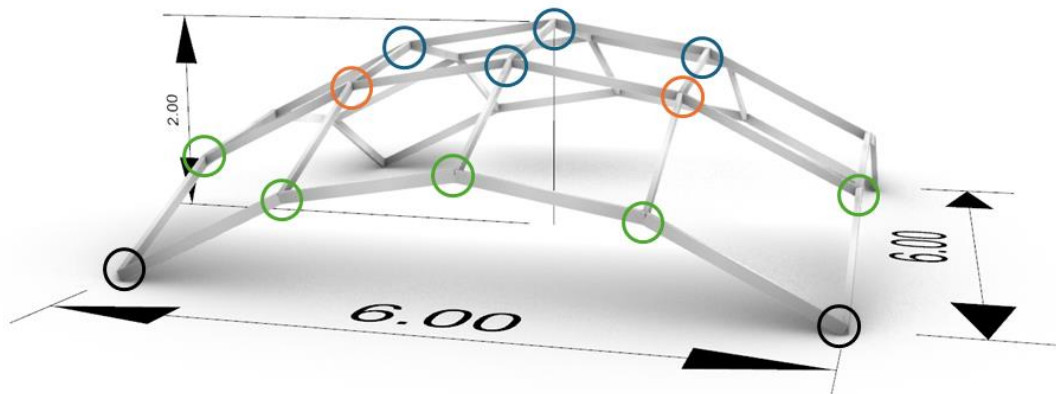
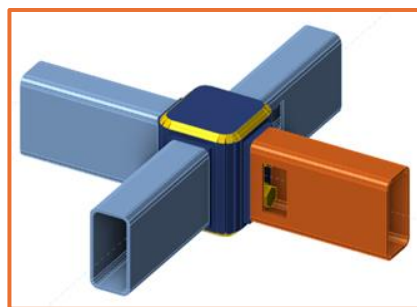
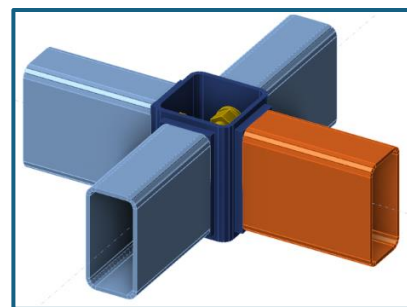


Figure 5.15: Final grid shell (Dimensions in meters)



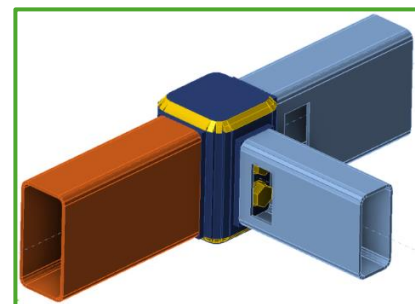
(a) Connections b and c ($m = 3,02 \text{ kg}$)



(b) Connections d, f, g and h ($m = 1,47 \text{ kg}$)



(c) Connection l ($m = 1,77 \text{ kg}$)



(d) Connections a, e, j, k and l ($m = 4,03 \text{ kg}$)

Figure 5.16: Final connection designs

Detailed structural analysis

For the detailed structural analysis, the structural model from Karamba3D can be loaded directly into RFEM. Geometry, support conditions, loads and stiffness of the connections are adopted one-on-one into the finite element model.

A second-order analysis is performed to assess the stresses in the different load combinations. A stability analysis of ULS 1 is performed to calculate the buckling factor. Figures 5.17, 5.18 and 5.19 show the stresses in load combination ULS1, ULS2 and ULS3 respectively. Figure 5.20 shows the buckling factor and the first buckling mode for ULS1. In table 5.20, the results from the analysis in RFEM are compared to the results from the analysis in Karamba3D.

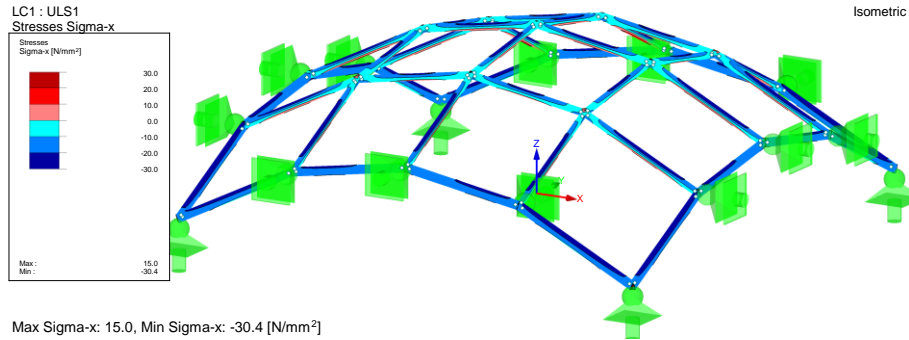


Figure 5.17: Axial stress results for ULS1

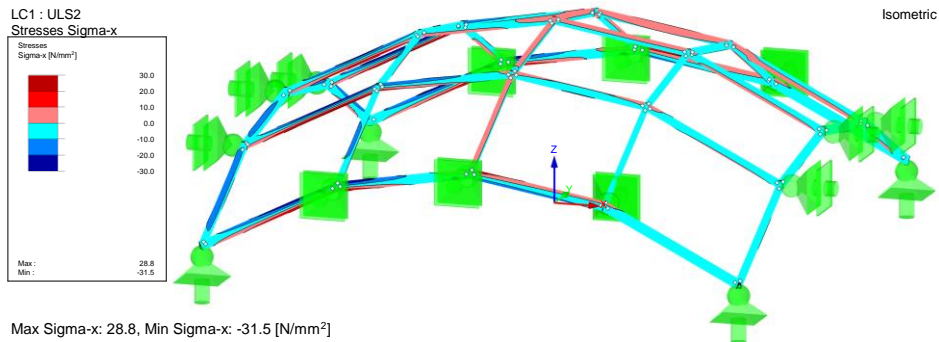


Figure 5.18: Axial stress results for ULS2

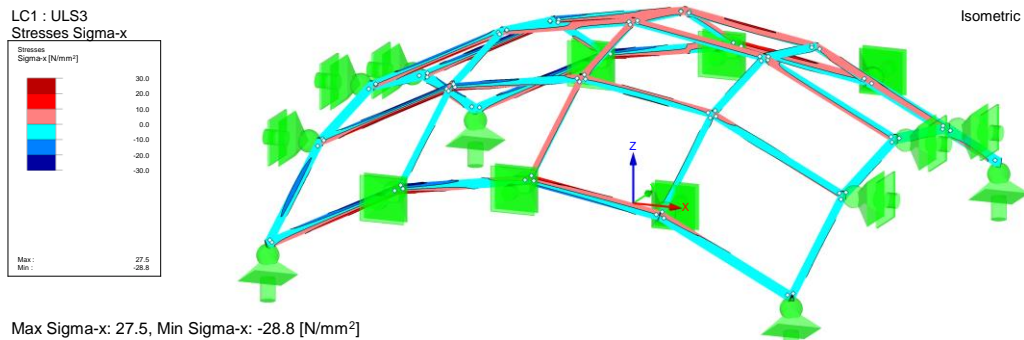


Figure 5.19: Axial stress results for ULS3

2.1 CRITICAL LOAD FACTORS

E-Value No.	Critical Load Factor f	Magnification Factor α
1	10.189	1.109
2	12.186	1.089
3	12.645	1.086
4	12.645	1.086

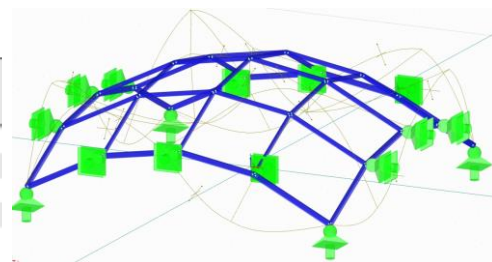


Figure 5.20: Buckling factor results and the first buckling mode for ULS1 found by RFEM

	ULS1			ULS2			ULS3		
	Karamba	RFEM	\Delta	Karamba	RFEM	\Delta	Karamba	RFEM	\Delta
σ_{\max} (N/mm ²)	15,0	15,0	0%	31,2	28,8	7,7%	30,0	27,5	9%
σ_{\min} (N/mm ²)	-30,6	-30,4	0,7%	-33,1	-31,5	5,1%	-30,4	-28,8	5,3%
BLfac	10,19	10,19	0%	-	-		-	-	

Table 5.17: Results of the structural analysis in RFEM compared to the results from the design in Karamba

The loads on the nodes are extracted from RFEM. These loads are tabulated in appendix G. The governing loading condition for each node type is determined from these tables. The normative values are marked by borders in similar colours as the joint design in figure 5.14. The normative loads are determined based on two criteria. Maximum bending moment in any direction, as the connections are symmetric around the horizontal axis, and the maximum axial load.

For these load combinations, a stress-strain analysis is performed in IDEA StatiCa. Because of the angles between the members in the structural model, equilibrium was not achieved in all connections. Where necessary, one or more of the loads on the connections were increased until equilibrium in the node was achieved. The calculation report of the connections is included in appendix G.4. Design checks are presented in table 5.18. Visual results for the connection types are presented in figures 5.19, 5.20, 5.21 and 5.22. All connections satisfy the design criteria.

Connection a, e, j, k, l	Value	Check status
Analysis	100,0%	OK
Plates	0,0 < 5,0%	OK
Bolts	17,7 < 100%	OK
Welds	7,8 < 100%	OK
GMNA	Calculated	
Connection b, c	Value	Check status
Analysis	100,0%	OK
Plates	0,0 < 5,0%	OK
Bolts	12,0 < 100%	OK
Welds	6,2 < 100%	OK
GMNA	Calculated	
Connection d, f, g, h	Value	Check status
Analysis	100,0%	OK
Plates	0,0 < 5,0%	OK
Bolts	13,4 < 100%	OK
Welds	0,0 < 100%	OK
GMNA	Calculated	
Connection i	Value	Check status
Analysis	100,0%	OK
Plates	0,0 < 5,0%	OK
Bolts	1,1 < 100%	OK
Welds	0,0 < 100%	OK
GMNA	Calculated	

Table 5.18: Design checks of the connections

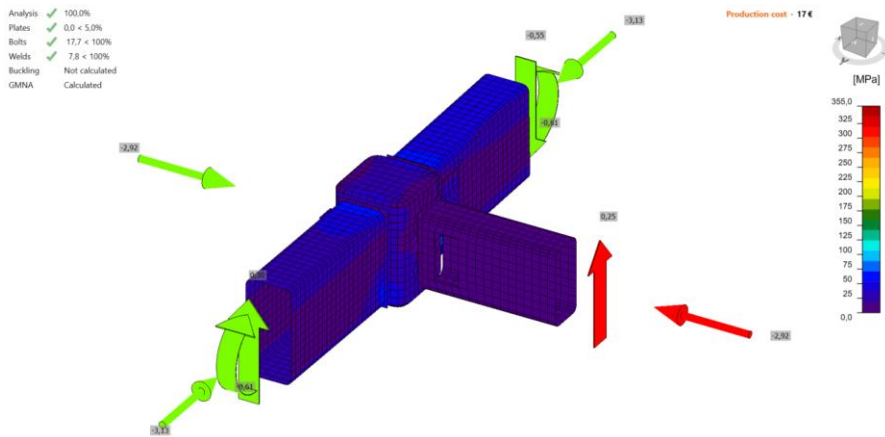


Figure 5.20: Governing stresses in connection type a, e, j, k, l (ULS2)

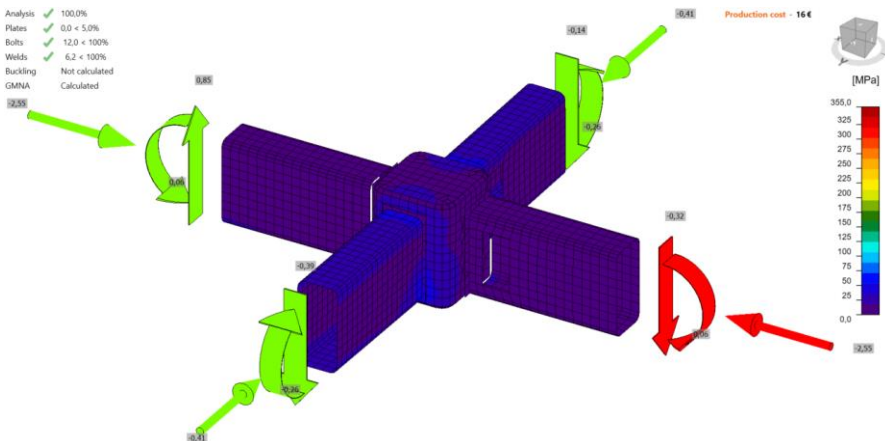


Figure 5.19: Governing stresses in connection type b, c (ULS2)

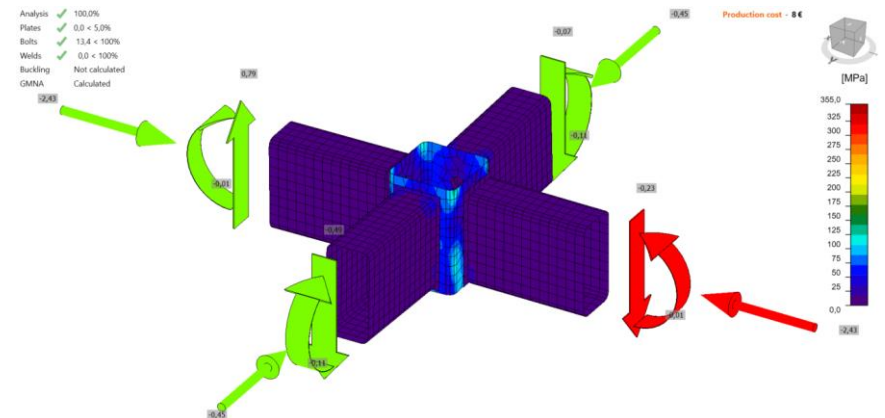


Figure 5.21: Governing stresses in connection type d, f, g, h (ULS2)

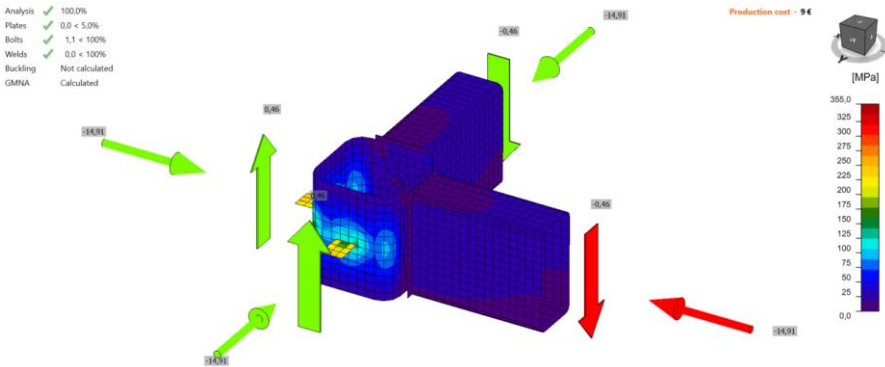


Figure 5.22: Governing stresses in connection type i (ULS1)

6 Case study: C30 Shell

In this chapter, the performed case study is presented. The goal of the case study is to apply the design strategy to a structure realised in practice to check if it can be combined with practical design aspects. The study considers the C30 shell, that is realised by Octatube in 2020 (Octatube, 2020). Section 6.1 presents the shell and discusses interesting aspects of the design. In section 6.2, an attempt is made to apply the design strategy that is presented in chapter 5 to the C30 Shell.

6.1 C30 Shell design

This section discusses the general aspects of the design, it pays specific attention to the joint design of the structure as well as considerations on constructability and sustainability that apply to the structure. Figure 6.1 shows the C30 shell.

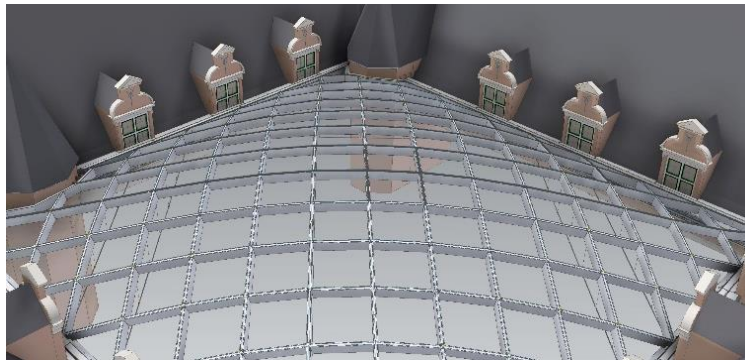


Figure 6.1: C30 Shell grid shell (Octatube,2020)

The C30 Shell is designed as a roof over an existing courtyard, which is surrounded by a monumental building. This resulted in several challenges for the design of the structure. No horizontal loads could be put on the existing walls as a result of the construction of the grid shell. In addition, it was complex to design a continuous edge to enclose the grid shell, because of several circular towers in the corners of the courtyard.

To combat these challenges, a combination of stiff edge beams and tension elements are included in the design. Pre-tension in the cables ensures stiffness of the structure, while simultaneously preventing horizontal loads on the existing structure. In this case study, the edge beams and the cables are not taken into account.

Due to the unique shape of the structure and the different element sizes and angles, a parametric approach is used for the design of the shell. Resulting in a double curved grid with beams of different length and glass panels of different size and curvature. (Octatube, 2020)

Joint stiffness design

Focussing on the joint design of the shell, two types of connections can be found in the shell structure. The first type is a welded connections that is used for assembling several ladder frames. The second type is a bolted connection to connect pre-fabricated frames on site. Both connections are shown in figure 6.2.

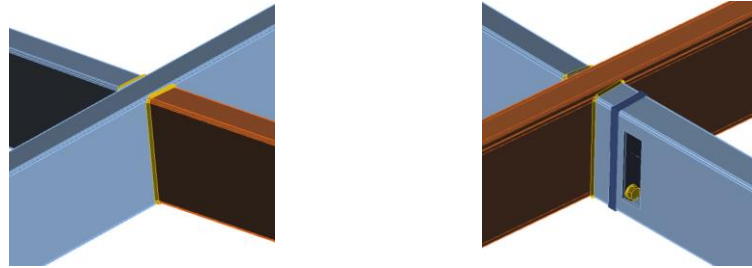


Figure 6.2: Connection in the C30 shell

The connection design considers the semi-rigidity of the connections according to NEN-EN 1993-1-8 for steel connection design (*EC3 part 1-8, 2011*). A value for the stiffness of the connections is determined based on a component based finite element calculation in IDEA StatiCa. The axial load on the connections is included in the design of the stiffness.

The stiffness analysis is performed for all load combinations that are investigated as potentially governing combinations for the connections. The lowest stiffness resulting for the analysis is then applied to all connections of that type in the structural model. In case bending moments exceed $2/3$ of the joint moment capacity, $S_{j,ini}/\eta$ is applied as the stiffness of the connection.

The design is checked for two possible governing situations:

- a. Semi-rigid connections: here the value of the calculated stiffness is used. This situation is governing for the stability and stiffness of the structure as well as for bending moment in the beams.
- b. Rigid connections: This situation is governing for the bending moments in the nodes.

Constructability and sustainability

In terms of constructability, the design provides some interesting solutions for challenges encountered during the project. Because of the limitations of the surrounding courtyard the shell had to be self-supporting during the construction phase. To this end, the design is divided in several welded ladder frames up-to maximum transportable dimensions. The centre of the structure is constructed from four reciprocal ladder frames that support each other. Figure 6.3 shows the divisions made in the design of the structure. The elements in the ladder frames are welded together. The individual parts are then bolted together on site.

A first assessment of this design showed that the shell is very rigid. The rigidity of the bolted connections had limited effect on the performance of the structure. In addition, the connection design as shown in figure 6.2 is not optimal for showing the proposed design method for grid shell connections. Therefore, in the case study a different division of the structure is proposed to be able to test the proposed design method for semi-rigid joints.

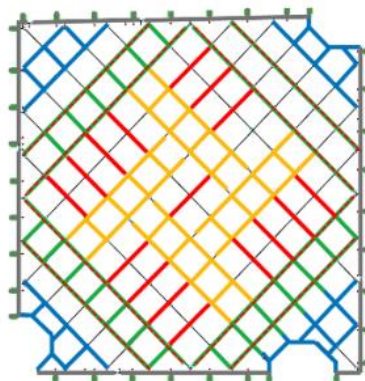


Figure 6.3: Division of pre-fabricated elements in the C30 shell

The division of the structure in figure 6.3 is selected based on constructability of the structure. Sections are only limited by the maximum transportable sizes. However, the division of the structure can also be made based on sustainability of the transport. In that case, it is preferable to divide the structure in segments that can be transported in regular trucks. Maximum truck dimensions according to EU regulations are a length of 12 m, a height of 4 m and a width of 2,55 m (Raad van de Europese Unie, 1996). If any of these dimensions is exceeded, the transport must be categorised as exceptional transport.

The division of the structure as presented in figure 6.4 results in structural elements that satisfy these transportation requirements. This division results in a clustering of the connections into five different groups based on the location in the structure. This creates uniformity in the structure. However, the distribution of bolted connections is not based on structural requirements.

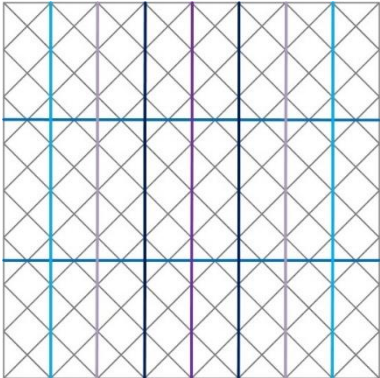


Figure 6.4: Proposed division of the C30 shell in transportable pre-fabricated segments

6.2 Case study design

Geometric design and technical details

The dimensions and grid parameters of the shell are presented in table 6.1

Parameter	Value	Unit
Lx	28	m
Ly	28	m
Division x	8	-
Division y	8	-

Table 6.1: Geometric parameters of the structural model

The shape of the shell is determined through form-finding. The particle-spring method is applied to find the shape. This is done with the Kangaroo plug-in for grasshopper (TU Delft, 2014). The parameters for the form-finding are adjusted so that the height of the structure in the model matches the height of the C30 shell. The height of the structure is 3.84 m.

To simulate the stabilising effect of the edge beam in combination with the cables, in the model, the points along the edges are supported for translation and free for rotations, resulting in a pinned support. The edge beams are modelled in the structure in order to generate accurate loading conditions near the edge of the structure. However, the edge beams do not contribute to stability and stiffness of the shell.

The resulting structure is presented in figure 6.5.

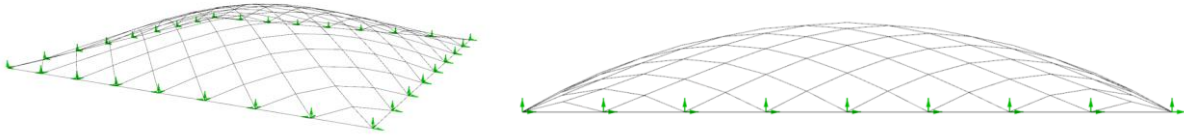


Figure 6.5: Structural model

The stiffness of the joints is defined as shown in table 6.2. For the bolted connection, the shear stiffness value is selected that represents a rigid joint for translational deformation ($k > 0,01EA m^{-1}$). To avoid in-plane bending moment and torsional moment in the structure, the joints are assumed pinned for in-plane bending and torsional stiffness. For the welded connections, a stiffness analysis has been performed for bending moments M_y and M_z separately. The results of this analysis are also included in table 6.2.

Parameter	Bolted connection	Welded connection	Unit
k_a	1000000	∞	kN/m
K_{sy}	200000	∞	kN/m
K_{sz}	200000	∞	kN/m
K_t	0.1	∞	kNm/rad
K_{by}	Variable	1000000	kNm/rad
K_{bz}	0.1	26700	kNm/rad

Table 6.2. Joint stiffness

Loads are defined as surface loads on the shell. The surface loads on the shell are translated to beam loads. For each surface, the total load is uniformly distributed over the structural elements that enclose it. Load cases are defined according to the load cases listed below. The resulting loads that are inserted into the structural model are presented in table 6.3.

LC 1: Deadload $g = 10 m/s^2$

- Structural self-weight: $G_{steel} = 7850 kg/m^3$
- Deadload glass cladding: $G_{glass} = 25 kN/m^3$, $t_{glass} = 18 mm (3x6mm)$
 $G * t = 25 * 0,018 = 0,45 kN/m^2$

LC 2: Snow load *As defined in NEN EN 1991-1-3 5.3.5 case I (EC1 part 1-3, 2019)*

$$S = \mu_4 * C_e * C_t * S_k = 0,56 kN/m^2$$

- $S_k = 0,7 kN/m^2$
- $\mu_4 = 0,8$
- $C_e * C_t = 1$

LC3: Asymmetric snow load *As in NEN EN 1991-1-3 5.3.5 case ii (EC1 part 1-3, 2019)*

$$S1 = \mu_4 * C_e * C_t * S_k = 1,12 kN/m^2$$

$$S2 = 0,5\mu_4 * C_e * C_t * S_k = 0,56 kN/m^2$$

- $S_k = 0,7 kN/m^2$
- $\alpha < 60 \rightarrow \mu_4 = 0,2 + 10 * f/b = 0,2 + 10 * (3,84/28) = 1.6$
- $C_e * C_t = 1$

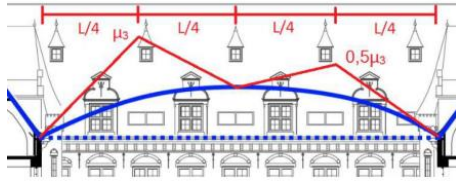


Figure 6.6: Asymmetric snow load distribution

LC 4: Wind load As defined in NEN EN 1991-1-4 (EC1 part 1-4, 2011)

$$P_A = C_s C_d * C_p * q_p(z_e) = -1,19 \text{ kN/m}^2$$

$$P_B = C_s C_d * C_p * q_p(z_e) = -0,82 \text{ kN/m}^2$$

$$P_C = C_s C_d * C_p * q_p(z_e) = -0,46 \text{ kN/m}^2$$

$$- C_s C_d = 1$$

$$\text{Zone 2, Urban, } z_e = 20,7\text{m} \rightarrow q_p = 0,91 \text{ kN/m}^2$$

$$- h/d = 0,6, f/d = 0,14 \rightarrow C_{p,A} = -1,3$$

$$C_{p,B} = -0,9$$

$$C_{p,C} = -0,5$$

LC1 Self-weight	Structural steel	In software ($g = 10\text{m/s}^2$)
	Glass cladding	0,45 kN/m ²
LC2 Snow load	Symmetric	0,56 kN/m ²
LC3 Asymmetric snow load	S ₁ (μ ₄)	1,12 kN/m ²
	S ₂ (0.5 μ ₄)	0,56 kN/m ²
LC4 Wind load	P _A	-1,19 kN/m ²
	P _B	-0,82 kN/m ²
	P _C	-0,46 kN/m ²

Table 6.3. Load cases

For strength verification of the structure, the following load combinations are investigated.

$$ULS1 = 1,2 * LC1 + 1,5 * LC2$$

$$ULS2 = 1,2 * LC1 + 1,5 * LC3$$

$$ULS3 = 0,9 * LC1 + 1,5 * LC3$$

$$ULS4 = 1,2 * LC1 + 1,5 * LC4$$

$$ULS5 = 0,9 * LC1 + 1,5 * LC4$$

Serviceability limit state load combinations are not considered. Therefore, deformations do not provide a hard criterium in the design. However, if deformations in the ULS load combinations satisfy the deformation limit ($u < L/250 = 28000/250 = 112 \text{ mm}$), then the deformation can be assumed fulfil the requirements.

For the case study, the applied cross-section would be based on the cross-section used in the C30 shell. Therefore, a cross-section of RHS300x100x8 is selected for all members in the structure.

Connection design

Based on the division of the structure as shown in figure 6.4, two types of connections can be defined. Welded connections, where the structural elements are welded to the centre node on all four sides, and bolted connections, for which two of the elements are bolted to the node and two elements are welded. Table 6.4 describes the base connections as shown in figure 6.7.

Welded connection		Bolted connection	
Cross-section	RHS300x100x8	Cross-section	RHS300x100x8
Centre box	SHS180x180x16 (L=300 mm)	Centre box	SHS160x160x10 (L=300 mm)
Endplate	-	Endplate	300x100x8
Welds	Butt welds	Bolts	M16 8.8 (s=100 mm)

Table 6.7: Connection design parameters for the base connections

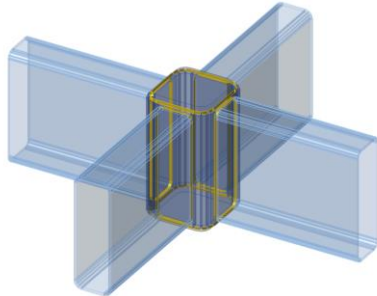


Figure 6.7: Welded connection

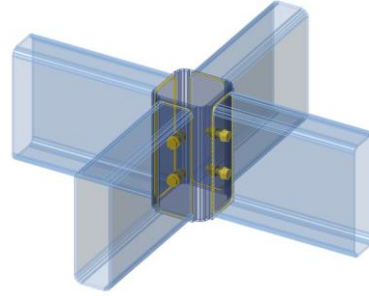


Figure 6.8: Bolted connection

Welded connections are not influenced by the load ratio, as they are in full contact with the node both in tension and in compression. As these nodes are prefabricated, it is easier to achieve a higher stiffness. The stiffness analysis returns a rigid stiffness for the welded connections. The values applied in the model are included in table 6.2.

Connection design diagram

Table 6.8 lists the design adjustments that are made to create the stiffness ranges for the connections. Stiffness analyses of these models are performed to generate the design diagram presented in figure 6.9.

Connection 2	Design changes	Mass (kg)
1. Base	See table 6.40	18,1
2. Spaced	$S_{bolts} = 230$ mm	18,1
3. Spaced M20	Bolts M20 8.8	18,5
4. SHS160	SHS160x160x12,5 and bolts M16 8.8	21,1
5. SHS160 M20	SHS160x160x12,5 and bolts M20 8.8	21,5
6. SHS160 $t_p=12$	Endplate 300x100x12	23,4
7. SHS180	Centre box: SHS180x180x16	30,5
8. SHS180 $t_p=16$	Endplate 300x100x16	32,4
9. Max	Centre box: length = 320 mm	34
Design operations	Caps	22,1 – 40,4

Table 6.8: Design adjustments to create the stiffness range for the bolted connection

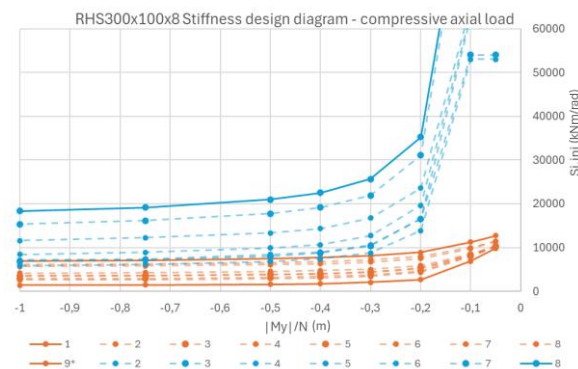


Figure 6.9: Design diagram for the bolted connection in figure 6.8 for the design in table 6.8

The design diagram presented in figure 6.9 is adjusted for the design of the shell. In practice, the peak values cannot be used safely as it is not possible to determine up to what value the results of the stiffness analysis are reliable. In addition, the design in chapter 5 showed that for the peak values estimates of the connection stiffness are difficult to make, because of the unpredictability of the results around the peak. Therefore, the design diagrams are capped-off at a load ratio of $|M_y|/N = -0,2$ m. The new design diagram that is used in the design is shown in figure 6.10. A full size version of the design diagram, including numerical data, is included in appendix D.3.

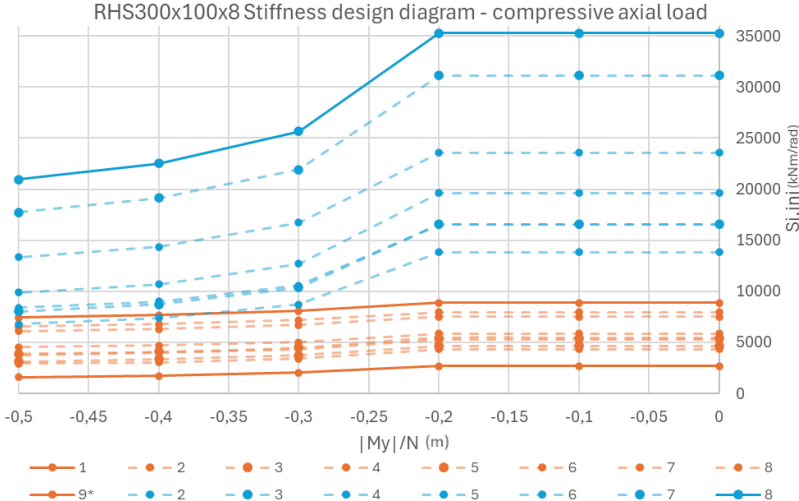


Figure 6.10: Adjusted design diagram to be used in the case study design

Initial stiffness design

Now, the initial design for the stiffness of the connection can be performed. The division of the structure leads to five different connections, that are clustered based on their location in the structure. Figure 6.11 shows the location of the connections labelled a, b, c, d and e.

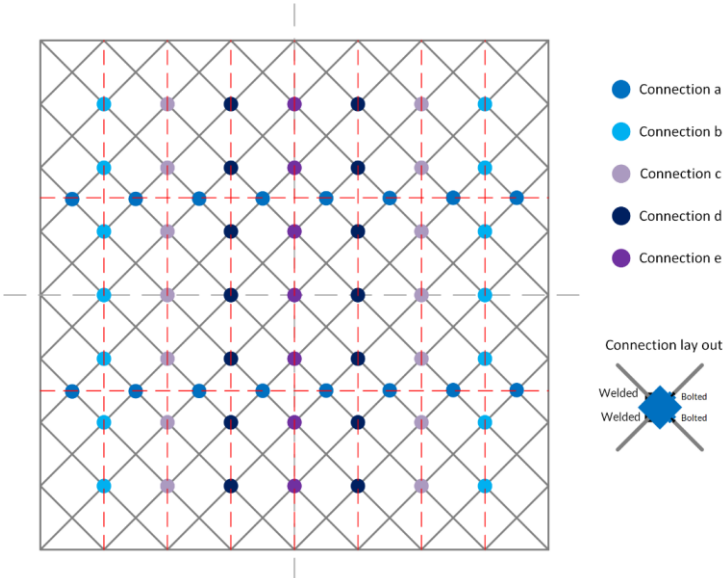


Figure 6.11: Clustering of the connections in the structure

The stiffness design is performed with an optimisation similar to the optimisation as presented in chapter 5. The optimisation is defined below. Boundary conditions for the penalty functions are determined based on the stiffness values in the design diagram and are, therefore, linked to mass and complexity of the connections.

General objective:

$$\begin{aligned} \min_{k_x} \quad & \text{Mass} \\ \text{s.t.} \quad & (\text{BLfac} \geq 10; \quad u \leq u_{max}; \quad \sigma_{Ed} \leq \sigma_{Rd}) \\ \text{Variables } k_x: \quad & k_x = \text{stiffness of connection } x \end{aligned}$$

Constrained optimisation function:

$$\begin{aligned} \min_{k_x} \quad & p(k_a) + p(k_b) + p(k_c) + p(k_d) + p(k_e) \\ \text{s.t.} \quad & \text{BLfac} = 10 \end{aligned}$$

Penalty function on mass and joint complexity

$$p(k_x) = \begin{cases} 0, & k_x \leq 2500 \\ 0.1, & 2500 < k_x \leq 4500 \\ 0.2, & 4500 < k_x \leq 9000 \\ 0.3, & 9000 < k_x \leq 14000 \\ 0.4, & 14000 < k_x \leq 35000 \\ 0.5, & k_x \geq 35000 \end{cases}$$

Unconstrained optimisation solver:

$$\min_{k_x} \quad |\text{BLfac} - 10| + p(k_a) + p(k_b) + p(k_c) + p(k_d) + p(k_e)$$

The optimisation results are shown in table 6.9. Two points of attention should be noticed. The optimisation shows that ULS4 and ULS5 for wind load proved to be stable and sufficiently strong if all the bolted connections would be hinged connections. The welded connections provided sufficient stability for the shell under these load conditions. Therefore, ULS4 and ULS5 are excluded from the design process and only have to be verified in the detailed structural analysis.

A second point is the difference in joint stiffness distribution between ULS 1 and ULS 2. The differences would lead to big differences in the initial design of the connections. This could create an oversized structure in all load combinations. To prevent this, a different design optimum has been manually found for ULS 2. This resulted in a similar optimum for the optimisation function, which makes it easier to define an appropriate connection design for all joints in the structure. The adjusted stiffness values are presented in table 6.10.

	ULS1	ULS2	ULS3	ULS4	ULS5
k_a	11800	13800	2500	1	1
k_b	18300	4800	8600	1	1
k_c	8500	7800	7500	1	1
k_d	31400	29500	9300	1	1
k_e	8800	13900	1700	1	1
BLfac	10,01	10,09	10,02	<0	<0

Table 6.9: Initial stiffness estimate based on the optimisation

	ULS1	ULS2	ULS3	ULS4	ULS5
k_a	11800	6200	2500	1	1
k_b	18300	10200	8600	1	1
k_c	8500	7800	7500	1	1
k_d	31400	29500	9300	1	1
k_e	8800	8000	1700	1	1
BLfac	10,01	10,09	10,02	<0	<0
UC	0,11	0,11	0,16	0,12	0,13
u	16,9	23,11	22,78	47,6	51,35

Table 6.10: Initial stiffness estimate adjusted for compatibility of the load combinations

Now, the load ratios on the connections can be determined in a similar way as for the design in chapter 5. However, the clusters of joints are of a larger size in the case study. Therefore, an extra step is needed to determine the governing situation for each connection design. As all considered load combinations result in compression, only negative load ratios are expected. Therefore, the minimal occurring load ratio in each cluster of connections is the governing one. Table 6.11 shows the governing load ratios for each connection.

$ M_y /N$	ULS1	ULS2	ULS3
a	-0,02	-0,06	-0,07
b	-0,05	-0,09	-0,10
c	-0,01	-0,11	-0,13
d	-0,02	-0,06	-0,08
e	-0,01	-0,08	-0,07

Table 6.11: Initial load ratio on the connections

Design iteration

Table 6.11 shows that all load ratios are between -0,2 and 0. This means that they all fall within the capped-off part of the design diagram. Therefore, for every connection in every load combination an estimate of the stiffness is made based on a load ratio $|M_y|/N = -0,2$. A subsequent consequence is that stiffness design iterations will not lead to changes in the design if the load ratios stay between -0,2 and 0, after the first selection of the connections has been made. This reduces the required design space to a one-dimensional stiffness range, from which connection designs can be immediately selected based on the required stiffness. Table 6.12 shows the selected connection design and the resulting estimate for the stiffness. Figure 6.12 shows the selection of the connections based on the design diagram.

Connection	Design (see table 6.8)	New stiffness (kNm/rad)	Mass (kg)
a	2. Spaced + Caps	13800	22,1
b	5. SHS160 M20 + Caps	19600	26,5
c	8. SHS180 tp = 16	8000	32,4
d	7. SHS180 + Caps	31100	36,9
e	9. Max	8900	34

Table 6.12: Design selection and stiffness estimate for the different connections

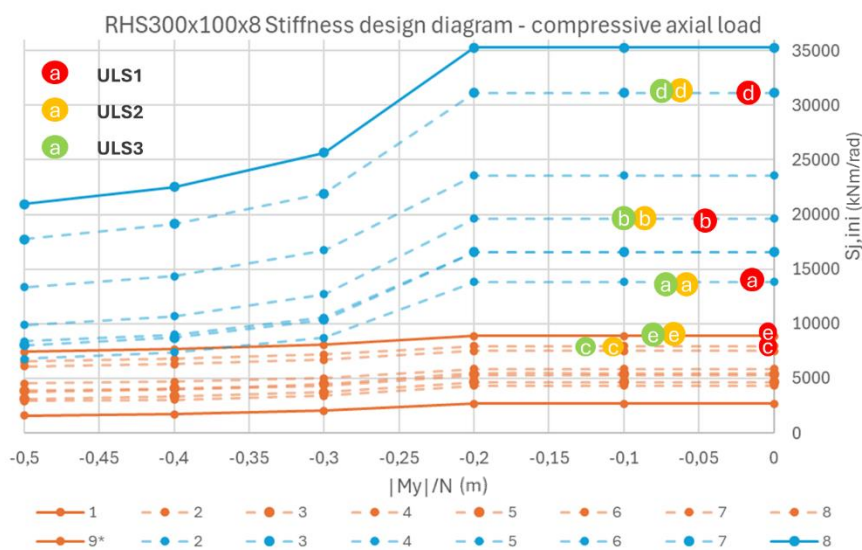


Figure 6.12: selection of the connection designs with the design diagram, based on load ratios and required stiffness

Stiffness analysis and structural verification

After the selection of the connection design the stiffness analysis can be performed to verify the stiffness estimates. For each connection, the largest axial force is applied and bending moment is increased to the point where $|M|/N = -0,2 \text{ m}$. This gives the stiffness that is used in the structural model. The results of the stiffness analysis are presented in table 6.13. Table 6.14 gives the results of the structural analysis after adjustment of the stiffness values. Figure 6.13 shows the first buckling mode of the structure, the buckling mode is similar in all load combinations. A global buckling behaviour can be observed.

Connection	Maximum axial force (N [kN])	Bending moment ($M = -0,2*N$)	Results stiffness analysis (kNm/rad)
a	-99	19,8	13840
b	-100	20	19607
c	-98	19,6	7945
d	-103	20,6	31112
e	-88	17,6	8763

Table 6.13: Input and results stiffness analysis

	Design criteria	ULS1	ULS2	ULS3	Check
Blfac	≥ 10	10,05	10,70	12,51	OK
UC	≤ 1	0,11	0,15	0,13	OK
U (mm)	≤ 112	16,9	22,7	20,9	OK

Table 6.14: Design criteria after structural verification

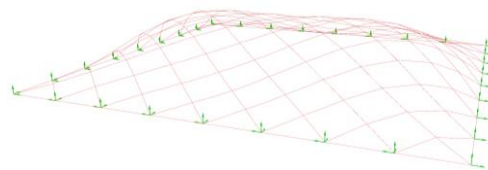


Figure 6.13: Buckling mode of the structure

Final design

Now, the design for the shell can be concluded. The final design of the connections is shown in figures 6.14 and 6.15. Figure 6.14 shows the location of the connections in the shell. Nodes without an assigned connection design are rigid joints. Figure 6.15 shows the specific connection designs that are selected from table 6.8.

Excluding the edges, the shell consists of 113 joints, of which 65 (58%) are partly reversible, with two elements welded to the node and two elements bolted to the nodes during installation. The other 48 joints (42%) are rigid and pre-assembled by welding the elements to the nodes.

The weight of the different connections is listed in table 6.15. The total weight of the connections is 3480 kg, which is approximately 11% of the mass of the structural elements.

The mass of the rigid connections is 32,2 kg and the average mass of the reversible connections is 29,7 kg. The choice for bolted connections instead of welded connection does not lead to significant advantages in material use. However, the bolted connections are essential for the constructability of the shell. Furthermore, the weight of the reversible connections can be improved by a more detailed approach to the clustering of the joints in the design phase.

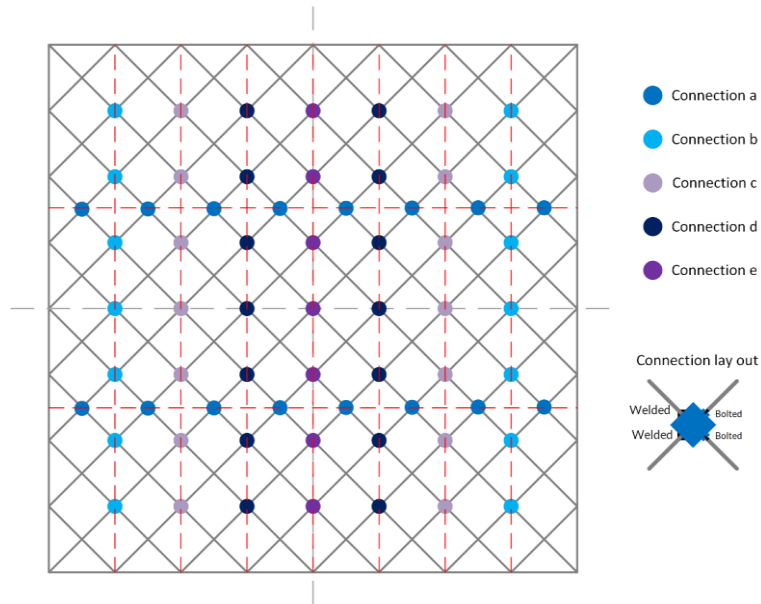


Figure 6.14: Connection design in the shell structure

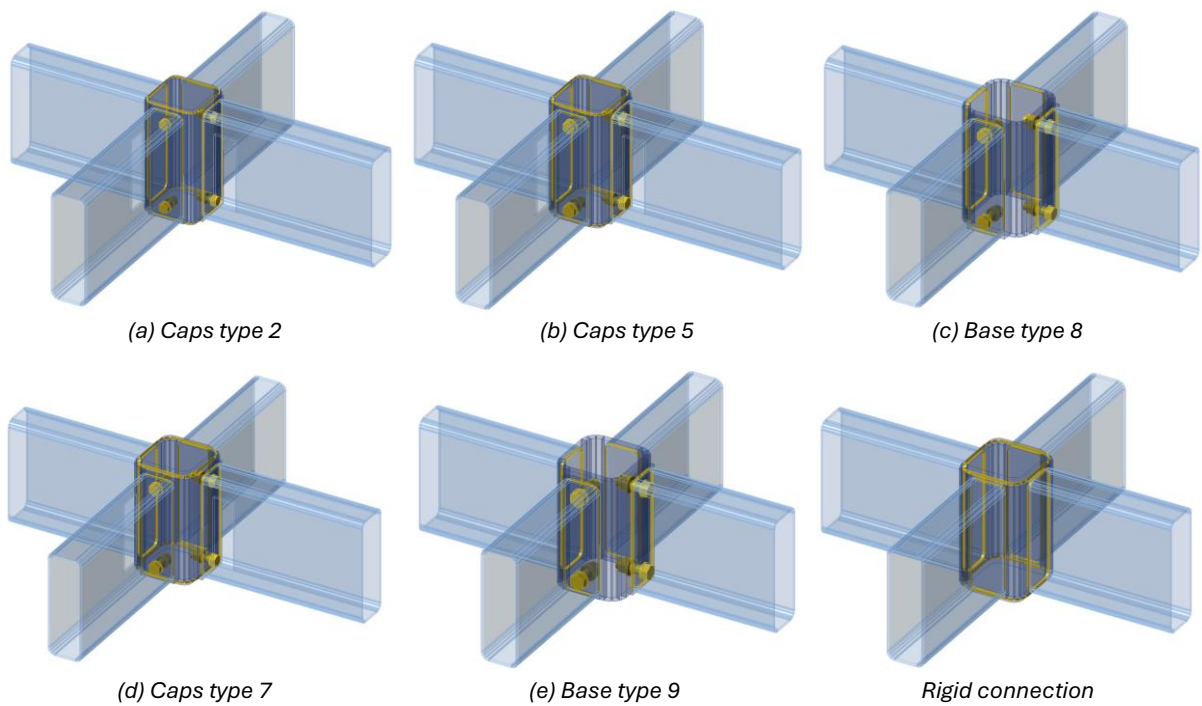


Figure 6.15: Selected connection designs for the case study, selected from table 6.8

Connection	Mass of one connection (kg)	Number of nodes in the structure	Total mass of the connection type (kg)
a	22,1	16	354
b	26,5	14	371
c	32,4	14	454
d	36,9	14	517
e	34	7	238
Rigid	32,2	48	1546

Table 6.15: Mass of the connections

6.3 Additional fictional load combination

Section 6.2 presents the application of the design method for the case study. It is found, that in load combinations ULS1, ULS2 and ULS3 the structure is highly compressive, which results in small load-ratios. Additionally, in ULS4 and ULS5 the upward wind loading in combination with the rigid connections already leads to a sufficiently stiff and stable structure in the case that the bolted connections are classified as hinged. The remaining design load ratios for ULS1, 2 and 3 then all fall within the capped-off peak of the design diagram, which simplifies the design process by eliminating the need for iterations.

However, for sake of showing the functioning of the design method, it is more interesting to see the full functionality of the method. Therefore, in this section, a fictional load combination will be applied to the structure of the case study. This load combination is designed to create higher bending moments in the structure, resulting in larger load ratios.

The fictional load case is an asymmetric load with downward load on half of the structure and a smaller upward loading on the other half. The load case is shown over a cross-section of the shell in figure 6.16. The fictional load combination is written below.

$$ULS6 = LC1 (self-weight) + fictional load case$$

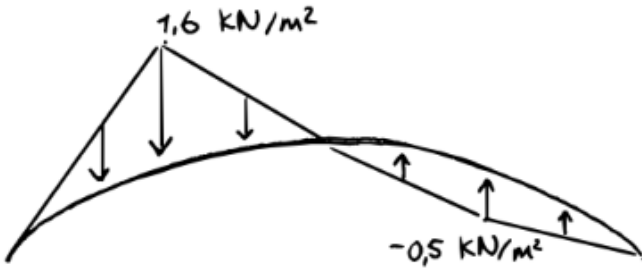


Figure 6.16. Fictional load case

For the connection design, the same design diagram as shown in figure 6.9 can be used. Therefore, we proceed immediately to the initial stiffness design. Table 6.16 presents the results and the resulting load ratios.

	k (kNm/rad)	Load ratios (m)	Connection design
a	7793	-0,36	9. Max or 2. Spaced + caps
b	9000	-0,71	5. SHS160 M20 + caps
c	6355	-0,22	8. SHS180 t _p =16
d	19000	-0,61	8. SHS180 t _p =16 + caps
e	2350	-0,26	1. Base

Table 6.16. Results of the initial stiffness optimisation

With the design diagram and the initial stiffness design, the design iterations for the structure can be performed for the fictional load combination. Figure 6.17 shows the locations of the different connections in the design diagram, based on the stiffness and load ratio a neighbouring design is selected, these designs are also included in table 6.16. This is indicated by the blue circles in the figure. The results of the design for ULS1, 2 and 3 are also included in the figure for reference.

As explained in chapter 5, in the first iteration the design of the connections is selected separately for every load combination. However, in the final design the design of the connection should be equal in every load combination. Therefore, some of the design choices must be adjusted. As can be seen in figure 6.17.

For connection a, at a stiffness of 7800 kNm/rad and a load ratio of -0,36 m, there are two possibilities for the connection design. These are connection 9. Max or connection 2. Spaced with added stiffener caps. Based on joint complexity connection 9 would be preferred over a connection with stiffener caps. However, the diagram shows that based on the requirements in the other load combinations, only connection 2 with stiffener caps satisfies the requirements for connection a in every load combination. Therefore, connection 2 Spaced + caps should be selected.

For both connection b and c, it can be seen that the connection design for the fictional load combination is the same as the connection design based on the other combinations. Therefore, the selected connection design can be used (5. SHS160 M20 + caps and 8. SHS180 $t_p = 16$ respectively).

For connection d, the diagram shows that the requirements for the connection design in the fictional load combination are governing of the requirements in the other load combinations. To ensure a connection design that satisfies all load combinations, the design of the initial case study should be adjusted to 8. SHS180 $t_p=16$ + Caps.

For connection e, the opposite happens where the requirements for ULS1, ULS2, and ULS3 are stricter than the requirements for the fictional load combination. Here the connection design for the fictional load combination should be adjusted to connection 9. Max.

The adjustments are indicated with arrows in figure 6.17. Table 6.17 presents the new stiffness estimates that result from the changes, concluding the first iteration.

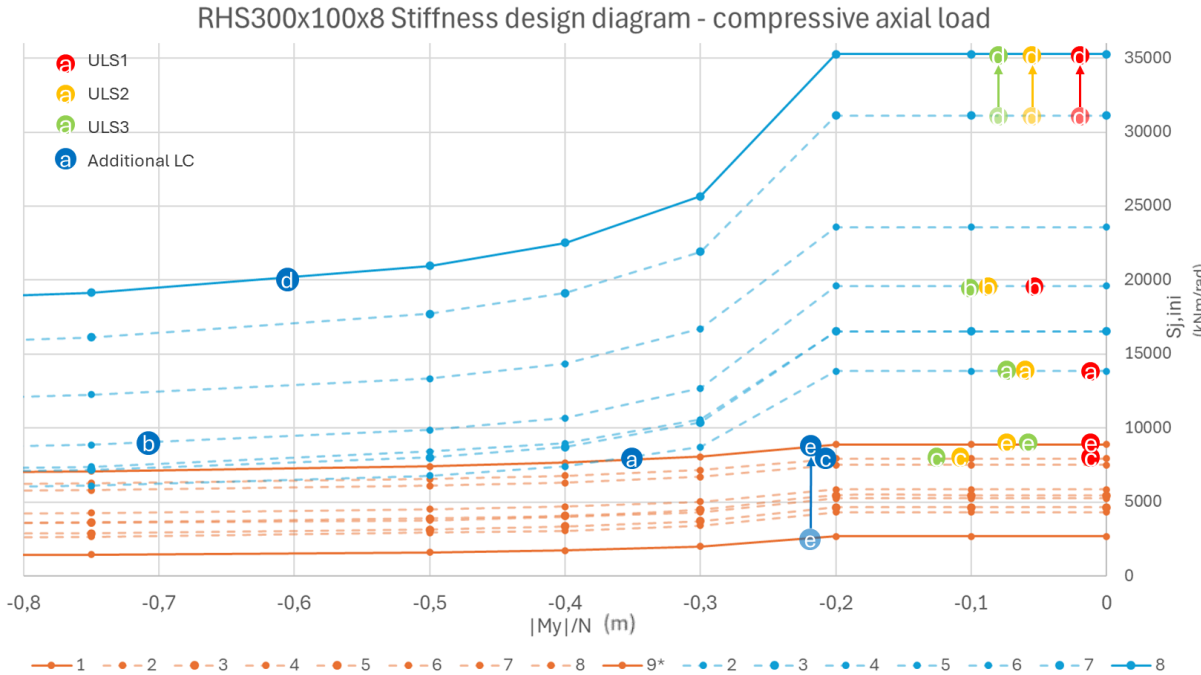


Figure 6.17. Design diagram with selection of connection designs for the fictional load combination

	Connection design	New stiffness estimate
a	2. Spaced + caps	8202
b	5. SHS160 M20 + caps	9110
c	8. SHS180 $t_p=16$	7700
d	8. SHS180 $t_p=16$ + caps	20160
e	9. Max	8400

Table 6.17. Adjusted selection of the connection design and adjusted stiffness estimates

The second iteration starts with the evaluation of the changed load ratios resulting from the new stiffness distribution. In this and the next iterations, the stiffness can be estimated with the design diagrams, based on the connection design and load ratios. The iterations are shown in table 6.18. The difference between iteration 2 and iteration 3 is sufficiently small to terminate the design loop after iteration 3. The process of the iterations is also illustrated in the design diagram in figure 6.18.

	Results iteration 1		Iteration 2		Iteration 3	
	Connection design	Stiffness estimate	Load ratio	Stiffness estimate	Load ratio	Stiffness estimate
a	2.+caps	8202	-0,36	8202	-0,36	8202
b	5. + caps	9110	-0,74	8910	-0,74	8910
c	8.	7700	-0,28	7325	-0,27	7400
d	8. + caps	20160	-0,65	19880	-0,65	19880
e	9.	8400	-0,17	8763	-0,17	8763

Table 6.18. Design iterations

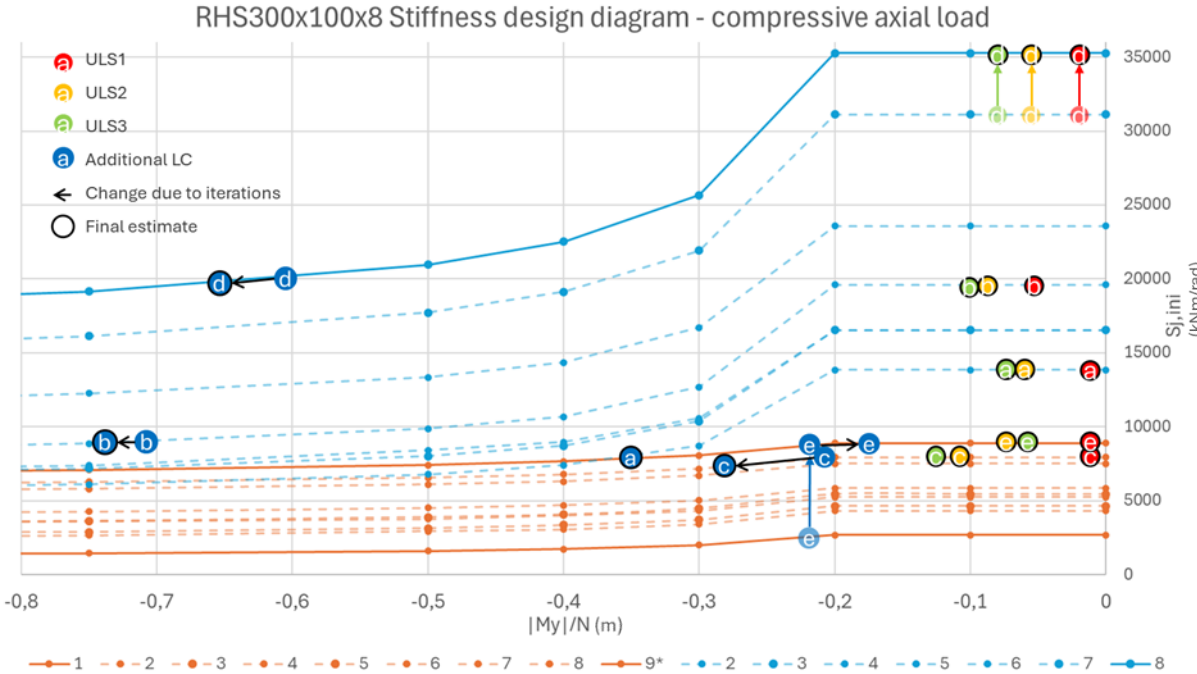


Figure 6.18: Iteration of the stiffness of the connections

With the design iterations concluded, the finalisation of the design can be performed analogous to the method as presented in chapter 5 and section 6.2. A simple verification of the new design including the fictional load case is presented in table 6.19.

The application of the fictional load cases leads to a very similar design of the grid shell. With as only difference the change of connection d from connection type 7 with stiffener caps to connection type 8 with stiffener caps.

	Design criteria	ULS1	ULS2	ULS3	Fictional combination
Blfac	≥10	10,07	10,72	12,52	10,42
UC	≤1	0,11	0,15	0,14	0,17
U (mm)	≤112	16,9	22,7	20,9	27,5

Table 6.19. Design verification including the fictional load combination

7 Discussion

7.1 Connection design

The literature review shows that limited research is available on the general aspects of grid shell connections. Codes and guidelines mainly focus on common steel frame connections. Therefore, studies on grid shell connections are often directed at testing a specific connection design (*Feng et al., 2015; Ge et al., 2020; Lopez et al., 2007; Ma et al., 2016*). This provides little background for a general design method for grid shell connections.

Grid shell connections differ from regular frame connections. They are often loaded in axial direction, whereas frame connections are generally subjected to bending moments and experience axial loads to a lesser extent. Because of these specific characteristics of grid shell connections, structural analysis is best performed with finite element methods. Nevertheless, the component method, that is widely used for the design of steel connections, provides a desirable basis for parametric design of the connections. The component based finite element method (CBFEM) combines the component method with a finite element analysis. Therefore, CBFEM can be considered an adequate approach for the design and calculation of grid shell connections. It returns more accurate results than the standard component method based on analytical formulations, but allows for easier parametrisation of the connection, than with most FEM software.

Influence of the load ratio: The research in chapter 3 is founded on the assumption that the axial loads on grid shell connections play an important role in their structural behaviour. Compression could significantly influence the stiffness of the connection. When this assumption is used in the design of the connection, the design deviates from the Eurocodes. Research on the connection, that is defined in section 3.2, shows that compressive loads can significantly increase the rotational stiffness of a grid shell connection.

Results presented in section 3.3 indeed show the increase in rotational stiffness for small M/N-ratios. However, some inconsistent results are found for very small load ratios. Figure 3.12 shows a decrease in the stiffness for very small load ratios. Under these load conditions, rotations in the model are too small for accurate calculation of the stiffness. Several investigations have been performed to determine for which load ratios the results of the stiffness analysis do give reliable results. A parametric study shows that inconsistencies in the definition of the model are likely not the cause. Furthermore, patterns in the results, hand calculations based on the Eurocode, and design diagrams in later stages of the project seem to indicate that the increase in rotational stiffness for high axial loads is valid. However, this cannot be concluded with certainty from the performed investigation. Physical testing or improvements in the finite element software must be performed to demonstrate the validity of the proposed assumption. Therefore, in practice the point up to which the results of the calculation are true cannot be safely assumed.

Parameters for connection design: Section 3.4 researches the influence on several design parameters on the rotational stiffness of the grid shell connection. The spacing of the bolts, the dimensions of the centre box and the thickness of the endplate can be applied to increase the stiffness. For the base connection, as described in section 3.2.1, a range of stiffness can be achieved between 85 kNm/rad and 137 kNm/rad. Thus, an increase of 61% could be achieved for the stiffness of the connection by adjusting the design parameters.

The stiffness can be increased further with different design operations. Which are, for example, the addition of stiffeners or an extra bolt row. With the addition of stiffeners the stiffness of the connection increased to a range from 175 kNm/rad for the base connection to 378 kNm/rad when the design parameters are adjusted. This is an increase of 116% by adjusting the three design parameters. When a bolt row was added to the design a range of 419 – 766 kNm/rad could be realised. For the base connection a range of stiffness from 85 kNm/rad to 766 kNm/rad could be achieved by adjustment of predetermined design adjustments, which is an increase of 801% compared to the base connection.

However, it should be noted that the effectiveness of the design parameters and design operations depends on the connection type and the loading conditions. The range above is achieved for a load ratio of $M_y/N = -0,1$ m. The result will be different for other load conditions. This can be seen in the design diagram in figure 3.17, for as load ratio of $M_y/N = -2,0$ the achieved range is 58 – 475 kNm/rad (an increase of 711 %). Also, during the design phase of the project, results show that the effectiveness of parameters depends on the loading conditions. For example, bolt diameter and thickness of the endplate are most effective for connections that are loaded mostly in bending. The tensile stiffness of the bolts and bending of the endplate do not contribute to the stiffness of the connection when the connection is mostly loaded in compression.

Furthermore, the list of considered design parameters is not exhaustive. Depending on the connection design other design parameters might work just as well.

Connection design from requirements: The research on the connection design is concluded with the generation of a design diagram, which can be used to select a connection design based on the required stiffness and the corresponding load ratio on a joint.

The generation of the design diagram does still require the design and evaluation of multiple connection designs. However, these designs originate from an easy to define base connection. The design diagram provides a framework in which a motivated choice for a connection design can be made. This eliminates the trial-and-error in the approach towards connection design. From the design phase of the project, it can be concluded that the design diagrams can help with accurate estimates of the connection stiffness during the design of a grid shell with semi-rigid joints.

7.2 Joint stiffness in grid shell structures

Research on grid shells focusses on different important characteristics of grid shell design. However, studies on the influence of joint stiffness on grid shell structures are not widely available. Results are focussed on dome grid shells with a triangular grid (*Lopez et al., 2007; Fan et al., 2011; Ye & Lu, 2020*). In practice, quadrangular grid shells and shells with free edges are much more common. Also, studies investigating the effect of the separate joint stiffness parameters are scarce (*Li & Taniguchi, 2020*). Studies researching the effect of boundary conditions and bracing on grid shell stability provide some insight (*Venuti & Bruno, 2018; Venuti, 2021; Feng et al, 2012; Wang et al., 2016*). However, general rules for design with semi-rigid joints cannot be formulated.

That the research is mostly focussed on specific grid shells is understandable. Different types of grid shell can have a different structural behaviour. For example, the support conditions can strengthen shell behaviour and the choice for a triangular or quadrangular grid determines whether the shell behaves isotropic or orthotropic. This study investigates a quadrangular grid shell with different boundary conditions. Therefore, results from this project are also specific to a certain type of grid shell structure. Still, the case study shows that lessons regarding the design of grid shells can also be adapted to grid shells with different shapes and grid orientations.

Influence of different stiffness parameters: Section 4.2 researches the influence of the six stiffness parameters (axial stiffness (k_a), in-plane shear stiffness (k_{sy}), out-of-plane shear stiffness (k_{sz}), torsional stiffness (k_t), out-of-plane bending stiffness (k_{by}), and in-plane bending stiffness (k_{bz})) on the structural performance of the quadrangular grid shell. Results show that the axial stiffness and the out-of-plane bending stiffness are important for the stability and stiffness of a grid shell. Boundary conditions provide in-plane stiffness of the grid, when the shell has free edges the in-plane shear stiffness and in-plane bending stiffness of the joints become relevant for stability of the shell. For larger grid shell structures or grid shell structures that approximate the funicular shape more closely, the relevance of the in-plane stiffness parameters for the structural performance also increases. This is shown in figure 4.18. For a small shell of 6x6 m with fully supported edges (FC-shell), changing the in-plane bending stiffness from rigid to pinned reduced the buckling load factor from 116,5 to 77,6, which is a reduction of 33%. For a shell of 18x18 m the buckling load factor was reduced from 8,5 to 2,5, a reduction 67%. For a shell with laterally supported edges (PC-shell) the differences is even greater, the reduction in buckling load factor for the small shell was 33% from 39,5 to 26,6, while the reduction for the larger shell was 85% from 3.51 to 0.53. Out-of-plane shear stiffness and torsional stiffness have limited influence on the structural behaviour of the researched grid shell.

Using these results requires some precautions. The research is performed with other parameters in rigid state. Interaction between the parameters is not studied but could significantly influence the structural behaviour.

Stiffness and load ratios: The consequence of the inclusion of the axial load in the determination of the connection stiffness is that the load ratios that result from the structural analysis influence the stiffness of the connections. This will lead to an iterative design process.

The influence of the out-of-plane bending stiffness of the joints on the loads on the connections is investigated. The effect varies greatly over the different load combinations and is, therefore, unpredictable. In a symmetric load combination, the influence shows an expected response. However, for asymmetric conditions such as wind loads, the load ratios are more unpredictable and varies throughout the structure. This is caused by variations in the axial stress throughout the structure in these load combinations. Also, the occurrence of tensile forces can increase the irregularity of the results.

The research does not consider the effect of axial stiffness on the load ratios. Section 4.2 does show an effect of axial stiffness on the buckling, displacement and utilisation of the shell. Thus, it can be assumed that the effect on the load ratios is considerable. In this thesis, this is not included, in the design phase connections are assumed to have a rigid axial stiffness.

7.3 Design of a grid shell with semi-rigid joints

In figure 5.1, a methodology for the design of grid-shells with semi-rigid joints is proposed. This methodology is applied to two different structures in chapters 5 and 6. In this section, the results, applicability, limitations and challenges of the method are discussed. An evaluation of the design method is performed based on the design challenges that are identified as a result of the research phase, these challenges are mentioned in section 4.4.

In section 5.2 an example design is performed on a simple shell structure. The structure consisted of 40 beams and 25 nodes. All of the nodes are reversible. The total mass of the nodes is 75 kg, which is 20% of the mass of the structural elements.

In section 6.2 the design method is applied to a case study of the C30 Shell. Because of the increased size, rigid connections were required that provided in-plane stability of the grid. The design resulted in a structure with 113 joints, of which 58% (65 joints) are designed as reversible

connections. The remainder are welded connections. The total mass of the connections was 3480 kg, which made up approximately 11% of the weight of the structural members. The average mass of the reversible joints was slightly lower than the mass of the rigid connections (29,7 kg vs. 32,2 kg). The weight of the reversible connections varied between 22,1 kg and 36,9 kg. Therefore, although the average weight of the welded connections is higher, the heaviest connections in the structure were reversible designs. However, the possibility for design of reversible connections is beneficial for the constructability of the grid shell.

Iterative stiffness design: The interdependency of the joint stiffness and the load ratios result in an iterative design process for the determination of the stiffness of the selected connection designs. Chapter 5 showed that the design loop converged sufficiently quickly. Within three iterations after the selection of the connection designs, the changes in the load ratios and stiffness became almost zero. The design loop showed to be a good method to quickly arrive at a feasible design.

Also, the stiffness estimates that are made using the design diagram are accurate. For ULS 2 and 3 in chapter 5, an average deviation 2,2% of the results of the stiffness analysis from the estimates was found. This justifies the use of the design diagrams for estimating the stiffness of the selected connection designs. For ULS1 the estimates deviated more (approximately 8,9%). This is because these estimates were made for load ratios around the peak in the stiffness diagram. The exact peak was not captured in the design diagram. This can be solved by either determining the exact location of the peak value, creating extra data points around the peak values or by capping the values before the results become unpredictable.

In the case study in chapter 6, the last of these options is applied. For this specific case, this had the result that the design space was simplified to a one dimensional design space, because the load ratios occurring in all of the relevant load combinations were inside the capped-off range. This resulted in an elimination of the iterative process for determining the stiffness of the connections. Reducing the complexity of the design process. Assessment of an additional fictional load combination showed that the design diagrams could also accommodate the iterative process in this case.

Normative load combinations: The consideration of the effect of the load ratio on the stiffness of a connection creates an increased complexity in the evaluation of the load combinations. The stiffness of a connection can be different in every load combination. Therefore, loads are no longer the only main factor in determining the governing load combinations. In chapter 5, this is solved by defining the required connection design for every load combination separately. After that, the connection design that has a sufficient stiffness for the occurring load ratio in every load combination can be selected. A second consequence is that extra load combinations might be required compared to a design with a fixed joint stiffness. In case of a fixed joint stiffness, ULS 3 (asymmetric snow load with favourable self-weight) would not be normative in the design of the case study. However, in this case the uniform loading from the self-weight reduces while the asymmetric snow load remained equal. This increases the moments in the construction and reduces the axial load, resulting in larger load ratios and, therefore, potentially a lower stiffness.

Joint stiffness optimisation: in the current design methodology the initial stiffness design plays a very important role. Therefore, it is important to have an adequate optimisation strategy. Unfortunately, the stiffness of the connections is not linearly linked to the mass or the constructability of the connections. In the performed design approach, the optimisation is linked to the design diagram that is used for the selection of the connections in the next step. This way, both mass and constructability of the connections is considered in the optimisation. However,

the optimisation is still set-up through trial-and-error. In chapter 5, the optimisation seems to result in a satisfactory distribution, resulting in an efficient structure. In the case study, the optimisation also resulted in different stiffness distributions. However, the distribution over different load combinations seemed to achieve different local minima creating large differences in the requirements. Had the initial result of the optimisation been used, this would have resulted in an oversized structure in all load combinations.

The confusion in the load optimisation of the different stiffness values in the case study could also be caused by an ineffective clustering of the joints. In the performed design, loading on the different joints did not vary much. Here it could help to have a better understanding of the interaction between different connections. It can be helpful to determine how the stiffness of certain joints influences the performance of others and which ones are normative at a given stiffness distribution. This could help to improve the clustering of the joints at the start of the design, which is essential for a satisfactory result.

Design of larger grid shells: An increase in the size of the designed shell is assumed to increase the complexity of the application of the design method for multiple reasons. The importance of in-plane stiffness parameters has shown to increase for larger shells, an increase in size results in a quadratically increasing number of connections, and load combinations become increasingly harder to analyse with increasing size.

In the case study, the problem of an increasing importance of in-plane bending stiffness has been solved by segmentation of the shell into pre-fabricated parts. This allowed for rigid connections to be included in the design, resulting in sufficient in-plane stability.

The increase in number of connections is approached by clustering the connections into comparable groups. However, in the design the clusters were defined based on geometry. Optimisation results and results from chapter 5 seem to indicate that clustering based on structural requirements might be more suitable. How this would need to be performed requires extra research.

Besides the previously expected challenges, some other learnings can be drawn from the performed design exercises. Also, some limitations of the method and opportunities are discussed.

First, it is important to identify if the combination of standard load combinations with the application of varying stiffness results in the governing loading situations. To determine this, it needs to be clear that a reduction in the loads from the different load combinations cannot lead to a more critical situation. In the design, three load situations can be identified. In case of a uniformly distributed downward loading (ULS 1 in both designs), this is not expected to lead to problems. A decrease in loads is not expected to affect the load ratio on the joints. This changes with asymmetric load combinations. In case of the asymmetric snow load, an overestimation of the permanent loading reduces the load ratios. In the case study, this can be seen in ULS 3, although here loads are lower, the load ratios in ULS 3 are the highest. In the case study, this did not result in any adjustments in the design, because of the capping of the design diagram. In general, for asymmetric load combinations the ULS load is assumed to be governing. A reduce in the asymmetric load can be expected to reduce the load ratios and the magnitude of the loads.

A second aspects that comes forward in the design process is that the proposed method does not take over the work of the structural engineer. The design method aids the process and helps to structure the design. However, the method does not dictate any design choices. Manipulation of the results to arrive at a satisfactory design still needs to be done manually. This is seen in the connection design and generation of the stiffness ranges, the adjusting of the optimisation results

in the case study to prevent an oversized structure, the definition for the clustering of similar connections, and the determination and evaluation of the governing load combinations. What the method does do is help structure a design space for the connection design, enabling an efficient design choice for connections based on pre-determined requirements. It also provides a framework for an iteration towards the actual interaction between joint stiffness and load ratios. Resulting in a structures design methodology for grid shell with semi-rigid connections.

Limitations and opportunities

- In the current method, it is not possible to design for more than one stiffness parameter, which is the out-of-plane bending stiffness. Influence of in-plane bending stiffness and axial stiffness could be considerable but is left out of the design for now.
- Only a linear stiffness definition can be applied at this point. Inclusion of joint moment capacity or non-linear stiffness definitions for the connections could increase the performance of the design method. The consideration of elasto-plastic behaviour of the connections could improve the design efficiency. Also, relating the stiffness directly to the load ratios in the structure could streamline and simplify the design process.
- This report does not extensively consider the production and installation of the grid shell and the connections. It is aimed at defining a feasible framework. Characteristics of the connection design and segmentation of the structure should be kept in mind.
- The design method might not only be applicable to grid shell structures. The method could be beneficial for special structures with steel connections loaded in bending and normal force. Also, in frame connections the method could be applied. Because the connections are mostly loaded in bending, this would result in a one dimensional design space for these types of structures.

8 Conclusion and recommendations

8.1 Conclusion

The research question to be answered in this project is:

How can a semi-rigid approach to steel connection design and considering the semi-rigidity of the joints be combined in a parametric design strategy for grid shells?

Based on the performed research and design exercise, an answer to the research question can be formulated. A semi-rigid approach to connection design and the inclusion of semi-rigidity of the joints in the structural design of a grid shell can be combined in the design of a grid shell. This can be achieved by defining a relation between the connection design and the joint stiffness design. This way, a design space can be created that links the connection design to pre-determined stiffness requirements and load ratios in the structural design. Which allows for efficient design iterations and eliminates guesswork in the design of both the connection and the joint stiffness distribution of the shell.

Conclusions

Some specific conclusions can be drawn to clarify the answer to the research question:

- A design method is defined which enables the design of a grid shell with semi-rigid connections based on results from an optimisation of the joint stiffness. For a small grid shell of 6x6 m this resulted in a design with 100% reversible connections that were designed based on specific stiffness requirements. The case study of a larger shell resulted in a structure with 58% reversible connections. The mass of the connections compared to 20% of the mass of the structural member for the small shell and 11% for the larger shell.
- Considering the effect of axial loading on the rotational stiffness of a grid shell connection can lead to a significant increase in the achieved stiffness of the connection. Which is beneficial in compressive structures, such as grid shells. However, stiffness results for very small load ratios should be used with caution.
- Parametrisation of a basic connection design can be applied to create a design space, which can be used to aid in the selection of a connection design, based on pre-determined stiffness requirements.
- The influence of joint stiffness on the structural performance of a grid shell depends on the characteristics of the shell. In general, it can be assumed that out-of-plane bending stiffness is relevant for the structural performance. Axial stiffness can play an important role, but its relevance depends on the connection design. The relevance of other stiffness parameters depends on the rigidity of the design, which is a consequence of support conditions, grid design, size, and shape of the shell.

- The combination of a joint stiffness optimisation and a parametrised connection design space can be combined to create a feasible design method. When the ratio between the axial loading and the bending moment on the joints is considered, this will result in an iterative process. This iteration seems to converge within 3 iterations, when a design space based on the connection design and load ratios is used. At the end of the iterations, estimates made using reliable parts of the design diagrams had an average deviation of 2,2% compared to the results from the CBFEM stiffness analysis. Around the peak values this increased to 8,9%, but this can be avoided by capping of the peak before the results become unpredictable.
- The initial design of the grid shell is important for an efficient result of the design method. The initial stiffness optimisation, the segmentation of the structure, and the clustering of the joints are essential for the method to result in an efficient grid shell design.

8.2 Recommendations

For application of the proposed design method

- The design method does not replace the expertise of the structural engineer. For adequate implementation of the design method, it is important to thoroughly understand the structure. This is necessary to adjust and verify intermediate results of the design process when that is required.
- When considering the effect of the load interaction on the stiffness of the connections, it is important to realise that the stiffness can be different in different load combinations. Therefore, it is essential to have a clear overview of the governing load combinations and to regard all potentially normative situations.
- A structured parametric approach will significantly reduce the effort that is required to perform the initial design and the design iterations. The differentiation of the stiffness of the joints creates a lot of extra variation in the input and results of the calculation. It is easy to lose the overview when the approach is not structured well.
- The segmentation of the shell, for production, transport and stability, and the clustering of the separate joints, for reduction of computational complexity, influences the result of the joint stiffness design. To successfully benefit from the opportunities that the design method offers for the connection design, the structural requirements of the structure should be regarded when determining the starting points of the design.

For engineers and designers

- When designing spatial structures with connections that are loaded in compression, it can be beneficial to consider the influence of the axial loading on the stiffness of the connection. The current method as prescribed by the Eurocode for steel connections results in a conservative estimate for the joint stiffness in compressive structures.

- Consider the use of parametric design methods for complex structures. The application of these methods can help structure structural challenges and make it possible to efficiently evaluated many different design solutions.
- Be aware of the limitations of the calculation software that is used in the structural evaluation of structures and connections. Approaches that are verified for general use might become unreliable when they are applied unaltered to new structural problems.

For future research and development

- The research indicates that axial loads significantly influence the initial stiffness of a connection. However, stiffness calculation can be unreliable in case axial loads exceed bending moments. The effect of axial load on the stiffness of the connections should be further investigated. Specific attention should be given to very small load ratios.
- The increase of joint stiffness as a result of compressive forces can be interesting for the design of connections. For example, the use of prestressed bolts to achieve this effect artificially can be researched.
- Research showed that axial stiffness of the connections can have a considerable impact on the structural performance of grid shells. However, this has not been considered in the design. To get a better understanding of the influence of axial stiffness on the design, further research on the effect of axial stiffness on the structural behaviour grid shells and the axial stiffness that is achieved in the connection design should be performed.
- In the current design method, only one stiffness parameter can be considered. However, research has shown that multiple stiffness parameters can affect the design simultaneously. The design method can be developed further to assess possibilities for the inclusion of multiple stiffness parameters.
- The interaction between joints with different stiffness values in a grid shell structure is not well understood and difficult to oversee. Further research on the effect of varying the joint stiffness throughout the structure could improve the initial stiffness design, by realising a better base for an initial stiffness optimisation.

Bibliography

- Adriaenssens, S., Ney, L., Bodarwe, E., & Williams, C. (2010, February). Dutch Maritime Museum: Form-finding of an irregular faceted skeletal shell-Part b. In Symposium of the International Association for Shell and Spatial Structures (50th. 2009. Valencia). Evolution and Trends in Design, Analysis and Construction of Shell and Spatial Structures: Proceedings. Editorial Universitat Politècnica de València.
- Adriaenssens, S., Block, P., Veenendaal, D., & Williams, C. (2014). Shell structures for architecture: form finding and optimization. Routledge.
- Beckh, M., & Barthel, R. (2009). The first doubly curved gridshell structure-Shukhovs building for the plate rolling workshop in Vyksa. In Third International Congress on Construction History, Brandenburg University of Technology Cottbus, Germany, 20th-24th May 2009 (p. 1).
- Blaauwendraad, J., & Hoefakker, J. H. (2013). Structural shell analysis : understanding and application (Ser. Solid mechanics and its applications, v. 200). Springer.
- Broeders, K. (2021). A software-based optimization for design of steel halls: for steel halls with open sections and bolted end-plate connections
- Brühwiler, E. (2020). Heinz Isler's twin shell roof in Deitingen—preservation of a 'timeless wing beat'. Proceedings of the Institution of Civil Engineers-Engineering History and Heritage, 174(3), 133-138.
- Brütting, J., De Wolf, C., & Fivet, C. (2019). The reuse of load-bearing components. IOP Conference Series: Earth and Environmental Science, 225(1), 012025.
- Bulenda, T., & Knippers, J. (2001). Stability of grid shells. Computers & Structures, 79(12), 1161-1174.
- Çelik, H.K., & Şakar, G. (2022). Semi-Rigid connections in steel structures State-of-the-Art report on modelling, analysis and design. Steel and composite structures, vol.45, no.1, 1-21.
- Coenders, J. L. (2008). Structural Design – Special Structures. Reader for CT5251
- Crielaard, R. & Terwel, K.C. (2020). Dictaat constructief ontwerpen. CTB2320-17 Ontwerpen van Constructies en Funderingen 2.
- Díaz, C., Martí, P., Victoria, M., & Querin, O. M. (2011). Review on the modelling of joint behaviour in steel frames. Journal of constructional steel research, 67(5), 741-758.
- EC1 part 1-3. (2019). European committee for standardization, Eurocode 1: Actions on structures - Part 1-3: General actions – Snow loads. 2011.
- EC1 part 1-4. (2011). European committee for standardization, Eurocode 1: Actions on structures - Part 1-4: General actions – Wind loads. 2011.
- EC3 part 1-8. (2011). European committee for standardization, Eurocode 3: Design of steel structures - Part 1-8: Design of joints. 2011.

- Feng, R. Q., Yao, B., & Ye, J. H. (2012). The stability of elliptic paraboloid grid shell lighting roofs with semi-rigid joints. *Advanced Materials Research*, 374, 2148-2151.
- Feng, R. Q., Ye, J., & Zhu, B. (2015). Behavior of bolted joints of cable-braced grid shells. *Journal of Structural Engineering*, 141(12), 04015071.
- Fan, F., Ma, H., Cao, Z., & Shen, S. (2011). A new classification system for the joints used in lattice shells. *Thin-walled structures*, 49(12), 1544-1553.
- Ge, H. B., Wan, H. P., Zheng, Y., & Luo, Y. (2020). Experimental and numerical study on stability behavior of reticulated shell composed of plate members. *Journal of Constructional Steel Research*, 171, 106102.
- Grande, E., Imbimbo, M., & Tomei, V. (2020). Optimization strategies for grid shells: the role of joints. *Journal of Architectural Engineering*, 26(1), 04019028.
- Gohnert, M. (2022). *Shell structures: theory and application*. Springer Nature.
- IDEA StatiCa. (n.d.-a). *Connection design*. <https://www.ideastatica.com/connection-design>
- IDEA StatiCa. (n.d.-b). IDEA StatiCa Connection – Structural design of steel connections. <https://www.ideastatica.com/support-center/general-theoretical-background>
- IDEA StatiCa. (n.d.-c). *Steel Connection Material model*. <https://www.ideastatica.com/support-center/material-model>
- IDEA StatiCa. (n.d.-d). Stiffness analysis and deformation capacity of steel joints. IDEA StatiCa. <https://www.ideastatica.com/support-center/stiffness-analysis-and-deformation-capacity>
- Isufi, F. (2021). Parametric design of a grid shell roof over existing building, with a focus on connection design.
- Jaspart, J.-P. and Weynand, K. (2016). *Design of joints in steel and composite structures: Eurocode 3: Design of steel structure, Part 1-8-Design of joints; Eurocode 4: Design of composite steel and concrete structures, Part 1-1-general rules and rules for building*. Brussels: ECCS, 2016
- Koronaki, A., Shepherd, P., & Evernden, M. (2023). Fabrication-Aware Joint Clustering in Freeform Space-Frames. *Buildings*, 13(4), 962.
- Li, H.J., & Taniguchi, Y. (2020). Effect of joint stiffness and size on stability of three-way single-layer cylindrical reticular shell. *International Journal of Space Structures*, 35(3), 90-107.
- Liu, F., Feng, R., & Tsavdaridis, K. D. (2021, June). Form finding of assembled lattice structure considering the effect of joint stiffness. In *Structures* (Vol. 31, pp. 1096-1105). Elsevier
- López, A., Puente, I., & Serna, M. A. (2007). Numerical model and experimental tests on single-layer latticed domes with semi-rigid joints. *Computers & structures*, 85(7-8), 360-374.
- Ma, H., Fan, F., Zhong, J., & Cao, Z. (2013). Stability analysis of single-layer elliptical paraboloid latticed shells with semi-rigid joints. *Thin-walled structures*, 72, 128-138.
- Ma, H., Ren, S., & Fan, F. (2016). Experimental and numerical research on a new semi-rigid joint for single-layer reticulated structures. *Engineering Structures*, 126, 725-738.

- Malek, S. R. (2012). The effect of geometry and topology on the mechanics of grid shells (Doctoral dissertation, Massachusetts Institute of Technology).
- Malek, S., Wierzbicki, T., & Ochsendorf, J. (2014). Buckling of spherical cap gridshells: A numerical and analytical study revisiting the concept of the equivalent continuum. *Engineering Structures*, 75, 288-298.
- Mesnil, R., Douthe, C., Baverel, O., & Léger, B. (2017). Linear buckling of quadrangular and kagome gridshells: a comparative assessment. *Engineering Structures*, 132, 337-348.
- Mode Lab, Akos, G., & Parsons, P. (2014). *Foundations: The Grasshopper Primer Third Edition*.
- Octatube. (2020). C30 Shell. https://www.octatube.nl/nL_NL/project-item/projectitem/216-c30-shell.html
- Octatube. (2022). (Grid)shells. Octatube.com. Geraadpleegd op 15 januari 2023, van https://www.octatube.nl/nL_NL/systemen/systemitem/12-grid-shells.html
- Pottmann, H., Asperl, A., Hofer, M., & Kilian, A. (2007). *Architectural geometry*. (D. Bentley, Ed.) (1st ed.). Bentley Institute Press.
- Pottmann, H., Eigensatz, M., Vaxman, A., & Wallner, J. (2015). *Architectural geometry*. *Computers & graphics*, 47, 145-164.
- Preisinger, C. (2013), Linking Structure and Parametric Geometry. *Architectural Design*, 83: 110-113. DOI: 10.1002/ad.1564.
- Raad van de Europese Unie. (1996). Richtlijn 96/53/EG van de Raad. Publikatieblad van de Europese Gemeenschappen.
- Rutten, D. (2011). Evolutionary Principles applied to Problem Solving. I Eat Bugs For Breakfast. <https://ieatbugsforbreakfast.wordpress.com/2011/03/04/epatps01/>
- Rust, W. (2015). *Non-linear finite element analysis in structural mechanics*. Springer.
- Schlaich, M. (2011). *Conceptual design of light-weight structures*.
- Schober, H. (2015). *Transparent shells: Form, topology, structure*. John Wiley & Sons.
- Schueller, W. (1983). *Horizontal-span building structures*. John Wiley & Sons.
- Seifi, H., Javan, A. R., Xu, S., Zhao, Y., & Xie, Y. M. (2018). Design optimization and additive manufacturing of nodes in gridshell structures. *Engineering Structures*, 160, 161-170.
- Stephan, S., Sanchez-Alvarez, J., & Knebel, K. (Eds.). (2004). *Reticulated Structures on Free-Form Surfaces*. ResearchGate.
- Tomei, V. (2023). The effect of joint stiffness on optimization design strategies for gridshells: The role of rigid, semi-rigid and hinged joints. In *Structures* (Vol. 48, pp. 147-158). Elsevier.
- Tomei, V., Grande, E., & Imbimbo, M. (2023, September). Influence of joint rotational stiffness on the design optimization of grid shells. In *AIP Conference Proceedings* (Vol. 2928, No. 1). AIP Publishing.
- Van der Linden, L. P. L. (2015). *Innovative joints for gridshells*.
- TU Delft, Faculty of Architecture. (2014). *Grasshopper Kangaroo*. TOI-Pedia. http://wiki.bk.tudelft.nl/toi-pedia/Grasshopper_Kangaroo

- Venuti, F. (2021). Influence of pattern anisotropy on the structural behaviour of free-edge single-layer gridshells. *Curved and Layered Structures*, 8(1), 119-129.
- Venuti, F., & Bruno, L. (2018). Influence of in-plane and out-of-plane stiffness on the stability of free-edge gridshells: A parametric analysis. *Thin-Walled Structures*, 131, 755-768.
- Wang, X., Feng, R. Q., Yan, G. R., Liu, F. C., & Xu, W. J. (2016). Effect of joint stiffness on the stability of cable-braced grid shells. *International Journal of Steel Structures*, 16, 1123-1133.
- Williams, C. J. (2001). The analytic and numerical definition of the geometry of the British Museum Great Court Roof. *Mathematics & design*, 200, 434-440.
- Ye, J., & Lu, M. (2020). Design optimization of domes against instability considering joint stiffness. *Journal of Constructional Steel Research*, 169, 105757.
- Yeung, J., Walbridge, S., Haas, C., & Saari, R. (2016). Understanding the total life cycle cost implications of reusing structural steel. *Environment Systems and Decisions*, 37(1), 101–120.
- Yin, T., Wang, Z., Zheng, K., & Lu, S. (2022a). A New Method for Design of the Semi-Rigid Steel Frame—The Integration of Joint Inverse Design and Structural Design. *Buildings*, 12(7), 938.
- Yin, T., Wang, Z., Pan, J., Zheng, K., Liu, D., & Lu, S. (2022b). A Design Method for Semi-Rigid Steel Frame via Pre-Established Performance-Based Connection Database. *Buildings*, 12(10), 1634.
- Zuo, W., Chen, M. T., Chen, Y., Zhao, O., Cheng, B., & Zhao, J. (2023). Additive manufacturing oriented parametric topology optimization design and numerical analysis of steel joints in Gridshell structures. *Thin-Walled Structures*, 188, 110817.

Appendix A. Influence of load ratio M_y/N on initial rotational stiffness

To investigate the peak in initial rotational stiffness ($S_{j,ini}$) for low values of M_y/N .

Contents

Introduction.....	102
A.1 The connection	103
A.2 Influence of the load ratio on the initial rotational stiffness	103
A.3 Parametric investigation	105
A.4 Communication with IDEA StatiCa.....	108
A.5 Hand calculation of the initial rotational stiffness	109
A.6 Results on the mechanic behaviour	112
A.7 Conclusion	113

Introduction

This appendix contains the investigation of the increase and decrease of the initial rotational stiffness for small load ratios for the connection design that is discussed in chapter 3. This peak in the results is not as expected and some of the results are assumed to be unreliable. This appendix aims to investigate why the peak occurs and which values of the calculation can be assumed to be reliable and can, therefore, be used in the design of the grid shell.

The investigation starts with an introduction of the problem in sections A.1 and A.2. Then in section A.3 a parametric investigation is performed to verify if the input of the calculation is consistent. Section A.4 reviews communication with IDEA Statica about the issue. Then, section A.5 includes a hand calculation based on the Eurocode for steel connection design. Lastly, the mechanic behaviour of the connection that is revealed in results throughout the project is reviewed in section A.6. Section A.7 provides a conclusion on how the problem is approached in the thesis.

A.1 The connection

Figure A.1 shows the joint that is evaluated in the research. Structural rectangular hollow sections (RHS) are connected to a centre box by bolts that fasten the endplate to the centre box. The endplate is welded to the beam cross-section with butt welds.

Structural cross section:	RHS100x60x8
Endplate:	100x60x5
Bolts:	M12 8.8
Centre box:	SHS80x80x5
Steel:	S355

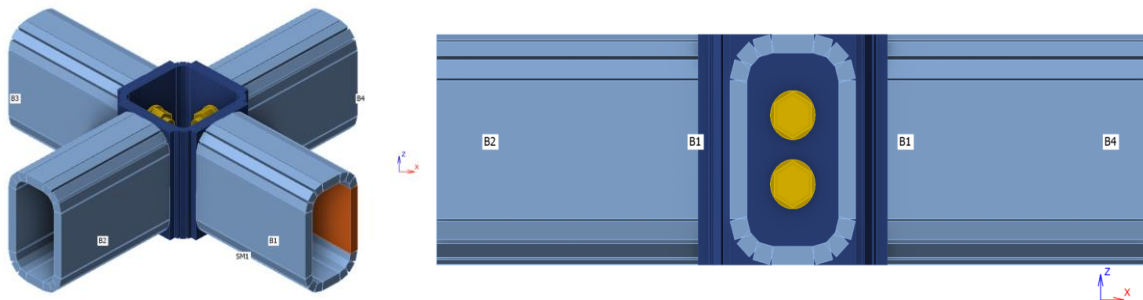


Figure A.1: Investigated connection

A.2 Influence of the load ratio on the initial rotational stiffness

The initial stiffness of the connection is calculated with the stiffness analysis of IDEA StatiCa software. IDEA StatiCa determines the moment-rotation diagram of the connection and specific loads. This is done by calculating the deformation of the connection for different factors of the loading. For this the loads are multiplied so that their ratio remains the same (*IDEA StatiCa, n.d.-d*). Therefore, the initial stiffness of the connection is only influenced by the ratio between the axial load and the bending moment. The magnitude of the loading does not affect the initial stiffness. Only the ultimate utilisation and the secant stiffness at the point of the applied loads is different.

Table A.1 gives the input and results of the assessment in IDEA StatiCa of the influence of the load ratio M_y/N on the initial stiffness of the connection. The initial rotational stiffness is plotted against the M_y/N -ratio in the diagram in figure A.2.

The results shows that the stiffness increases for low values of the M_y/N -ratio. The increase of stiffness for low load ratios can be explained by the schemes shown in figure A.3. Compression in the cross-section stabilises and stiffens the connection. For low load ratios a greater area of the cross section is in compression. Therefore, the connection has a higher initial stiffness. For higher load ratios the approach of a stable value can be explained by the fact that in the current configuration (compressive load and bending moment around the neutral axis) the area in compression can never be smaller than half the area of the entire cross-section.

However, further research into the lower range of the load ratios reveals an unexpected result. When decreasing the load ratio the initial rotational stiffness increases further. Only, after a certain value the stiffness starts decreasing, creating a peak in the initial stiffness. This creates a peak that can be seen in figure A.2. This peak cannot be explained through assumptions of the mechanical behaviour of the connection.

Name	Input			Initial stiffness				Secant stiffness		
	Comp.	Loads	M_{Ed} [kNm]	N [kN]	$M_{j,Rd}$ [kNm]	$S_{j,ini}$ [kNm/rad]	Φ_c [mrad]	L [m]	S_{js} [kNm/rad]	Φ [mrad]
B1	My	LE1	0,01	-2	0,79	96,7	8,18	1,5	96,7	0,1
	My	LE2	0,02	-2	1,4	128,9	10,82	1,5	128,9	0,16
	My	LE3	0,03	-2	1,81	248,2	13,97	1,5	248,2	0,12
	My	LE4	0,04	-2	2,09	272,8	15,49	1,5	272,8	0,15
	My	LE5	0,05	-2	2,23	252,8	21,25	1,5	252,8	0,2
	My	LE6	0,06	-2	2,28	213	23,56	1,5	217,8	0,28
	My	LE7	0,07	-2	2,28	181	24,17	1,5	184,5	0,38
	My	LE8	0,08	-2	2,33	152,9	29,58	1,5	158,8	0,5
	My	LE9	0,09	-2	2,33	135,9	31,23	1,5	140,8	0,64
	My	LE10	0,1	-2	2,28	125,2	32,29	1,5	127,4	0,78
	My	LE11	0,15	-2	2,19	96,9	38,35	1,5	96,9	1,55
	My	LE12	0,2	-2	2,14	85,6	41,31	1,5	85,6	2,34
	My	LE13	0,25	-2	2,05	79,6	38,8	1,5	79,6	3,14
	My	LE14	0,3	-2	2	75,9	38	1,5	75,9	3,96
	My	LE15	0,5	-2	1,91	68,7	36,3	1,5	68,7	7,27
	My	LE16	1	-2	1,86	62,2	37,06	1,5	62,2	16,08
	My	LE17	2	-2	1,86	59	38,82	1,5	43,8	45,64

Table A.1. Results from IDEA StatiCa for initial rotational stiffness at different load ratios

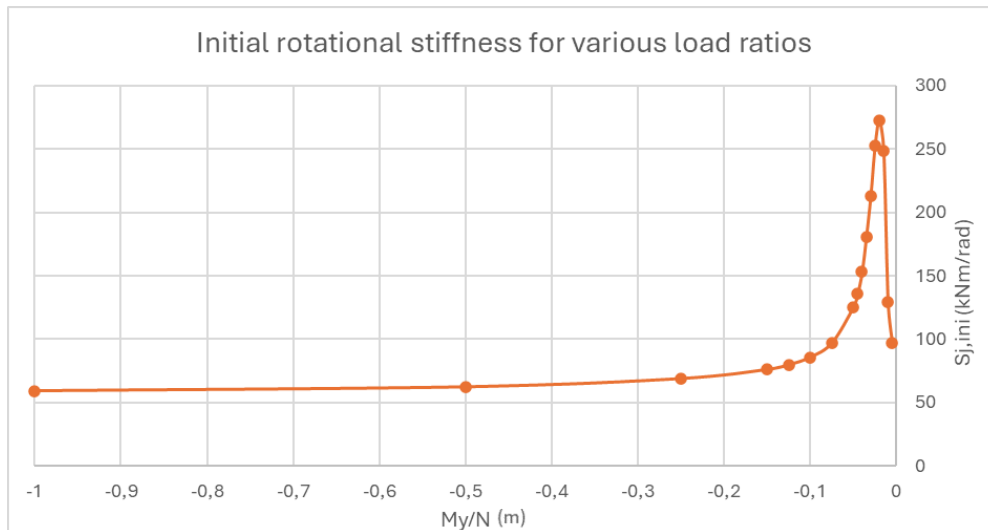


Figure A.2. Influence of the load ratio (M_y/N) on the initial rotational stiffness ($S_{j,ini}$)

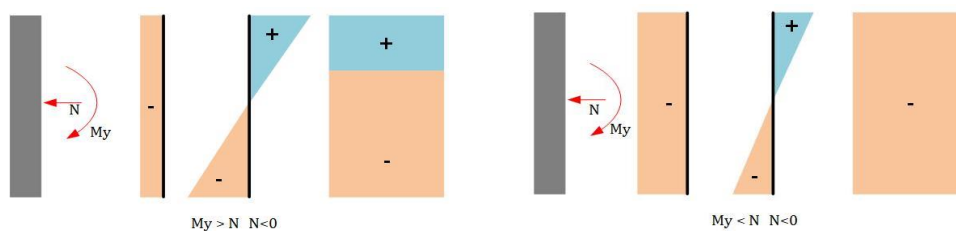


Figure A.3. Influence of the load ratio on the size of the area of the cross-section that is in compression

A.3 Parametric investigation

A parametric study is performed in an attempt to explain the peak that occurs in the stiffness values for low load ratios as shown in figure A.2. Five calculations are performed to identify the cause of these results.

The results are shown in figure A.4. Afterwards a discussion is formulated that discusses the formed peak in the results.

- 1.) The first model is equal to the previous research, where the axial load is kept constant ($N = -2\text{kN}$) and the bending moment is varied from $M_y = 0,01\text{ kNm}$ up to $M_y = 2\text{ kNm}$.
- 2.) In the second model the bending moment is kept constant ($M_y = 1\text{ kNm}$), and the axial load is varied from $N = -200\text{ kN}$ to $N = -1,01\text{ kN}$ ¹. Although the stiffness for very low load ratios is different, still a peak can be seen in the results.
- 3.) In the third model the theoretical length of the connected elements is changed from 1.5 m to 3 m. The results show that this does not influence the initial rotational stiffness of the connection. Only the values for the pinned and rigid boundaries are affected.
- 4.) The fourth model shows the results for the connection if it was designed with only one bolt instead of two, representing a connection that is less rigid. As expected, the initial stiffness of this connection is lower than the other results. However, still a peak value can be seen at the same load ratio as in the other models.
- 5.) In the fifth model both the bending moment and the axial load are scaled by a factor of 10 compared to the first model. For example, the load case with $M_y = 0,1\text{ kNm}$ and $N = -2\text{ kN}$ has changed to $M_y = 1\text{ kNm}$ and $N = -20\text{ kN}$. Results of model 5 are equal to the results of model 1. Which can be expected based on the calculation method, where loads are applied in increments in which the load ratio remain the same throughout the analysis.

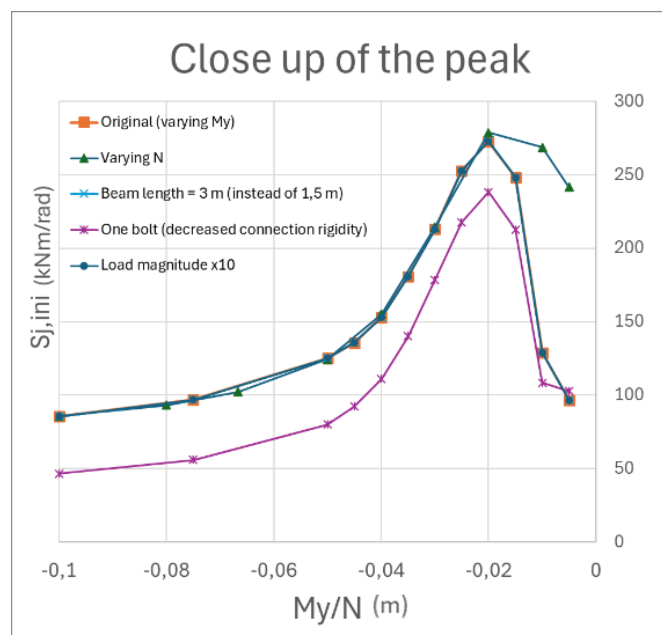


Figure A.4. Close-up of the peak values from the diagram in figure 5.

¹ The stiffness analysis in IDEA StatiCa does not run for $N \leq 1\text{ kN}$

Discussion

Unfortunately, the results from the parametric study are inconclusive regarding the cause of the occurring peak in the initial rotational stiffness for low values of the M_y/N -ratio. All models show a similar pattern where the stiffness initially increases for a decreasing load ratio until a peak value is reached, after which the stiffness decreases. The varied load parameter, length of the element, rigidity of the connection and magnitude of the load are likely not the cause of the peak.

The increase in stiffness for low load ratios as well as the asymptotic behaviour of the stiffness for higher load ratios can be explained with the mechanics presented in figure 2. This is under the assumption that compression in the connection pushes the element together, restricting their movement. Therefore, compression increases the stiffness of the connection.

For this reason, the increase of the stiffness in the results can be valid. To investigate this, an estimation is made of the location of the peak based on the stresses in the cross-section. This calculation is shown in figure 7 on the next page. The assumption that compression increases the stiffness implies that the maximum value of the stiffness is reached when the entire cross section is in compression. Based on this the load ratio for maximum initial bending stiffness can be estimated with the equation below. This is elaborated in figure 7.

$$\sigma_N = \sigma_b$$
$$\frac{N}{A} = \frac{M_y * z}{I_y}$$

Assuming a compressive load of $N = -2$ kN and a cross section RHS100x60x8, this results in a bending moment $M_y = 0,047$ kNm. Which gives a load ratio $M_y/N = 0,024$. This load ratio is close to the load ratio at which the peak in the results occurs, which is approximately $M_y/N = 0,02$.

Furthermore, if the assumptions in this hand calculation are correct, this would also explain why the magnitude of the load, the rigidity of the connection and the length of the elements do not influence the location of the peak. Only the profile of the cross section will have an impact. To verify this an extra investigation is performed for a cross-section of RHS120x60x8. According to the hand calculation this should result in a peak in stiffness at a slightly higher load ratio ($M_y/N = 0,028$). Figure 8 shows the results from IDEA StatiCa. The figure indeed shows that the peak of the stiffness occurs at a higher load ratio than the peak of the connection with RHS100x60x8 cross section. As expected, the increase in cross-section also lead to a more rigid connection. However, the parametric study showed that only changing the rigidity of the connection does not affect the location of the peak.

Based on this parametric study, it is not possible to draw a conclusion on the reliability of the results of the stiffness calculation in IDEA StatiCa. The following section will dive deeper into the problem.

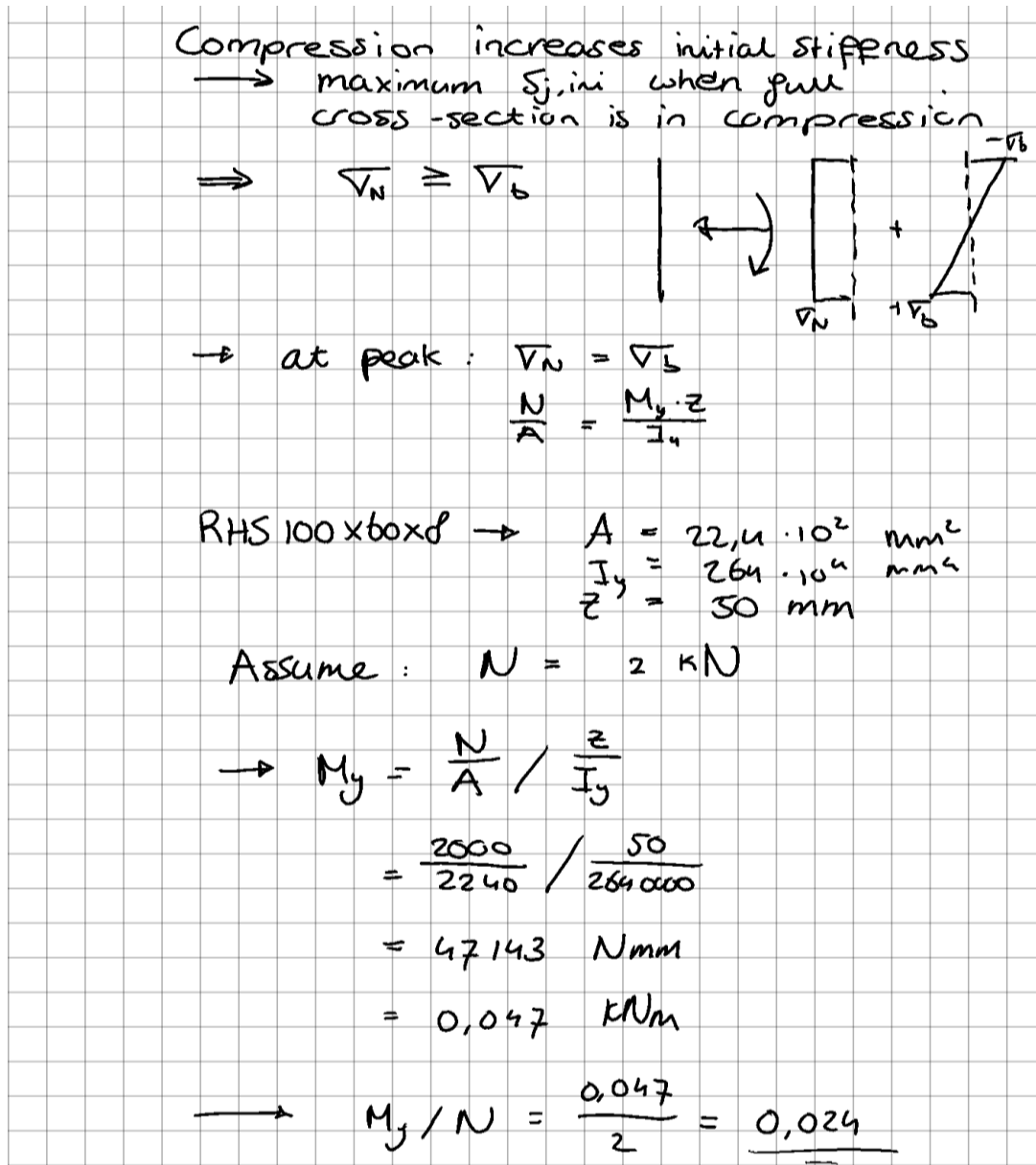


Figure A.5. Estimate of the location of the peak in initial rotational stiffness

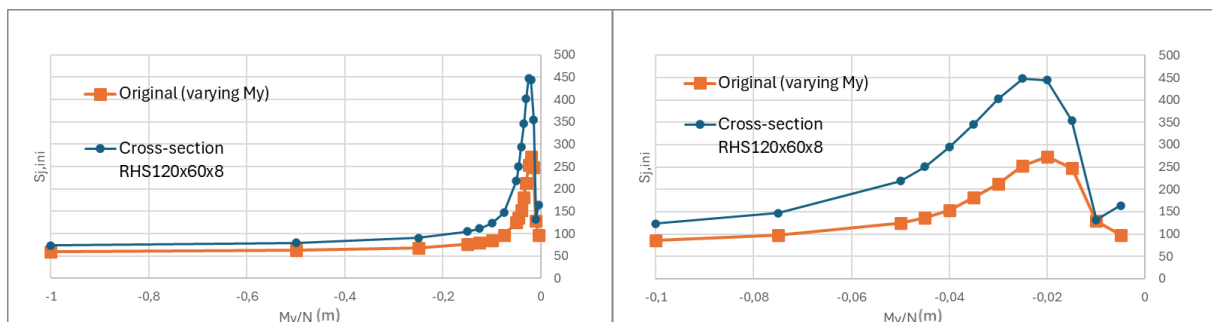


Figure A.6. Stiffness of RHS100x60x8 and RHS120x60x8 for different load ratios (left) and close-up of the peak values (Right)

A.4 Communication with IDEA StatiCa

The described problem has been discussed with IDEA StatiCa. Correspondence regarding the model led to the conclusion that the results for small M_y/N -ratios are not reliable and should not be considered. The error is caused by the small rotations in the calculation. The rotations as a result of the small load ratios are too small to accurately calculate the moment-rotation relation in the connection, which is used to determine the stiffness.

The question that remains is from which load ratio the results of the stiffness are reliable. To determine this the diagram in figure A.7 has been constructed by IDEA StatiCa. The diagram includes the 17 load cases that are shown in table A.1. For each load case the moment-rotation diagram has been plotted. The increase in the angle of the lines shows the increase in initial stiffness of the connection for lower load ratios. However, the results for LE1, 2 and 3 are between the rest of the results. The results show a consistent result up until LE4. Based on the discontinuation of the pattern IDEA StatiCa advises to disregard LE1, LE2 and LE3. This would lead to the diagram from figure A.2 to be changed to the diagram in figure A.8. If stiffness values are needed for load ratios that do not give a reliable result, the values in the diagram in figure A.8 could be either extrapolated or kept constant as indicated by the red lines in the figure.

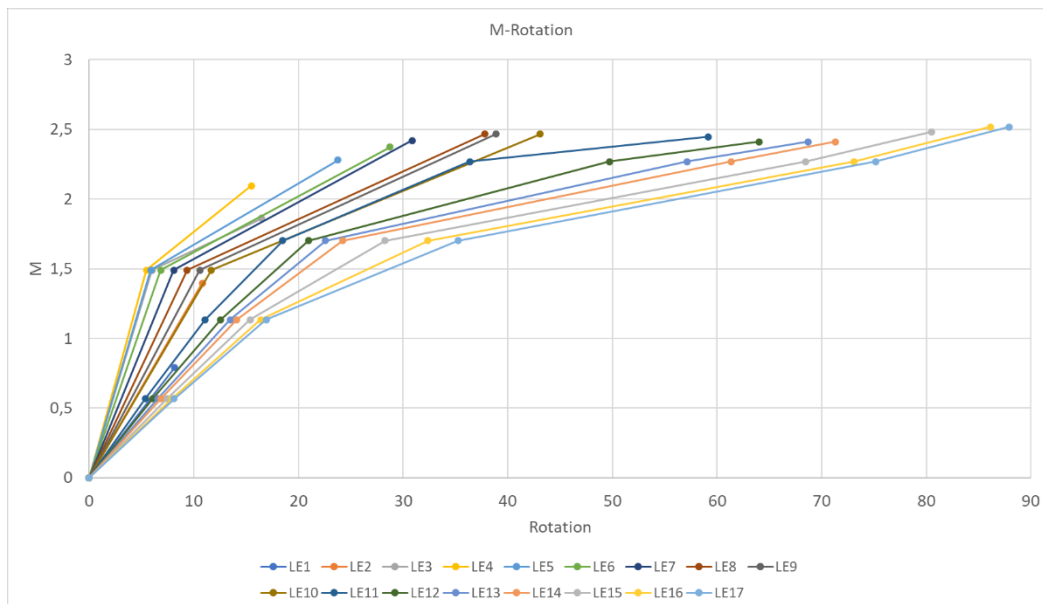


Figure A.7. Moment-rotation relations for each load case as presented in table A.1

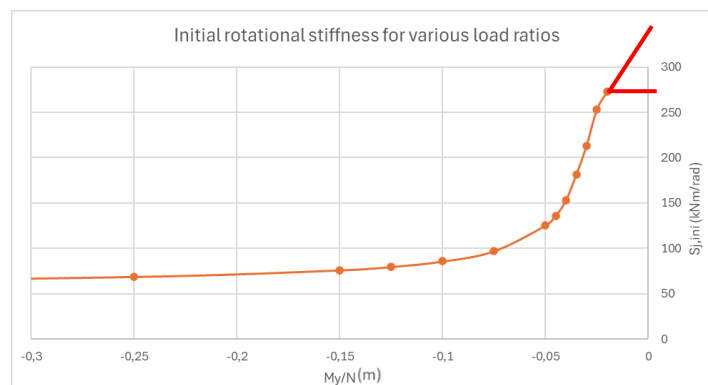


Figure A.8. Adjusted diagram for the influence of load ratios on the initial rotational stiffness

A.5 Hand calculation of the initial rotational stiffness

This section presents a hand calculation of the stiffness of the connection based on the component method as described in the Eurocode (NEN EN 1993-1-8 section 6.3). Although this method is designed for connection of open sections, an attempt has been made to apply this to the researched connection. The results are compared to the results from the stiffness analysis in IDEA StatiCa.

NEN EN 1993-1-8 section 6.3

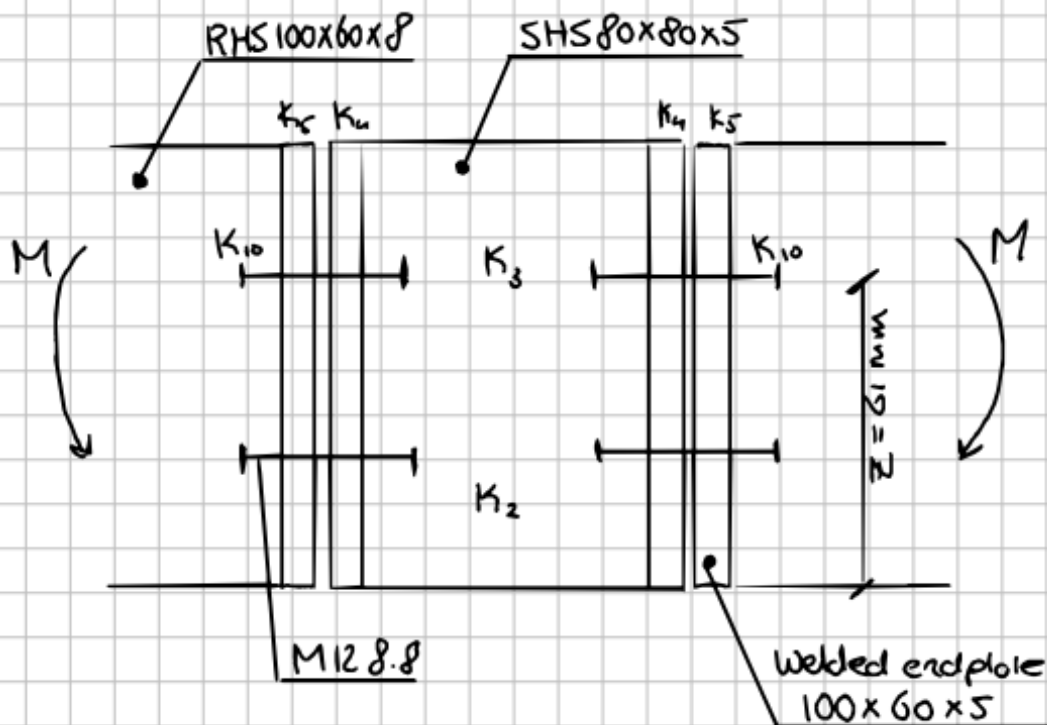
6.3.1.(4) eq. 6.27

$$S_j = \frac{E \cdot z^2}{\mu \cdot \sum_i \frac{1}{k_i}}$$

for $M_{ed} \leq \frac{2}{3} M_{j,Rd}$: $\mu = 1$

6.3.1 table 6.9

$$\sum \frac{1}{k_i} = \frac{1}{k_2} + \frac{1}{k_3} + \frac{1}{k_4} + \frac{1}{k_5} + \frac{1}{k_{10}}$$



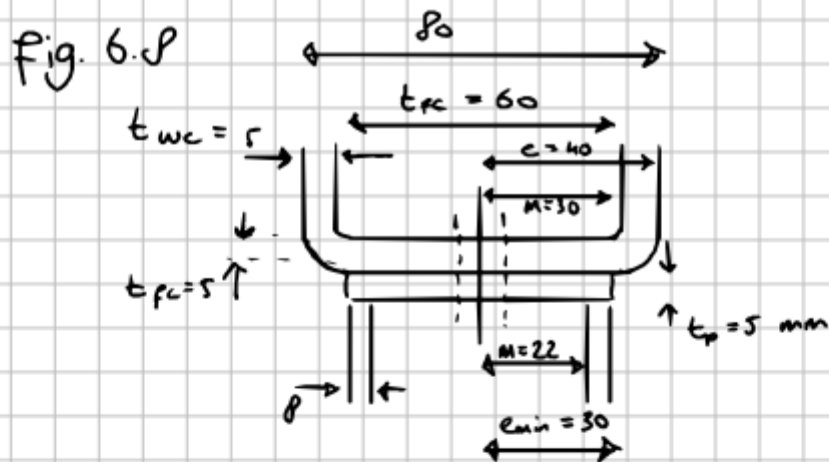


table 6.11

K_2 : $b_{\text{eff},c,wc} = t_f + 2\sqrt{2}a_f + 5(t_{fc} + 5) + t_w$
 $= d + 0 + 5(5 + 0) + 5 = 38 \text{ mm}$
 $K_2 = \frac{0,7 \cdot b_{\text{eff},c,wc} \cdot t_{wc}}{d_c} = \frac{0,7 \cdot 38 \cdot 5}{70} = 1,9$

K_3 : $b_{\text{eff},e,wc} = l_{\text{eff},cp} = \min(2\pi M; \pi M + 2e)$
 $= \min(188; 174) = 174 \text{ mm}$
 $K_3 = \frac{0,7 \cdot b_{\text{eff},e,wc} \cdot t_{wc}}{d_c} = \frac{0,7 \cdot 174 \cdot 5}{70} = 8,7$

For K_4 and K_5 table 6.11 is not applicable to hollow sections. Therefore the following forget-me-not is used

$$w = \frac{1}{48} \cdot \frac{FL^3}{EI}$$

$$K = \frac{48 I_{\text{plate}}}{L^3}$$

E is included in eq. 6.27

$$K_4: I_{\text{plate}} = \frac{1}{12} b h^3 = \frac{1}{12} \cdot 50 \cdot 5^3 = 521$$

$$L = 75 \text{ mm}$$

$$K_4 = \frac{48 \cdot I}{L^3} = \frac{48 \cdot 521}{75^3} = 0,059$$

$$K_5: I_{\text{plate}} = \frac{1}{12} b h^3 = \frac{1}{12} \cdot 50 \cdot 5^3 = 521$$

$$L = 50 \text{ mm}$$

$$K_5 = \frac{48 I}{L^3} = \frac{48 \cdot 521}{50^3} = 0,2$$

$$K_{10}: A_{s, \text{ME}} = 84,3 \text{ mm}^2$$

$$L_s = 5 + 5 + 2 + 10 = 22 \text{ mm}$$

$$K_{10} = 1,6 A_s / L_s = 6,16$$

$$\rightarrow \sum_i \frac{1}{k_i} = \frac{1}{1,9} + \frac{1}{8,7} + \frac{1}{0,059} + \frac{1}{0,2} + \frac{1}{6,16}$$

$$= 22,75$$

$$\rightarrow S_{j, \text{ini}} = \frac{E z^2}{22,75} = \frac{210000 \cdot 61^2}{22,75} = 34,3 \frac{\text{KNm}}{\text{rad}}$$

Which is in the same order of magnitude as the stiffness in IDEA StatiCa for large load ratios (where $M > N$)

However for low M_y/N -ratios
only compression

→ k_3, k_4, k_5 and k_{10} have no influence

$$\rightarrow \sum \frac{1}{k_i} = \frac{1}{2k_2} = \frac{1}{3,8} = 1,06$$

$$\Rightarrow S_j = \frac{210000 \cdot 61^2}{1,06} = 737 \text{ kNm/rod}$$

→ Which is considerably higher than the peak stiffness value. which is 250 kNm/rod

$$\frac{737}{250} \approx 3$$

The component method as described in the Eurocode calculates the stiffness based on only the bending moment. Assuming half the connection to be in compression and half of the connection to be in tension. According to this assumption the stiffness can be calculated for large M_y/N -ratios. The resulting stiffness of 34,4 kNm/rad is in the same order of magnitude as the results from IDEA StatiCa (approximately 50 kNm/rad). Some inconsistencies in the simplifications and the three dimensional characteristics of the connection design in IDEA StatiCa may have caused the difference.

However, at the 'peak-values' of the results the connection cross-section is assumed to be completely in compression. Therefore, the tensile stiffness parameters from the hand calculation are eliminated from the calculation in the case of small load ratios. This results in the stiffness of the centre box in compression to be the only stiffness parameter. This increases the stiffness to a value of 737 kNm/rad, which is considerably higher than the results from IDEA StatiCa.

In the next section, this assumption that the tensile stiffness parameters (bolts in tension, endplate in bending, column flange in bending and column web in tension) can be excluded from the calculation is investigated in results from the design phase of the project.

A.6 Results on the mechanic behaviour

Figure A.9 shows the design diagram for the connections of the RHS100x50x3 profiles in the design of the grid shell in chapter 5. For this research the focus is on the connection with stiffening cap (the blue lines). The analysis considers 5 different connection designs.

1. The base connection for the RHS100x50x3 profile

2. Increased spacing of the bolts
3. Increased centre box dimensions (to SHS80x80x6.3)
4. Increased centre box dimensions (to SHS90x90x8)
5. Increased thickness of the endplate

For general load combinations each of these adjustments is expected to increase the stiffness of the connection. As can be seen in the stiffness values for a load ratio $M_y/N = -0,1$. However, at the peak value $M_y/N = -0,025$, the results show that the increased bolt spacing, or the increased thickness of the endplate do not influence the stiffness of the connection. Only the increase in the size of the centre box, which determines the compressive stiffness parameters, leads to an increase of the stiffness for this small load ratio. This indicates that the assumption made in the hand calculation, that the tensile stiffness parameters can be excluded from the calculation in the case that the entire cross-section is in compression, might be valid.

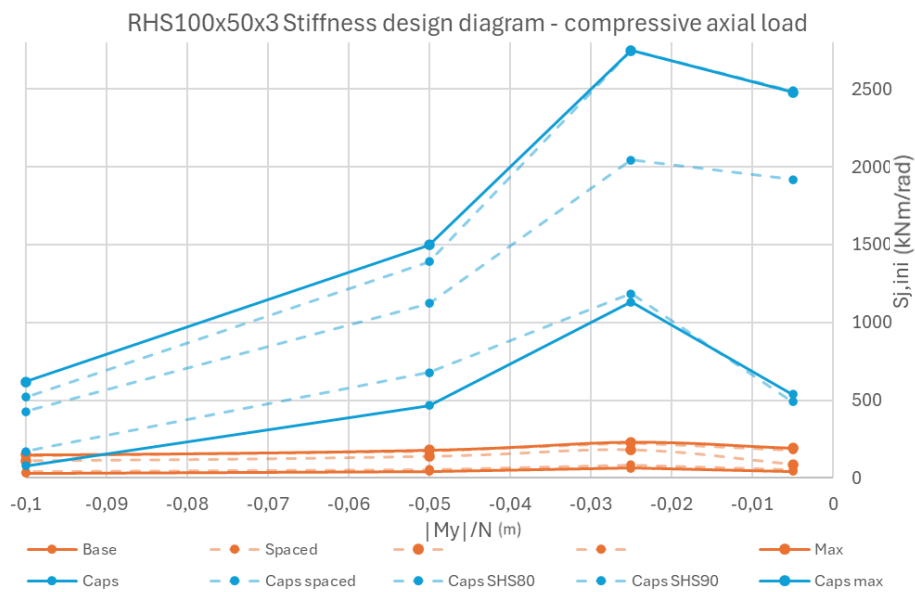


Figure A.9. Design diagram as defined in the design phase in chapter 5

A.7 Discussion and conclusion

The results shows that the stiffness increases for small values of the M_y/N -ratio. Compression in the cross-section stabilises and stiffens the connection. For low load ratios a greater area of the cross section is in compression. Therefore, the connection has a higher initial stiffness.

However, further research into the lower range of the load ratios reveals an unexpected result. When the initial stiffness is calculated for load ratios where the axial force is much larger than the bending moment a peak occurs in the stiffness values. For ratios lower than the peak value the stiffness seems to decrease. This peak cannot be explained through assumptions of the mechanical behaviour of the connection.

A parametric investigation shows that the peak in the results is not caused by inconsistencies in the input of data into the model. Varying the axial load instead of the bending moment, the beam length, the design rigidity and the magnitude of the loading do not influence the location of the peak that occurs. The height of the cross-section does influence the location of the peak. This could indicate that the assumption that compression stabilises the connection. When the stress from the axial load is equated to the minimum bending stress, the location of the peak can be approximated.

In communication with the software developer IDEA StatiCa it has been established that the results of the stiffness analysis for very low M_y/N -ratios are unreliable. It can be said with sufficient certainty that the decrease in stiffness for load ratios after the peak does not represent actual structural behaviour. However, the question remains up to which load ratio the results are reliable. Solely based on the continuation of a pattern in the results the stiffness values until the peak could all be valid.

A hand calculation to determine the stiffness of the connection is performed. This calculation is based in the component method for connection of open section as specified in EC3. The determination of the stiffness values at the peak are based on the assumption that the connection is only subjected to compressive forces. Difference in the compression between the top and bottom of the cross-section cause the rotation in the connection.

Based on this assumption a stiffness of the peak value of 739 kNm/rad is calculated, this is almost three times as high as the stiffness of calculated by IDEA StatiCa (250 kNm/rad). This is another indication that stiffness values up until the peak in stiffness might be reliable. In addition, results from the design phase of the problem support the assumption that the tensile elements of the connection do not influence the stiffness at load ratios around the peak in stiffness.

When the entirety of the research presented in this appendix is reviewed it can be said that the increase in stiffness for lower load ratios is representative of the actual behaviour of the connection. However, it can not be said with any certainty up to which values the result from the stiffness analysis in IDEA StatiCa are reliable. They, therefore, have to be handled with care when applied in the design of a structure. In the different stages of the design of a grid shell in this project the way the peak values of the stiffness are handled will be discussed specifically.

B.2 Structural analysis with Karamba

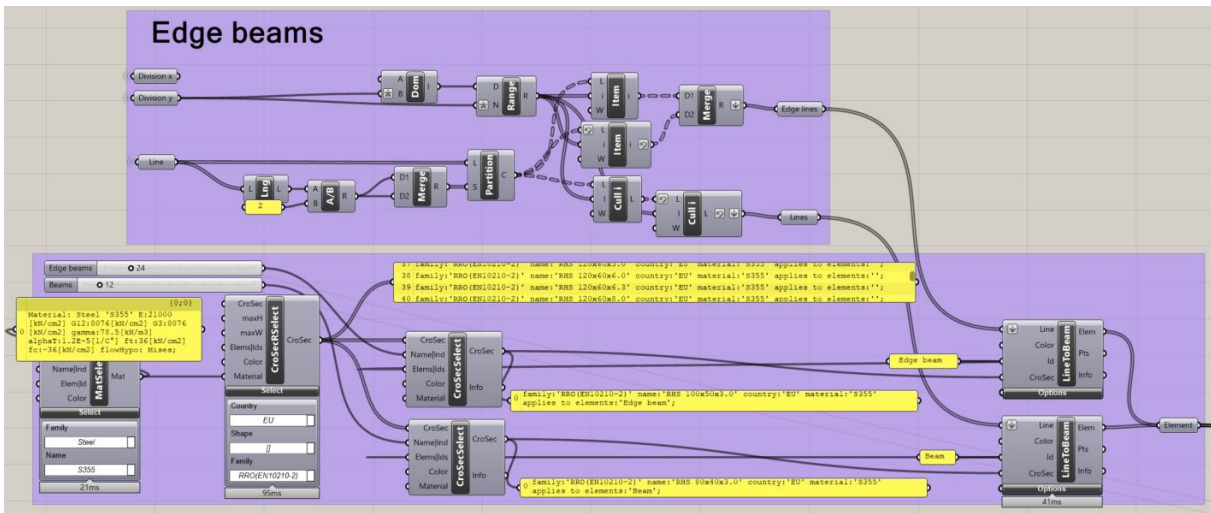


Figure B.5: Selection of elements

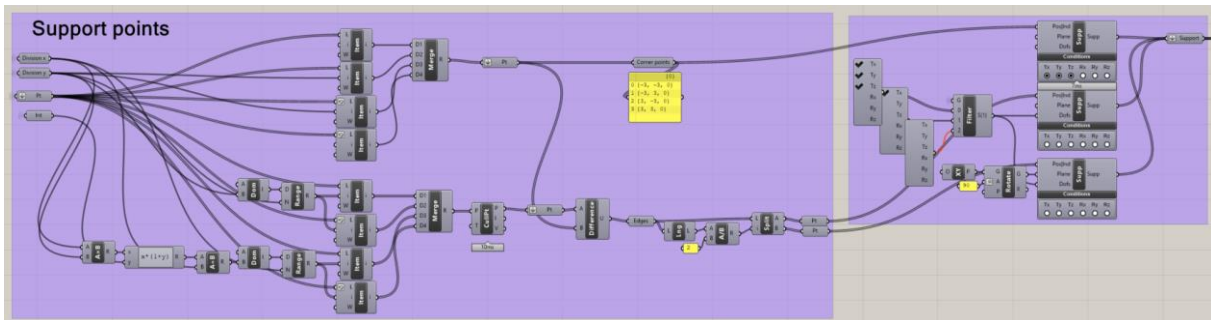


Figure B.6: Definition of support conditions

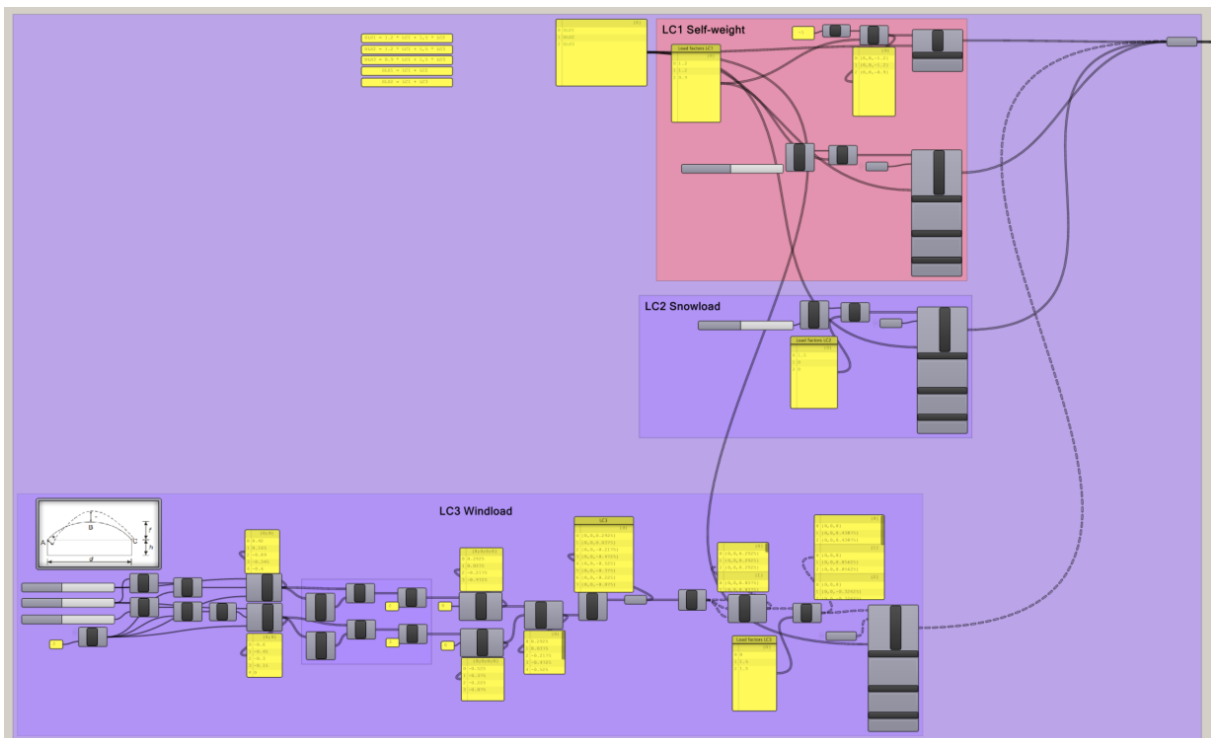


Figure B.7: Definition of load cases and load combinations

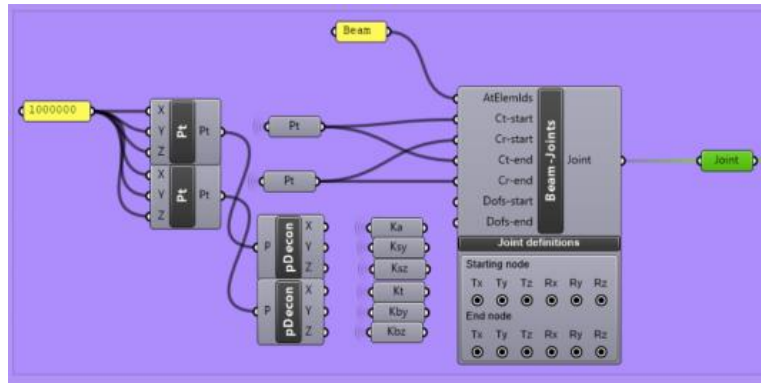


Figure B.8: Definition of joint stiffness

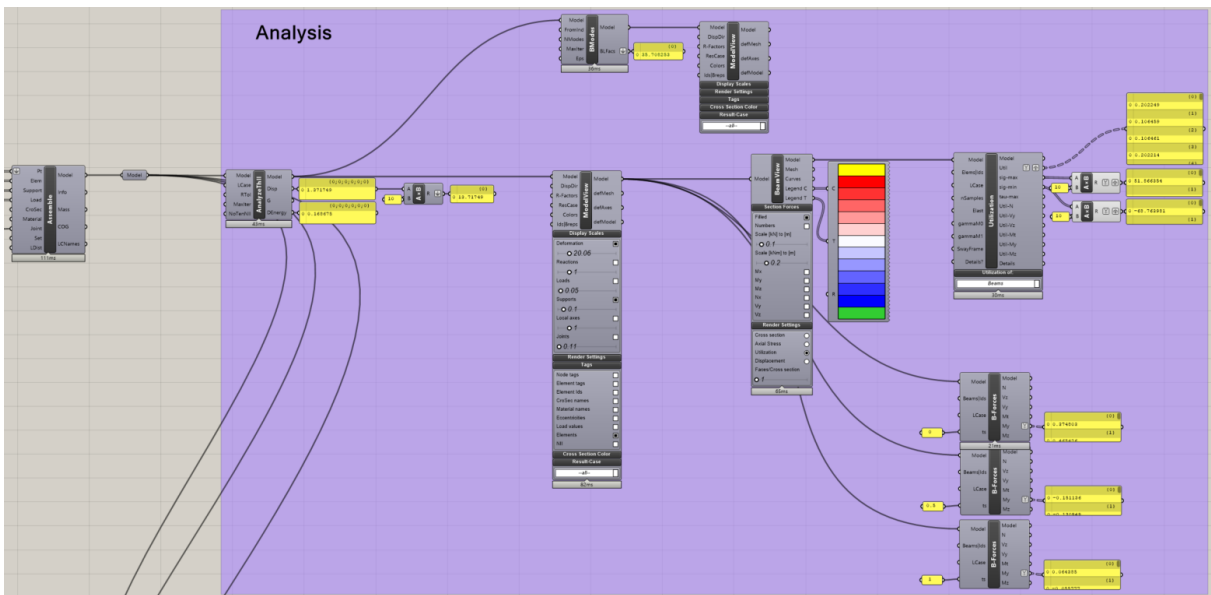
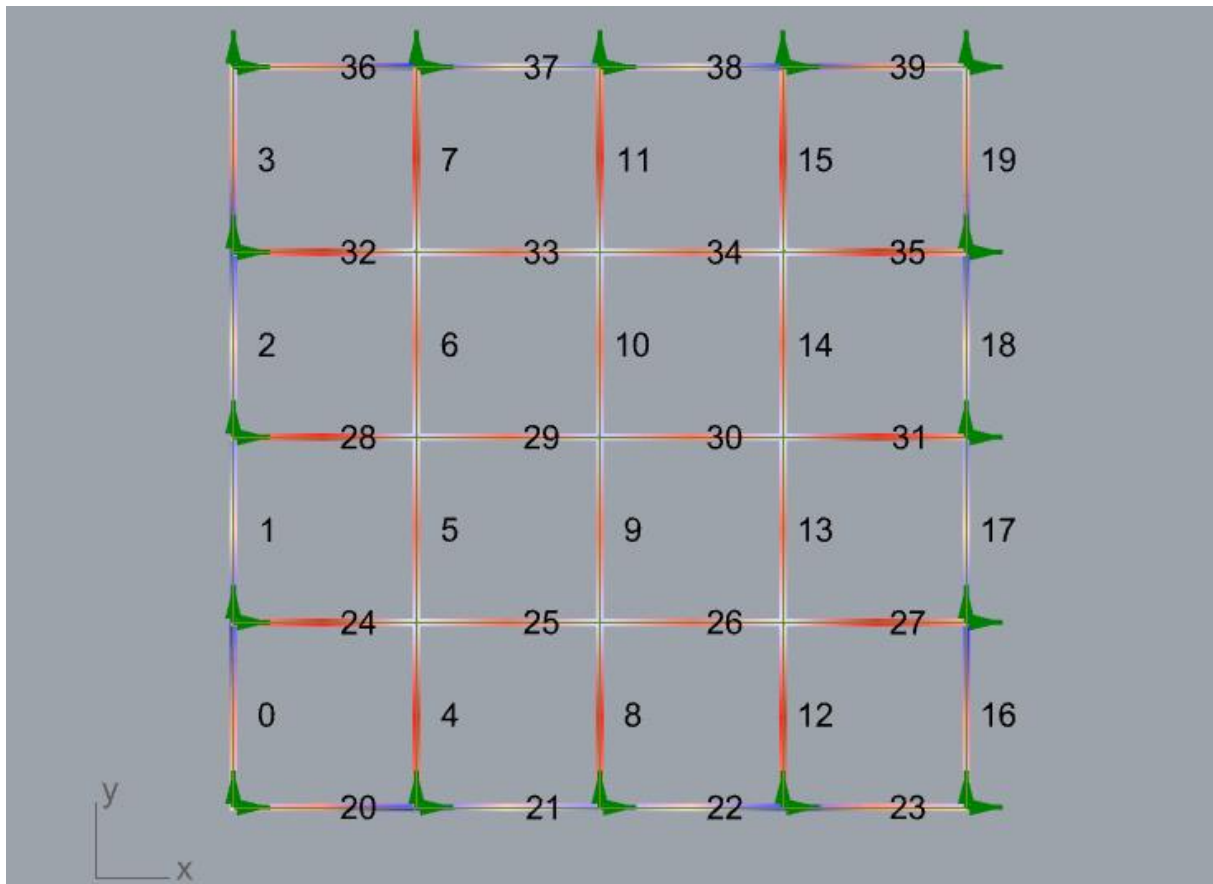
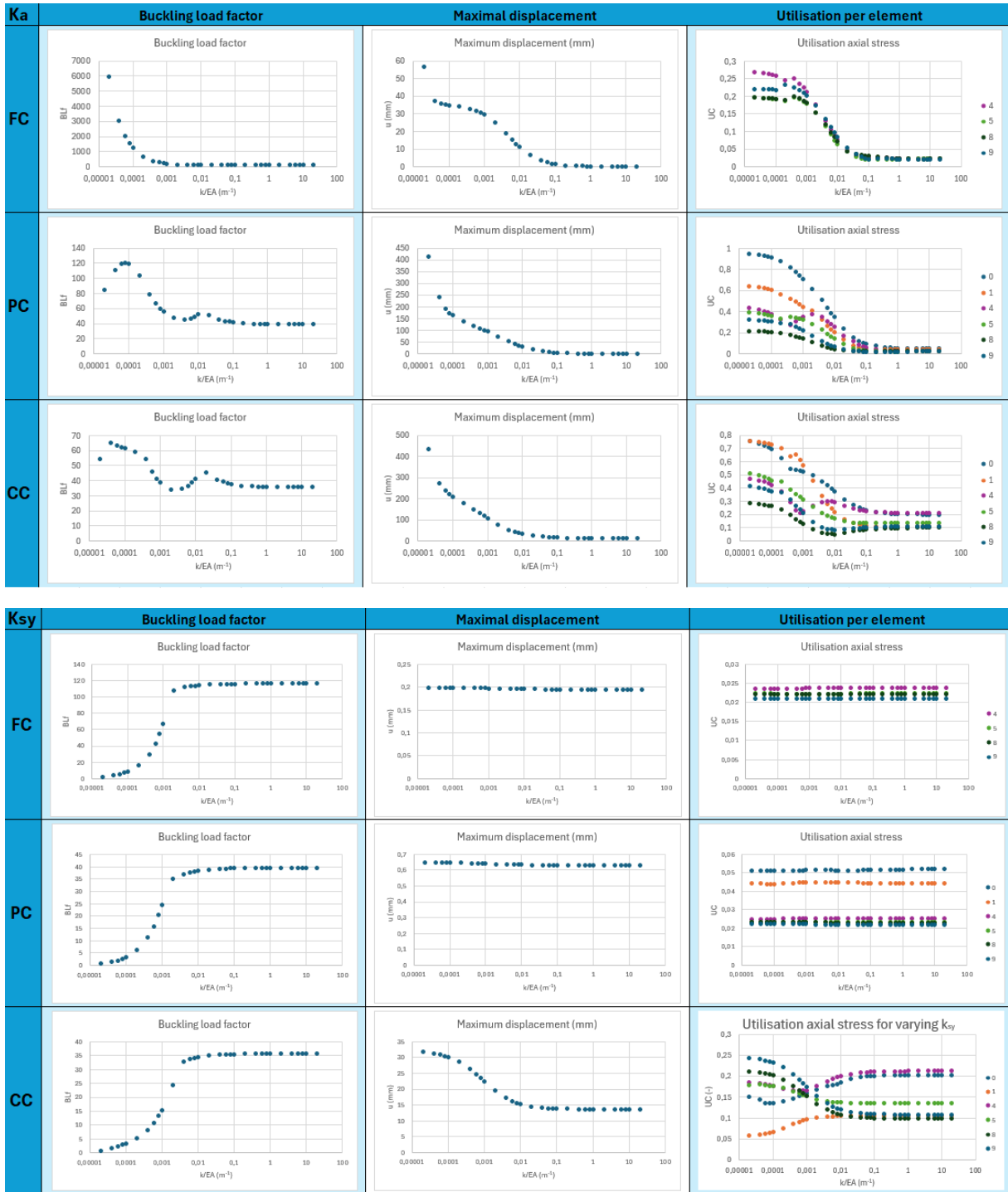


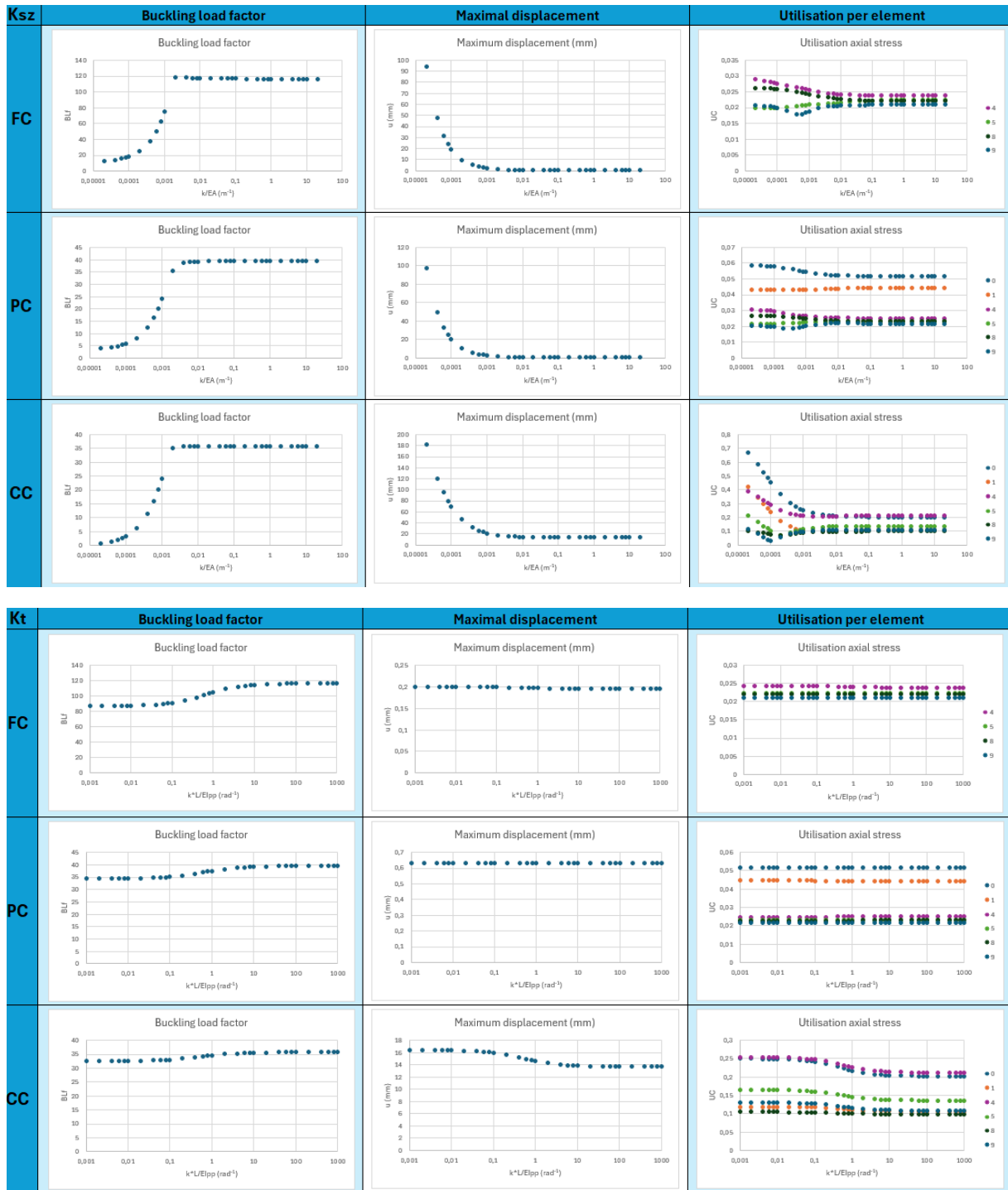
Figure B.9: Structural analysis with Karamaba 3D

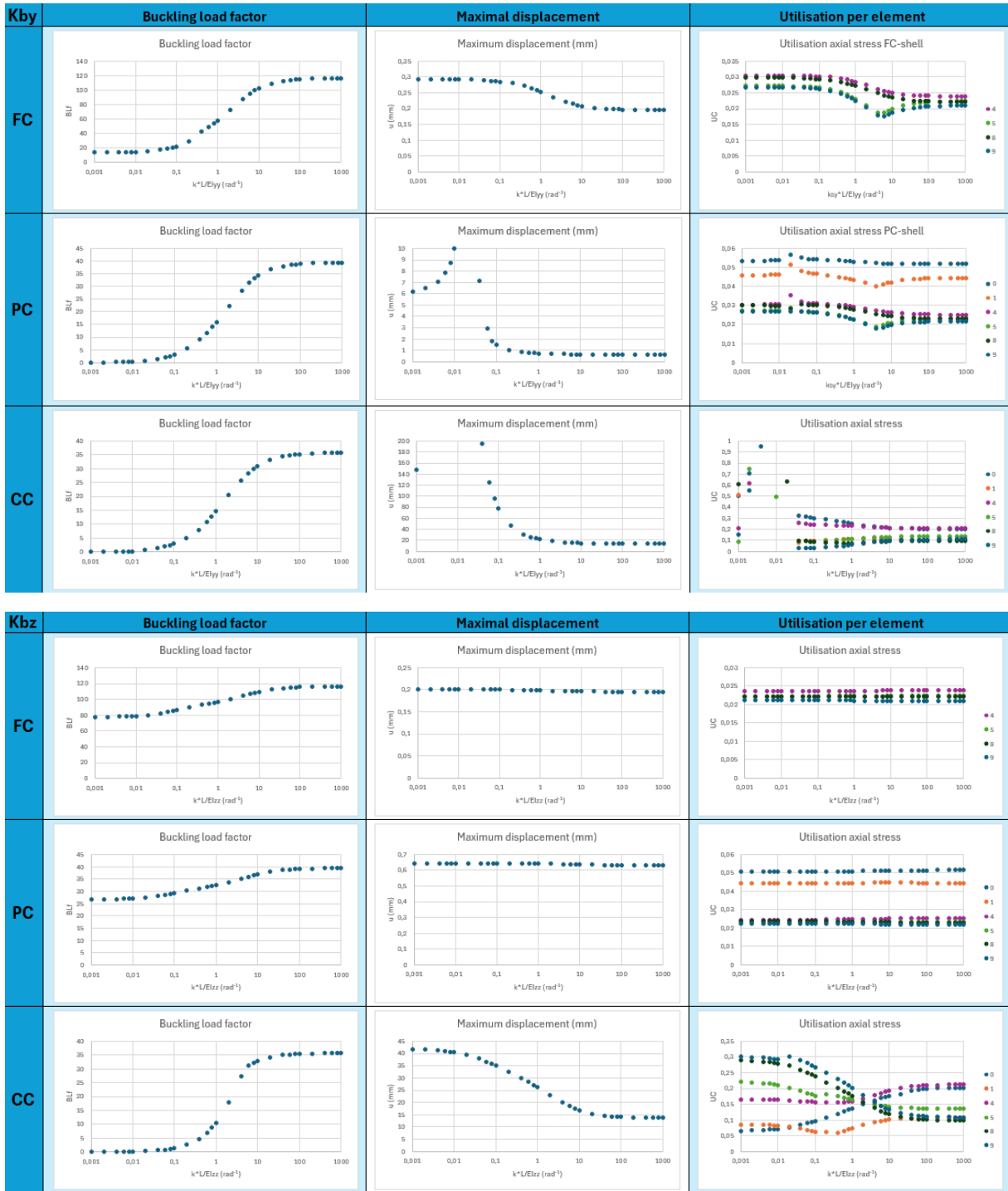
Appendix C: Results Parameter study joint stiffness influence

C.1 Small shell

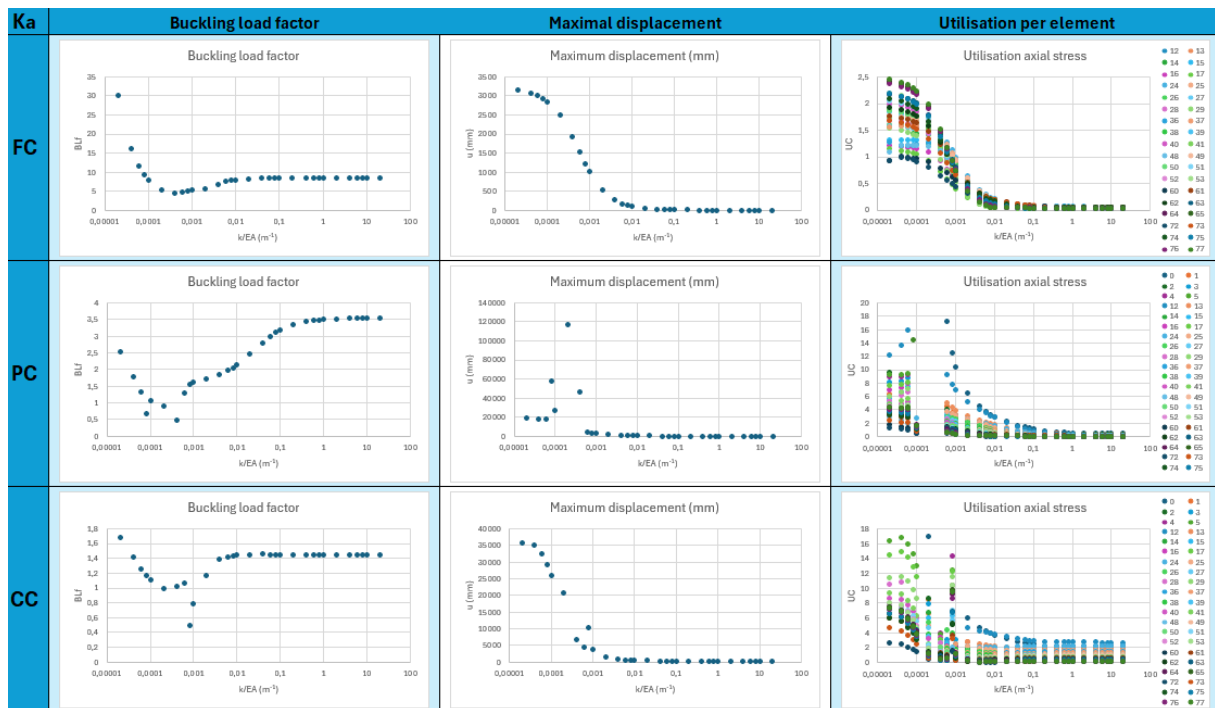
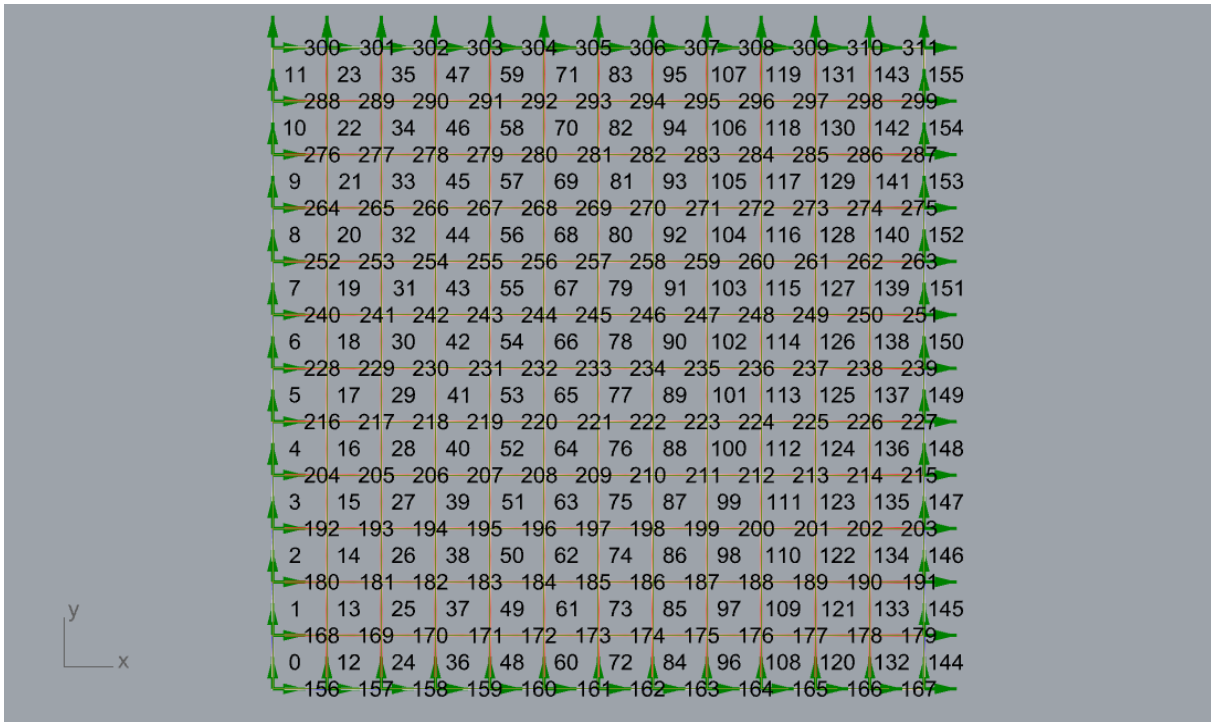


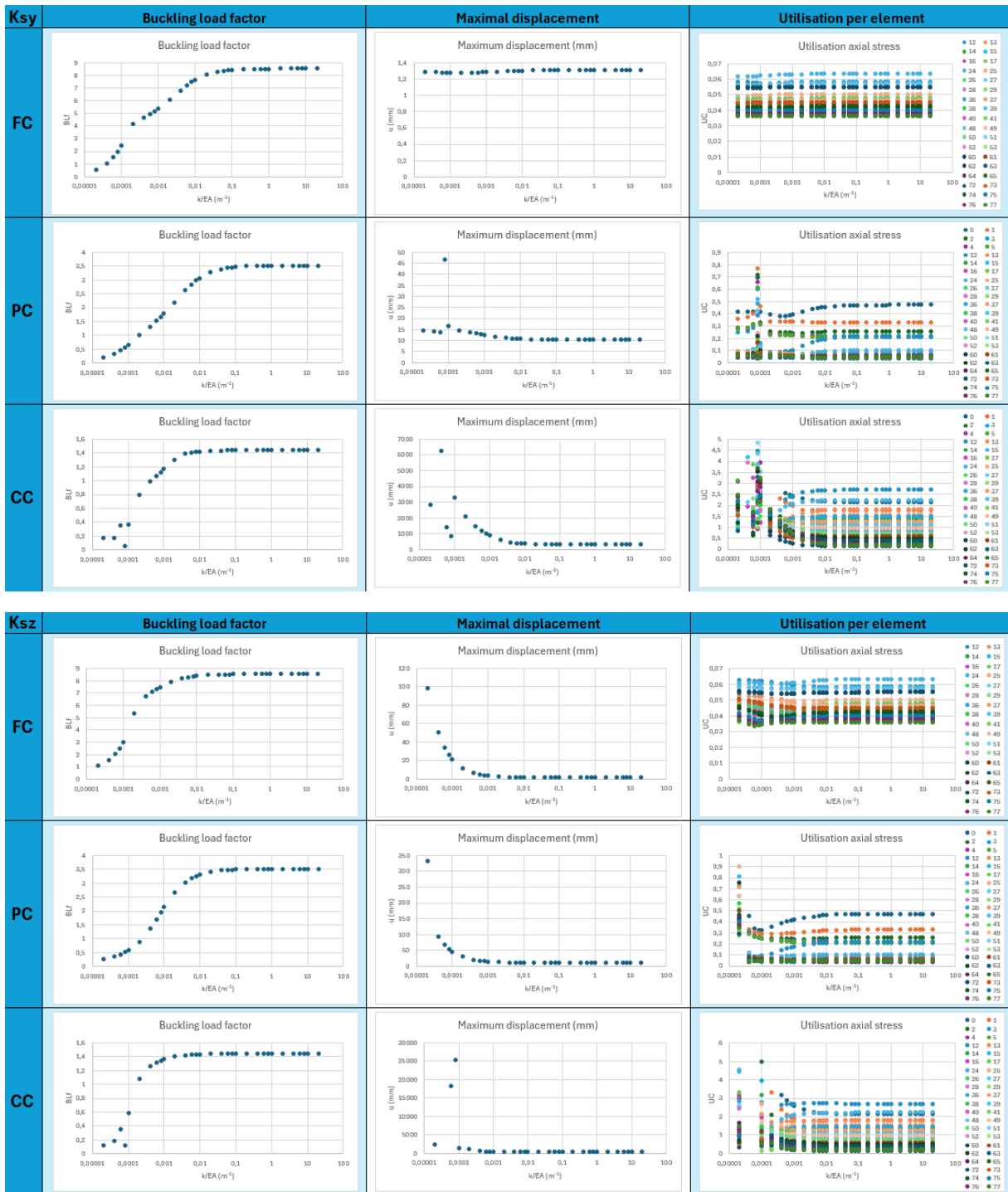


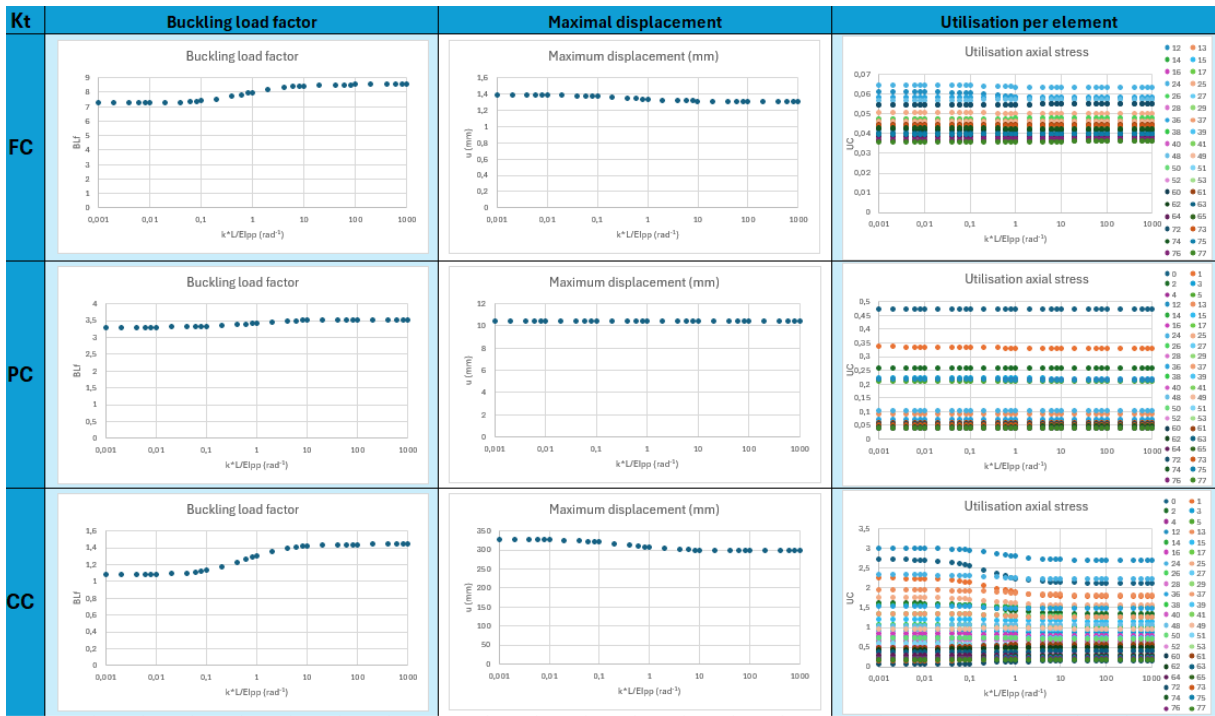


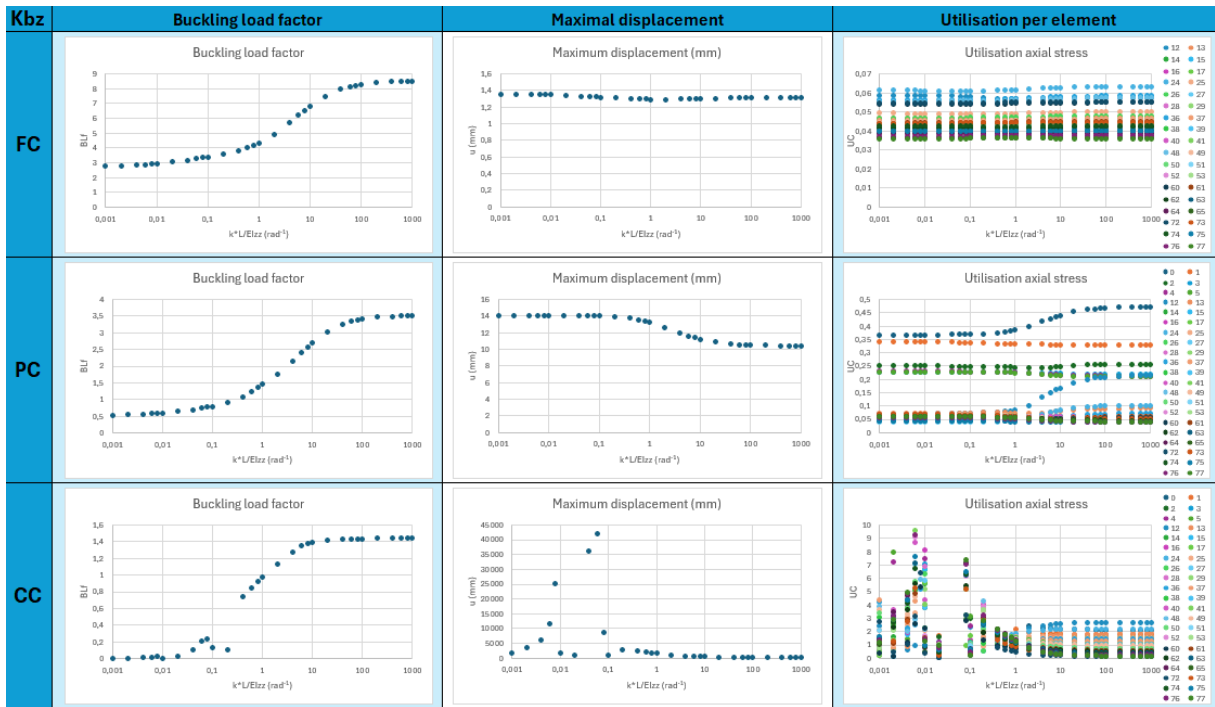


C.2 Big shell





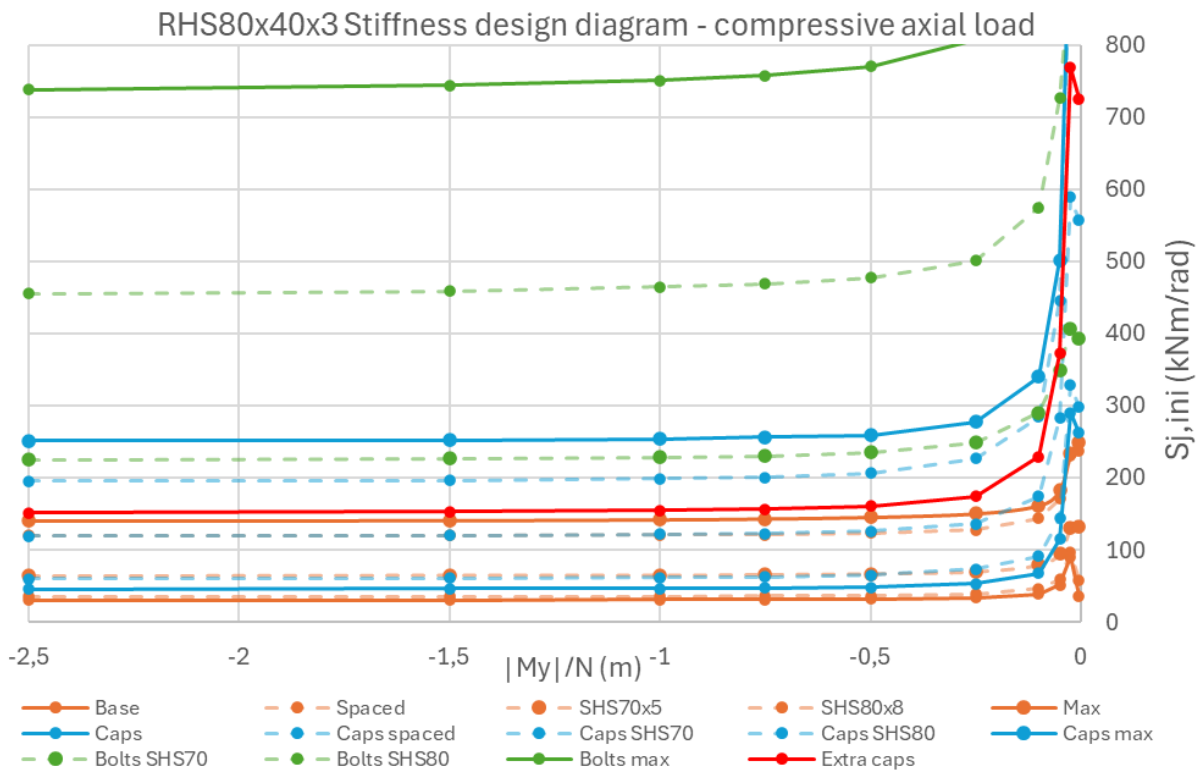




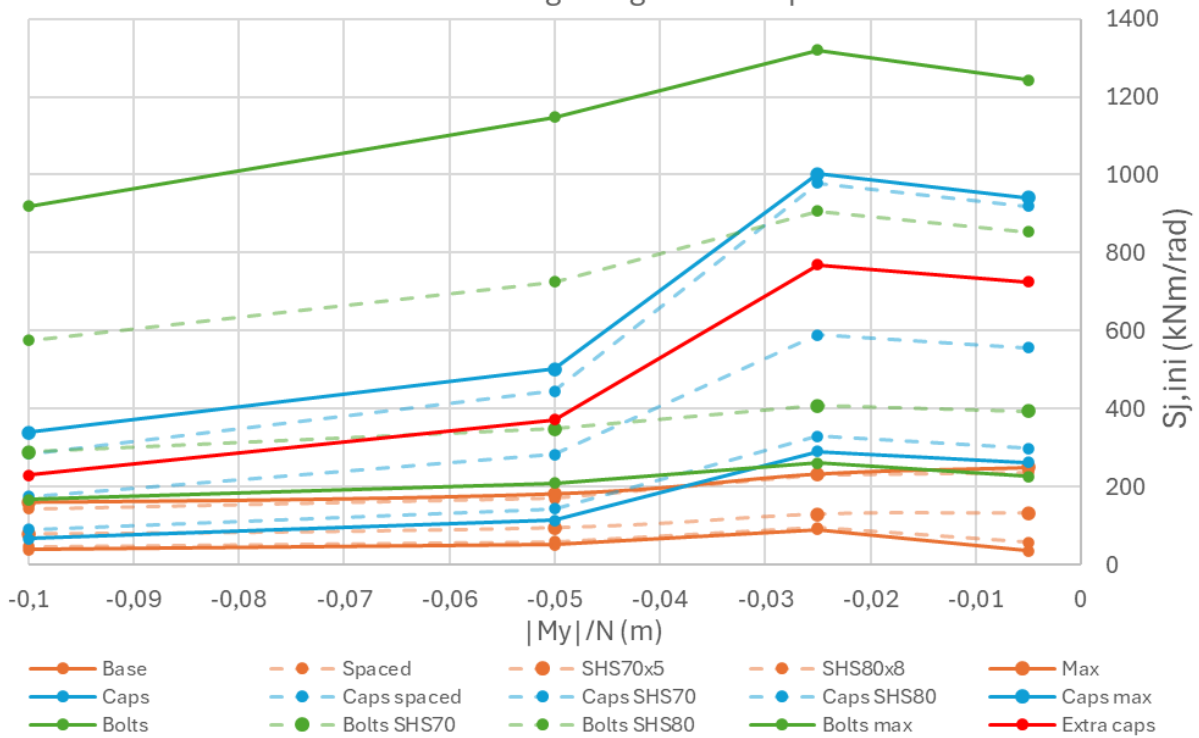
Appendix D: Connection design diagrams

D.1 Connection 1: RHS80x40x3

Axial compression



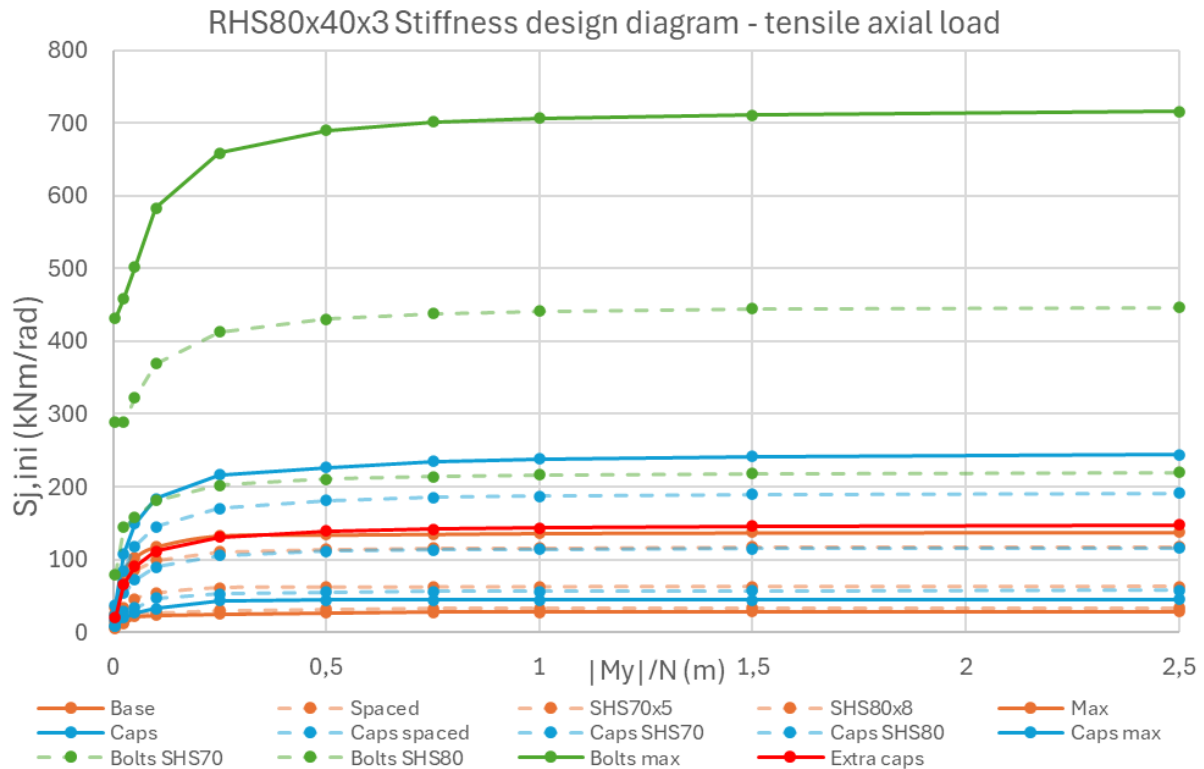
RHS80x40x3 Stiffness design diagram - compressive axial load



My/N	Base	Spaced	SHS70x5	SHS80x8	Max	Caps	Caps spa	Caps SHS	Caps SHS	Caps max
-2,5	30	35	64	120	140	46	60	119	195	251
-1,5	30	35	65	120	141	46	61	120	196	253
-1	31	35	65	121	142	46	62	121	199	254
-0,75	31	36	66	121	143	47	63	123	201	256
-0,5	32	36	67	123	145	48	65	126	206	259
-0,25	34	39	70	128	150	53	74	136	227	278
-0,1	39	46	79	144	161	68	91	175	284	340
-0,05	51	59	95	171	183	115	143	283	446	502
-0,025	90	96	130	231	233	291	330	589	979	1003
-0,005	36	58	133	238	250	262	298	557	920	941

My/N	Bolts	Bolts SHS	Bolts SHS	Bolts ma	Extra bas
-2,5	124	225	455	738	152
-1,5	125	227	459	744	153
-1	126	229	464	751	155
-0,75	127	230	469	758	157
-0,5	129	235	478	770	161
-0,25	139	249	501	807	174
-0,1	167	290	575	919	230
-0,05	209	349	726	1147	372
-0,025	261	407	907	1319	769
-0,005	227	393	854	1244	725

Axial tension

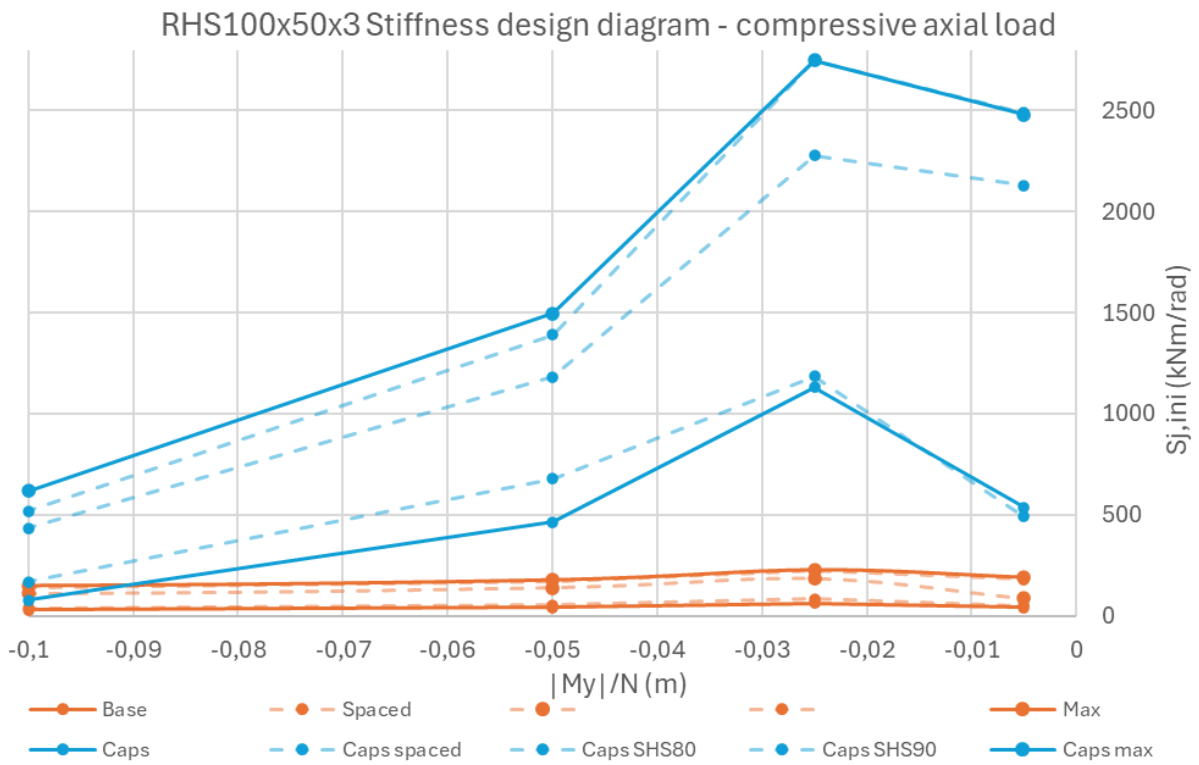
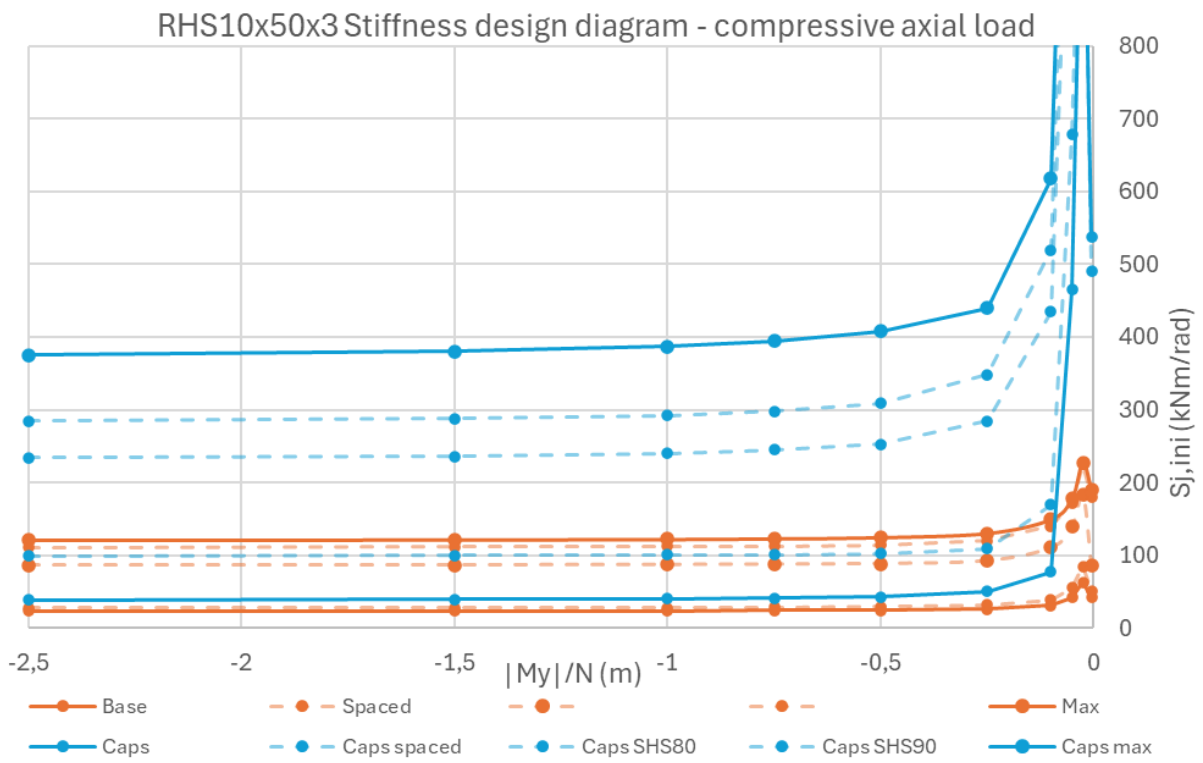


My/N	Base	Spaced	SHS70	SHS80	Max	Caps	Caps spa	Caps SHS70	Caps SHS80	Caps max
0,005	5	7	14	25	34	8	10	17	24	38
0,025	12	14	34	68	83	20	29	54	85	108
0,05	22	25	46	85	102	27	33	72	118	149
0,1	23	27	53	99	118	33	47	90	145	184
0,25	25	30	61	110	133	43	53	106	170	216
0,5	27	32	62	114	134	44	55	111	181	227
0,75	28	33	62	115	135	44	56	113	185	235
1	28	33	62	116	136	44	57	114	187	238
1,5	28	33	63	117	137	45	57	115	189	242
2,5	29	34	63	118	138	45	58	116	191	244

My/N	Bolts	Bolts SHS70	Bolts SHS80	Bolts max	Extra bas
0,005	19	79	288	431	20
0,025	81	144	289	459	66
0,05	86	158	322	502	90
0,1	99	181	370	583	112
0,25	112	202	413	659	131
0,5	117	211	431	690	139
0,75	119	214	438	701	142
1	119	216	442	706	144
1,5	120	218	444	711	146
2,5	121	220	447	716	147

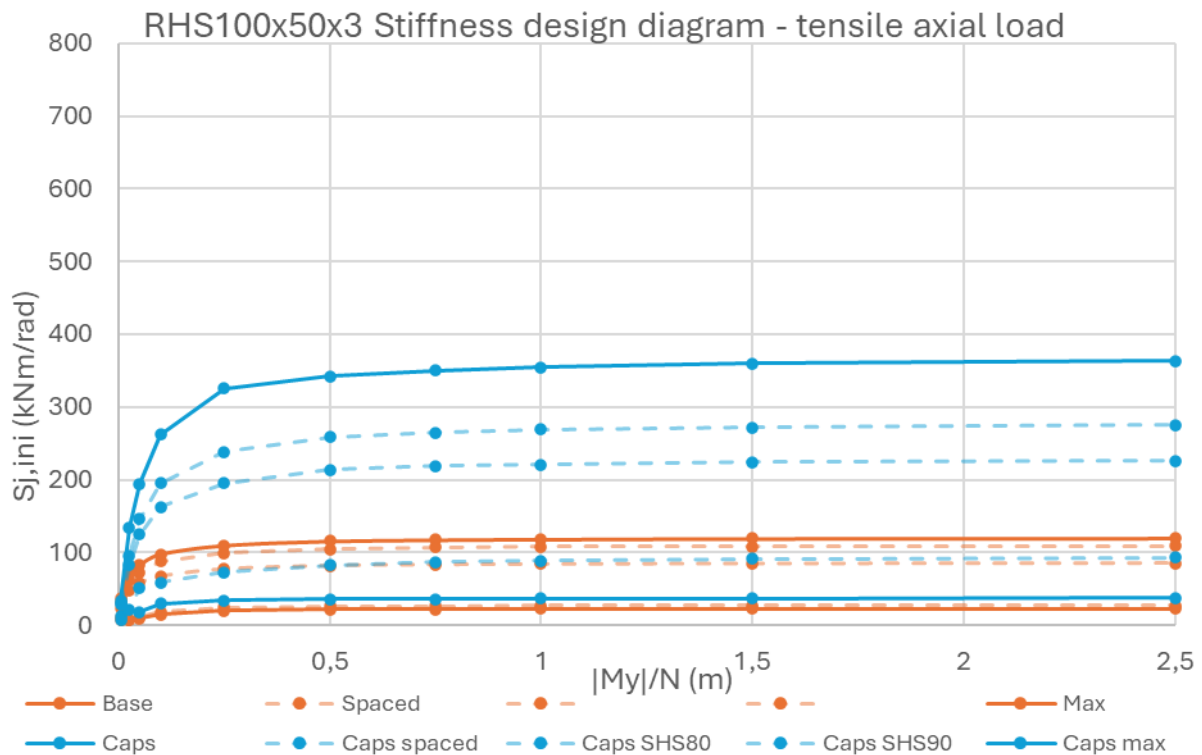
D.2 Connection 2: RHS100x50x3

Axial compression



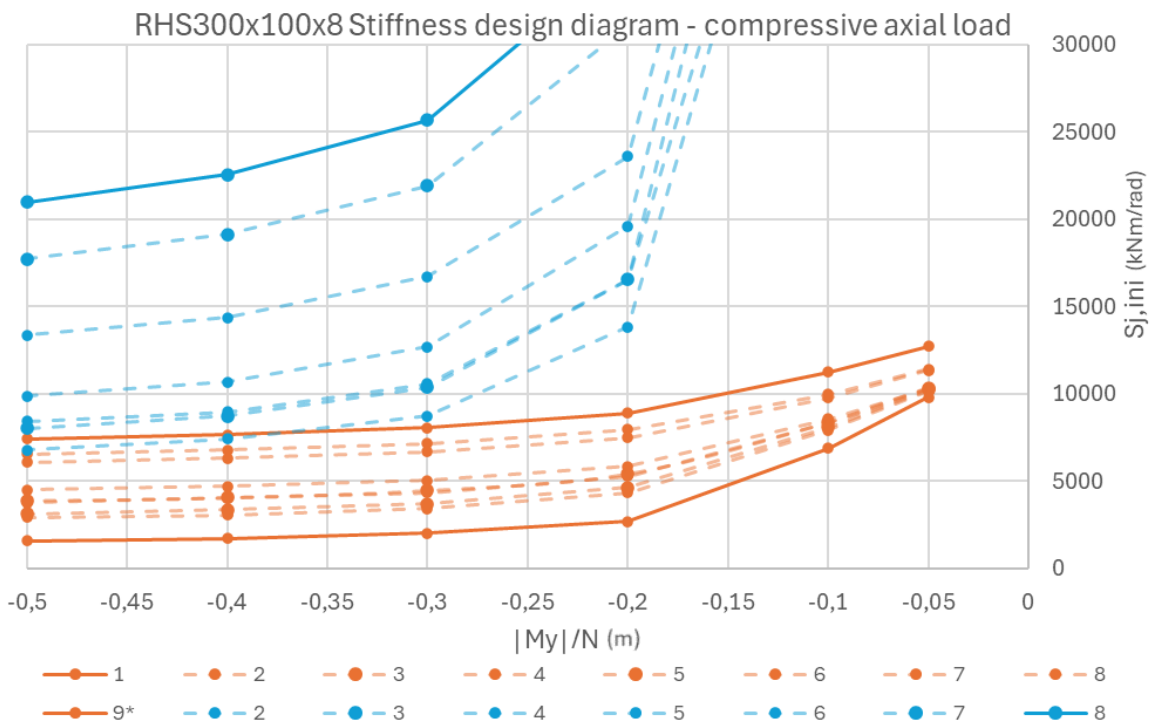
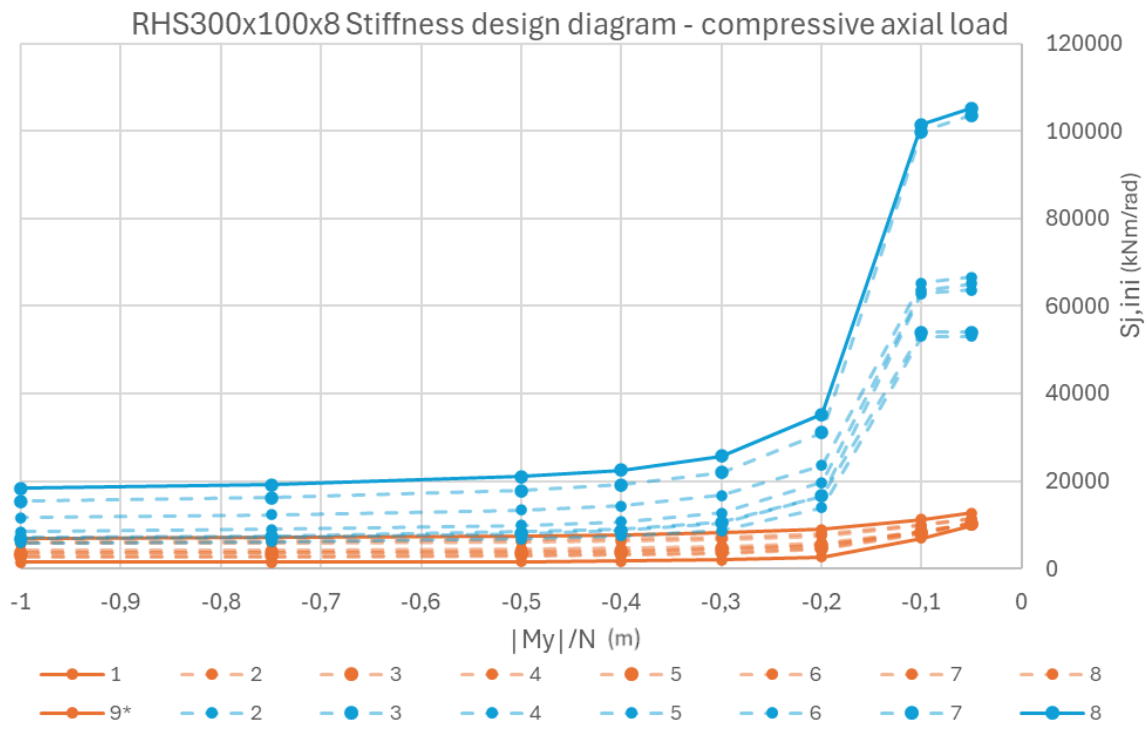
My/N	Base	Spaced	SHS80	SHS90	Max	Caps	Caps spa	Caps SHS	Caps SHS	Caps SHS	Caps max
-2,5	23	28	87	111	121	39	99	234	284	376	
-1,5	23	28	87	112	122	39	100	236	288	381	
-1	24	28	87	112	122	40	101	240	292	387	
-0,75	24	28	88	113	123	41	101	245	298	394	
-0,5	24	29	89	114	125	43	102	253	309	408	
-0,25	26	32	93	120	130	51	109	285	348	440	
-0,1	31	39	110	141	150	77	169	434	520	617	
-0,05	42	55	140	171	178	465	678	1183	1390	1497	
-0,025	63	85	183	225	228	1130	1185	2278	2749	2747	
-0,005	42	51	86	180	191	538	490	2131	2488	2479	

Axial tension



My/N	Base	Spaced	SHS80	SHS90	Max	Caps	Caps spa	Caps SHS	Caps SHS	Caps SHS	Caps max
0,005	7	11	24	33	37	7	13	28	30	34	
0,025	7	8	48	61	70		21	82	96	134	
0,05	9	11	58	73	82	18	52	125	146	195	
0,1	15	18	67	87	98	30	59	163	196	262	
0,25	20	24	77	99	110	34	73	195	238	325	
0,5	21	26	82	105	116	35	83	214	258	342	
0,75	22	26	83	107	117	36	87	219	265	350	
1	22	27	84	108	118	37	89	221	269	354	
1,5	22	27	85	108	119	37	91	224	272	360	
2,5	23	27	85	109	120	38	93	226	276	364	

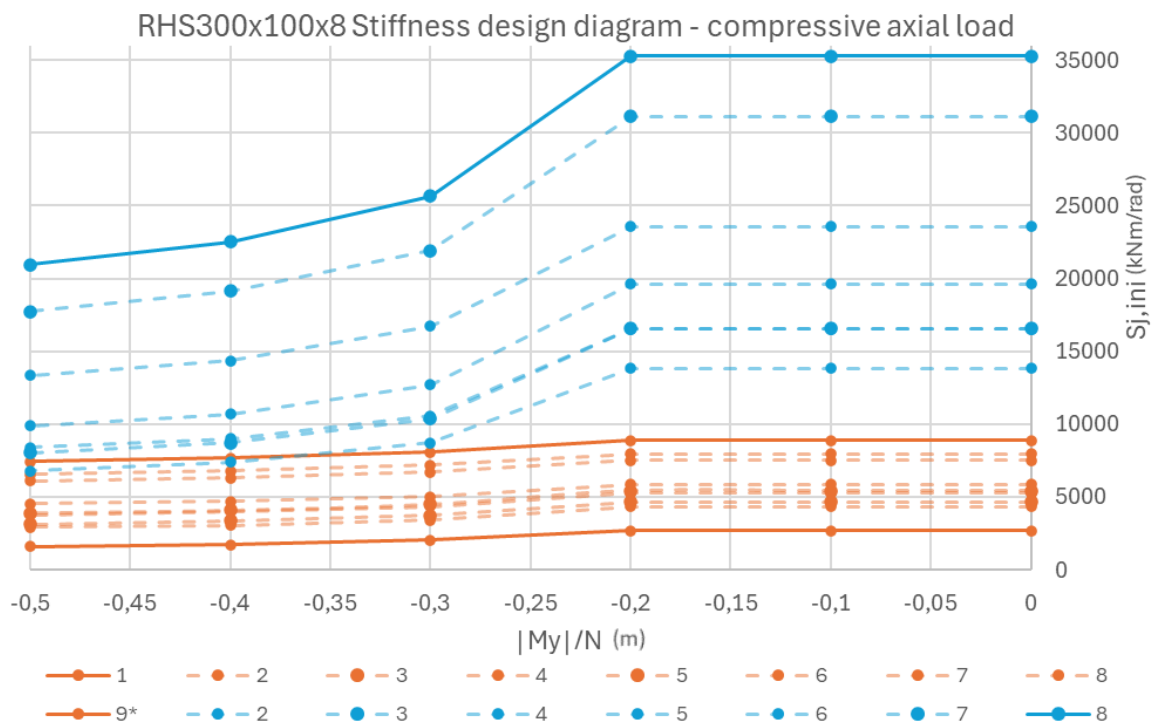
D.3 Case study: Connection RHS300x100x8



My/N	1	2	3	4	5	6	7	8	9*
-0,05	9813	10134	10224	10357	10304	10292	11355	11417	12723
-0,1	6884	7935	8080	8343	8377	8575	9775	9985	11229
-0,2	2687	4331	4647	5264	5437	5851	7506	7945	8897
-0,3	2021	3424	3708	4330	4492	5028	6700	7169	8068
-0,4	1728	3058	3373	4027	4075	4706	6310	6782	7658
-0,5	1596	2927	3138	3768	3905	4512	6097	6561	7410
-0,75	1454	2664	2901	3582	3641	4268	5809	6278	7096
-1	1400	2562	2834	3509	3530	4154	5670	6139	6937
-2,5	1328	2416	2668	3235	3347	3984	5445	5908	6676

My/N	1	2	3	4	5	6	7	8
-0,05	50916	53043	54000	63705	65180	66617	103634	105263
-0,1	51409	53006	54025	62799	63578	65284	99896	101458
-0,2	5186	13841	16546	16542	19607	23571	31112	35279
-0,3	2954	8732	10371	10585	12693	16716	21910	25664
-0,4	2471	7407	8731	8980	10671	14359	19130	22529
-0,5	2242	6792	8020	8414	9876	13352	17727	20959
-0,75	2001	6113	7200	7383	8872	12267	16133	19157
-1	1891	5838	6856	7148	8452	11592	15363	18361
-2,5	1723	5275	6312	6500	7805	10976	14314	17079

Adjusted for design application



Appendix E: Design Iterations

E.1 Iteration 1

Output ULS1								
Connectio S _{j,ini}	N	M	M/N					
ajk	1	-6,68	0,00	0,00				
bc	641	-5,85	0,15	-0,03				
cb	641	-5,87	0,15	-0,03				
dfg	90	-5,60	0,09	-0,02				
el	1	-5,61	0,00	0,00				
fdg	90	-4,76	0,11	-0,02				
gdf	90	-4,87	0,11	-0,02				
h	30	-4,60	0,02	0,00				
i	1	-14,91	0,00	0,00				
jak	2140	-14,47	-0,07	0,00				
kaj	2140	-13,36	-0,07	-0,01				
le	2140	-13,21	0,16	-0,01				
Output ULS2								
Connectio S _{j,ini}	N	M	M/N	N	M	M/N		
ajk	1	-0,51	0,00	0,00	-0,79	0,00	0,00	
bc	30	-0,13	-0,15	-1,15	-0,41	0,06	-0,14	
cb	30	-0,30	-0,15	-0,51	-0,34	0,06	-0,16	
dfg	30	-0,18	0,09	-0,48	-0,22	0,09	-0,38	
el	1	-0,71	0,00	0,00	-1,00	0,00	0,00	
fdg	30	-0,33	-0,13	-0,40	-0,61	0,06	-0,09	
gdf	30	-0,49	-0,13	-0,27	-0,53	0,06	-0,11	
h	30	-0,37	0,07	-0,18	-0,41	0,07	-0,16	
i	1	-3,38	0,00	0,00	-3,25	0,00	0,00	
jak	210	-3,15	-0,77	-0,24	-3,02	0,26	-0,09	
kaj	210	-2,68	-0,77	-0,29	-2,80	0,26	-0,09	
le	210	-2,61	0,34	-0,13	-2,73	0,34	-0,12	
Output ULS3								
Connectio S _{j,ini}	N	M	M/N	N	M	M/N		
ajk	1	0,21	0,00	0,00	-0,07	0,00	0,00	
bc	17	0,50	-0,14	0,29	0,22	0,05	0,24	
cb	17	0,33	-0,14	0,43	0,29	0,05	0,18	
dfg	20	0,42	0,09	0,20	0,38	0,09	0,23	
el	1	-0,08	0,00	0,00	-0,36	0,00	0,00	
fdg	20	0,21	-0,15	0,71	-0,07	0,05	-0,72	
gdf	20	0,06	-0,15	2,36	0,02	0,05	2,67	
h	1	0,15	0,00	0,03	0,11	0,00	0,04	
i	1	-1,65	0,00	0,00	-1,53	0,00	0,00	
jak	108	-1,48	-0,75	-0,50	-1,36	0,26	-0,19	
kaj	108	-1,14	-0,75	-0,66	-1,26	0,26	-0,21	
le	108	-1,08	0,35	-0,33	-1,20	0,35	-0,29	

E.2 Iteration 2

Output ULS1								
Connectio	Sj,ini	N	M	M/N				
ajk	1	-6,65	0,00	0,00				
bc	690	-5,83	0,15	-0,03				
cb	690	-5,84	0,15	-0,03				
dfg	82	-5,57	0,09	-0,02				
el	1	-5,65	0,00	0,00				
fdg	82	-4,80	0,11	-0,02				
gdf	82	-4,91	0,11	-0,02				
h	82	-4,63	0,03	-0,01				
i	1	-14,92	0,00	0,00				
jak	2050	-14,48	-0,06	0,00				
kaj	2050	-13,36	-0,06	0,00				
le	2050	-13,22	0,16	-0,01				
Output ULS2								
Connectio	Sj,ini	N	M	M/N	N	M	M/N	
ajk	1	-0,54	0,00	0,00	-0,75	0,00	0,00	
bc	154	-0,16	-0,30	-1,95	-0,37	0,11	-0,29	
cb	160	-0,26	-0,30	-1,17	-0,33	0,11	-0,33	
dfg	32	-0,14	0,07	-0,46	-0,21	0,07	-0,31	
el	1	-0,68	0,00	0,00	-0,97	0,00	0,00	
fdg	32	-0,29	-0,11	-0,38	-0,59	0,05	-0,08	
gdf	34	-0,46	-0,11	-0,24	-0,50	0,05	-0,10	
h	35	-0,35	0,06	-0,19	-0,39	0,06	-0,17	
i	1	-3,35	0,00	0,00	-3,28	0,00	0,00	
jak	285	-3,12	-0,63	-0,20	-3,05	0,19	-0,06	
kaj	275	-2,70	-0,63	-0,23	-2,80	0,19	-0,07	
le	400	-2,63	0,34	-0,13	-2,73	0,34	-0,12	
Output ULS3								
Connectio	Sj,ini	N	M	M/N	N	M	M/N	
ajk	1	0,20	0,00	0,00	-0,02	0,00	0,00	
bc	131	0,49	-0,30	0,61	0,26	0,09	0,34	
cb	116	0,38	-0,30	0,78	0,31	0,09	0,29	
dfg	24	0,47	0,05	0,12	0,40	0,05	0,13	
el	1	-0,04	0,00	0,00	-0,34	0,00	0,00	
fdg	28	0,25	-0,12	0,47	-0,05	0,04	-0,75	
gdf	29	0,08	-0,12	1,42	0,04	0,04	0,87	
h	12	0,17	0,03	0,18	0,13	0,03	0,23	
i	1	-1,62	0,00	0,00	-1,55	0,00	0,00	
jak	253	-1,45	-0,64	-0,44	-1,38	0,20	-0,14	
kaj	250	-1,15	-0,64	-0,56	-1,25	0,20	-0,16	
le	273	-1,10	0,33	-0,30	-1,20	0,33	-0,27	

E.3 Iteration 3

Output ULS1								
Connectio	Sj,ini	N	M	M/N				
ajk	1	-6,65	0,00	0,00				
bc	690	-5,83	0,15	-0,03				
cb	690	-5,84	0,15	-0,03				
dfg	82	-5,57	0,09	-0,02				
el	1	-5,65	0,00	0,00				
fdg	82	-4,80	0,11	-0,02				
gdf	82	-4,91	0,11	-0,02				
h	82	-4,63	0,03	-0,01				
i	1	-14,92	0,00	0,00				
jak	2050	-14,48	-0,06	0,00				
kaj	2050	-13,36	-0,06	0,00				
le	2050	-13,22	0,16	-0,01				
Output ULS2								
Connectio	Sj,ini	N	M	M/N	N	M	M/N	
ajk	1	-0,54	0,00	0,00	-0,76	0,00	0,00	
bc	153	-0,15	-0,29	-1,91	-0,37	0,10	-0,27	
cb	155	-0,26	-0,29	-1,11	-0,33	0,10	-0,31	
dfg	32	-0,14	0,06	-0,45	-0,21	0,06	-0,31	
el	1	-0,68	0,00	0,00	-0,97	0,00	0,00	
fdg	33	-0,29	-0,11	-0,37	-0,59	0,05	-0,08	
gdf	34	-0,46	-0,11	-0,24	-0,50	0,05	-0,09	
h	35	-0,35	0,06	-0,18	-0,38	0,06	-0,16	
i	1	-3,34	0,00	0,00	-3,27	0,00	0,00	
jak	331	-3,12	-0,65	-0,21	-3,04	0,19	-0,06	
kaj	302	-2,69	-0,65	-0,24	-2,79	0,19	-0,07	
le	400	-2,62	0,33	-0,13	-2,72	0,33	-0,12	
Output ULS3								
Connectio	Sj,ini	N	M	M/N	N	M	M/N	
ajk	1	0,20	0,00	0,00	-0,02	0,00	0,00	
bc	134	0,49	-0,30	0,62	0,27	0,09	0,34	
cb	131	0,38	-0,31	0,80	0,32	0,09	0,29	
dfg	23	0,47	0,05	0,11	0,40	0,05	0,13	
el	1	-0,05	0,00	0,00	-0,34	0,00	0,00	
fdg	27	0,24	-0,11	0,45	-0,05	0,04	-0,70	
gdf	28	0,08	-0,11	1,38	0,04	0,04	0,93	
h	24	0,17	0,05	0,31	0,13	0,05	0,41	
i	1	-1,62	0,00	0,00	-1,55	0,00	0,00	
jak	259	-1,45	-0,63	-0,43	-1,38	0,20	-0,14	
kaj	250	-1,15	-0,63	-0,55	-1,25	0,20	-0,16	
le	277	-1,10	0,32	-0,29	-1,20	0,32	-0,27	

E.4 Final design

Output ULS1								
Connectio	Sj,ini	N	M	M/N				
ajk	1	-6,65	0,00	0,00				
bc	690	-5,83	0,15	-0,03				
cb	690	-5,84	0,15	-0,03				
dfg	82	-5,57	0,09	-0,02				
el	1	-5,65	0,00	0,00				
fdg	82	-4,80	0,11	-0,02				
gdf	82	-4,91	0,11	-0,02				
h	82	-4,63	0,03	-0,01				
i	1	-14,92	0,00	0,00				
jak	2050	-14,48	-0,06	0,00				
kaj	2050	-13,36	-0,06	0,00				
le	2050	-13,22	0,16	-0,01				
Output ULS2								
Connectio	Sj,ini	N	M	M/N	N	M	M/N	
ajk	1	-0,54	0,00	0,00	-0,76	0,00	0,00	
bc	153	-0,15	-0,29	-1,92	-0,37	0,10	-0,28	
cb	155	-0,26	-0,29	-1,12	-0,33	0,10	-0,31	
dfg	32	-0,14	0,06	-0,45	-0,21	0,06	-0,31	
el	1	-0,68	0,00	0,00	-0,97	0,00	0,00	
fdg	33	-0,29	-0,11	-0,38	-0,59	0,05	-0,08	
gdf	34	-0,46	-0,11	-0,24	-0,50	0,05	-0,09	
h	36	-0,35	0,07	-0,19	-0,38	0,07	-0,17	
i	1	-3,35	0,00	0,00	-3,27	0,00	0,00	
jak	320	-3,12	-0,65	-0,21	-3,05	0,19	-0,06	
kaj	292	-2,70	-0,65	-0,24	-2,80	0,19	-0,07	
le	400	-2,62	0,33	-0,13	-2,73	0,33	-0,12	
Output ULS3								
Connectio	Sj,ini	N	M	M/N	N	M	M/N	
ajk	1	0,20	0,00	0,00	-0,02	0,00	0,00	
bc	134	0,49	-0,30	0,62	0,27	0,09	0,34	
cb	131	0,38	-0,30	0,80	0,32	0,09	0,29	
dfg	23	0,47	0,05	0,11	0,40	0,05	0,13	
el	1	-0,05	0,00	0,00	-0,34	0,00	0,00	
fdg	27	0,24	-0,11	0,45	-0,05	0,04	-0,70	
gdf	28	0,08	-0,11	1,37	0,04	0,04	0,93	
h	25	0,17	0,05	0,32	0,13	0,05	0,42	
i	1	-1,62	0,00	0,00	-1,55	0,00	0,00	
jak	260	-1,45	-0,63	-0,44	-1,38	0,20	-0,14	
kaj	255	-1,15	-0,63	-0,55	-1,25	0,20	-0,16	
le	277	-1,10	0,32	-0,29	-1,20	0,32	-0,27	

E.5 After stiffness analysis

Output ULS1								
Connectio	Sj,ini	N	M	M/N				
ajk	1	-6,66	0,00	0,00				
bc	744	-5,83	0,15	-0,02				
cb	744	-5,84	0,15	-0,02				
dfg	76	-5,58	0,09	-0,02				
el	1	-5,63	0,00	0,00				
fdg	77	-4,78	0,11	-0,02				
gdf	76	-4,90	0,11	-0,02				
h	77	-4,62	0,02	0,00				
i	1	-14,92	0,00	0,00				
jak	2302	-14,48	-0,07	0,00				
kaj	2301	-13,36	-0,06	0,00				
le	2333	-13,22	0,16	-0,01				
Output ULS2								
Connectio	Sj,ini	N	M	M/N	N	M	M/N	
ajk	1	-0,54	0,00	0,00	-0,75	0,00	0,00	
bc	151	-0,15	-0,30	-1,95	-0,37	0,10	-0,28	
cb	153	-0,26	-0,30	-1,15	-0,33	0,10	-0,32	
dfg	32	-0,14	0,07	-0,46	-0,21	0,07	-0,31	
el	1	-0,68	0,00	0,00	-0,97	0,00	0,00	
fdg	34	-0,29	-0,11	-0,39	-0,59	0,05	-0,08	
gdf	35	-0,46	-0,11	-0,25	-0,50	0,05	-0,10	
h	34	-0,34	0,06	-0,19	-0,38	0,06	-0,17	
i	1	-3,35	0,00	0,00	-3,27	0,00	0,00	
jak	299	-3,12	-0,65	-0,21	-3,05	0,19	-0,06	
kaj	287	-2,70	-0,65	-0,24	-2,80	0,19	-0,07	
le	377	-2,63	0,33	-0,13	-2,73	0,33	-0,12	
Output ULS3								
Connectio	Sj,ini	N	M	M/N	N	M	M/N	
ajk	1	0,20	0,00	0,00	-0,02	0,00	0,00	
bc	136	0,49	-0,31	0,63	0,27	0,09	0,34	
cb	136	0,38	-0,31	0,81	0,32	0,09	0,29	
dfg	23	0,47	0,05	0,11	0,40	0,05	0,13	
el	1	-0,04	0,00	0,00	-0,34	0,00	0,00	
fdg	27	0,24	-0,11	0,45	-0,05	0,04	-0,71	
gdf	28	0,08	-0,11	1,35	0,04	0,04	0,90	
h	26	0,17	0,06	0,33	0,13	0,06	0,43	
i	1	-1,62	0,00	0,00	-1,55	0,00	0,00	
jak	257	-1,45	-0,63	-0,43	-1,38	0,20	-0,14	
kaj	250	-1,15	-0,63	-0,54	-1,25	0,20	-0,16	
le	275	-1,10	0,32	-0,29	-1,20	0,32	-0,27	

Appendix F: Stiffness analysis

F.1 Stiffness analysis: Design chapter 5

Project data

Project name	Stiffness analysis
Project number	Chapter 5
Author	Friso van Spengler
Description	
Date	2024.05
Code	EN

Material

Steel	S 355
-------	-------

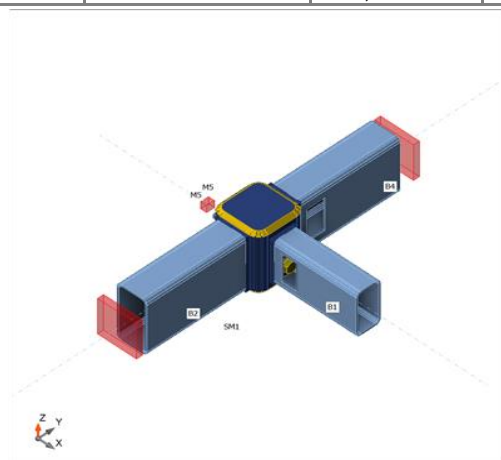
a

Analysis: Stiffness

Members

Geometry

Name	Cross-section	β - Direction [°]	γ - Pitch [°]	α - Rotation [°]	Offset ex [mm]	Offset ey [mm]	Offset ez [mm]
B1	1 - RHS80/40/3.0	0,0	0,0	0,0	0	0	0
B2	6 - RHS100/50/3.0	-90,0	0,0	0,0	0	0	0
B4	6 - RHS100/50/3.0	90,0	0,0	0,0	0	0	0
M5	7 - FLA20/8	180,0	0,0	0,0	0	0	0



Material

Steel	S 355 (EN)
Bolts	M12 8.8

Load effects

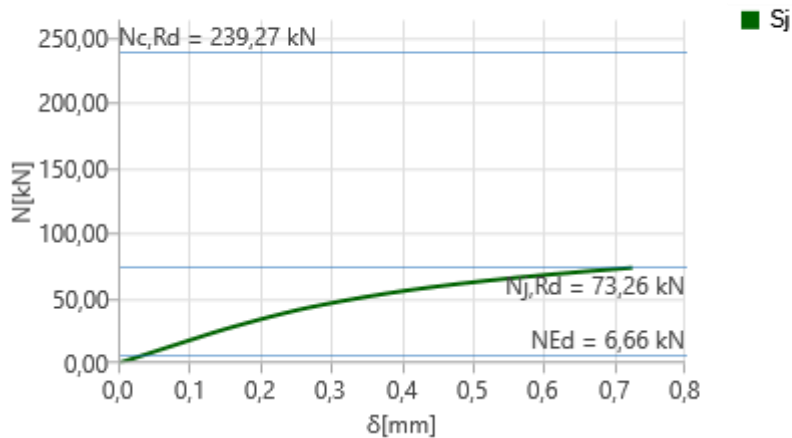
Name	Member	N	Vy	Vz	Mx	My	Mz
------	--------	---	----	----	----	----	----

		[kN]	[kN]	[kN]	[kNm]	[kNm]	[kNm]
ULS1	B1 / End	-6,66	0,00	0,00	0,00	0,00	0,00
	B2 / End	0,00	0,00	0,00	0,00	0,00	0,00
	B4 / End	0,00	0,00	0,00	0,00	0,00	0,00
	M5 / End	0,00	0,00	0,00	0,00	0,00	0,00

Axial stiffness

Name	Component	Loads	N [kN]	N _{j,Rd} [kN]	dx [mm]	St [kN/m]
B1	N	ULS1	-6,66	-73,26	0	175953

N - δ



Stiffness diagram N - δ, ULS1

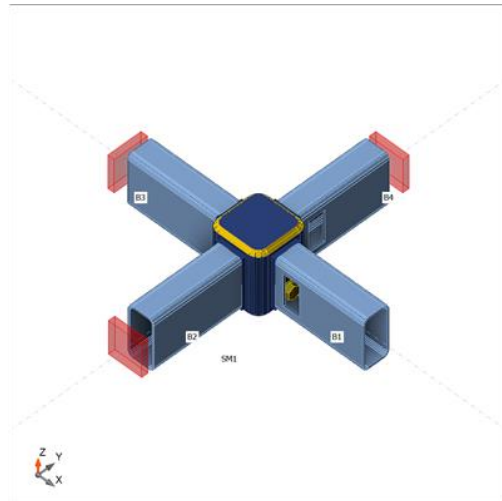
b

Analysis: Stiffness

Members

Geometry

Name	Cross-section	β - Direction [°]	γ - Pitch [°]	α - Rotation [°]	Offset ex [mm]	Offset ey [mm]	Offset ez [mm]
B1	1 - RHS80/40/3.0	0,0	0,0	0,0	0	0	0
B2	1 - RHS80/40/3.0	-90,0	0,0	0,0	0	0	0
B3	1 - RHS80/40/3.0	180,0	0,0	0,0	0	0	0
B4	1 - RHS80/40/3.0	90,0	0,0	0,0	0	0	0



Material

Steel	S 355 (EN)
Bolts	M12 8.8

Load effects

Name	Member	N [kN]	Vy [kN]	Vz [kN]	Mx [kNm]	My [kNm]	Mz [kNm]
ULS1	B1 / End	-5,84	0,00	0,00	0,00	0,18	0,00
	B2 / End	0,00	0,00	0,00	0,00	0,00	0,00
	B3 / End	0,00	0,00	0,00	0,00	0,00	0,00
	B4 / End	0,00	0,00	0,00	0,00	0,00	0,00
ULS2a	B1 / End	-1,07	0,00	0,00	0,00	-2,06	0,00
	B2 / End	0,00	0,00	0,00	0,00	0,00	0,00
	B3 / End	0,00	0,00	0,00	0,00	0,00	0,00
	B4 / End	0,00	0,00	0,00	0,00	0,00	0,00
ULS2b	B1 / End	-1,12	0,00	0,00	0,00	0,31	0,00
	B2 / End	0,00	0,00	0,00	0,00	0,00	0,00
	B3 / End	0,00	0,00	0,00	0,00	0,00	0,00
	B4 / End	0,00	0,00	0,00	0,00	0,00	0,00
ULS3a	B1 / End	1,28	0,00	0,00	0,00	-0,91	0,00
	B2 / End	0,00	0,00	0,00	0,00	0,00	0,00
	B3 / End	0,00	0,00	0,00	0,00	0,00	0,00
	B4 / End	0,00	0,00	0,00	0,00	0,00	0,00
ULS3b	B1 / End	1,01	0,00	0,00	0,00	0,36	0,00
	B2 / End	0,00	0,00	0,00	0,00	0,00	0,00
	B3 / End	0,00	0,00	0,00	0,00	0,00	0,00
	B4 / End	0,00	0,00	0,00	0,00	0,00	0,00

Rotational stiffness

Name	Comp.	Loads	Mj,Rd [kNm]	Sj,ini [kNm/rad]	Φc [mrad]	L [m]	Sj,R [kNm/rad]	Sj,P [kNm/rad]	Class.
B1	My	ULS1	2,37	743,7	14,26	1,50	1897,0	37,9	Semi-rigid
	My	ULS2a	-3,06	151,2	40,42	1,50	1897,0	37,9	Semi-rigid
	My	ULS2b	3,28	172,2	42,90	1,50	1897,0	37,9	Semi-rigid
	My	ULS3a	-2,92	141,4	39,32	1,50	1897,0	37,9	Semi-rigid
	My	ULS3b	2,82	135,5	39,01	1,50	1897,0	37,9	Semi-rigid

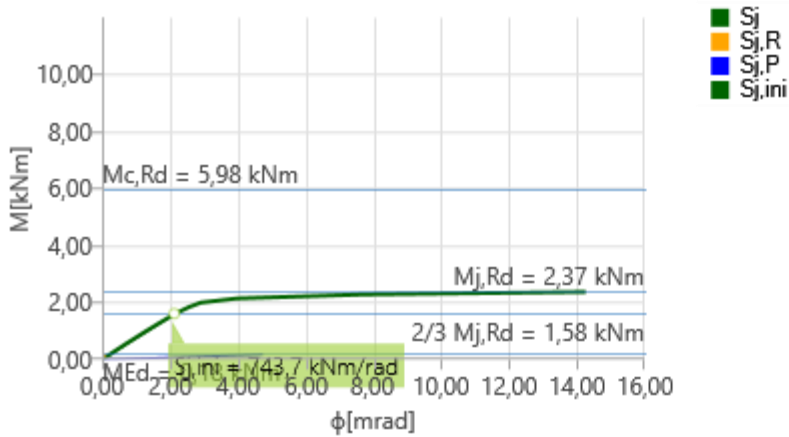
Secant rotational stiffness

Name	Comp.	Loads	M [kNm]	Sjs [kNm/rad]	Φ [mrad]
B1	My	ULS1	0,18	799,6	0,23
	My	ULS2a	-2,06	150,1	13,73
	My	ULS2b	0,31	188,5	1,64

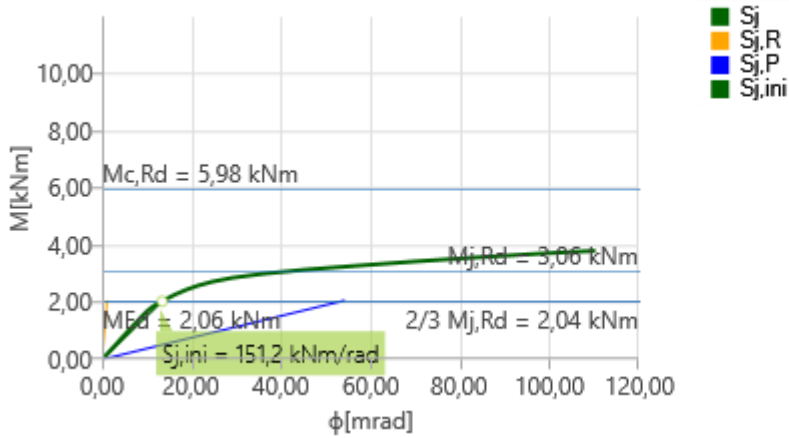
	My	ULS3a	-0,91	161,5	5,63
	My	ULS3b	0,36	155,6	2,31

Symbol explanation

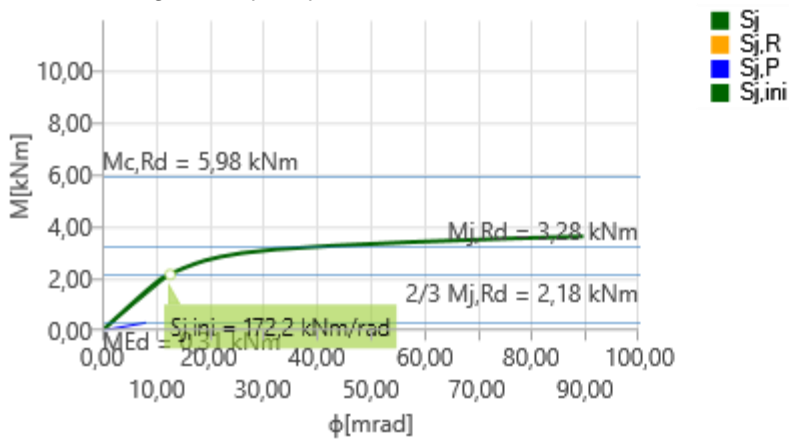
- $M_{j,Rd}$ Bending resistance
- $S_{j,ini}$ Initial rotational stiffness
- $S_{j,s}$ Secant rotational stiffness
- Φ Rotational deformation
- Φ_c Rotational capacity
- $S_{j,R}$ Limit value - rigid joint
- $S_{j,P}$ Limit value - nominally pinned joint



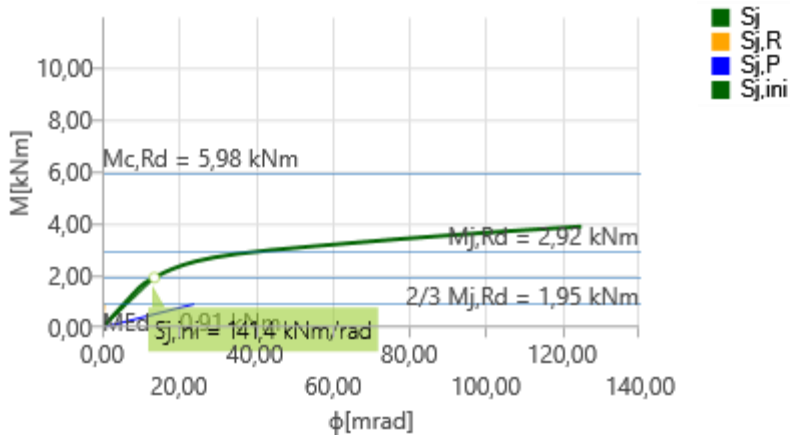
Stiffness diagram My - ϕ , ULS1



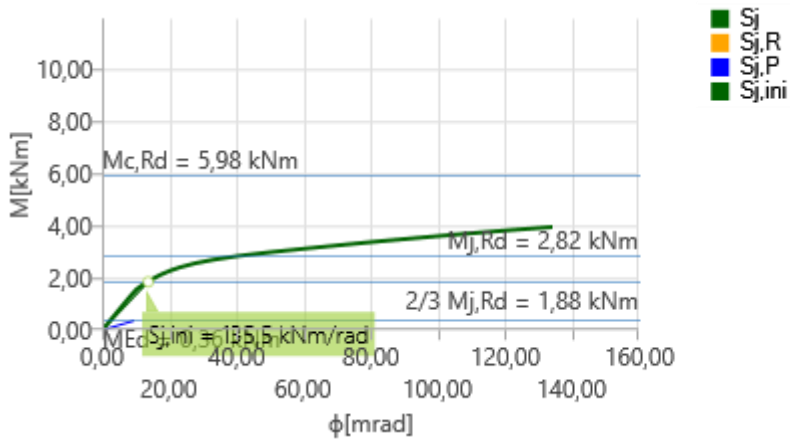
Stiffness diagram My - ϕ , ULS2a



Stiffness diagram My - ϕ , ULS2b



Stiffness diagram $M_y - \phi_y$, ULS3a

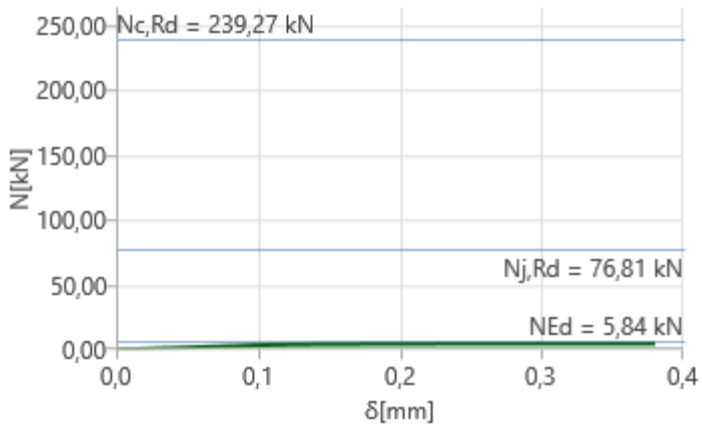


Stiffness diagram $M_y - \phi_y$, ULS3b

Axial stiffness

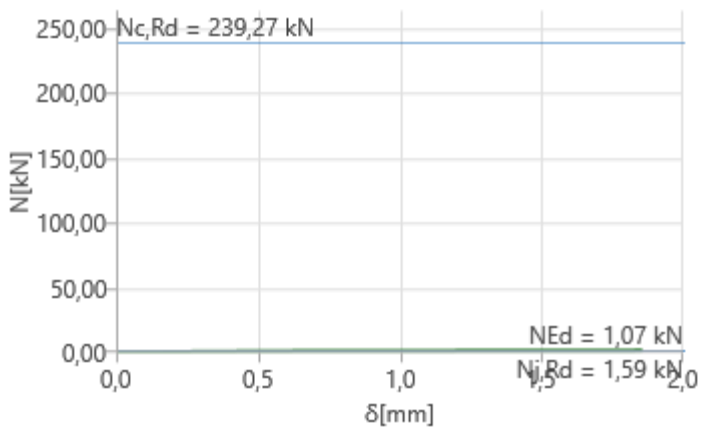
Name	Component	Loads	N [kN]	Nj,Rd [kN]	dx [mm]	St [kN/m]
B1	N	ULS1	-5,84	-76,81	0	2763050
		ULS2a	-1,07	-1,59	1	1073
		ULS2b	-1,12	-11,83	1	1665
		ULS3a	1,28	4,11	1	1019
		ULS3b	1,01	7,92	1	695

N - δ



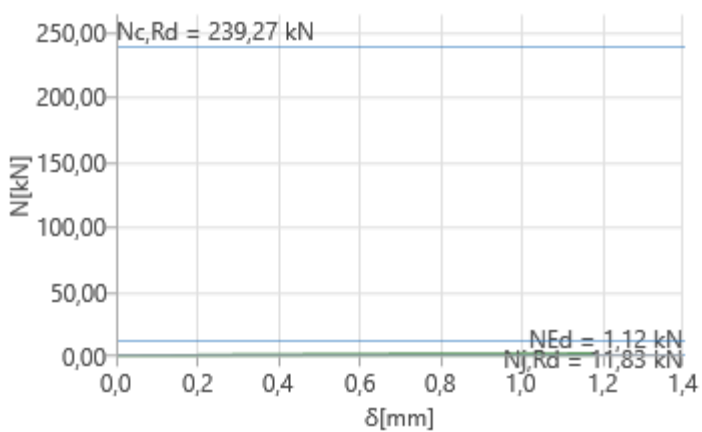
Stiffness diagram N - δ , ULS1

N - δ



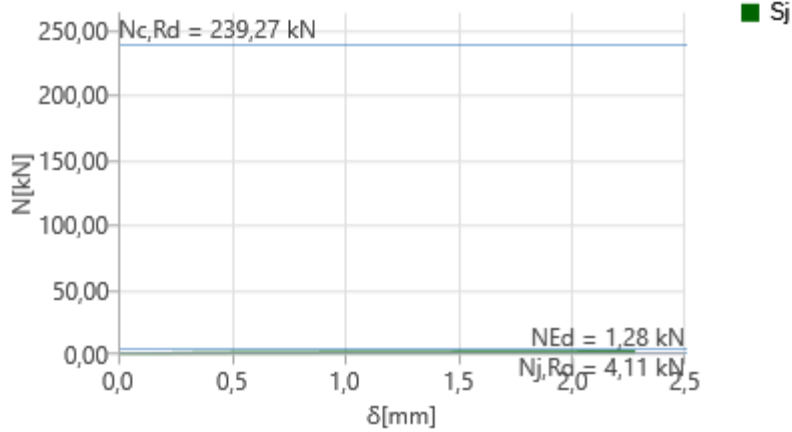
Stiffness diagram N - δ , ULS2a

N - δ



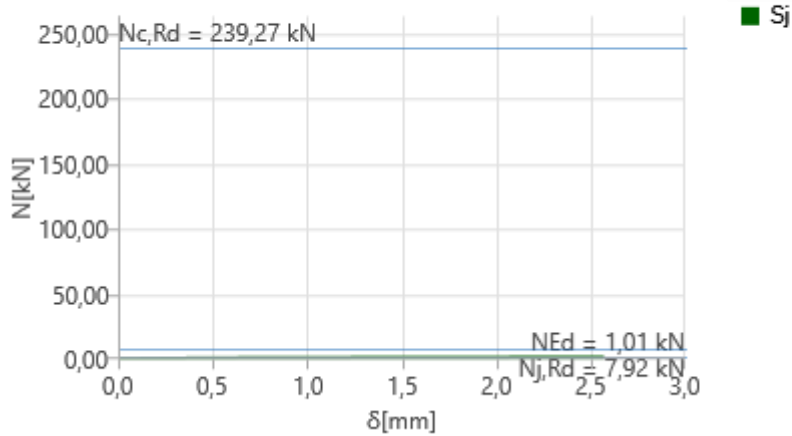
Stiffness diagram N - δ , ULS2b

N - δ



Stiffness diagram N - δ , ULS3a

N - δ



Stiffness diagram N - δ , ULS3b

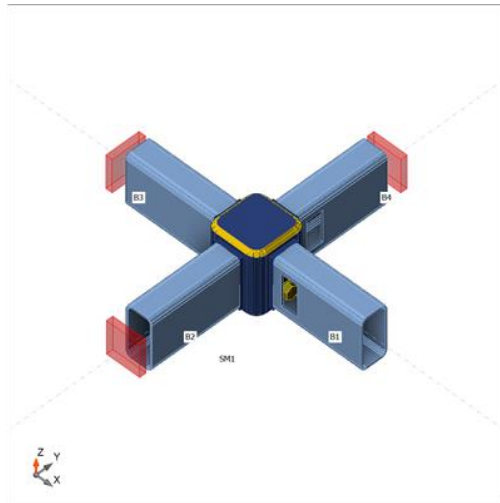
C

Analysis: Stiffness

Members

Geometry

Name	Cross-section	β - Direction [°]	γ - Pitch [°]	α - Rotation [°]	Offset ex [mm]	Offset ey [mm]	Offset ez [mm]
B1	1 - RHS80/40/3.0	0,0	0,0	0,0	0	0	0
B2	1 - RHS80/40/3.0	-90,0	0,0	0,0	0	0	0
B3	1 - RHS80/40/3.0	180,0	0,0	0,0	0	0	0
B4	1 - RHS80/40/3.0	90,0	0,0	0,0	0	0	0



Material

Steel	S 355 (EN)
Bolts	M12 8.8

Load effects

Name	Member	N [kN]	Vy [kN]	Vz [kN]	Mx [kNm]	My [kNm]	Mz [kNm]
ULS1	B1 / End	-5,85	0,00	0,00	0,00	0,18	0,00
	B2 / End	0,00	0,00	0,00	0,00	0,00	0,00
	B3 / End	0,00	0,00	0,00	0,00	0,00	0,00
	B4 / End	0,00	0,00	0,00	0,00	0,00	0,00
ULS2a	B1 / End	-1,05	0,00	0,00	0,00	-1,18	0,00
	B2 / End	0,00	0,00	0,00	0,00	0,00	0,00
	B3 / End	0,00	0,00	0,00	0,00	0,00	0,00
	B4 / End	0,00	0,00	0,00	0,00	0,00	0,00
ULS2b	B1 / End	-1,31	0,00	0,00	0,00	0,41	0,00
	B2 / End	0,00	0,00	0,00	0,00	0,00	0,00
	B3 / End	0,00	0,00	0,00	0,00	0,00	0,00
	B4 / End	0,00	0,00	0,00	0,00	0,00	0,00
ULS3a	B1 / End	1,53	0,00	0,00	0,00	-1,22	0,00
	B2 / End	0,00	0,00	0,00	0,00	0,00	0,00
	B3 / End	0,00	0,00	0,00	0,00	0,00	0,00
	B4 / End	0,00	0,00	0,00	0,00	0,00	0,00
ULS3b	B1 / End	1,01	0,00	0,00	0,00	0,36	0,00
	B2 / End	0,00	0,00	0,00	0,00	0,00	0,00
	B3 / End	0,00	0,00	0,00	0,00	0,00	0,00
	B4 / End	0,00	0,00	0,00	0,00	0,00	0,00

Rotational stiffness

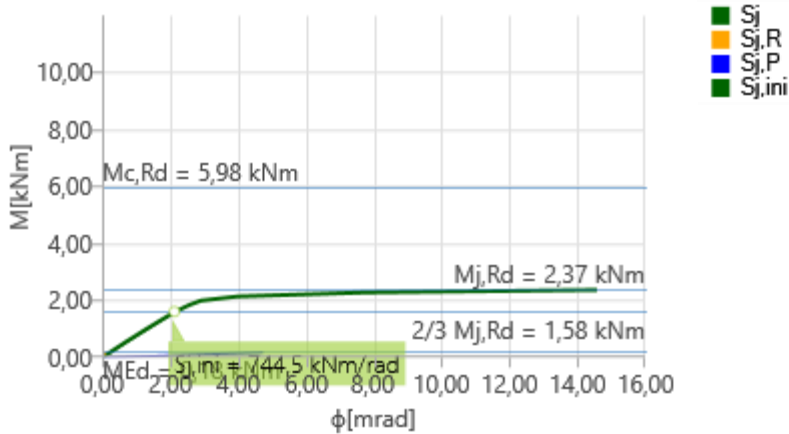
Name	Comp.	Loads	Mj,Rd [kNm]	Sj,ini [kNm/rad]	Φc [mrad]	L [m]	Sj,R [kNm/rad]	Sj,P [kNm/rad]	Class.
B1	My	ULS1	2,37	744,5	14,58	1,50	1897,0	37,9	Semi-rigid
	My	ULS2a	-3,09	153,3	40,66	1,50	1897,0	37,9	Semi-rigid
	My	ULS2b	3,25	169,0	42,36	1,50	1897,0	37,9	Semi-rigid
	My	ULS3a	-2,93	142,2	39,26	1,50	1897,0	37,9	Semi-rigid
	My	ULS3b	2,82	135,5	39,01	1,50	1897,0	37,9	Semi-rigid

Secant rotational stiffness

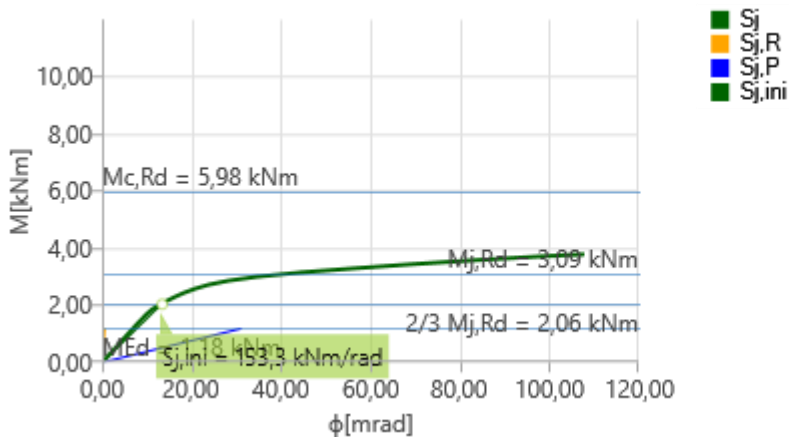
Name	Comp.	Loads	M [kNm]	S _{j,s} [kNm/rad]	Φ [mrad]
B1	My	ULS1	0,18	800,2	0,22
	My	ULS2a	-1,18	172,1	6,86
	My	ULS2b	0,41	185,8	2,21
	My	ULS3a	-1,22	161,7	7,54
	My	ULS3b	0,36	155,6	2,31

Symbol explanation

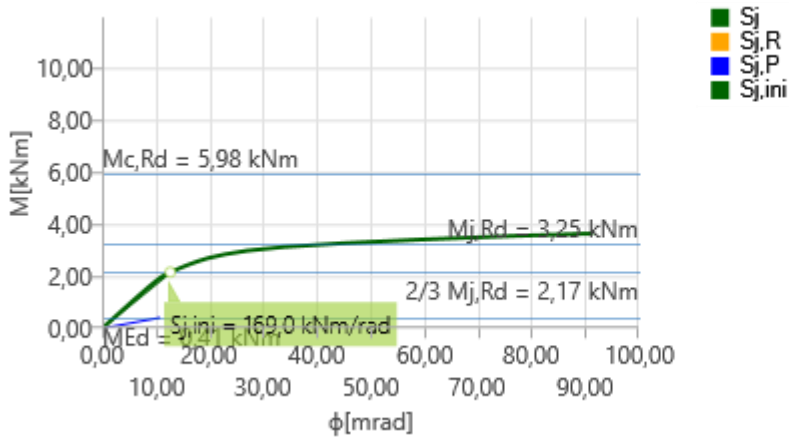
- M_{j,Rd} Bending resistance
- S_{j,ini} Initial rotational stiffness
- S_{j,s} Secant rotational stiffness
- Φ Rotational deformation
- Φ_c Rotational capacity
- S_{j,R} Limit value - rigid joint
- S_{j,P} Limit value - nominally pinned joint



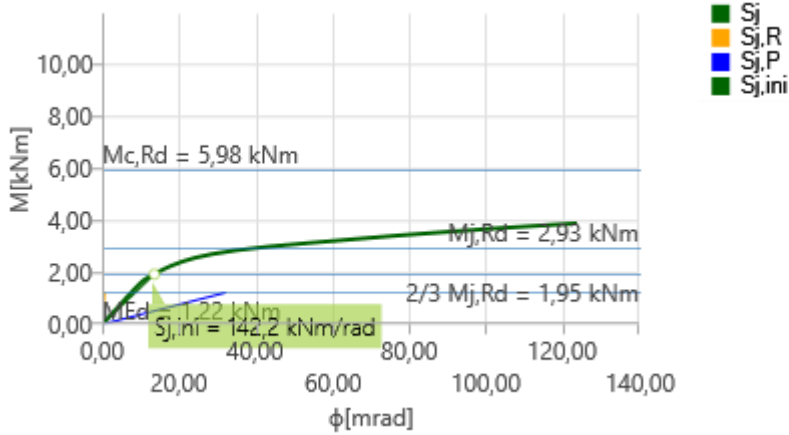
Stiffness diagram My - ϕ , ULS1



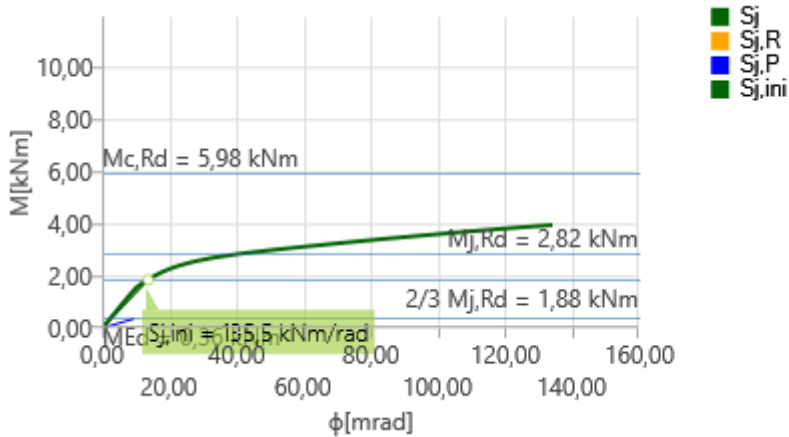
Stiffness diagram My - ϕ , ULS2a



Stiffness diagram $M_y - \phi_y$, ULS2b



Stiffness diagram $M_y - \phi_y$, ULS3a

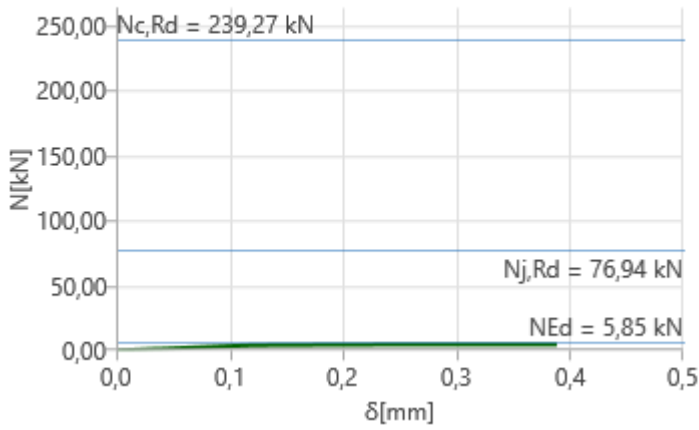


Stiffness diagram $M_y - \phi_y$, ULS3b

Axial stiffness

Name	Component	Loads	N [kN]	N _{j,Rd} [kN]	dx [mm]	St [kN/m]
B1	N	ULS1	-5,85	-76,94	0	2762626
		ULS2a	-1,05	-2,75	1	1103
		ULS2b	-1,31	-10,38	1	1850
		ULS3a	1,53	3,67	1	1239
		ULS3b	1,01	7,92	1	695

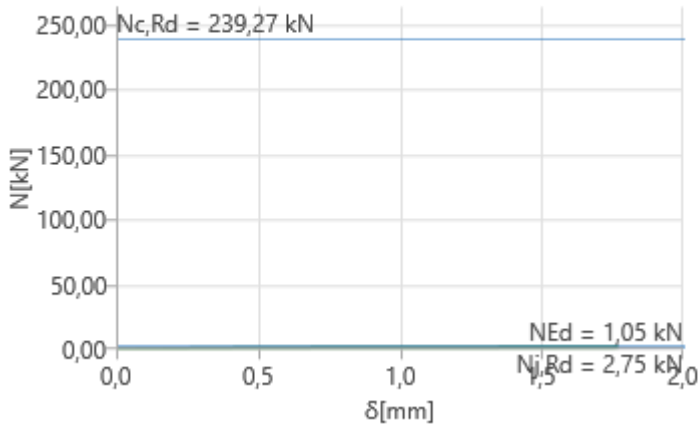
N - δ



■ Sj

Stiffness diagram N - δ , ULS1

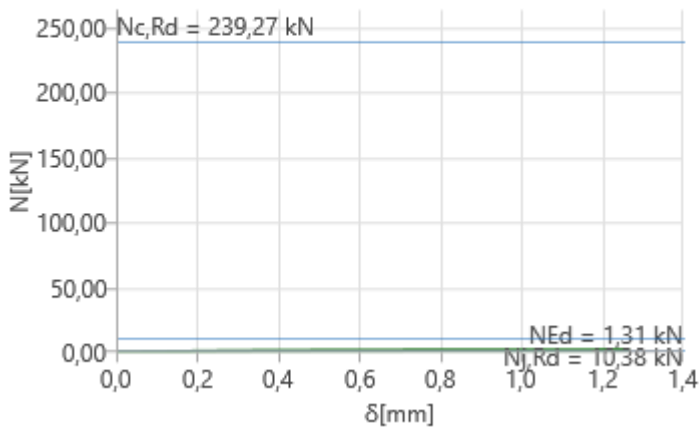
N - δ



■ Sj

Stiffness diagram N - δ , ULS2a

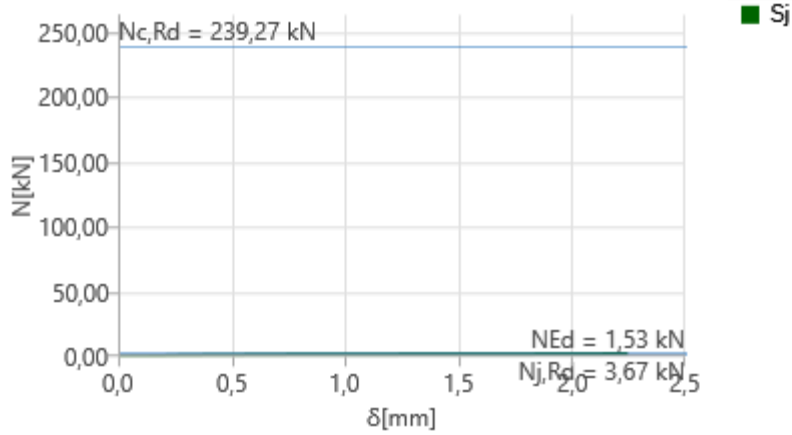
N - δ



■ Sj

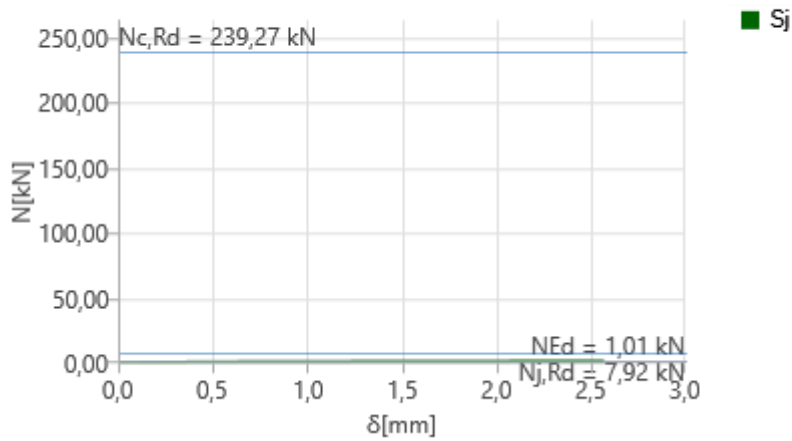
Stiffness diagram N - δ , ULS2b

N - δ



Stiffness diagram N - δ , ULS3a

N - δ



Stiffness diagram N - δ , ULS3b

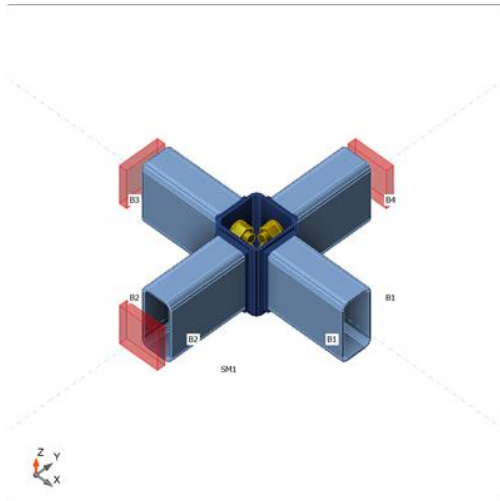
d

Analysis: Stiffness

Members

Geometry

Name	Cross-section	β - Direction [°]	γ - Pitch [°]	α - Rotation [°]	Offset ex [mm]	Offset ey [mm]	Offset ez [mm]
B1	1 - RHS80/40/3.0	0,0	0,0	0,0	0	0	0
B2	1 - RHS80/40/3.0	-90,0	0,0	0,0	0	0	0
B3	1 - RHS80/40/3.0	180,0	0,0	0,0	0	0	0
B4	1 - RHS80/40/3.0	90,0	0,0	0,0	0	0	0



Material

Steel	S 355 (EN)
Bolts	M12 8.8

Load effects

Name	Member	N [kN]	Vy [kN]	Vz [kN]	Mx [kNm]	My [kNm]	Mz [kNm]
ULS1	B1 / End	-5,58	0,00	0,00	0,00	0,17	0,00
	B2 / End	0,00	0,00	0,00	0,00	0,00	0,00
	B3 / End	0,00	0,00	0,00	0,00	0,00	0,00
	B4 / End	0,00	0,00	0,00	0,00	0,00	0,00
ULS2a	B1 / End	-1,01	0,00	0,00	0,00	0,45	0,00
	B2 / End	0,00	0,00	0,00	0,00	0,00	0,00
	B3 / End	0,00	0,00	0,00	0,00	0,00	0,00
	B4 / End	0,00	0,00	0,00	0,00	0,00	0,00
ULS2b	B1 / End	-1,05	0,00	0,00	0,00	0,32	0,00
	B2 / End	0,00	0,00	0,00	0,00	0,00	0,00
	B3 / End	0,00	0,00	0,00	0,00	0,00	0,00
	B4 / End	0,00	0,00	0,00	0,00	0,00	0,00
ULS3a	B1 / End	1,41	0,00	0,00	0,00	0,16	0,00
	B2 / End	0,00	0,00	0,00	0,00	0,00	0,00
	B3 / End	0,00	0,00	0,00	0,00	0,00	0,00
	B4 / End	0,00	0,00	0,00	0,00	0,00	0,00
ULS3b	B1 / End	1,21	0,00	0,00	0,00	0,16	0,00
	B2 / End	0,00	0,00	0,00	0,00	0,00	0,00
	B3 / End	0,00	0,00	0,00	0,00	0,00	0,00
	B4 / End	0,00	0,00	0,00	0,00	0,00	0,00

Rotational stiffness

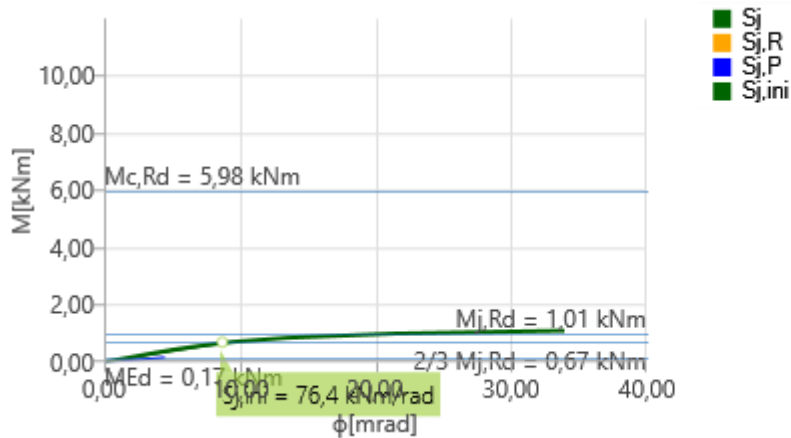
Name	Comp.	Loads	Mj,Rd [kNm]	Sj,ini [kNm/rad]	Φc [mrad]	L [m]	Sj,R [kNm/rad]	Sj,P [kNm/rad]	Class.
B1	My	ULS1	1,01	76,4	22,10	1,50	1897,0	37,9	Semi-rigid
	My	ULS2a	0,88	33,2	43,70	1,50	1897,0	37,9	Pinned
	My	ULS2b	0,88	34,1	40,13	1,50	1897,0	37,9	Pinned
	My	ULS3a	0,74	25,8	50,43	1,50	1897,0	37,9	Pinned
	My	ULS3b	0,76	26,5	49,62	1,50	1897,0	37,9	Pinned

Secant rotational stiffness

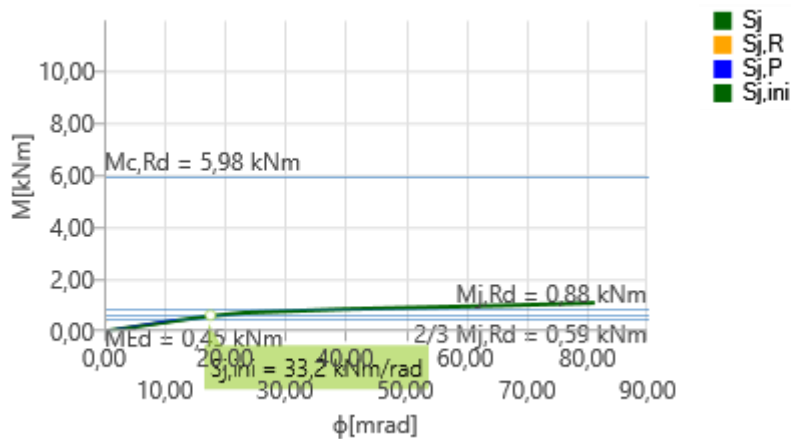
Name	Comp.	Loads	M [kNm]	S _{js} [kNm/rad]	Φ [mrad]
B1	My	ULS1	0,17	89,8	1,89
	My	ULS2a	0,45	34,3	13,11
	My	ULS2b	0,32	35,5	9,03
	My	ULS3a	0,16	27,7	5,78
	My	ULS3b	0,16	28,3	5,65

Symbol explanation

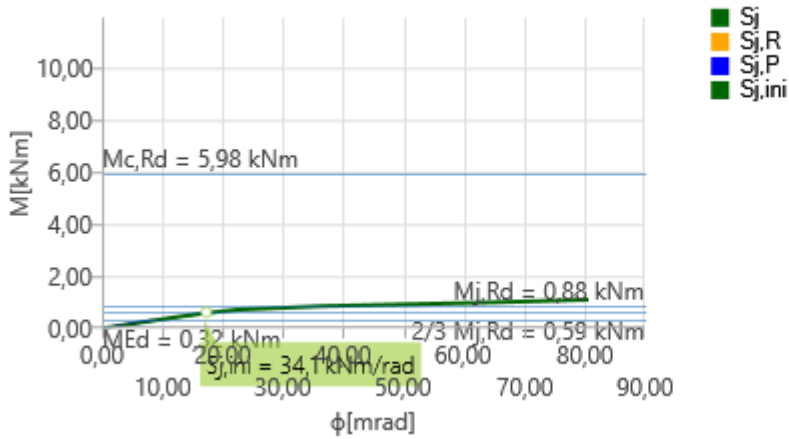
- M_{j,Rd} Bending resistance
- S_{j,ini} Initial rotational stiffness
- S_{j,s} Secant rotational stiffness
- Φ Rotational deformation
- Φ_c Rotational capacity
- S_{j,R} Limit value - rigid joint
- S_{j,P} Limit value - nominally pinned joint



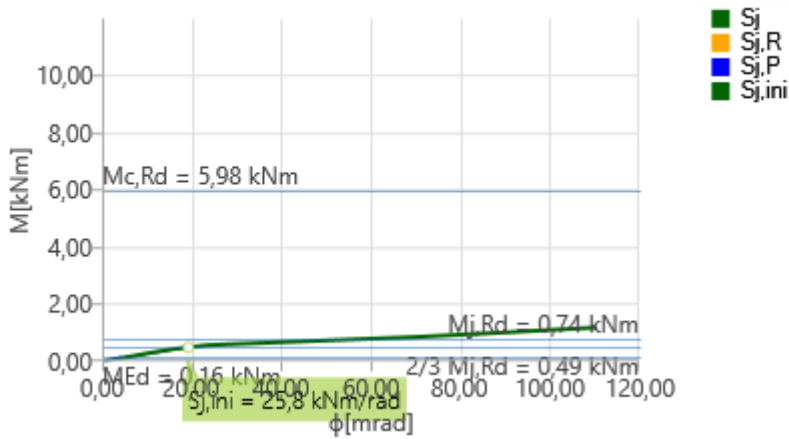
Stiffness diagram My - ϕ_y , ULS1



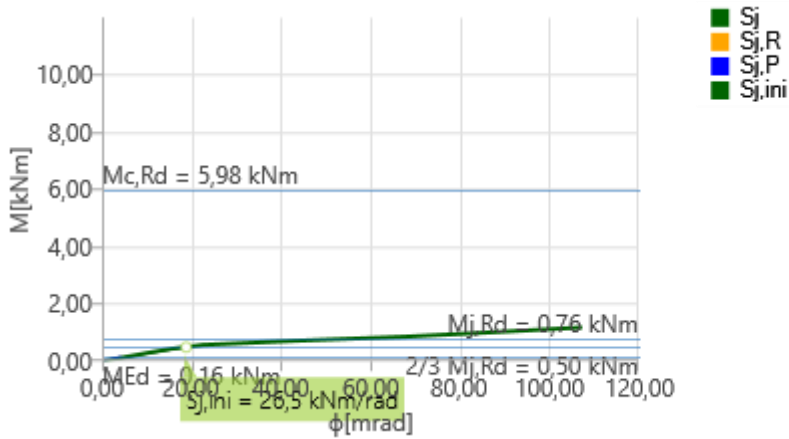
Stiffness diagram My - ϕ_y , ULS2a



Stiffness diagram $M_y - \phi_y$, ULS2b



Stiffness diagram $M_y - \phi_y$, ULS3a

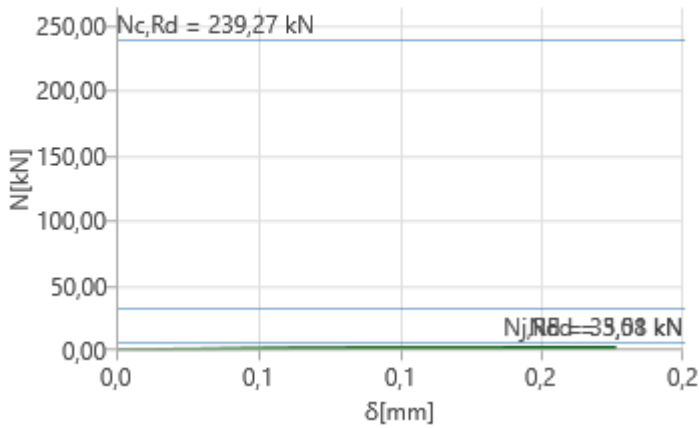


Stiffness diagram $M_y - \phi_y$, ULS3b

Axial stiffness

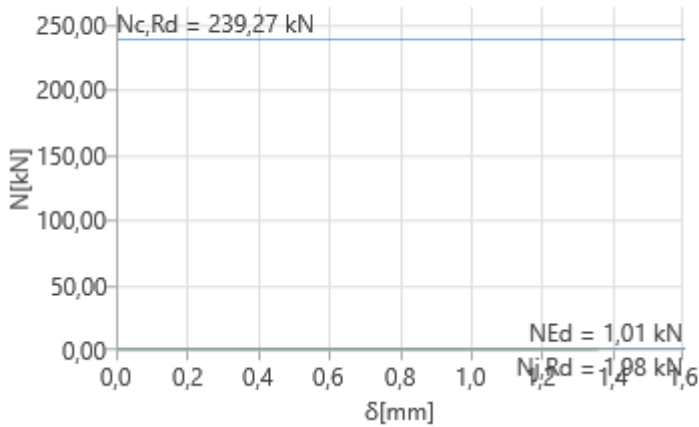
Name	Component	Loads	N [kN]	Nj,Rd [kN]	dx [mm]	St [kN/m]
B1	N	ULS1	-5,58	-33,01	0	2402013
		ULS2a	-1,01	-1,98	0	22039
		ULS2b	-1,05	-2,89	0	47633
		ULS3a	1,41	6,51	0	142269
		ULS3b	1,21	5,72	0	127731

N - δ



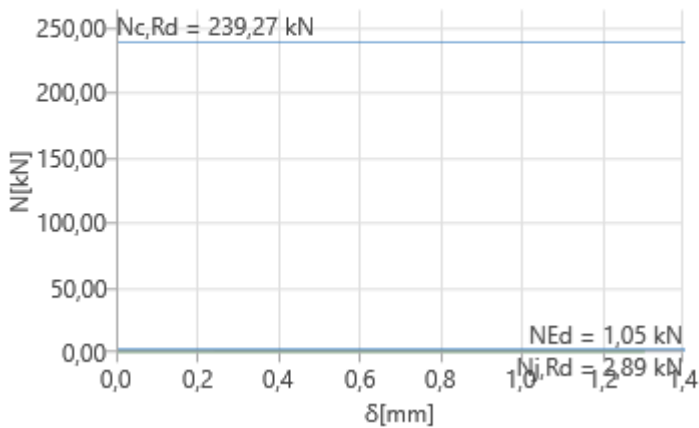
Stiffness diagram N - δ , ULS1

N - δ



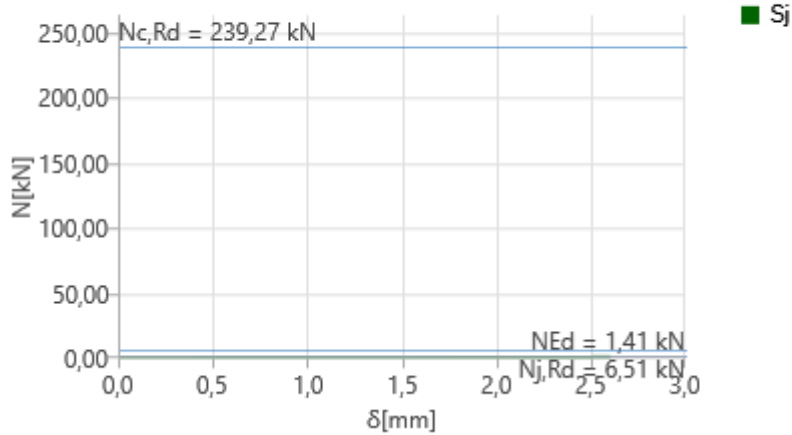
Stiffness diagram N - δ , ULS2a

N - δ



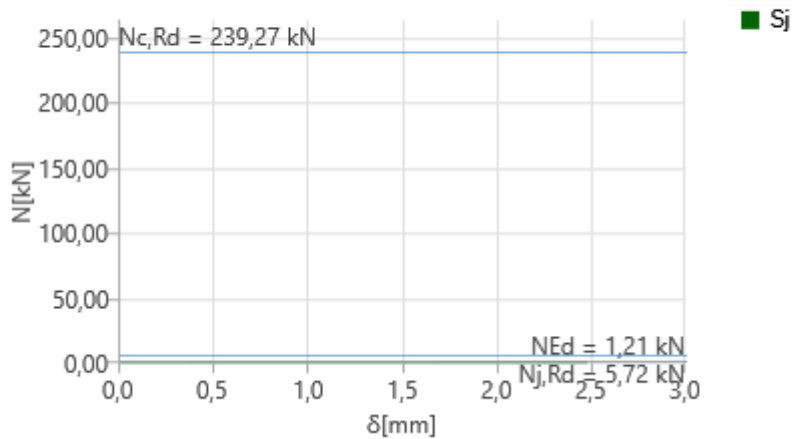
Stiffness diagram N - δ , ULS2b

N - δ



Stiffness diagram N - δ , ULS3a

N - δ



Stiffness diagram N - δ , ULS3b

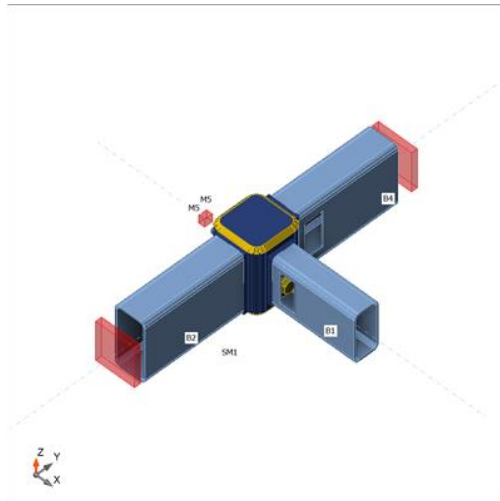
e

Analysis: Stiffness

Members

Geometry

Name	Cross-section	β - Direction [°]	γ - Pitch [°]	α - Rotation [°]	Offset ex [mm]	Offset ey [mm]	Offset ez [mm]
B1	1 - RHS80/40/3.0	0,0	0,0	0,0	0	0	0
B2	6 - RHS100/50/3.0	-90,0	0,0	0,0	0	0	0
B4	6 - RHS100/50/3.0	90,0	0,0	0,0	0	0	0
M5	7 - FLA20/8	180,0	0,0	0,0	0	0	0



Material

Steel	S 355 (EN)
Bolts	M12 8.8

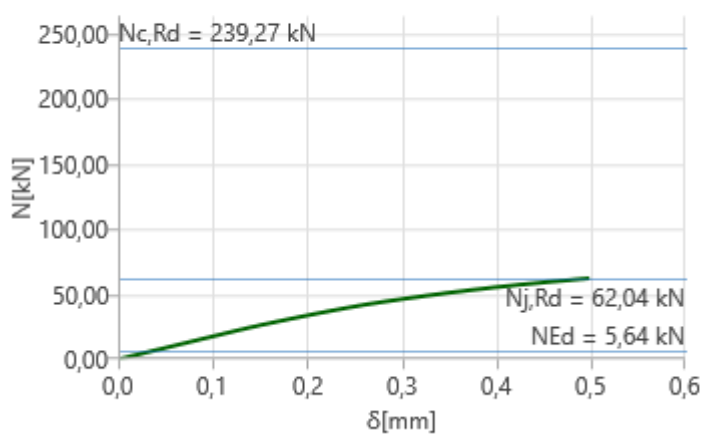
Load effects

Name	Member	N [kN]	Vy [kN]	Vz [kN]	Mx [kNm]	My [kNm]	Mz [kNm]
ULS1	B1 / End	-5,64	0,00	0,00	0,00	0,00	0,00
	B2 / End	0,00	0,00	0,00	0,00	0,00	0,00
	B4 / End	0,00	0,00	0,00	0,00	0,00	0,00
	M5 / End	0,00	0,00	0,00	0,00	0,00	0,00

Axial stiffness

Name	Component	Loads	N [kN]	Nj,Rd [kN]	dx [mm]	St [kN/m]
B1	N	ULS1	-5,64	-62,04	0	175992

N - δ



Stiffness diagram N - δ , ULS1

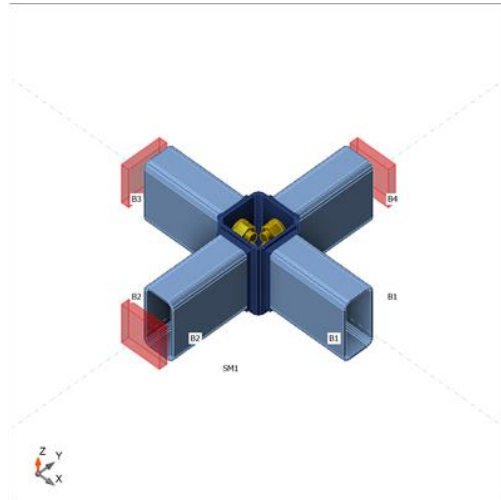
f

Analysis: Stiffness

Members

Geometry

Name	Cross-section	β - Direction [°]	γ - Pitch [°]	α - Rotation [°]	Offset ex [mm]	Offset ey [mm]	Offset ez [mm]
B1	1 - RHS80/40/3.0	0,0	0,0	0,0	0	0	0
B2	1 - RHS80/40/3.0	-90,0	0,0	0,0	0	0	0
B3	1 - RHS80/40/3.0	180,0	0,0	0,0	0	0	0
B4	1 - RHS80/40/3.0	90,0	0,0	0,0	0	0	0



Material

Steel	S 355 (EN)
Bolts	M12 8.8

Load effects

Name	Member	N [kN]	Vy [kN]	Vz [kN]	Mx [kNm]	My [kNm]	Mz [kNm]
ULS1	B1 / End	-4,79	0,00	0,00	0,00	0,15	0,00
	B2 / End	0,00	0,00	0,00	0,00	0,00	0,00
	B3 / End	0,00	0,00	0,00	0,00	0,00	0,00
	B4 / End	0,00	0,00	0,00	0,00	0,00	0,00
ULS2a	B1 / End	-1,17	0,00	0,00	0,00	-0,44	0,00
	B2 / End	0,00	0,00	0,00	0,00	0,00	0,00
	B3 / End	0,00	0,00	0,00	0,00	0,00	0,00
	B4 / End	0,00	0,00	0,00	0,00	0,00	0,00
ULS2b	B1 / End	-1,18	0,00	0,00	0,00	0,10	0,00
	B2 / End	0,00	0,00	0,00	0,00	0,00	0,00
	B3 / End	0,00	0,00	0,00	0,00	0,00	0,00
	B4 / End	0,00	0,00	0,00	0,00	0,00	0,00
ULS3a	B1 / End	1,21	0,00	0,00	0,00	-0,55	0,00
	B2 / End	0,00	0,00	0,00	0,00	0,00	0,00
	B3 / End	0,00	0,00	0,00	0,00	0,00	0,00
	B4 / End	0,00	0,00	0,00	0,00	0,00	0,00
ULS3b	B1 / End	-1,10	0,00	0,00	0,00	0,77	0,00
	B2 / End	0,00	0,00	0,00	0,00	0,00	0,00
	B3 / End	0,00	0,00	0,00	0,00	0,00	0,00

	B4 / End	0,00	0,00	0,00	0,00	0,00	0,00
--	----------	------	------	------	------	------	------

Rotational stiffness

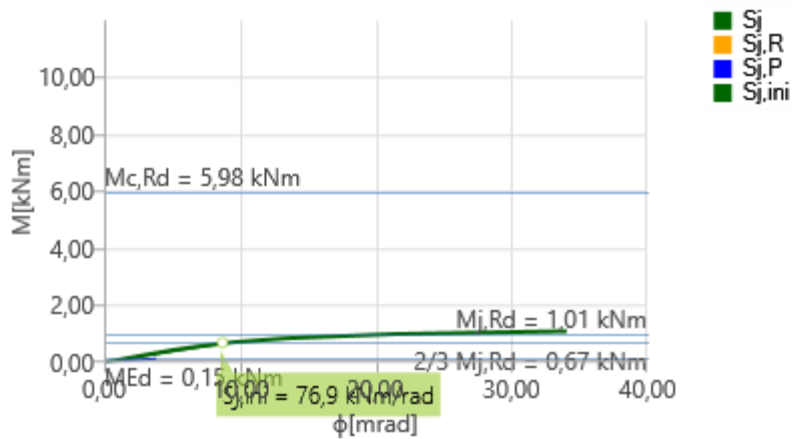
Name	Comp.	Loads	M _{j,Rd} [kNm]	S _{j,ini} [kNm/rad]	Φ _c [mrad]	L [m]	S _{j,R} [kNm/rad]	S _{j,P} [kNm/rad]	Class.
B1	My	ULS1	1,01	76,9	22,06	1,50	1897,0	37,9	Semi-rigid
	My	ULS2a	-0,88	33,6	42,28	1,50	1897,0	37,9	Pinned
	My	ULS2b	0,99	40,9	40,28	1,50	1897,0	37,9	Semi-rigid
	My	ULS3a	-0,84	26,6	43,38	1,50	1897,0	37,9	Pinned
	My	ULS3b	0,88	30,9	38,54	1,50	1897,0	37,9	Pinned

Secant rotational stiffness

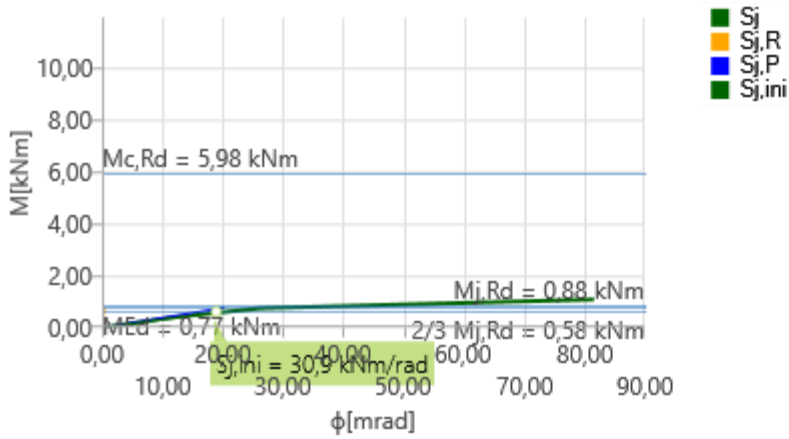
Name	Comp.	Loads	M [kNm]	S _{j,s} [kNm/rad]	Φ [mrad]
B1	My	ULS1	0,15	90,6	1,60
	My	ULS2a	-0,44	34,7	12,67
	My	ULS2b	0,10	43,8	2,28
	My	ULS3a	-0,55	26,9	20,45
	My	ULS3b	0,77	27,5	28,02

Symbol explanation

- M_{j,Rd} Bending resistance
- S_{j,ini} Initial rotational stiffness
- S_{j,s} Secant rotational stiffness
- Φ Rotational deformation
- Φ_c Rotational capacity
- S_{j,R} Limit value - rigid joint
- S_{j,P} Limit value - nominally pinned joint



Stiffness diagram My - φ_y, ULS1

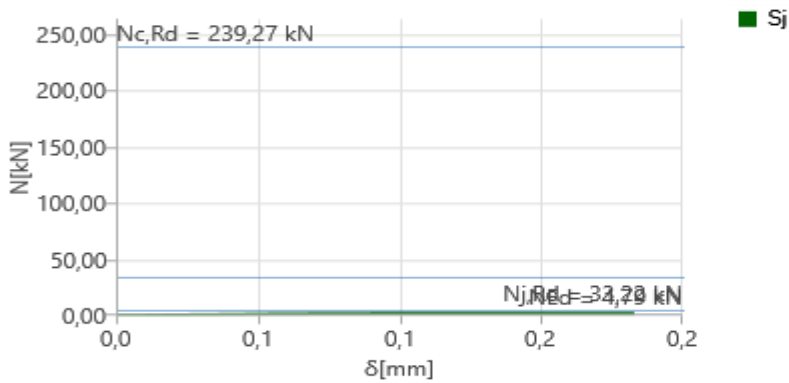


Stiffness diagram $M_y - \phi_y$, ULS3b

Axial stiffness

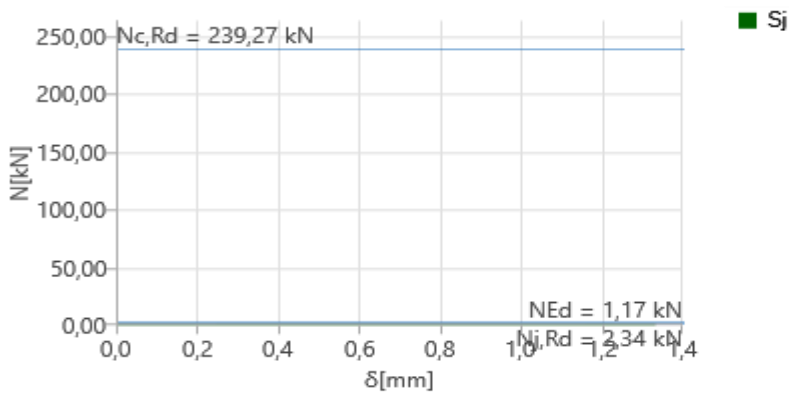
Name	Component	Loads	N [kN]	Nj,Rd [kN]	dx [mm]	St [kN/m]
B1	N	ULS1	-4,79	-33,22	0	2792763
		ULS2a	-1,17	-2,34	0	27384
		ULS2b	-1,18	-11,72	0	1015365
		ULS3a	1,21	1,85	0	13597
		ULS3b	-1,10	-1,25	1	6656

N - delta



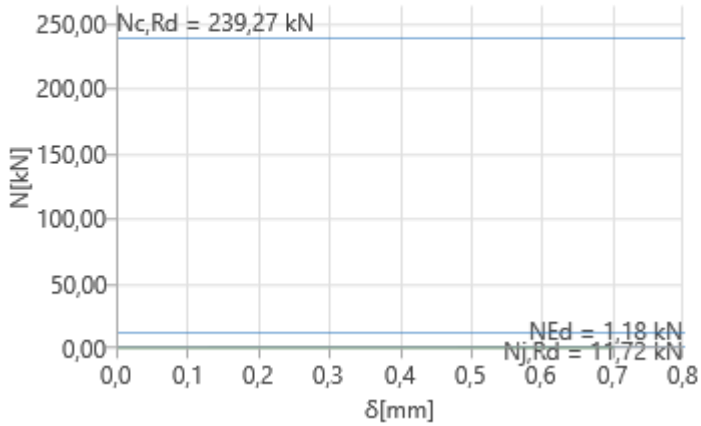
Stiffness diagram $N - \delta$, ULS1

N - delta



Stiffness diagram $N - \delta$, ULS2a

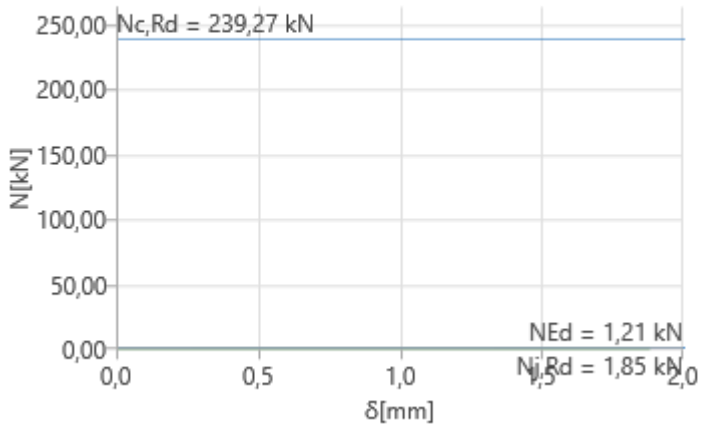
N - δ



■ Sj

Stiffness diagram N - δ , ULS2b

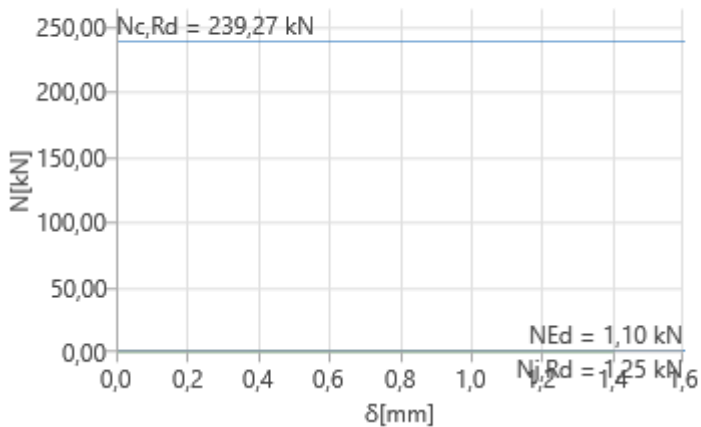
N - δ



■ Sj

Stiffness diagram N - δ , ULS3a

N - δ



■ Sj

Stiffness diagram N - δ , ULS3b

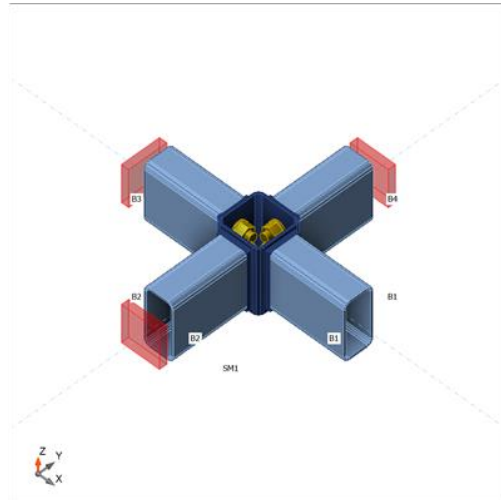
g

Analysis: Stiffness

Members

Geometry

Name	Cross-section	β - Direction [°]	γ - Pitch [°]	α - Rotation [°]	Offset ex [mm]	Offset ey [mm]	Offset ez [mm]
B1	1 - RHS80/40/3.0	0,0	0,0	0,0	0	0	0
B2	1 - RHS80/40/3.0	-90,0	0,0	0,0	0	0	0
B3	1 - RHS80/40/3.0	180,0	0,0	0,0	0	0	0
B4	1 - RHS80/40/3.0	90,0	0,0	0,0	0	0	0



Material

Steel	S 355 (EN)
Bolts	M12 8.8

Load effects

Name	Member	N [kN]	Vy [kN]	Vz [kN]	Mx [kNm]	My [kNm]	Mz [kNm]
ULS1	B1 / End	-4,91	0,00	0,00	0,00	0,15	0,00
	B2 / End	0,00	0,00	0,00	0,00	0,00	0,00
	B3 / End	0,00	0,00	0,00	0,00	0,00	0,00
	B4 / End	0,00	0,00	0,00	0,00	0,00	0,00
ULS2a	B1 / End	-1,39	0,00	0,00	0,00	-0,33	0,00
	B2 / End	0,00	0,00	0,00	0,00	0,00	0,00
	B3 / End	0,00	0,00	0,00	0,00	0,00	0,00
	B4 / End	0,00	0,00	0,00	0,00	0,00	0,00
ULS2b	B1 / End	-1,01	0,00	0,00	0,00	0,10	0,00
	B2 / End	0,00	0,00	0,00	0,00	0,00	0,00
	B3 / End	0,00	0,00	0,00	0,00	0,00	0,00
	B4 / End	0,00	0,00	0,00	0,00	0,00	0,00
ULS3a	B1 / End	1,03	0,00	0,00	0,00	-1,42	0,00
	B2 / End	0,00	0,00	0,00	0,00	0,00	0,00
	B3 / End	0,00	0,00	0,00	0,00	0,00	0,00
	B4 / End	0,00	0,00	0,00	0,00	0,00	0,00
ULS3b	B1 / End	1,03	0,00	0,00	0,00	0,96	0,00
	B2 / End	0,00	0,00	0,00	0,00	0,00	0,00
	B3 / End	0,00	0,00	0,00	0,00	0,00	0,00

	B4 / End	0,00	0,00	0,00	0,00	0,00	0,00
--	----------	------	------	------	------	------	------

Rotational stiffness

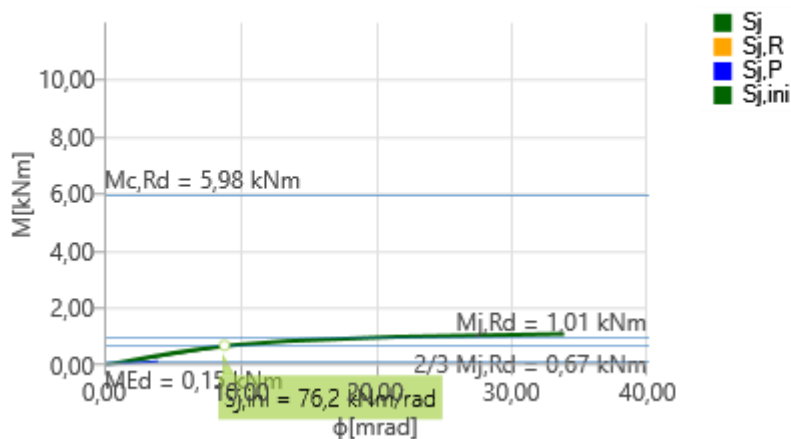
Name	Comp.	Loads	M _{j,Rd} [kNm]	S _{j,ini} [kNm/rad]	Φ _c [mrad]	L [m]	S _{j,R} [kNm/rad]	S _{j,P} [kNm/rad]	Class.
B1	My	ULS1	1,01	76,2	22,11	1,50	1897,0	37,9	Semi-rigid
	My	ULS2a	-0,90	34,7	39,94	1,50	1897,0	37,9	Pinned
	My	ULS2b	0,97	39,2	38,89	1,50	1897,0	37,9	Semi-rigid
	My	ULS3a	-0,85	28,3	40,50	1,50	1897,0	37,9	Pinned
	My	ULS3b	0,85	27,9	41,44	1,50	1897,0	37,9	Pinned

Secant rotational stiffness

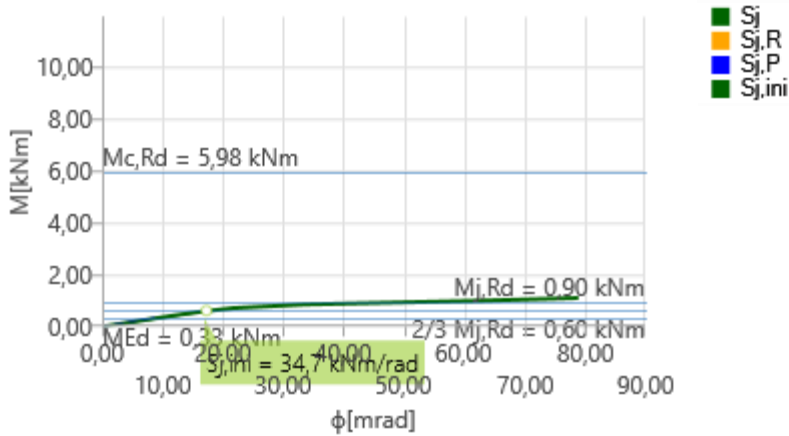
Name	Comp.	Loads	M [kNm]	S _{j,s} [kNm/rad]	Φ [mrad]
B1	My	ULS1	0,15	89,7	1,67
	My	ULS2a	-0,33	36,2	9,11
	My	ULS2b	0,10	41,9	2,39
	My	ULS3a	-1,42	0,0	136,08
	My	ULS3b	0,96	17,2	55,71

Symbol explanation

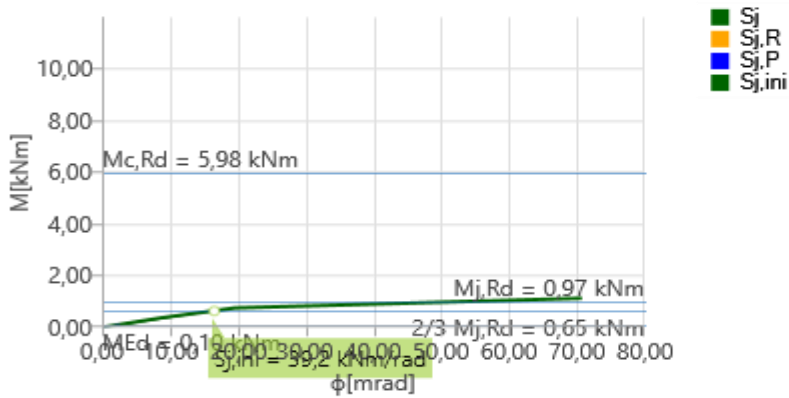
- M_{j,Rd} Bending resistance
- S_{j,ini} Initial rotational stiffness
- S_{j,s} Secant rotational stiffness
- Φ Rotational deformation
- Φ_c Rotational capacity
- S_{j,R} Limit value - rigid joint
- S_{j,P} Limit value - nominally pinned joint



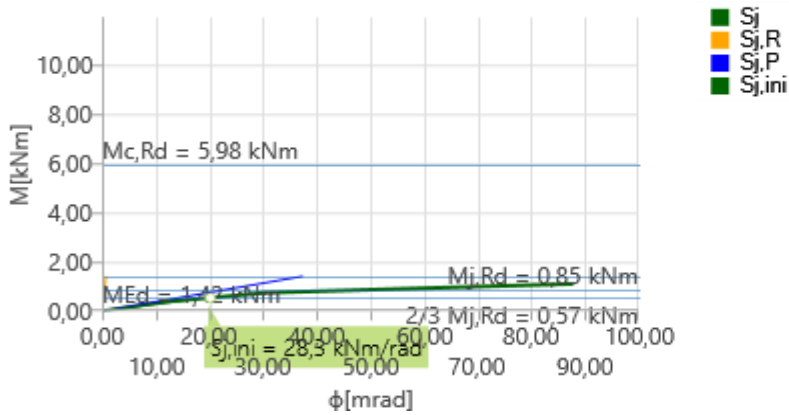
Stiffness diagram My - φ_y, ULS1



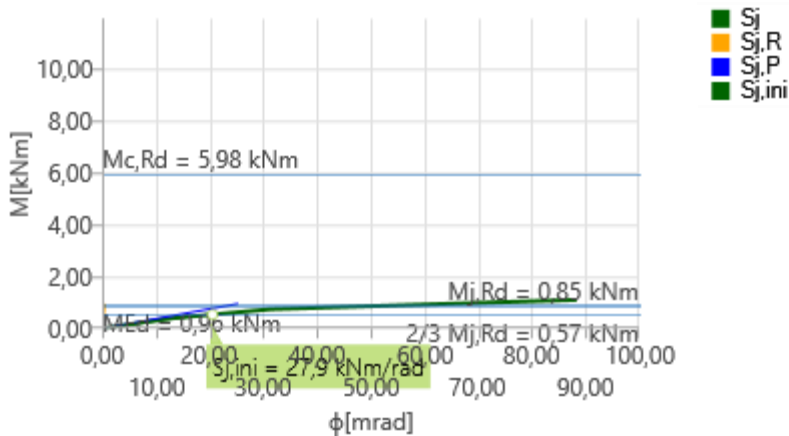
Stiffness diagram $M_y - \phi_y$, ULS2a



Stiffness diagram $M_y - \phi_y$, ULS2b



Stiffness diagram $M_y - \phi_y$, ULS3a

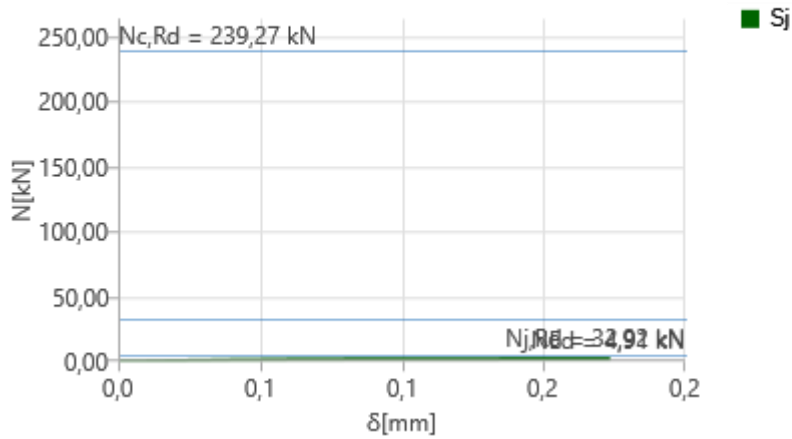


Stiffness diagram $M_y - \phi_y$, ULS3b

Axial stiffness

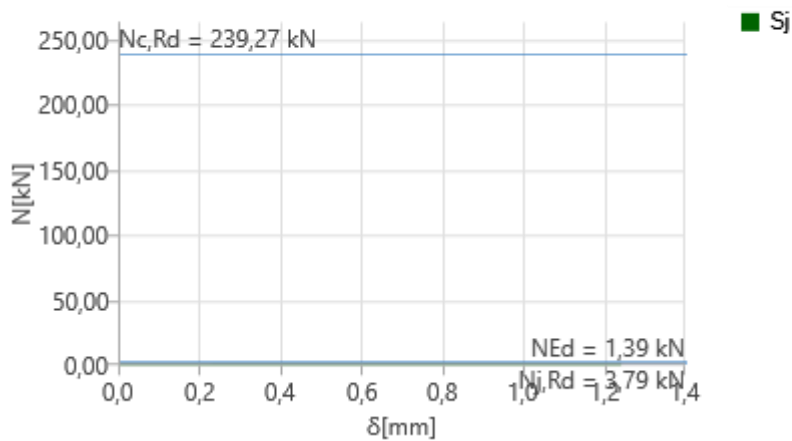
Name	Component	Loads	N [kN]	N _{j,Rd} [kN]	dx [mm]	St [kN/m]
B1	N	ULS1	-4,91	-32,92	0	2731874
		ULS2a	-1,39	-3,79	0	62754
		ULS2b	-1,01	-9,79	0	737425
		ULS3a	1,03	0,62	2	1116
		ULS3b	1,03	0,91	1	2151

N - δ



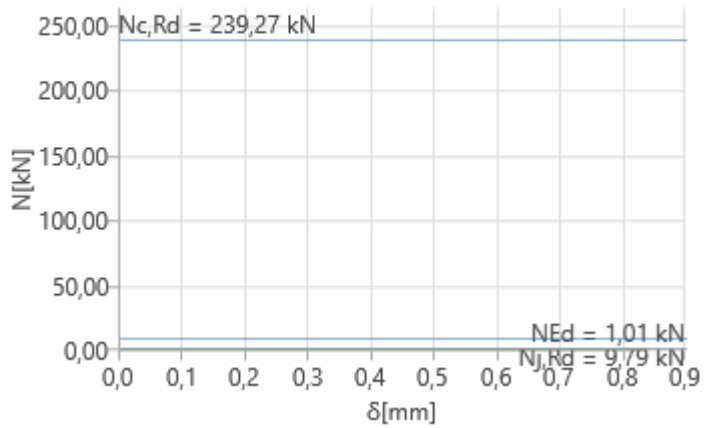
Stiffness diagram N - δ , ULS1

N - δ



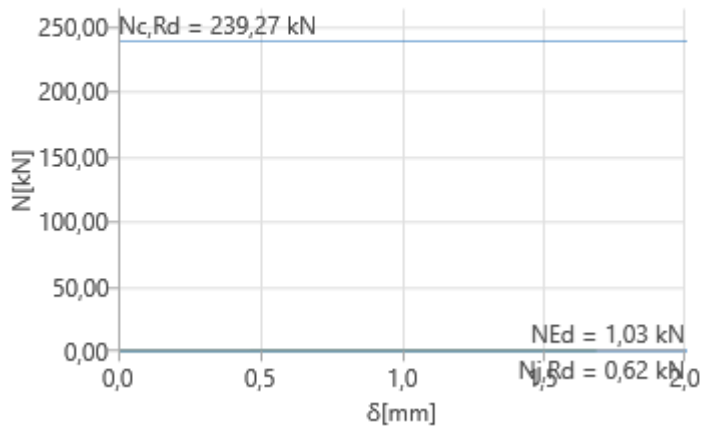
Stiffness diagram N - δ , ULS2a

N - δ



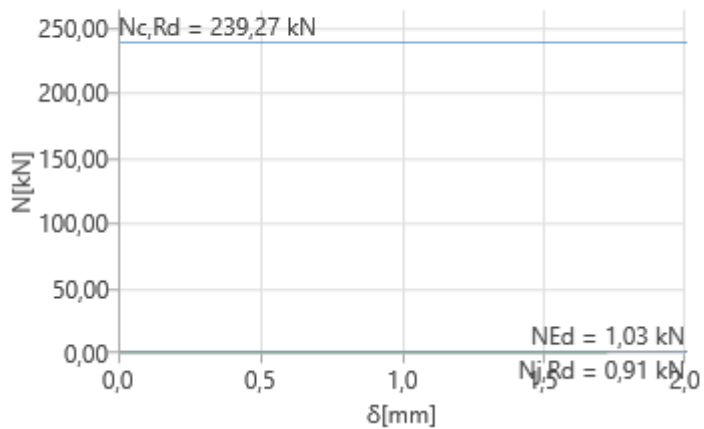
Stiffness diagram N - δ , ULS2b

N - δ



Stiffness diagram N - δ , ULS3a

N - δ



Stiffness diagram N - δ , ULS3b

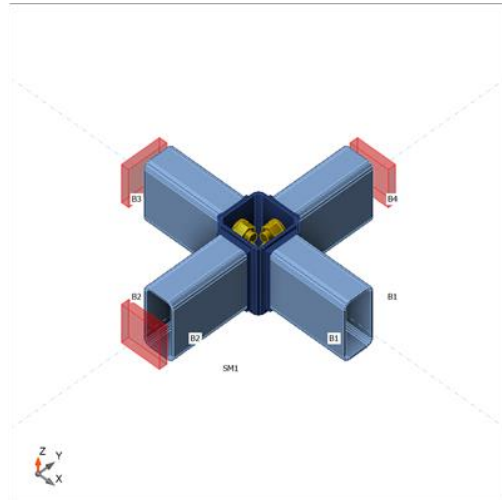
h

Analysis: Stiffness

Members

Geometry

Name	Cross-section	β - Direction [°]	γ - Pitch [°]	α - Rotation [°]	Offset ex [mm]	Offset ey [mm]	Offset ez [mm]
B1	1 - RHS80/40/3.0	0,0	0,0	0,0	0	0	0
B2	1 - RHS80/40/3.0	-90,0	0,0	0,0	0	0	0
B3	1 - RHS80/40/3.0	180,0	0,0	0,0	0	0	0
B4	1 - RHS80/40/3.0	90,0	0,0	0,0	0	0	0



Material

Steel	S 355 (EN)
Bolts	M12 8.8

Load effects

Name	Member	N [kN]	Vy [kN]	Vz [kN]	Mx [kNm]	My [kNm]	Mz [kNm]
ULS1	B1 / End	-4,63	0,00	0,00	0,00	0,14	0,00
	B2 / End	0,00	0,00	0,00	0,00	0,00	0,00
	B3 / End	0,00	0,00	0,00	0,00	0,00	0,00
	B4 / End	0,00	0,00	0,00	0,00	0,00	0,00
ULS2a	B1 / End	-1,04	0,00	0,00	0,00	0,20	0,00
	B2 / End	0,00	0,00	0,00	0,00	0,00	0,00
	B3 / End	0,00	0,00	0,00	0,00	0,00	0,00
	B4 / End	0,00	0,00	0,00	0,00	0,00	0,00
ULS2b	B1 / End	-1,15	0,00	0,00	0,00	0,20	0,00
	B2 / End	0,00	0,00	0,00	0,00	0,00	0,00
	B3 / End	0,00	0,00	0,00	0,00	0,00	0,00
	B4 / End	0,00	0,00	0,00	0,00	0,00	0,00
ULS3a	B1 / End	1,01	0,00	0,00	0,00	0,33	0,00
	B2 / End	0,00	0,00	0,00	0,00	0,00	0,00
	B3 / End	0,00	0,00	0,00	0,00	0,00	0,00
	B4 / End	0,00	0,00	0,00	0,00	0,00	0,00
ULS3b	B1 / End	1,04	0,00	0,00	0,00	0,44	0,00
	B2 / End	0,00	0,00	0,00	0,00	0,00	0,00
	B3 / End	0,00	0,00	0,00	0,00	0,00	0,00

	B4 / End	0,00	0,00	0,00	0,00	0,00	0,00
--	----------	------	------	------	------	------	------

Rotational stiffness

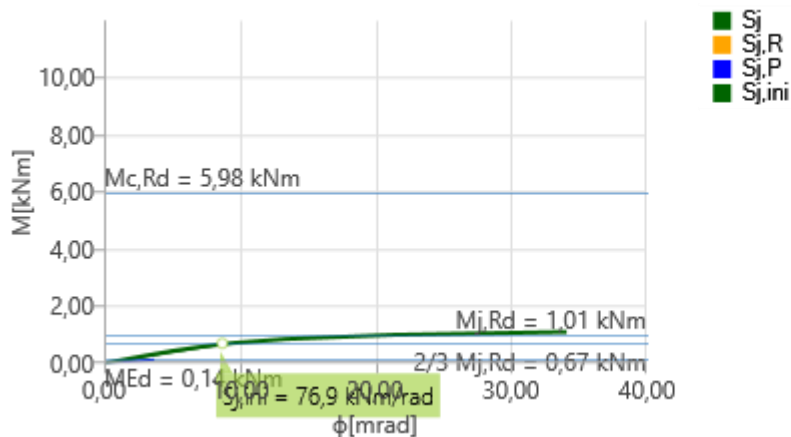
Name	Comp.	Loads	M _{j,Rd} [kNm]	S _{j,ini} [kNm/rad]	Φ _c [mrad]	L [m]	S _{j,R} [kNm/rad]	S _{j,P} [kNm/rad]	Class.
B1	My	ULS1	1,01	76,9	22,05	1,50	1897,0	37,9	Semi-rigid
	My	ULS2a	0,91	35,5	38,48	1,50	1897,0	37,9	Pinned
	My	ULS2b	0,92	35,9	38,53	1,50	1897,0	37,9	Pinned
	My	ULS3a	0,84	29,3	52,17	1,50	1897,0	37,9	Pinned
	My	ULS3b	0,85	29,8	52,46	1,50	1897,0	37,9	Pinned

Secant rotational stiffness

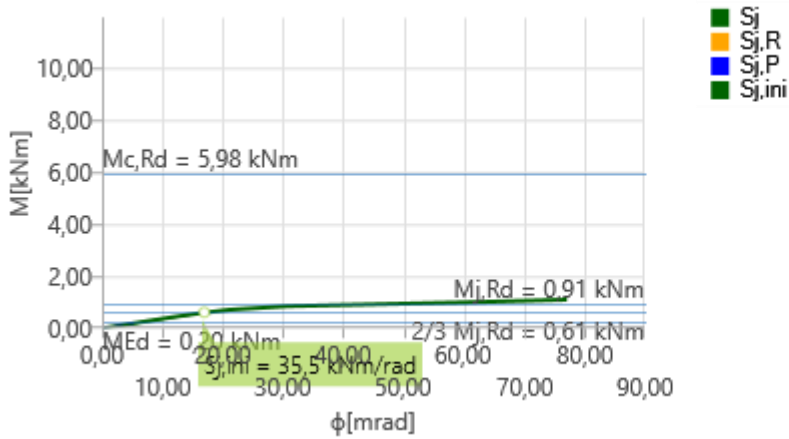
Name	Comp.	Loads	M [kNm]	S _{j,s} [kNm/rad]	Φ [mrad]
B1	My	ULS1	0,14	90,7	1,54
	My	ULS2a	0,20	37,2	5,38
	My	ULS2b	0,20	37,7	5,31
	My	ULS3a	0,33	30,9	10,68
	My	ULS3b	0,44	31,1	14,17

Symbol explanation

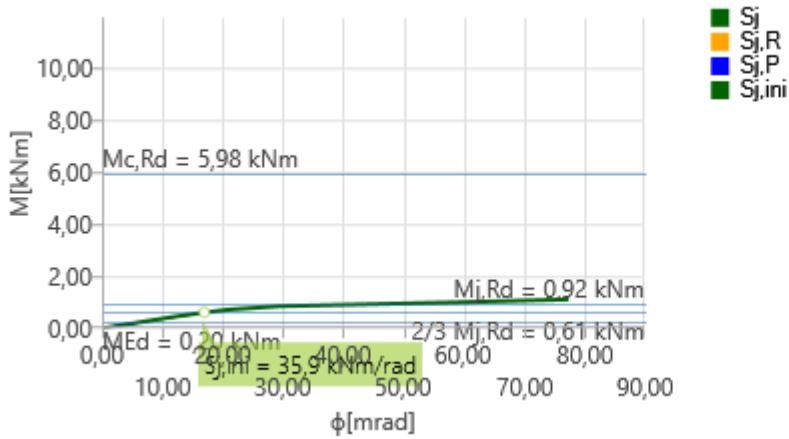
- M_{j,Rd} Bending resistance
- S_{j,ini} Initial rotational stiffness
- S_{j,s} Secant rotational stiffness
- Φ Rotational deformation
- Φ_c Rotational capacity
- S_{j,R} Limit value - rigid joint
- S_{j,P} Limit value - nominally pinned joint



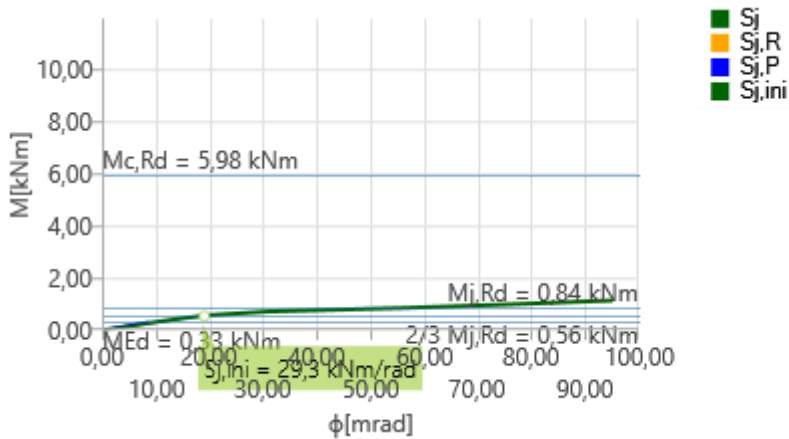
Stiffness diagram My - φ_y, ULS1



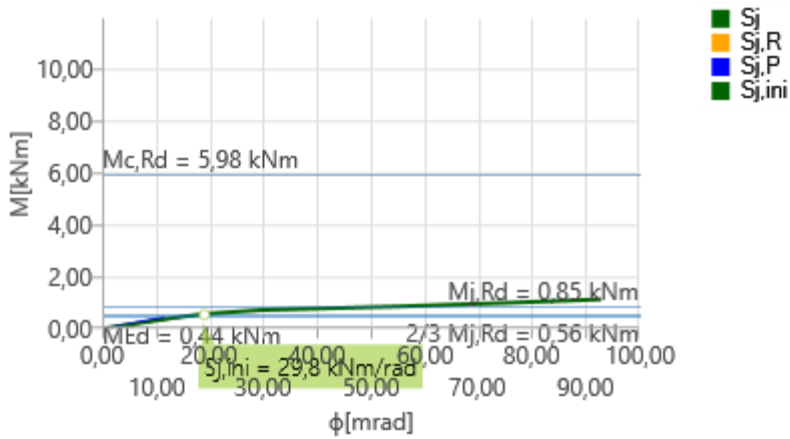
Stiffness diagram $M_y - \phi$, ULS2a



Stiffness diagram $M_y - \phi$, ULS2b



Stiffness diagram $M_y - \phi$, ULS3a

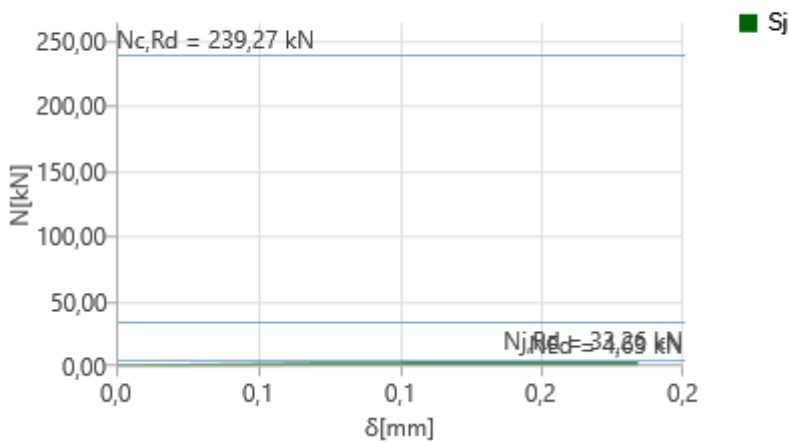


Stiffness diagram $M_y - \phi_y$, ULS3b

Axial stiffness

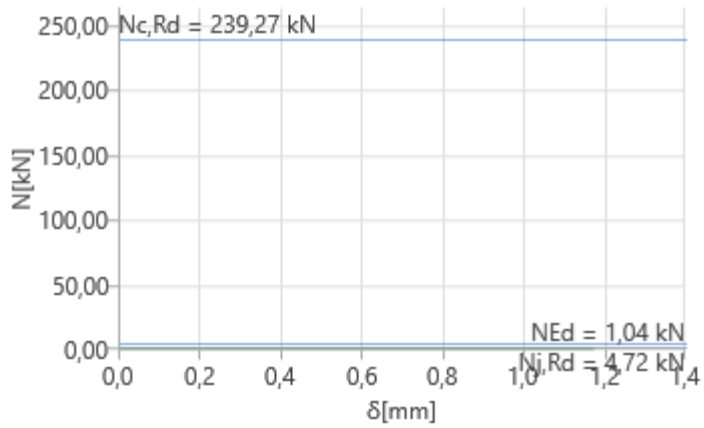
Name	Component	Loads	N [kN]	Nj,Rd [kN]	dx [mm]	St [kN/m]
B1	N	ULS1	-4,63	-33,26	0	2888316
		ULS2a	-1,04	-4,72	0	133617
		ULS2b	-1,15	-5,27	0	152928
		ULS3a	1,01	2,56	0	30819
		ULS3b	1,04	2,00	0	18504

N - delta



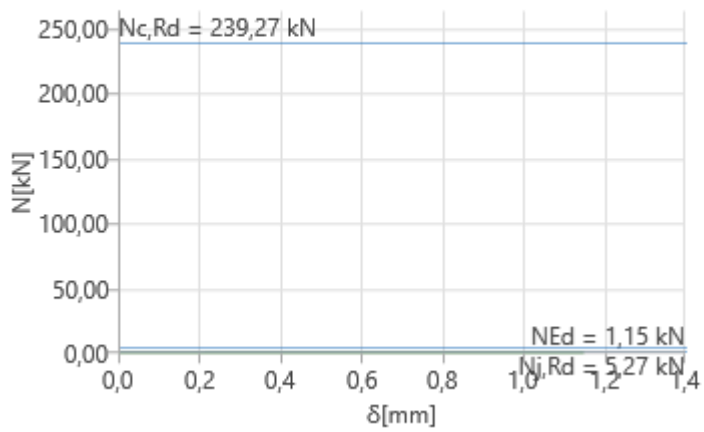
Stiffness diagram $N - \delta$, ULS1

N - δ



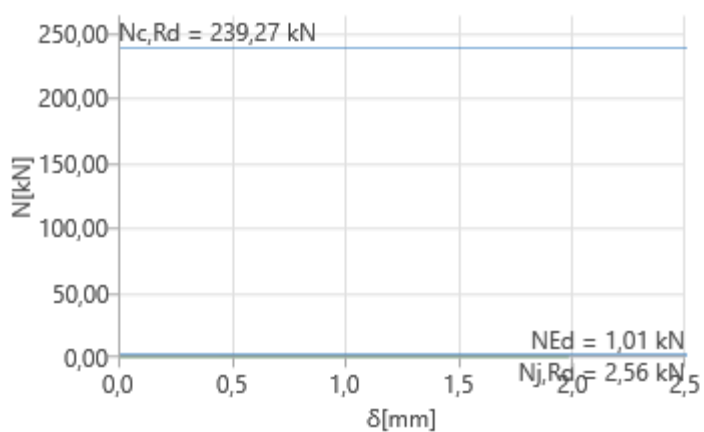
Stiffness diagram N - δ , ULS2a

N - δ



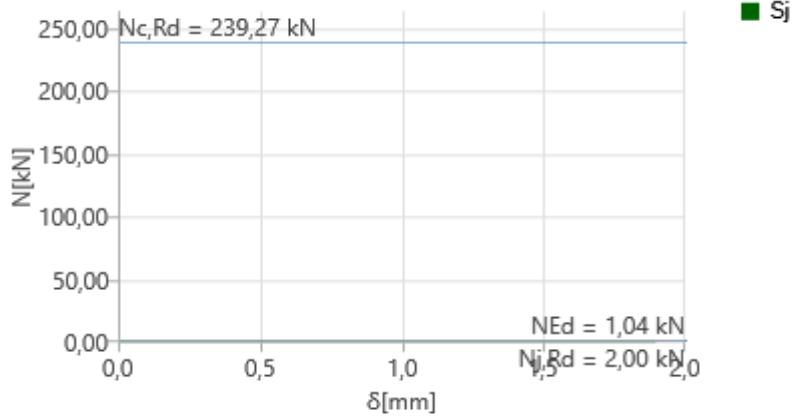
Stiffness diagram N - δ , ULS2b

N - δ



Stiffness diagram N - δ , ULS3a

N - δ



Stiffness diagram N - δ , ULS3b

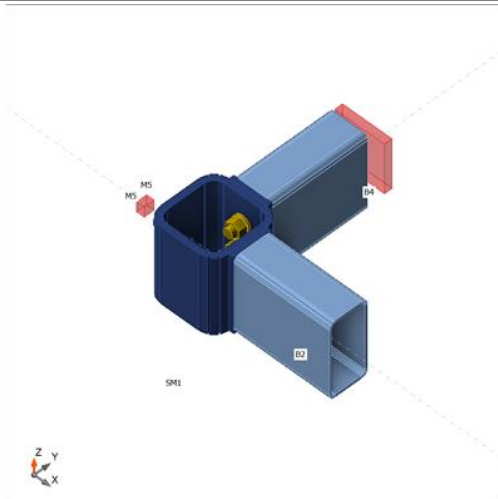
i

Analysis: Stiffness

Members

Geometry

Name	Cross-section	β - Direction [°]	γ - Pitch [°]	α - Rotation [°]	Offset ex [mm]	Offset ey [mm]	Offset ez [mm]
B2	6 - RHS100/50/3.0	0,0	0,0	0,0	0	0	0
B4	6 - RHS100/50/3.0	90,0	0,0	0,0	0	0	0
M5	7 - FLA20/8	180,0	0,0	0,0	0	0	0



Material

Steel	S 355 (EN)
Bolts	M12 8.8

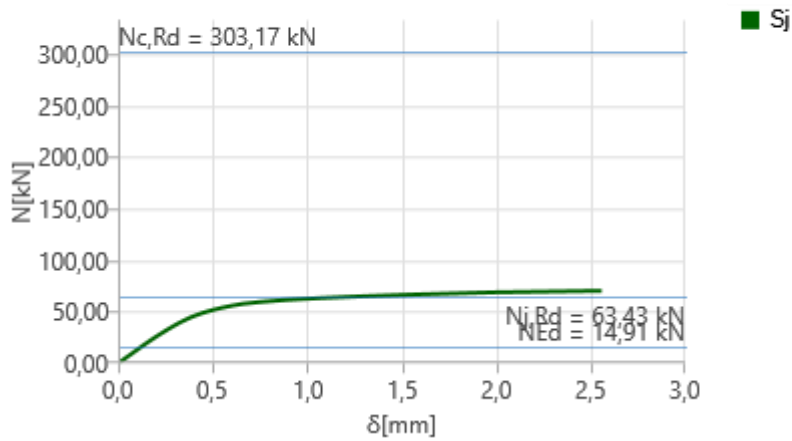
Load effects

Name	Member	N [kN]	Vy [kN]	Vz [kN]	Mx [kNm]	My [kNm]	Mz [kNm]
ULS1	B2 / End	-14,91	0,00	0,00	0,00	0,00	0,00
	B4 / End	0,00	0,00	0,00	0,00	0,00	0,00
	M5 / End	0,00	0,00	0,00	0,00	0,00	0,00

Axial stiffness

Name	Component	Loads	N [kN]	Nj,Rd [kN]	dx [mm]	St [kN/m]
B2	N	ULS1	-14,91	-63,43	0	131840

N - δ



Stiffness diagram N - δ , ULS1

j

Analysis: Stiffness

Members

Geometry

Name	Cross-section	β - Direction [°]	γ - Pitch [°]	α - Rotation [°]	Offset ex [mm]	Offset ey [mm]	Offset ez [mm]
B1	1 - RHS80/40/3.0	0,0	0,0	0,0	0	0	0
B2	6 - RHS100/50/3.0	-90,0	0,0	0,0	0	0	0
B4	6 - RHS100/50/3.0	90,0	0,0	0,0	0	0	0



Material

Steel	S 355 (EN)
Bolts	M12 8.8

Load effects

Name	Member	N [kN]	Vy [kN]	Vz [kN]	Mx [kNm]	My [kNm]	Mz [kNm]
ULS1	B1 / End	-2,00	0,00	0,00	0,00	0,01	0,00
	B2 / End	-14,48	0,00	0,00	0,00	-0,43	0,00
	B4 / End	0,00	0,00	0,00	0,00	0,00	0,00
ULS2a	B1 / End	-2,00	0,00	0,00	0,00	0,05	0,00
	B2 / End	-3,12	0,00	0,00	0,00	-0,65	0,00
	B4 / End	0,00	0,00	0,00	0,00	0,00	0,00
ULS2b	B1 / End	-2,00	0,00	0,00	0,00	0,10	0,00
	B2 / End	-3,05	0,00	0,00	0,00	0,19	0,00
	B4 / End	0,00	0,00	0,00	0,00	0,00	0,00
ULS3a	B1 / End	-2,00	0,00	0,00	0,00	0,20	0,00
	B2 / End	-1,45	0,00	0,00	0,00	-0,63	0,00
	B4 / End	0,00	0,00	0,00	0,00	0,00	0,00
ULS3b	B1 / End	-2,00	0,00	0,00	0,00	0,50	0,00
	B2 / End	-1,38	0,00	0,00	0,00	0,20	0,00
	B4 / End	0,00	0,00	0,00	0,00	0,00	0,00

Rotational stiffness

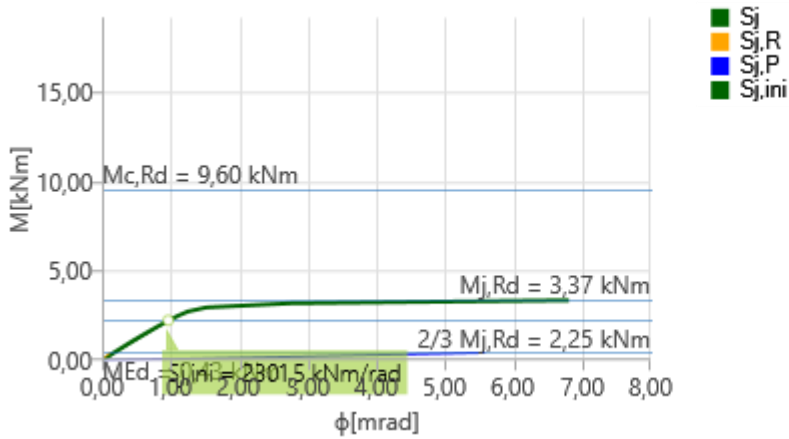
Name	Comp.	Loads	Mj,Rd [kNm]	Sj,ini [kNm/rad]	Φ_c [mrad]	L [m]	Sj,R [kNm/rad]	Sj,P [kNm/rad]	Class.
B2	My	ULS1	-3,37	2301,5	6,81	1,50	3850,0	77,0	Semi-rigid
	My	ULS2a	-4,73	298,9	36,86	1,50	3850,0	77,0	Semi-rigid
	My	ULS2b	4,51	708,2	14,09	1,50	3850,0	77,0	Semi-rigid
	My	ULS3a	-4,33	257,2	35,63	1,50	3850,0	77,0	Semi-rigid
	My	ULS3b	5,01	347,7	39,92	1,50	3850,0	77,0	Semi-rigid

Secant rotational stiffness

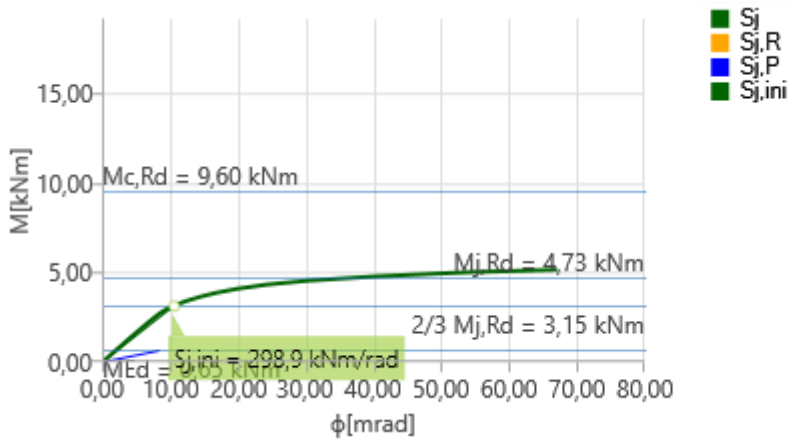
Name	Comp.	Loads	M [kNm]	Sjs [kNm/rad]	Φ [mrad]
B2	My	ULS1	-0,43	2535,2	0,17
	My	ULS2a	-0,65	332,5	1,95
	My	ULS2b	0,19	769,0	0,25
	My	ULS3a	-0,63	295,0	2,14
	My	ULS3b	0,20	374,5	0,53

Symbol explanation

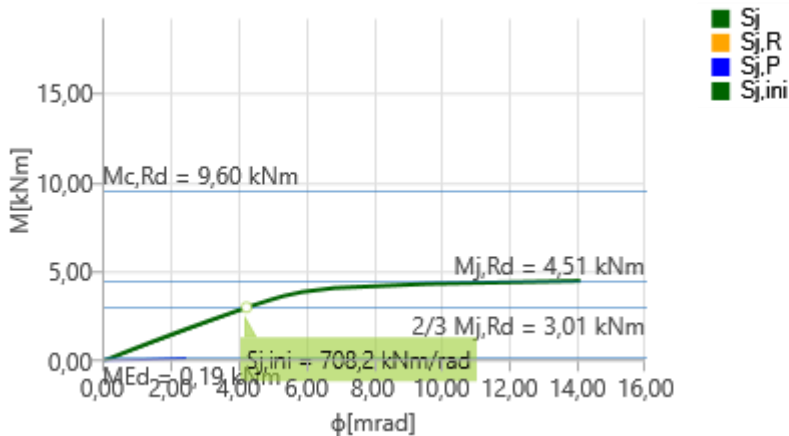
- M_{j,Rd} Bending resistance
- S_{j,ini} Initial rotational stiffness
- S_{j,s} Secant rotational stiffness
- Φ Rotational deformation
- Φ_c Rotational capacity
- S_{j,R} Limit value - rigid joint
- S_{j,P} Limit value - nominally pinned joint



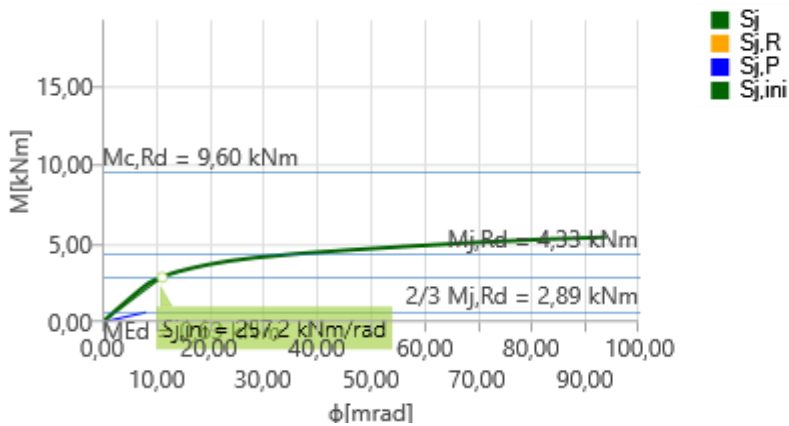
Stiffness diagram $M_y - \phi_y$, ULS1



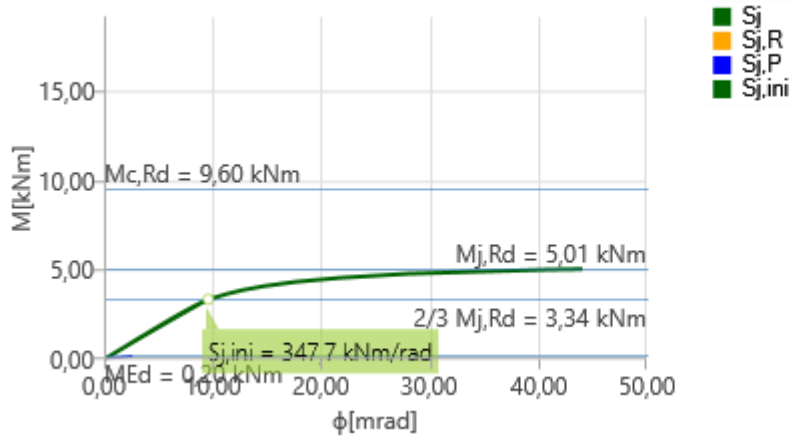
Stiffness diagram $M_y - \phi_y$, ULS2a



Stiffness diagram $M_y - \phi_y$, ULS2b



Stiffness diagram My - ϕ , ULS3a

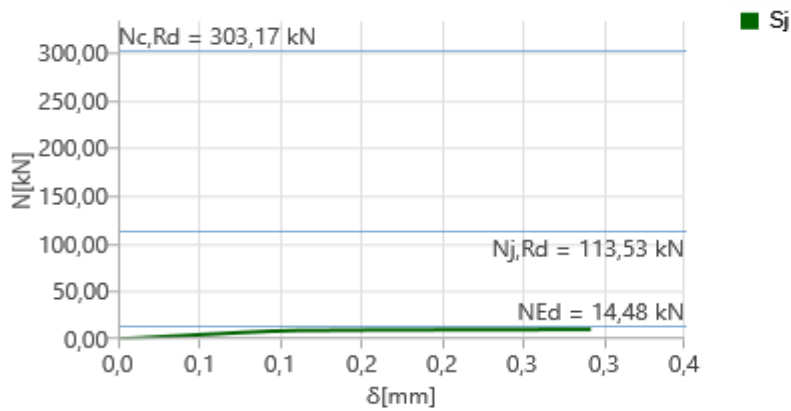


Stiffness diagram My - ϕ , ULS3b

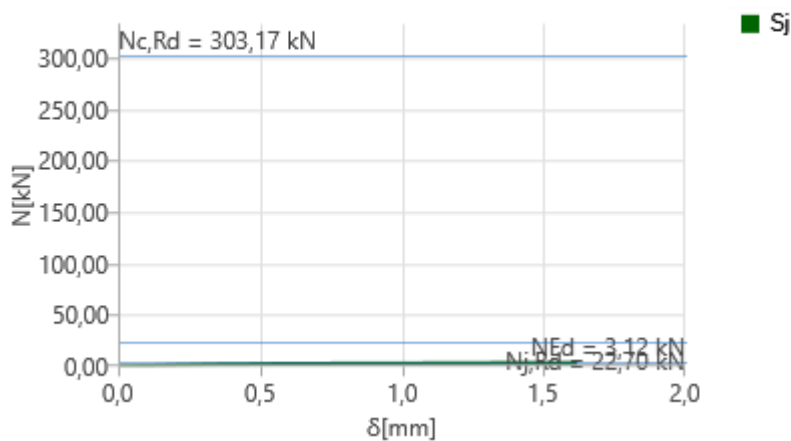
Axial stiffness

Name	Component	Loads	N [kN]	Nj,Rd [kN]	dx [mm]	St [kN/m]
B2	N	ULS1	-14,48	-113,53	0	2226099
		ULS2a	-3,12	-22,70	1	2376
		ULS2b	-3,05	-72,47	0	10096921
		ULS3a	-1,45	-9,96	2	760
		ULS3b	-1,38	-34,60	1	1632

N - δ

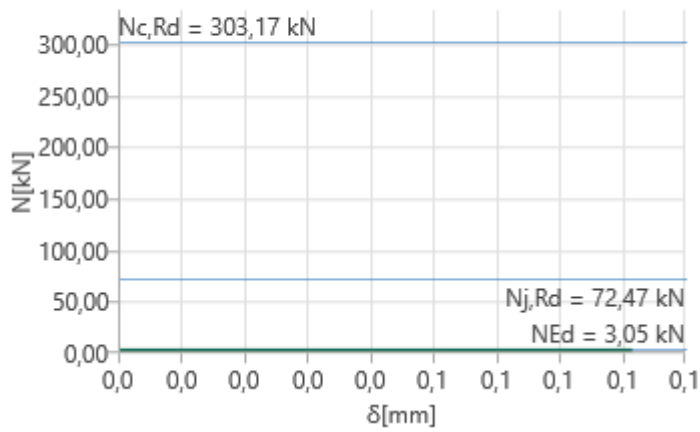


Stiffness diagram N - δ , ULS1



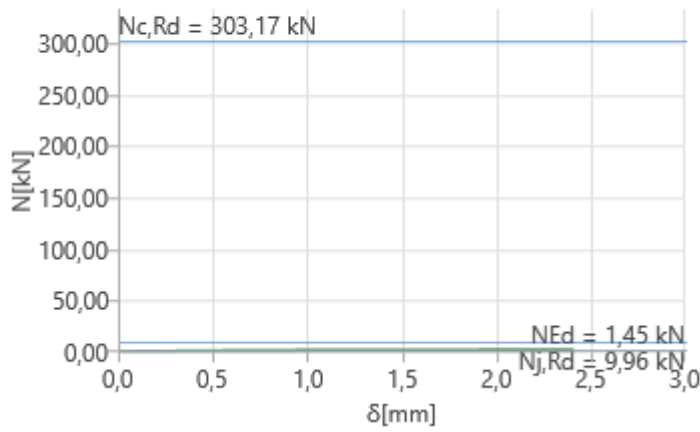
Stiffness diagram N - δ , ULS2a

N - δ



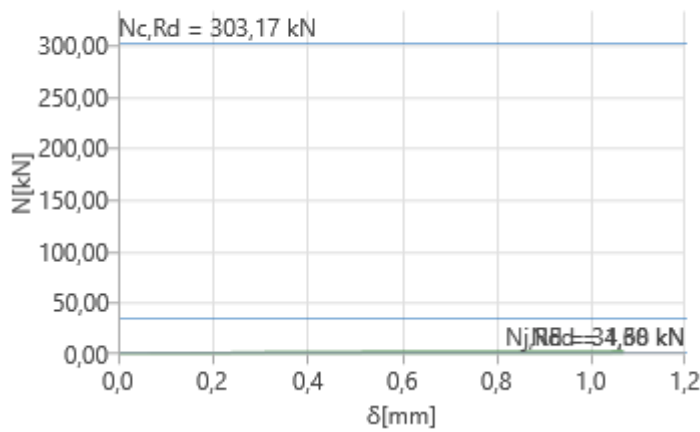
Stiffness diagram N - δ , ULS2b

N - δ



Stiffness diagram N - δ , ULS3a

N - δ



Stiffness diagram N - δ , ULS3b

k

Analysis: Stiffness

Members

Geometry

Name	Cross-section	β - Direction [°]	γ - Pitch [°]	α - Rotation [°]	Offset ex [mm]	Offset ey [mm]	Offset ez [mm]
B1	1 - RHS80/40/3.0	0,0	0,0	0,0	0	0	0
B2	6 - RHS100/50/3.0	-90,0	0,0	0,0	0	0	0
B4	6 - RHS100/50/3.0	90,0	0,0	0,0	0	0	0



Material

Steel	S 355 (EN)
Bolts	M12 8.8

Load effects

Name	Member	N [kN]	Vy [kN]	Vz [kN]	Mx [kNm]	My [kNm]	Mz [kNm]
ULS1	B1 / End	-2,00	0,00	0,00	0,00	0,01	0,00
	B2 / End	-13,36	0,00	0,00	0,00	-0,40	0,00
	B4 / End	0,00	0,00	0,00	0,00	0,00	0,00
ULS2a	B1 / End	-2,00	0,00	0,00	0,00	0,05	0,00
	B2 / End	-2,70	0,00	0,00	0,00	-0,65	0,00
	B4 / End	0,00	0,00	0,00	0,00	0,00	0,00
ULS2b	B1 / End	-2,00	0,00	0,00	0,00	0,10	0,00
	B2 / End	-2,80	0,00	0,00	0,00	0,19	0,00
	B4 / End	0,00	0,00	0,00	0,00	0,00	0,00
ULS3a	B1 / End	-2,00	0,00	0,00	0,00	0,20	0,00
	B2 / End	-1,15	0,00	0,00	0,00	-0,63	0,00
	B4 / End	0,00	0,00	0,00	0,00	0,00	0,00
ULS3b	B1 / End	-2,00	0,00	0,00	0,00	0,50	0,00
	B2 / End	-1,25	0,00	0,00	0,00	0,20	0,00
	B4 / End	0,00	0,00	0,00	0,00	0,00	0,00

Rotational stiffness

Name	Comp.	Loads	Mj,Rd [kNm]	Sj,ini [kNm/rad]	Φ_c [mrad]	L [m]	Sj,R [kNm/rad]	Sj,P [kNm/rad]	Class.
------	-------	-------	----------------	---------------------	--------------------	----------	-------------------	-------------------	--------

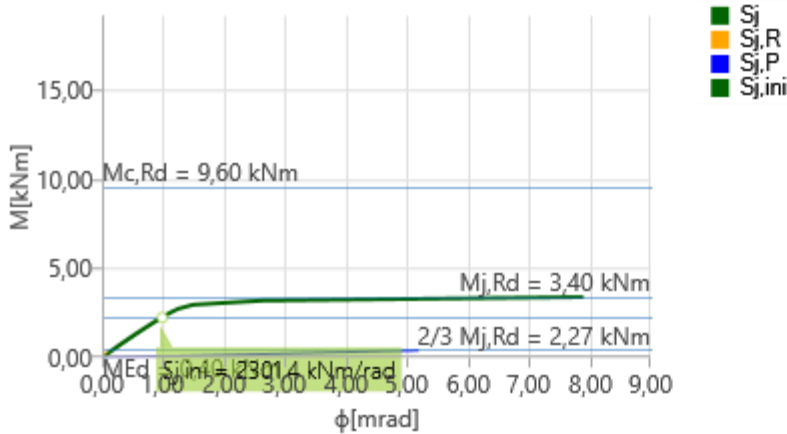
B2	My	ULS1	-3,40	2301,4	7,90	1,50	3850,0	77,0	Semi-rigid
	My	ULS2a	-4,63	286,8	36,45	1,50	3850,0	77,0	Semi-rigid
	My	ULS2b	4,60	624,1	15,10	1,50	3850,0	77,0	Semi-rigid
	My	ULS3a	-4,26	250,5	35,56	1,50	3850,0	77,0	Semi-rigid
	My	ULS3b	4,94	331,5	38,90	1,50	3850,0	77,0	Semi-rigid

Secant rotational stiffness

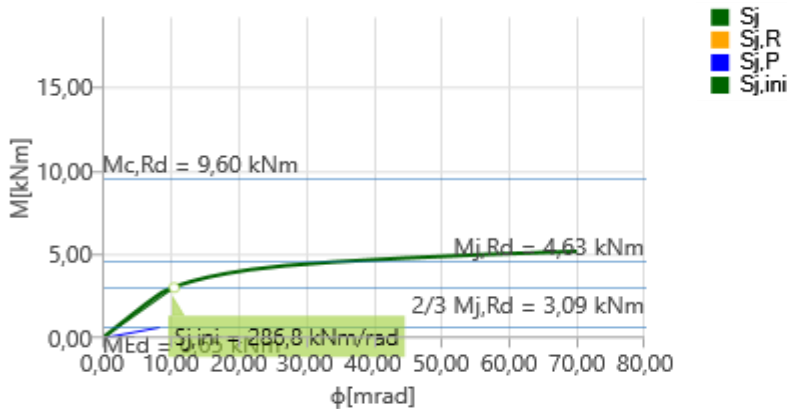
Name	Comp.	Loads	M [kNm]	Sjs [kNm/rad]	Φ [mrad]
B2	My	ULS1	-0,40	2539,8	0,16
	My	ULS2a	-0,65	321,9	2,02
	My	ULS2b	0,19	671,4	0,28
	My	ULS3a	-0,63	288,8	2,18
	My	ULS3b	0,20	361,1	0,55

Symbol explanation

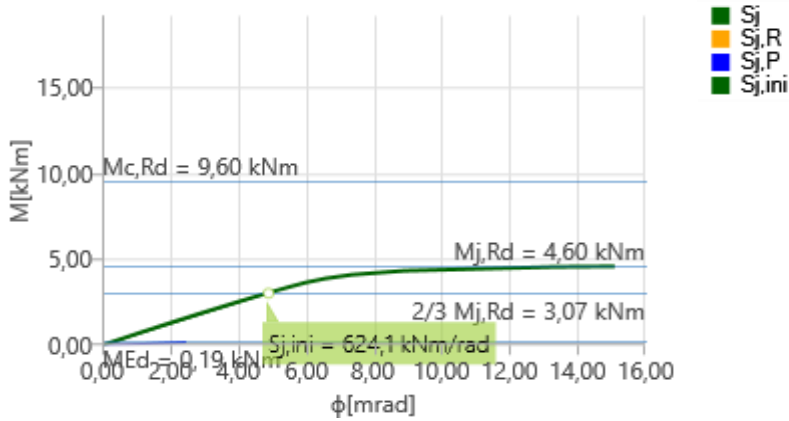
- $M_{j,Rd}$ Bending resistance
- $S_{j,ini}$ Initial rotational stiffness
- $S_{j,s}$ Secant rotational stiffness
- Φ Rotational deformation
- Φ_c Rotational capacity
- $S_{j,R}$ Limit value - rigid joint
- $S_{j,P}$ Limit value - nominally pinned joint



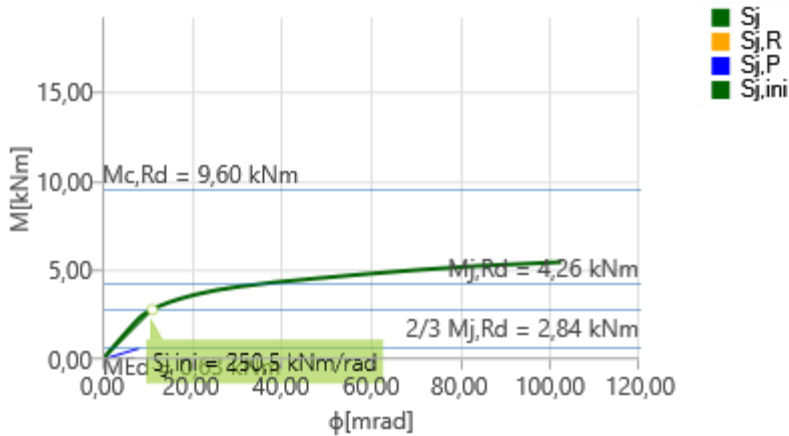
Stiffness diagram My - ϕ_y , ULS1



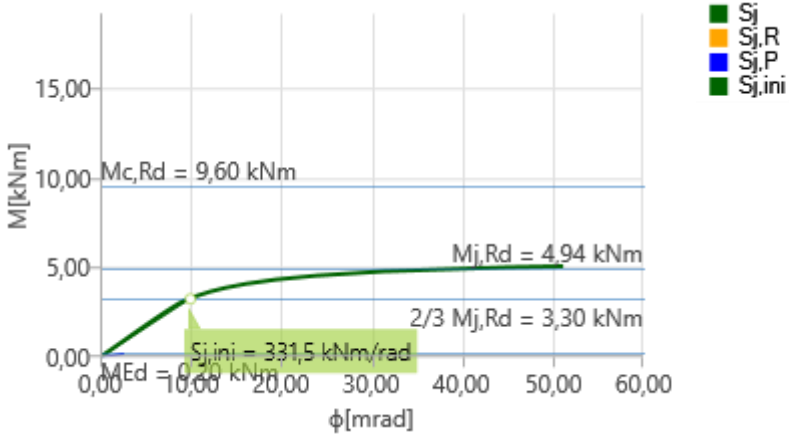
Stiffness diagram My - ϕ_y , ULS2a



Stiffness diagram My - ϕ , ULS2b



Stiffness diagram My - ϕ , ULS3a

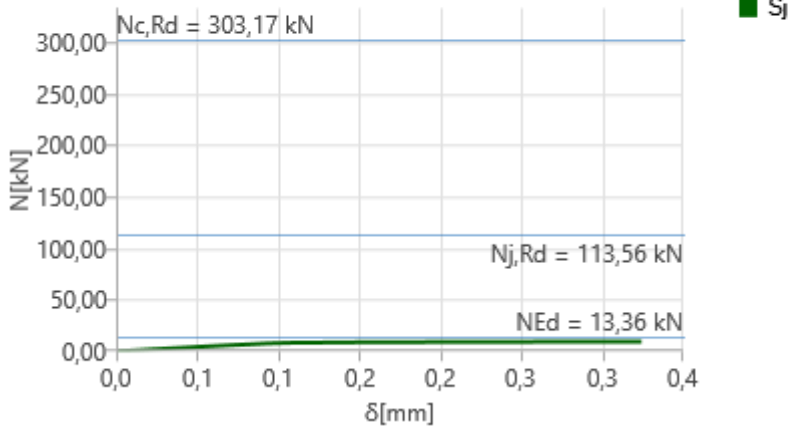


Stiffness diagram My - ϕ , ULS3b

Axial stiffness

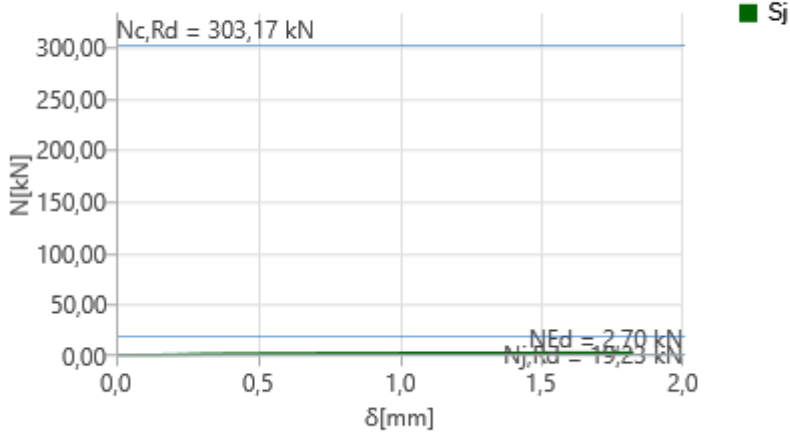
Name	Component	Loads	N [kN]	Nj,Rd [kN]	dx [mm]	St [kN/m]
B2	N	ULS1	-13,36	-113,56	0	2393395
		ULS2a	-2,70	-19,23	1	1834
		ULS2b	-2,80	-67,79	0	15135790
		ULS3a	-1,15	-7,77	2	570
		ULS3b	-1,25	-30,89	1	1288

N - δ



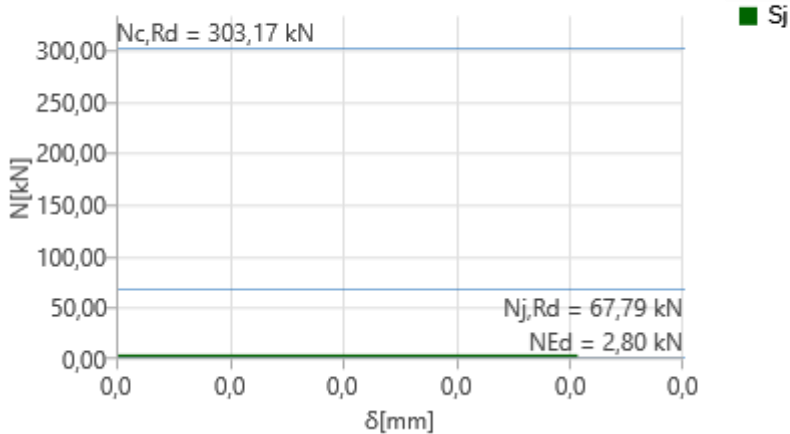
Stiffness diagram N - δ, ULS1

N - δ



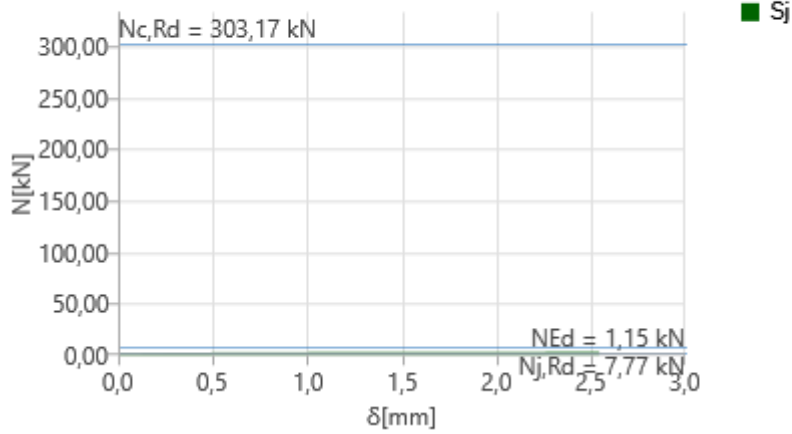
Stiffness diagram N - δ, ULS2a

N - δ



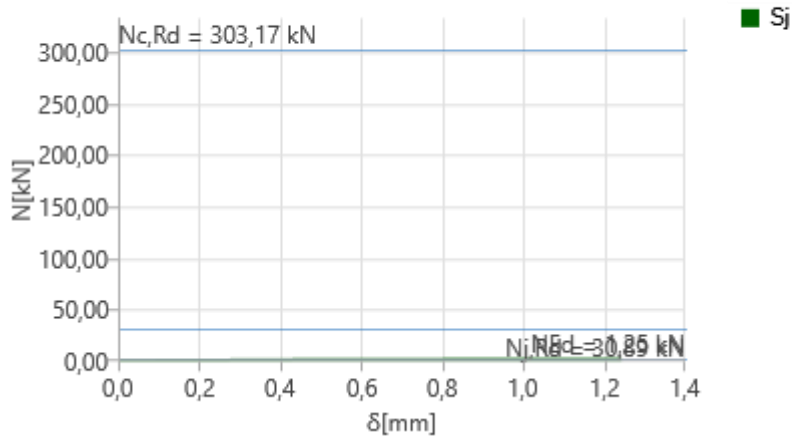
Stiffness diagram N - δ, ULS2b

N - δ



Stiffness diagram N - δ , ULS3a

N - δ



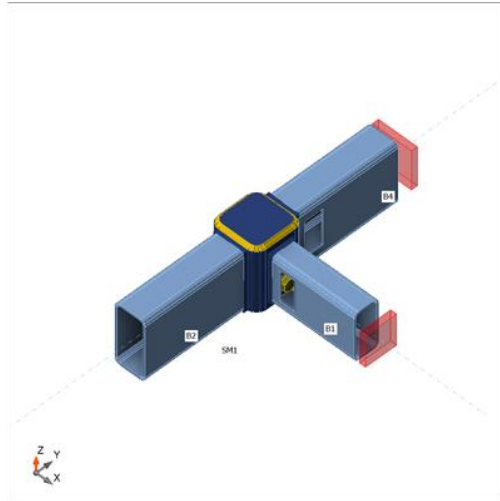
Stiffness diagram N - δ , ULS3b

Analysis: Stiffness

Members

Geometry

Name	Cross-section	β - Direction [°]	γ - Pitch [°]	α - Rotation [°]	Offset ex [mm]	Offset ey [mm]	Offset ez [mm]
B1	1 - RHS80/40/3.0	0,0	0,0	0,0	0	0	0
B2	6 - RHS100/50/3.0	-90,0	0,0	0,0	0	0	0
B4	6 - RHS100/50/3.0	90,0	0,0	0,0	0	0	0



Material

Steel	S 355 (EN)
Bolts	M12 8.8

Load effects

Name	Member	N [kN]	Vy [kN]	Vz [kN]	Mx [kNm]	My [kNm]	Mz [kNm]
ULS1	B1 / End	-2,00	0,00	0,00	0,00	0,01	0,00
	B2 / End	-13,22	0,00	0,00	0,00	0,40	0,00
	B4 / End	0,00	0,00	0,00	0,00	0,00	0,00
ULS2a	B1 / End	-2,00	0,00	0,00	0,00	0,05	0,00
	B2 / End	-2,62	0,00	0,00	0,00	0,33	0,00
	B4 / End	0,00	0,00	0,00	0,00	0,00	0,00
ULS2b	B1 / End	-2,00	0,00	0,00	0,00	0,10	0,00
	B2 / End	-2,73	0,00	0,00	0,00	0,33	0,00
	B4 / End	0,00	0,00	0,00	0,00	0,00	0,00
ULS3a	B1 / End	-2,00	0,00	0,00	0,00	0,20	0,00
	B2 / End	-1,10	0,00	0,00	0,00	0,32	0,00
	B4 / End	0,00	0,00	0,00	0,00	0,00	0,00
ULS3b	B1 / End	-2,00	0,00	0,00	0,00	0,50	0,00
	B2 / End	-1,20	0,00	0,00	0,00	0,32	0,00
	B4 / End	0,00	0,00	0,00	0,00	0,00	0,00

Rotational stiffness

Name	Comp.	Loads	Mj,Rd [kNm]	Sj,ini [kNm/rad]	Φc [mrad]	L [m]	Sj,R [kNm/rad]	Sj,P [kNm/rad]	Class.
B2	My	ULS1	3,40	2332,8	6,66	1,50	3850,0	77,0	Semi-rigid
	My	ULS2a	5,03	376,8	35,16	1,50	3850,0	77,0	Semi-rigid
	My	ULS2b	5,03	384,9	34,13	1,50	3850,0	77,0	Semi-rigid
	My	ULS3a	4,51	275,4	36,06	1,50	3850,0	77,0	Semi-rigid
	My	ULS3b	4,57	280,0	36,56	1,50	3850,0	77,0	Semi-rigid

Secant rotational stiffness

Name	Comp.	Loads	M [kNm]	Sjs [kNm/rad]	Φ [mrad]
B2	My	ULS1	0,40	2573,5	0,16
	My	ULS2a	0,33	397,8	0,83
	My	ULS2b	0,33	406,0	0,81
	My	ULS3a	0,32	312,1	1,03

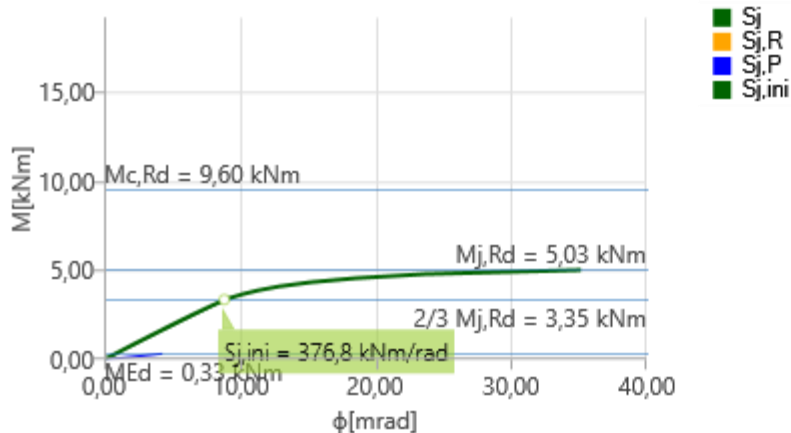
	My	ULS3b	0,32	316,8	1,01
--	----	-------	------	-------	------

Symbol explanation

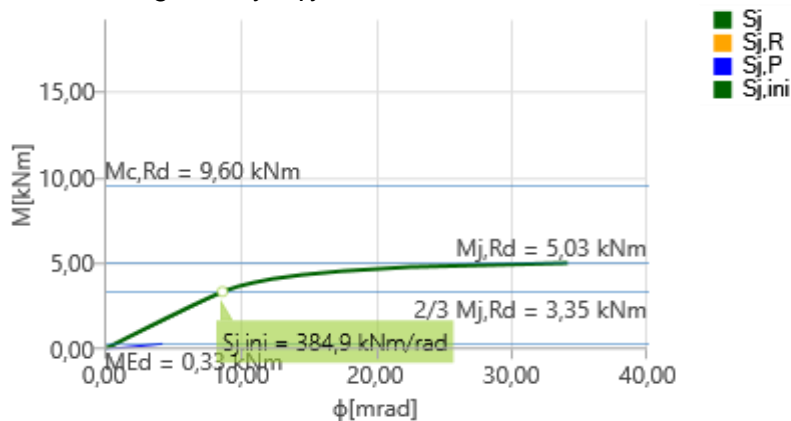
- $M_{j,Rd}$ Bending resistance
- $S_{j,ini}$ Initial rotational stiffness
- $S_{j,s}$ Secant rotational stiffness
- Φ Rotational deformation
- Φ_c Rotational capacity
- $S_{j,R}$ Limit value - rigid joint
- $S_{j,P}$ Limit value - nominally pinned joint



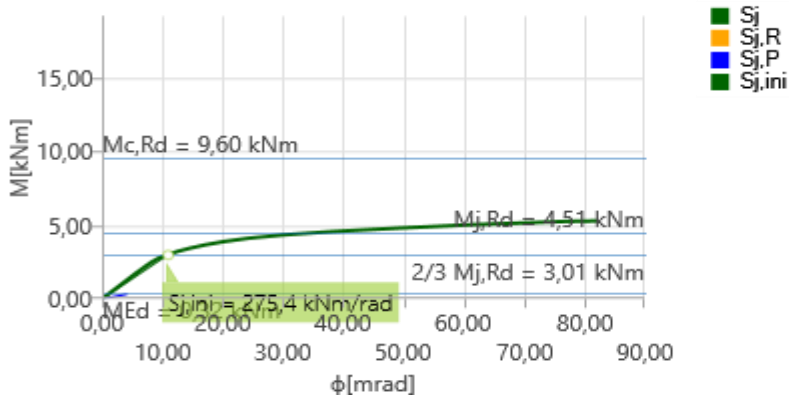
Stiffness diagram My - ϕ_y , ULS1



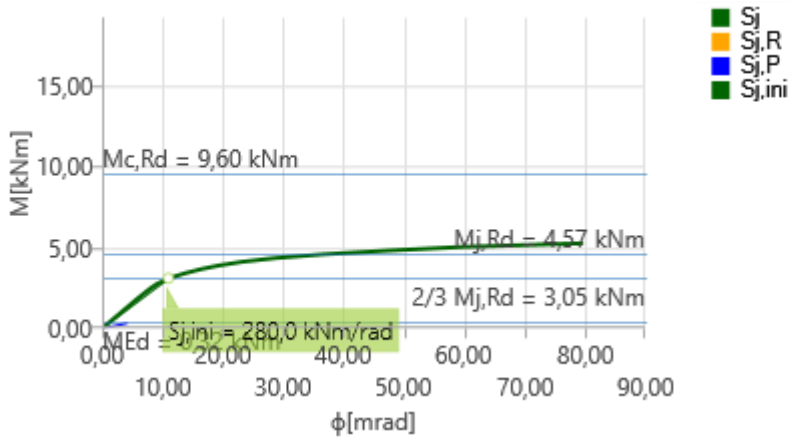
Stiffness diagram My - ϕ_y , ULS2a



Stiffness diagram My - ϕ_y , ULS2b



Stiffness diagram $M_y - \phi_y$, ULS3a

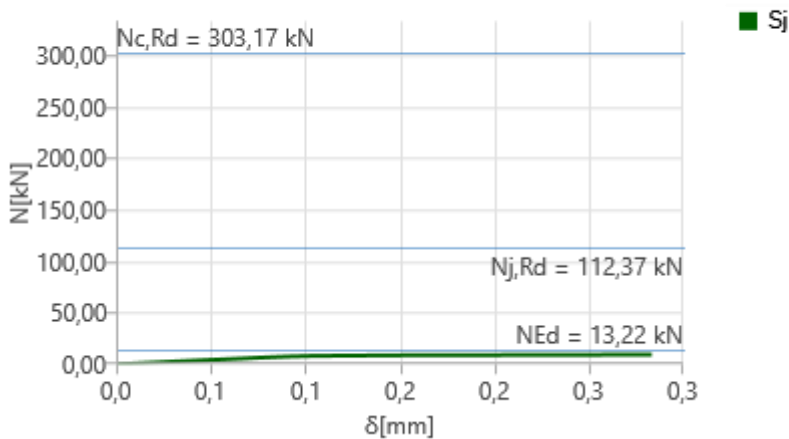


Stiffness diagram $M_y - \phi_y$, ULS3b

Axial stiffness

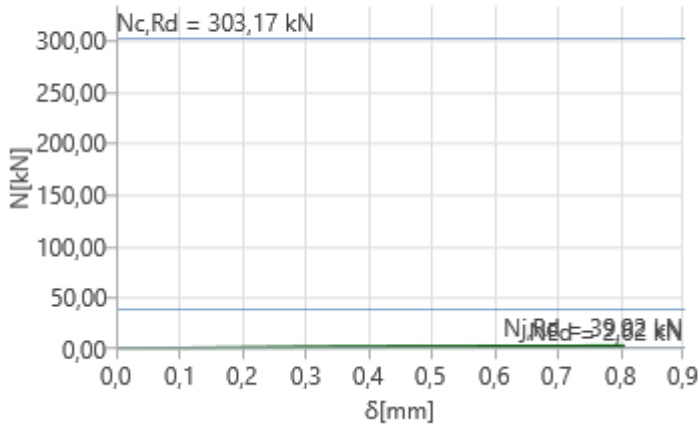
Name	Component	Loads	N [kN]	Nj,Rd [kN]	dx [mm]	St [kN/m]
B2	N	ULS1	-13,22	-112,37	0	2395655
		ULS2a	-2,62	-39,92	1	3865
		ULS2b	-2,73	-41,60	1	4333
		ULS3a	-1,10	-15,52	2	670
		ULS3b	-1,20	-17,14	2	766

N - delta



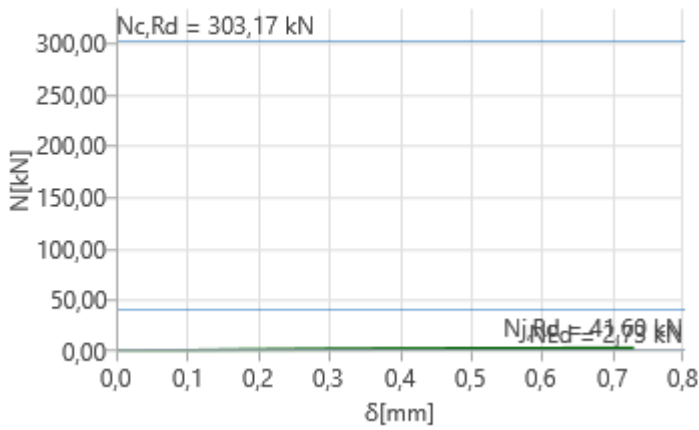
Stiffness diagram $N - \delta$, ULS1

N - δ



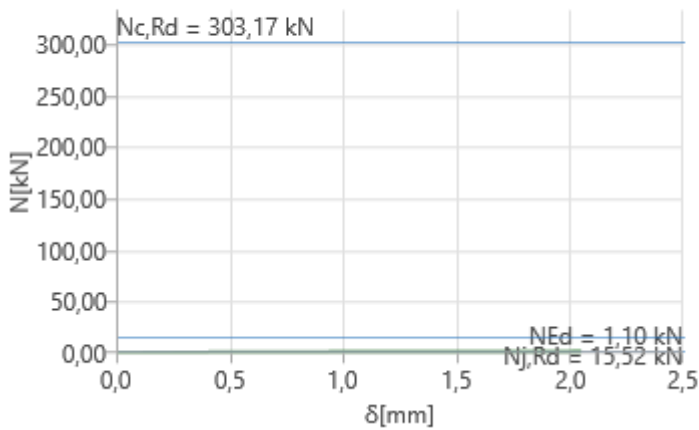
Stiffness diagram N - δ , ULS2a

N - δ



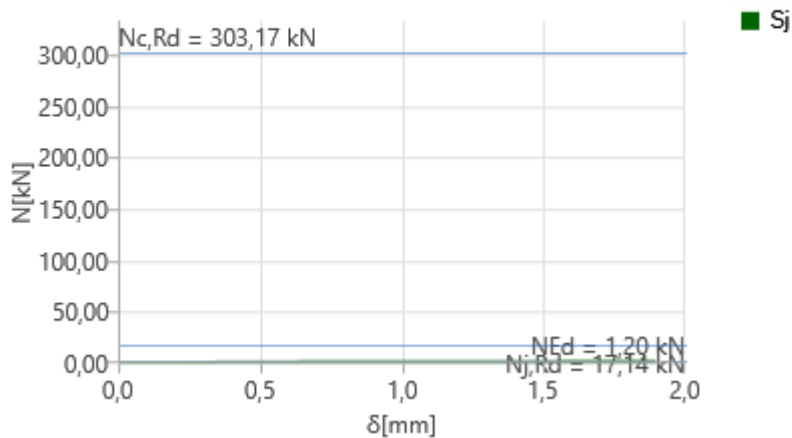
Stiffness diagram N - δ , ULS2b

N - δ



Stiffness diagram N - δ , ULS3a

N - δ



Stiffness diagram N - δ , ULS3b

Code settings

Item	Value	Unit	Reference
Safety factor γ_{M0}	1,00	-	EN 1993-1-1: 6.1
Safety factor γ_{M1}	1,00	-	EN 1993-1-1: 6.1
Safety factor γ_{M2}	1,25	-	EN 1993-1-1: 6.1
Safety factor γ_{M3}	1,25	-	EN 1993-1-8: 2.2
Safety factor γ_c	1,50	-	EN 1992-1-1: 2.4.2.4
Safety factor γ_{Inst}	1,20	-	EN 1992-4: Table 4.1
Joint coefficient β_j	0,67	-	EN 1993-1-8: 6.2.5
Effective area - influence of mesh size	0,10	-	
Friction coefficient - concrete	0,25	-	EN 1993-1-8
Friction coefficient in slip-resistance	0,30	-	EN 1993-1-8 tab 3.7
Limit plastic strain	0,05	-	EN 1993-1-5
Detailing	No		
Distance between bolts [d]	2,20	-	EN 1993-1-8: tab 3.3
Distance between bolts and edge [d]	1,20	-	EN 1993-1-8: tab 3.3
Concrete breakout resistance check	Both		EN 1992-4: 7.2.1.4 and 7.2.2.5
Use calculated a_b in bearing check.	Yes		EN 1993-1-8: tab 3.4
Cracked concrete	Yes		EN 1992-4
Local deformation check	No		CIDECT DG 1, 3 - 1.1
Local deformation limit	0,03	-	CIDECT DG 1, 3 - 1.1
Geometrical nonlinearity (GMNA)	Yes		Analysis with large deformations for hollow section joints
Braced system	No		EN 1993-1-8: 5.2.2.5

F.2 Stiffness analysis: Case study

Project data

Project name
 Project number
 Author
 Description
 Date 2024.05.14
 Code EN

Material

Steel S 355

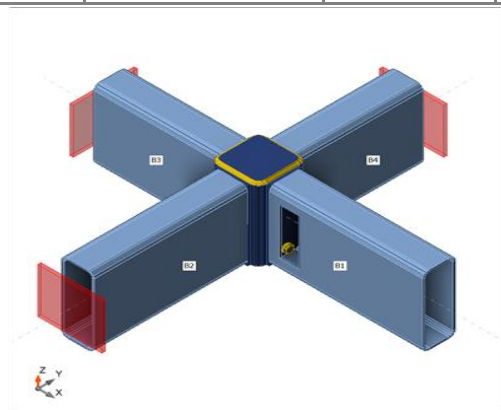
a

Analysis: Stiffness

Members

Geometry

Name	Cross-section	β - Direction [°]	γ - Pitch [°]	α - Rotation [°]	Offset ex [mm]	Offset ey [mm]	Offset ez [mm]
B1	1 - RHS300/100/8.0	0,0	0,0	0,0	0	0	0
B2	1 - RHS300/100/8.0	-90,0	0,0	0,0	0	0	0
B3	1 - RHS300/100/8.0	180,0	0,0	0,0	0	0	0
B4	1 - RHS300/100/8.0	90,0	0,0	0,0	0	0	0



Material

Steel	S 355 (EN)
Bolts	M16 8.8

Load effects

Name	Member	N [kN]	Vy [kN]	Vz [kN]	Mx [kNm]	My [kNm]	Mz [kNm]
LE1	B1 / End	-99,00	0,00	0,00	0,00	19,80	0,00
	B2 / End	0,00	0,00	0,00	0,00	0,00	0,00
	B3 / End	0,00	0,00	0,00	0,00	0,00	0,00
	B4 / End	0,00	0,00	0,00	0,00	0,00	0,00

Rotational stiffness

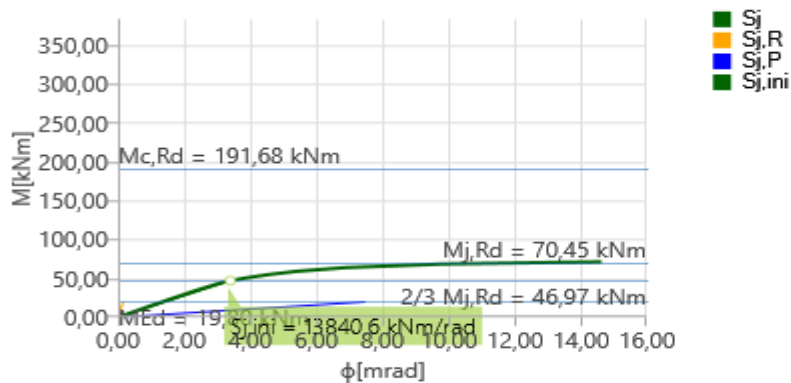
Name	Comp.	Loads	M _{j,Rd} [kNm]	S _{j,ini} [kNm/rad]	Φ _c [mrad]	L [m]	S _{j,R} [kNm/rad]	S _{j,P} [kNm/rad]	Class.
B1	My	LE1	70,45	13840,6	12,79	2,50	132405,0	2648,1	Semi-rigid

Secant rotational stiffness

Name	Comp.	Loads	M [kNm]	S _{j,s} [kNm/rad]	Φ [mrad]
B1	My	LE1	19,80	14844,1	1,33

Symbol explanation

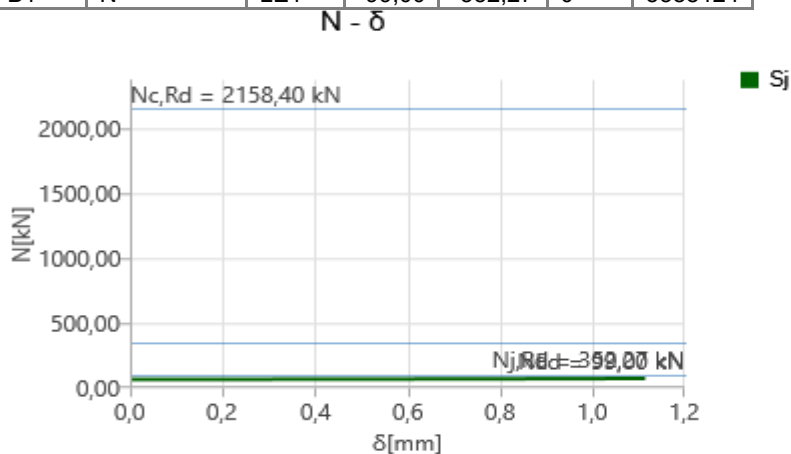
- M_{j,Rd} Bending resistance
- S_{j,ini} Initial rotational stiffness
- S_{j,s} Secant rotational stiffness
- Φ Rotational deformation
- Φ_c Rotational capacity
- S_{j,R} Limit value - rigid joint
- S_{j,P} Limit value - nominally pinned joint



Stiffness diagram My - φ_y, LE1

Axial stiffness

Name	Component	Loads	N [kN]	N _{j,Rd} [kN]	dx [mm]	St [kN/m]
B1	N	LE1	-99,00	-352,27	0	5388124



Stiffness diagram N - δ, LE1

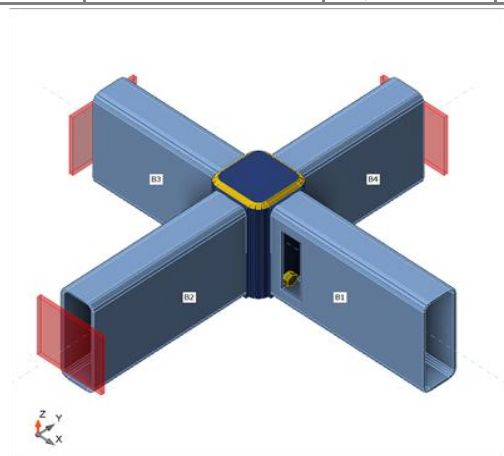
b

Analysis: Stiffness

Members

Geometry

Name	Cross-section	β - Direction [°]	γ - Pitch [°]	α - Rotation [°]	Offset ex [mm]	Offset ey [mm]	Offset ez [mm]
B1	1 - RHS300/100/8.0	0,0	0,0	0,0	0	0	0
B2	1 - RHS300/100/8.0	-90,0	0,0	0,0	0	0	0
B3	1 - RHS300/100/8.0	180,0	0,0	0,0	0	0	0
B4	1 - RHS300/100/8.0	90,0	0,0	0,0	0	0	0



Material

Steel	S 355 (EN)
Bolts	M20 8.8

Load effects

Name	Member	N [kN]	Vy [kN]	Vz [kN]	Mx [kNm]	My [kNm]	Mz [kNm]
LE1	B1 / End	-100,00	0,00	0,00	0,00	20,00	0,00
	B2 / End	0,00	0,00	0,00	0,00	0,00	0,00
	B3 / End	0,00	0,00	0,00	0,00	0,00	0,00
	B4 / End	0,00	0,00	0,00	0,00	0,00	0,00

Rotational stiffness

Name	Comp.	Loads	Mj,Rd [kNm]	Sj,ini [kNm/rad]	Φ_c [mrad]	L [m]	Sj,R [kNm/rad]	Sj,P [kNm/rad]	Class.
B1	My	LE1	74,16	19607,3	6,32	2,50	132405,0	2648,1	Semi-rigid

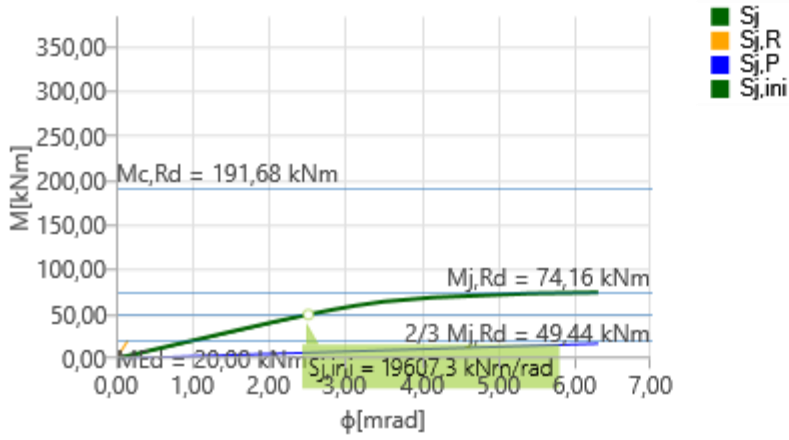
Secant rotational stiffness

Name	Comp.	Loads	M [kNm]	Sjs [kNm/rad]	Φ [mrad]
B1	My	LE1	20,00	20237,3	0,99

Symbol explanation

- M_{j,Rd} Bending resistance
- S_{j,ini} Initial rotational stiffness

- $S_{j,s}$ Secant rotational stiffness
- Φ Rotational deformation
- Φ_c Rotational capacity
- $S_{j,R}$ Limit value - rigid joint
- $S_{j,P}$ Limit value - nominally pinned joint

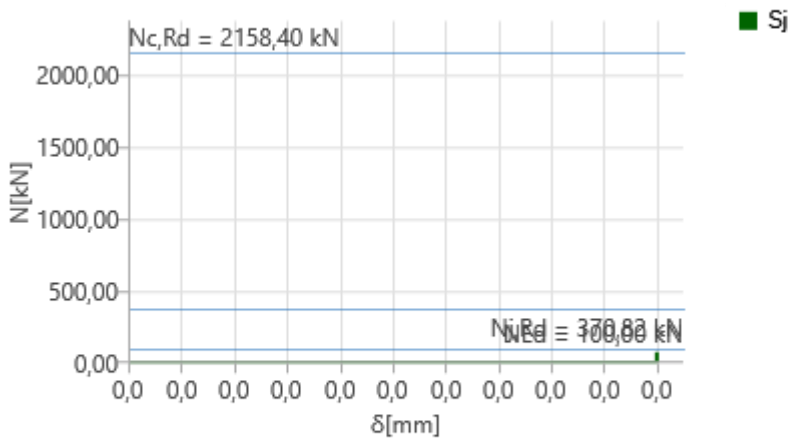


Stiffness diagram $M_y - \phi_y$, LE1

Axial stiffness

Name	Component	Loads	N [kN]	Nj,Rd [kN]	dx [mm]	St [kN/m]
B1	N	LE1	-100,00	-370,82	0	3849015

N - δ



Stiffness diagram $N - \delta$, LE1

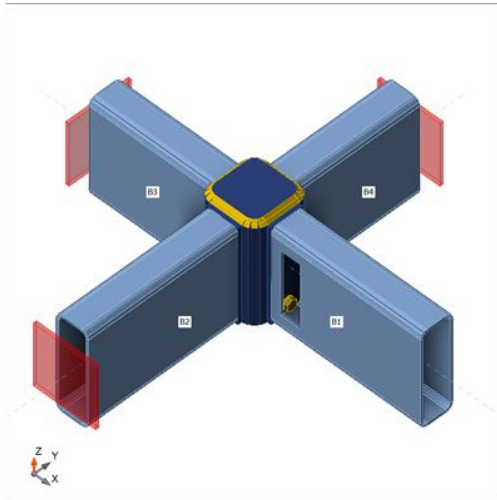
d

Analysis: Stiffness

Members

Geometry

Name	Cross-section	β - Direction [°]	γ - Pitch [°]	α - Rotation [°]	Offset ex [mm]	Offset ey [mm]	Offset ez [mm]
B1	1 - RHS300/100/8.0	0,0	0,0	0,0	0	0	0
B2	1 - RHS300/100/8.0	-90,0	0,0	0,0	0	0	0
B3	1 - RHS300/100/8.0	180,0	0,0	0,0	0	0	0
B4	1 - RHS300/100/8.0	90,0	0,0	0,0	0	0	0



Material

Steel	S 355 (EN)
Bolts	M20 8.8

Load effects

Name	Member	N [kN]	Vy [kN]	Vz [kN]	Mx [kNm]	My [kNm]	Mz [kNm]
LE1	B1 / End	-103,00	0,00	0,00	0,00	20,60	0,00
	B2 / End	0,00	0,00	0,00	0,00	0,00	0,00
	B3 / End	0,00	0,00	0,00	0,00	0,00	0,00
	B4 / End	0,00	0,00	0,00	0,00	0,00	0,00

Rotational stiffness

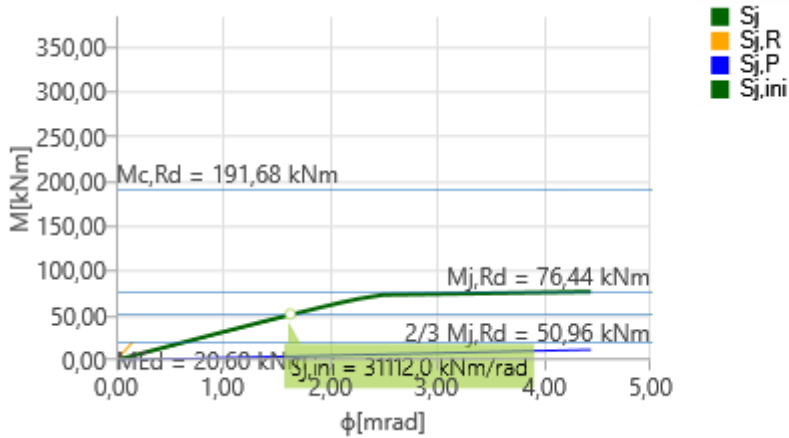
Name	Comp.	Loads	Mj,Rd [kNm]	Sj,ini [kNm/rad]	Φ c [mrad]	L [m]	Sj,R [kNm/rad]	Sj,P [kNm/rad]	Class.
B1	My	LE1	76,44	31112,0	4,44	2,50	132405,0	2648,1	Semi-rigid

Secant rotational stiffness

Name	Comp.	Loads	M [kNm]	Sjs [kNm/rad]	Φ [mrad]
B1	My	LE1	20,60	31797,6	0,65

Symbol explanation

- $M_{j,Rd}$ Bending resistance
- $S_{j,ini}$ Initial rotational stiffness
- $S_{j,s}$ Secant rotational stiffness
- Φ Rotational deformation
- Φ_c Rotational capacity
- $S_{j,R}$ Limit value - rigid joint
- $S_{j,P}$ Limit value - nominally pinned joint

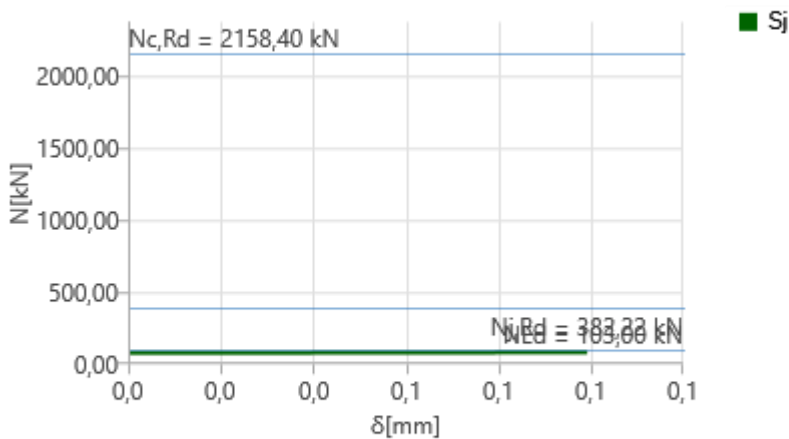


Stiffness diagram $M_y - \phi_y$, LE1

Axial stiffness

Name	Component	Loads	N [kN]	$N_{j,Rd}$ [kN]	dx [mm]	St [kN/m]
B1	N	LE1	-103,00	-382,22	0	3146225

$N - \delta$



Stiffness diagram $N - \delta$, LE1

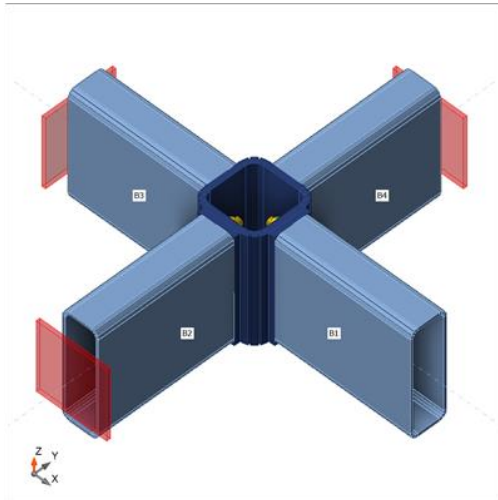
C

Analysis: Stiffness

Members

Geometry

Name	Cross-section	β - Direction [°]	γ - Pitch [°]	α - Rotation [°]	Offset ex [mm]	Offset ey [mm]	Offset ez [mm]
B1	1 - RHS300/100/8.0	0,0	0,0	0,0	0	0	0
B2	1 - RHS300/100/8.0	-90,0	0,0	0,0	0	0	0
B3	1 - RHS300/100/8.0	180,0	0,0	0,0	0	0	0
B4	1 - RHS300/100/8.0	90,0	0,0	0,0	0	0	0



Material

Steel	S 355 (EN)
Bolts	M20 8.8

Load effects

Name	Member	N [kN]	Vy [kN]	Vz [kN]	Mx [kNm]	My [kNm]	Mz [kNm]
LE1	B1 / End	-98,00	0,00	0,00	0,00	19,60	0,00
	B2 / End	0,00	0,00	0,00	0,00	0,00	0,00
	B3 / End	0,00	0,00	0,00	0,00	0,00	0,00
	B4 / End	0,00	0,00	0,00	0,00	0,00	0,00

Rotational stiffness

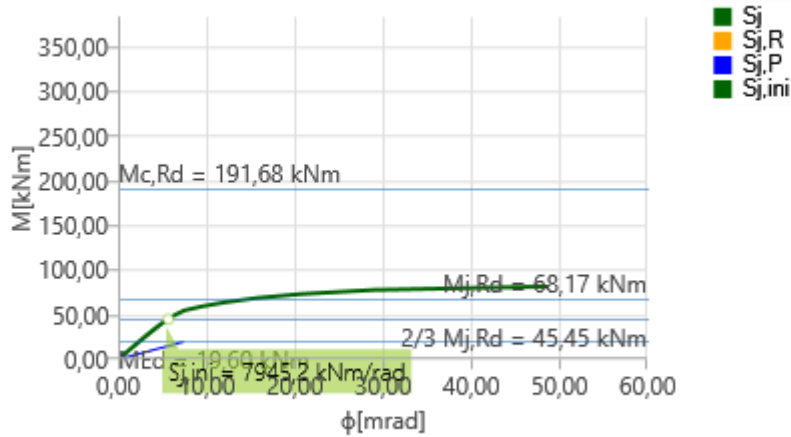
Name	Comp.	Loads	Mj,Rd [kNm]	Sj,ini [kNm/rad]	Φ c [mrad]	L [m]	Sj,R [kNm/rad]	Sj,P [kNm/rad]	Class.
B1	My	LE1	68,17	7945,2	15,34	2,50	132405,0	2648,1	Semi-rigid

Secant rotational stiffness

Name	Comp.	Loads	M [kNm]	Sjs [kNm/rad]	Φ [mrad]
B1	My	LE1	19,60	8462,1	2,32

Symbol explanation

- $M_{j,Rd}$ Bending resistance
- $S_{j,ini}$ Initial rotational stiffness
- $S_{j,s}$ Secant rotational stiffness
- Φ Rotational deformation
- Φ_c Rotational capacity
- $S_{j,R}$ Limit value - rigid joint
- $S_{j,P}$ Limit value - nominally pinned joint

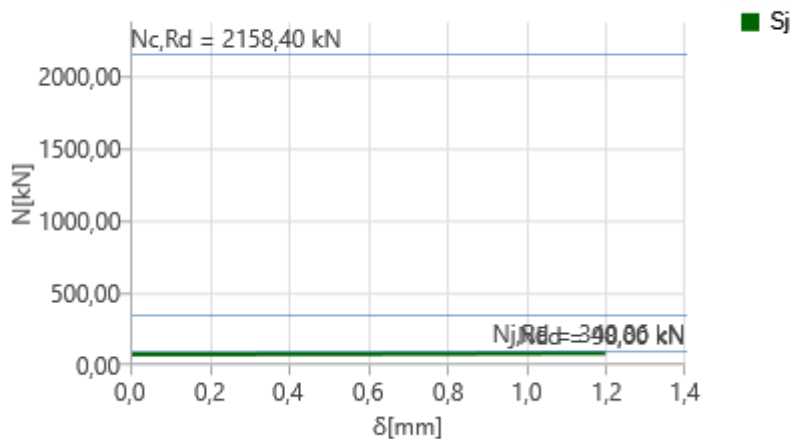


Stiffness diagram $M_y - \phi_y$, LE1

Axial stiffness

Name	Component	Loads	N [kN]	$N_{j,Rd}$ [kN]	dx [mm]	St [kN/m]
B1	N	LE1	-98,00	-340,86	0	2742704

$N - \delta$



Stiffness diagram $N - \delta$, LE1

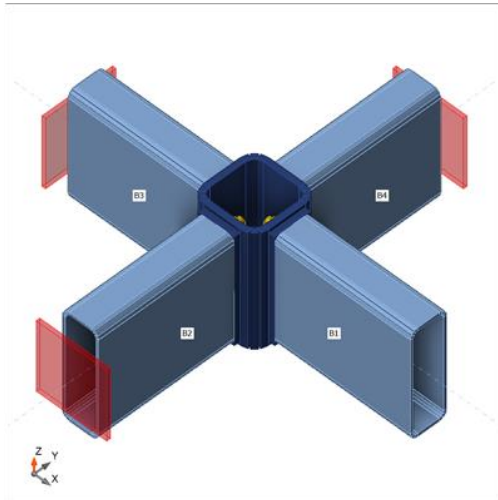
e

Analysis: Stiffness

Members

Geometry

Name	Cross-section	β - Direction [°]	γ - Pitch [°]	α - Rotation [°]	Offset ex [mm]	Offset ey [mm]	Offset ez [mm]
B1	1 - RHS300/100/8.0	0,0	0,0	0,0	0	0	0
B2	1 - RHS300/100/8.0	-90,0	0,0	0,0	0	0	0
B3	1 - RHS300/100/8.0	180,0	0,0	0,0	0	0	0
B4	1 - RHS300/100/8.0	90,0	0,0	0,0	0	0	0



Material

Steel	S 355 (EN)
Bolts	M24 8.8

Load effects

Name	Member	N [kN]	Vy [kN]	Vz [kN]	Mx [kNm]	My [kNm]	Mz [kNm]
LE1	B1 / End	-88,00	0,00	0,00	0,00	17,60	0,00
	B2 / End	0,00	0,00	0,00	0,00	0,00	0,00
	B3 / End	0,00	0,00	0,00	0,00	0,00	0,00
	B4 / End	0,00	0,00	0,00	0,00	0,00	0,00

Rotational stiffness

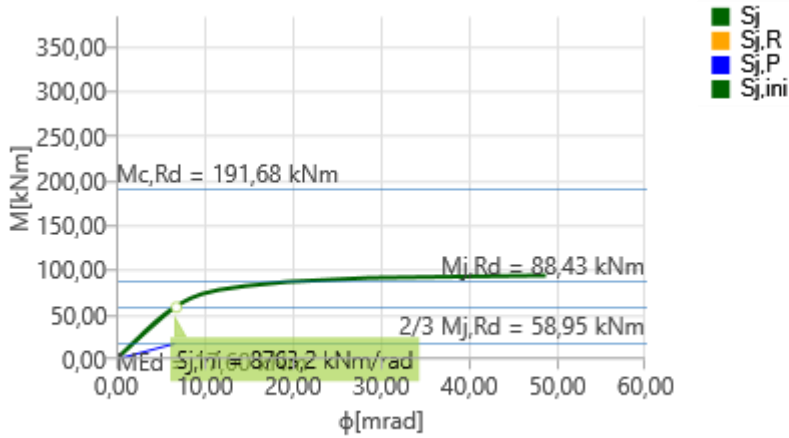
Name	Comp.	Loads	Mj,Rd [kNm]	Sj,ini [kNm/rad]	Φ c [mrad]	L [m]	Sj,R [kNm/rad]	Sj,P [kNm/rad]	Class.
B1	My	LE1	88,43	8763,2	22,18	2,50	132405,0	2648,1	Semi-rigid

Secant rotational stiffness

Name	Comp.	Loads	M [kNm]	Sjs [kNm/rad]	Φ [mrad]
B1	My	LE1	17,60	9644,6	1,82

Symbol explanation

- $M_{j,Rd}$ Bending resistance
- $S_{j,ini}$ Initial rotational stiffness
- $S_{j,s}$ Secant rotational stiffness
- Φ Rotational deformation
- Φ_c Rotational capacity
- $S_{j,R}$ Limit value - rigid joint
- $S_{j,P}$ Limit value - nominally pinned joint

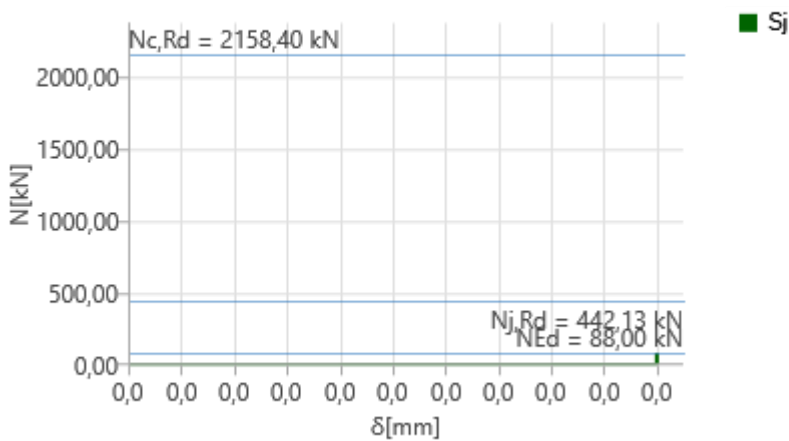


Stiffness diagram $M_y - \phi_y$, LE1

Axial stiffness

Name	Component	Loads	N [kN]	$N_{j,Rd}$ [kN]	dx [mm]	St [kN/m]
B1	N	LE1	-88,00	-442,13	0	2979390

$N - \delta$



Stiffness diagram $N - \delta$, LE1

Code settings

Item	Value	Unit	Reference
Safety factor γ_{M0}	1,00	-	EN 1993-1-1: 6.1
Safety factor γ_{M1}	1,00	-	EN 1993-1-1: 6.1
Safety factor γ_{M2}	1,25	-	EN 1993-1-1: 6.1
Safety factor γ_{M3}	1,25	-	EN 1993-1-8: 2.2
Safety factor γ_c	1,50	-	EN 1992-1-1: 2.4.2.4
Safety factor γ_{Inst}	1,20	-	EN 1992-4: Table 4.1
Joint coefficient β_j	0,67	-	EN 1993-1-8: 6.2.5
Effective area - influence of mesh size	0,10	-	
Friction coefficient - concrete	0,25	-	EN 1993-1-8
Friction coefficient in slip-resistance	0,30	-	EN 1993-1-8 tab 3.7
Limit plastic strain	0,05	-	EN 1993-1-5
Detailing	No		
Distance between bolts [d]	2,20	-	EN 1993-1-8: tab 3.3
Distance between bolts and edge [d]	1,20	-	EN 1993-1-8: tab 3.3
Concrete breakout resistance check	Both		EN 1992-4: 7.2.1.4 and 7.2.2.5
Use calculated a_b in bearing check.	Yes		EN 1993-1-8: tab 3.4
Cracked concrete	Yes		EN 1992-4
Local deformation check	No		CIDECT DG 1, 3 - 1.1
Local deformation limit	0,03	-	CIDECT DG 1, 3 - 1.1
Geometrical nonlinearity (GMNA)	Yes		Analysis with large deformations for hollow section joints
Braced system	No		EN 1993-1-8: 5.2.2.5

Appendix G: Nodal forces (RFEM Output)

G.1 ULS1

Member	Node	N	Vy	Vz	Mt	My	Mz
1	1	-6.66	0.00	0.74	0.00	0.00	0.00
33	1	-14.48	0.00	-0.41	0.00	-0.07	0.00
	1	-13.36	0.00	0.28	0.00	-0.07	0.00
8	10	-5.63	0.00	-0.79	0.00	0.00	0.00
38	10	-13.22	0.00	-0.57	0.00	0.16	0.00
	10	-13.22	0.00	0.57	0.00	0.16	0.00
	11	-6.66	0.00	0.74	0.00	0.00	0.00
35	11	-13.36	0.00	-0.28	0.00	-0.07	0.00
	11	-14.48	0.00	0.41	0.00	-0.07	0.00
9	12	-5.83	0.00	-0.92	0.00	0.15	0.00
	12	-5.84	0.00	0.84	0.00	0.15	0.00
15	12	-5.84	0.00	-0.84	0.00	0.15	0.00
	12	-5.83	0.00	0.92	0.00	0.15	0.00
10	13	-5.58	0.00	-0.76	0.00	0.09	0.00
	13	-5.58	0.00	0.76	0.00	0.09	0.00
19	13	-4.90	0.00	-0.87	0.00	0.11	0.00
	13	-4.78	0.00	0.91	0.00	0.11	0.00
11	14	-5.84	0.00	-0.84	0.00	0.15	0.00
	14	-5.83	0.00	0.92	0.00	0.15	0.00
23	14	-5.84	0.00	-0.84	0.00	0.15	0.00
	14	-5.83	0.00	0.92	0.00	0.15	0.00
12	15	-6.66	0.00	-0.74	0.00	0.00	0.00
39	15	-13.36	0.00	-0.28	0.00	-0.07	0.00
	15	-14.48	0.00	0.41	0.00	-0.07	0.00
	16	-6.66	0.00	0.74	0.00	0.00	0.00
25	16	-14.48	0.00	-0.41	0.00	-0.07	0.00
	16	-13.36	0.00	0.28	0.00	-0.07	0.00
16	17	-6.66	0.00	-0.74	0.00	0.00	0.00
29	17	-14.48	0.00	-0.41	0.00	-0.07	0.00
	17	-13.36	0.00	0.28	0.00	-0.07	0.00
	18	-5.63	0.00	0.79	0.00	0.00	0.00
26	18	-13.22	0.00	-0.57	0.00	0.16	0.00
	18	-13.22	0.00	0.57	0.00	0.16	0.00
20	19	-5.63	0.00	-0.79	0.00	0.00	0.00
30	19	-13.22	0.00	-0.57	0.00	0.16	0.00
	19	-13.22	0.00	0.57	0.00	0.16	0.00
1	2	-5.83	0.00	-0.92	0.00	0.15	0.00
	2	-5.84	0.00	0.84	0.00	0.15	0.00
13	2	-5.83	0.00	-0.92	0.00	0.15	0.00
	2	-5.84	0.00	0.84	0.00	0.15	0.00
	20	-6.66	0.00	0.74	0.00	0.00	0.00
27	20	-13.36	0.00	-0.28	0.00	-0.07	0.00
	20	-14.48	0.00	0.41	0.00	-0.07	0.00
24	21	-6.66	0.00	-0.74	0.00	0.00	0.00
31	21	-13.36	0.00	-0.28	0.00	-0.07	0.00
	21	-14.48	0.00	0.41	0.00	-0.07	0.00
	22	-14.91	0.00	0.46	0.00	0.00	0.00
	22	-14.91	0.00	0.46	0.00	0.00	0.00
28	23	-14.91	0.00	-0.46	0.00	0.00	0.00
	23	-14.91	0.00	0.46	0.00	0.00	0.00
	24	-14.91	0.00	0.46	0.00	0.00	0.00
36	24	-14.91	0.00	-0.46	0.00	0.00	0.00
32	25	-14.91	0.00	-0.46	0.00	0.00	0.00
40	25	-14.91	0.00	-0.46	0.00	0.00	0.00
2	3	-5.58	0.00	-0.76	0.00	0.09	0.00
	3	-5.58	0.00	0.76	0.00	0.09	0.00
17	3	-4.78	0.00	-0.91	0.00	0.11	0.00
	3	-4.90	0.00	0.87	0.00	0.11	0.00
3	4	-5.84	0.00	-0.84	0.00	0.15	0.00
	4	-5.83	0.00	0.92	0.00	0.15	0.00
21	4	-5.83	0.00	-0.92	0.00	0.15	0.00
	4	-5.84	0.00	0.84	0.00	0.15	0.00
4	5	-6.66	0.00	-0.74	0.00	0.00	0.00
37	5	-14.48	0.00	-0.41	0.00	-0.07	0.00
	5	-13.36	0.00	0.28	0.00	-0.07	0.00
	6	-5.63	0.00	0.79	0.00	0.00	0.00
34	6	-13.22	0.00	-0.57	0.00	0.16	0.00
	6	-13.22	0.00	0.57	0.00	0.16	0.00
5	7	-4.78	0.00	-0.91	0.00	0.11	0.00
	7	-4.90	0.00	0.87	0.00	0.11	0.00
14	7	-5.58	0.00	-0.76	0.00	0.09	0.00
	7	-5.58	0.00	0.76	0.00	0.09	0.00
6	8	-4.62	0.00	-0.77	0.00	0.02	0.00
	8	-4.62	0.00	0.77	0.00	0.02	0.00
18	8	-4.62	0.00	-0.77	0.00	0.02	0.00
	8	-4.62	0.00	0.77	0.00	0.02	0.00
7	9	-4.90	0.00	-0.87	0.00	0.11	0.00
	9	-4.78	0.00	0.91	0.00	0.11	0.00
22	9	-5.58	0.00	-0.76	0.00	0.09	0.00
	9	-5.58	0.00	0.76	0.00	0.09	0.00
No.	No.	N	Vy	Vz	Mt	My	Mz
Member	Node	Forces [kN]			Moments [kNm]		

Normative combinations marked

G.2 ULS2

Member	Node	N	Vy	Vz	Mt	My	Mz
1	1	-2.92	-0.01	0.25	0.00	0.00	0.00
33	1	-3.13	0.03	0.05	0.00	-0.61	0.00
	1	-2.73	0.07	-0.55	0.00	-0.61	0.00
8	10	-0.22	0.00	0.13	0.00	0.00	0.00
38	10	-2.66	0.07	-0.71	0.00	0.36	0.00
	10	-2.74	-0.09	0.21	0.00	0.36	0.00
	11	-1.55	0.08	0.10	0.00	0.00	0.00
35	11	-2.81	-0.09	0.13	0.00	0.11	0.00
	11	-2.93	0.03	0.22	0.00	0.11	0.00
9	12	-1.16	-0.08	-0.07	0.00	-0.02	0.00
	12	-1.26	0.07	0.08	0.00	-0.02	0.00
15	12	-0.58	-0.12	0.01	0.00	0.06	0.00
	12	-0.35	0.04	0.27	0.00	0.06	0.00
10	13	-1.15	-0.07	-0.13	0.00	0.01	0.00
	13	-1.15	0.07	0.13	0.00	0.01	0.00
19	13	-0.47	0.00	0.07	0.00	0.03	0.00
	13	-0.25	0.00	0.24	0.00	0.03	0.00
11	14	-1.26	-0.07	-0.08	0.00	-0.02	0.00
	14	-1.16	0.08	0.07	0.00	-0.02	0.00
23	14	-0.58	0.12	0.01	0.00	0.06	0.00
	14	-0.35	-0.04	0.27	0.00	0.06	0.00
12	15	-1.55	-0.08	-0.10	0.00	0.00	0.00
39	15	-2.81	0.09	0.13	0.00	0.11	0.00
	15	-2.93	-0.03	0.22	0.00	0.11	0.00
	16	-0.79	-0.05	0.70	0.00	0.00	0.00
25	16	-5.28	-0.06	-0.34	0.00	-0.05	0.00
	16	-4.93	0.06	0.26	0.00	-0.05	0.00
16	17	-0.73	-0.04	-0.20	0.00	0.00	0.00
29	17	-2.86	-0.02	-0.18	0.00	-0.02	0.00
	17	-2.75	0.01	0.16	0.00	-0.02	0.00
	18	-0.62	0.00	0.62	0.00	0.00	0.00
26	18	-4.86	-0.06	-0.39	0.00	0.04	0.00
	18	-4.86	0.06	0.39	0.00	0.04	0.00
20	19	-0.64	0.00	-0.21	0.00	0.00	0.00
30	19	-2.67	-0.01	-0.20	0.00	0.01	0.00
	19	-2.67	0.01	0.20	0.00	0.01	0.00
1	2	-2.54	0.01	-0.32	0.00	0.06	0.00
	2	-2.55	-0.01	0.32	0.00	0.06	0.00
13	2	-0.41	0.05	-0.39	0.00	-0.26	0.00
	2	-0.54	0.09	-0.14	0.00	-0.26	0.00
	20	-0.79	0.05	0.70	0.00	0.00	0.00
27	20	-4.93	-0.06	-0.26	0.00	-0.05	0.00
	20	-5.28	0.06	0.34	0.00	-0.05	0.00
24	21	-0.73	0.04	-0.20	0.00	0.00	0.00
31	21	-2.75	-0.01	-0.16	0.00	-0.02	0.00
	21	-2.86	0.02	0.18	0.00	-0.02	0.00
	22	-5.50	0.06	0.39	0.00	0.00	0.00
	22	-3.35	-0.03	0.66	0.00	0.00	0.00
28	23	-5.50	-0.06	-0.39	0.00	0.00	0.00
	23	-3.35	0.03	0.66	0.00	0.00	0.00
	24	-3.09	0.02	0.20	0.00	0.00	0.00
36	24	-3.16	-0.03	-0.09	0.00	0.00	0.00
32	25	-3.09	-0.02	-0.20	0.00	0.00	0.00
40	25	-3.16	0.03	-0.09	0.00	0.00	0.00
2	3	-2.43	0.01	-0.23	0.00	-0.01	0.00
	3	-2.43	-0.01	0.23	0.00	-0.01	0.00
17	3	-0.24	0.00	-0.49	0.00	-0.11	0.00
	3	-0.45	0.00	-0.07	0.00	-0.11	0.00
3	4	-2.55	0.01	-0.32	0.00	0.06	0.00
	4	-2.54	-0.01	0.32	0.00	0.06	0.00
21	4	-0.41	-0.05	-0.39	0.00	-0.26	0.00
	4	-0.54	-0.09	-0.14	0.00	-0.26	0.00
4	5	-2.92	0.01	-0.25	0.00	0.00	0.00
37	5	-3.13	-0.03	0.05	0.00	-0.61	0.00
	6	-2.73	-0.07	-0.55	0.00	-0.61	0.00
	6	-0.22	0.00	-0.13	0.00	0.00	0.00
34	6	-2.66	-0.07	-0.71	0.00	0.36	0.00
	6	-2.74	0.09	0.21	0.00	0.36	0.00
5	7	0.17	0.00	0.14	0.00	-0.01	0.00
	7	0.02	0.00	-0.08	0.00	-0.01	0.00
14	7	-0.42	-0.09	-0.29	0.00	0.07	0.00
	7	-0.47	0.12	-0.01	0.00	0.07	0.00
6	8	0.14	0.00	0.06	0.00	0.00	0.00
	8	0.14	0.00	-0.06	0.00	0.00	0.00
18	8	-0.33	0.00	-0.19	0.00	0.08	0.00
	8	-0.35	0.00	0.01	0.00	0.08	0.00
7	9	0.02	0.00	0.08	0.00	-0.01	0.00
	9	0.17	0.00	-0.14	0.00	-0.01	0.00
22	9	-0.42	0.09	-0.29	0.00	0.07	0.00
	9	-0.47	-0.12	-0.01	0.00	0.07	0.00
No.	No.	N	Vy	Vz	Mt	My	Mz
Member	Node	Forces [kN]			Moments [kNm]		

Normative combinations marked

G.3 ULS3

Member	Node	N	Vy	Vz	Mt	My	Mz
	1	-2.21	-0.01	0.16	0.00	0.00	0.00
33	1	-1.46	0.03	0.10	0.00	-0.59	0.00
	1	-1.19	0.07	-0.59	0.00	-0.59	0.00
8	10	0.44	0.00	0.22	0.00	0.00	0.00
38	10	-1.14	0.07	-0.65	0.00	0.36	0.00
	10	-1.21	-0.09	0.14	0.00	0.36	0.00
	11	-0.83	0.08	0.00	0.00	0.00	0.00
35	11	-1.27	-0.09	0.17	0.00	0.12	0.00
	11	-1.26	0.03	0.17	0.00	0.12	0.00
9	12	-0.54	-0.08	0.03	0.00	-0.03	0.00
	12	-0.64	0.07	-0.01	0.00	-0.03	0.00
15	12	0.05	-0.12	0.10	0.00	0.05	0.00
	12	0.29	0.04	0.17	0.00	0.05	0.00
10	13	-0.55	-0.07	-0.04	0.00	0.01	0.00
	13	-0.55	0.07	0.04	0.00	0.01	0.00
19	13	0.08	0.00	0.15	0.00	0.02	0.00
	13	0.29	0.00	0.14	0.00	0.02	0.00
11	14	-0.64	-0.07	0.01	0.00	-0.03	0.00
	14	-0.54	0.08	-0.03	0.00	-0.03	0.00
23	14	0.05	0.12	0.10	0.00	0.05	0.00
	14	0.29	-0.04	0.17	0.00	0.05	0.00
12	15	-0.83	-0.08	0.00	0.00	0.00	0.00
39	15	-1.27	0.09	0.17	0.00	0.12	0.00
	15	-1.26	-0.03	0.17	0.00	0.12	0.00
	16	-0.06	-0.05	0.61	0.00	0.00	0.00
25	16	-3.61	-0.06	-0.29	0.00	-0.03	0.00
	16	-3.39	0.06	0.22	0.00	-0.03	0.00
16	17	0.00	-0.04	-0.11	0.00	0.00	0.00
29	17	-1.20	-0.02	-0.13	0.00	0.00	0.00
	17	-1.21	0.01	0.12	0.00	0.00	0.00
	18	0.02	0.00	0.53	0.00	0.00	0.00
26	18	-3.34	-0.06	-0.32	0.00	0.04	0.00
	18	-3.34	0.06	0.32	0.00	0.04	0.00
20	19	0.00	0.00	-0.12	0.00	0.00	0.00
30	19	-1.16	-0.01	-0.14	0.00	0.01	0.00
	19	-1.16	0.01	0.14	0.00	0.01	0.00
1	2	-1.93	0.01	-0.23	0.00	0.05	0.00
	2	-1.93	-0.01	0.23	0.00	0.05	0.00
13	2	0.22	0.05	-0.29	0.00	-0.27	0.00
	2	0.10	0.09	-0.23	0.00	-0.27	0.00
	20	-0.06	0.05	0.61	0.00	0.00	0.00
27	20	-3.39	-0.06	-0.22	0.00	-0.03	0.00
	20	-3.61	0.06	0.29	0.00	-0.03	0.00
24	21	0.00	0.04	-0.11	0.00	0.00	0.00
31	21	-1.21	-0.01	-0.12	0.00	0.00	0.00
	21	-1.20	0.02	0.13	0.00	0.00	0.00
	22	-3.78	0.06	0.32	0.00	0.00	0.00
	22	-1.63	-0.03	0.60	0.00	0.00	0.00
28	23	-3.78	-0.06	-0.32	0.00	0.00	0.00
	23	-1.63	0.03	0.60	0.00	0.00	0.00
	24	-1.37	0.02	0.14	0.00	0.00	0.00
36	24	-1.43	-0.03	-0.03	0.00	0.00	0.00
32	25	-1.37	-0.02	-0.14	0.00	0.00	0.00
40	25	-1.43	0.03	-0.03	0.00	0.00	0.00
2	3	-1.84	0.01	-0.14	0.00	-0.02	0.00
	3	-1.84	-0.01	0.14	0.00	-0.02	0.00
17	3	0.30	0.00	-0.39	0.00	-0.11	0.00
	3	0.10	0.00	-0.15	0.00	-0.11	0.00
3	4	-1.93	0.01	-0.23	0.00	0.05	0.00
	4	-1.93	-0.01	0.23	0.00	0.05	0.00
21	4	0.22	-0.05	-0.29	0.00	-0.27	0.00
	4	0.10	-0.09	-0.23	0.00	-0.27	0.00
4	5	-2.21	0.01	-0.16	0.00	0.00	0.00
37	5	-1.46	-0.03	0.10	0.00	-0.59	0.00
	5	-1.19	-0.07	-0.59	0.00	-0.59	0.00
	6	0.44	0.00	-0.22	0.00	0.00	0.00
34	6	-1.14	-0.07	-0.65	0.00	0.36	0.00
	6	-1.21	0.09	0.14	0.00	0.36	0.00
5	7	0.73	0.00	0.24	0.00	-0.01	0.00
	7	0.58	0.00	-0.17	0.00	-0.01	0.00
14	7	0.18	-0.09	-0.20	0.00	0.05	0.00
	7	0.14	0.12	-0.10	0.00	0.05	0.00
6	8	0.67	0.00	0.15	0.00	0.01	0.00
	8	0.67	0.00	-0.15	0.00	0.01	0.00
18	8	0.19	0.00	-0.09	0.00	0.07	0.00
	8	0.17	0.00	-0.08	0.00	0.07	0.00
7	9	0.58	0.00	0.17	0.00	-0.01	0.00
	9	0.73	0.00	-0.24	0.00	-0.01	0.00
22	9	0.18	0.09	-0.20	0.00	0.05	0.00
	9	0.14	-0.12	-0.10	0.00	0.05	0.00
No.	No.	N	Vy	Vz	Mt	My	Mz
Member	Node	Forces [kN]			Moments [kNm]		

G.4 Stress-strain analysis of the connections

Project data

Project name	Stiffness analysis
Project number	Chapter 5
Author	Friso van Spengler
Description	
Date	2024.04.17
Code	EN

Material

Steel S 355

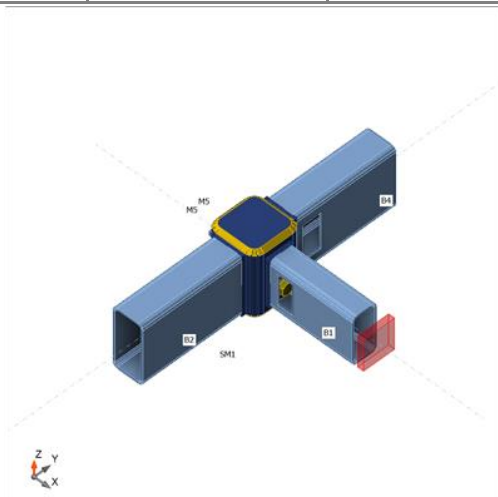
a, e, j, k, l (green)

Analysis: Stress, strain/ loads in equilibrium

Members

Geometry

Name	Cross-section	β - Direction [°]	γ - Pitch [°]	α - Rotation [°]	Offset ex [mm]	Offset ey [mm]	Offset ez [mm]
B1	1 - RHS80/40/3.0	0,0	0,0	0,0	0	0	0
B2	6 - RHS100/50/3.0	-90,0	0,0	0,0	0	0	0
B4	6 - RHS100/50/3.0	90,0	0,0	0,0	0	0	0
M5	7 - FLA20/8	180,0	0,0	0,0	0	0	0



Material

Steel	S 355 (EN)
Bolts	M12 8.8

Load effects (forces in equilibrium)

Name	Member	N [kN]	Vy [kN]	Vz [kN]	Mx [kNm]	My [kNm]	Mz [kNm]
ULS1, 1	B1 / End	-6,66	0,00	-0,74	0,00	0,00	0,00
	B2 / End	-14,48	0,00	-0,41	0,00	-0,07	0,00
	B4 / End	-14,48	0,00	1,15	0,00	-0,07	0,00
	M5 / End	-6,66	0,00	0,00	0,00	0,00	0,00
ULS1, 6	B1 / End	-5,63	0,00	0,79	0,00	0,00	0,00
	B2 / End	-13,22	0,00	-1,36	0,00	-0,07	0,00
	B4 / End	-13,22	0,00	0,57	0,00	-0,07	0,00
	M5 / End	-5,63	0,00	0,00	0,00	0,00	0,00
ULS2, 1	B1 / End	-2,92	0,00	0,25	0,00	0,00	0,00
	B2 / End	-3,13	0,00	0,30	0,00	-0,61	0,00
	B4 / End	-3,13	0,00	-0,55	0,00	-0,61	0,00
	M5 / End	-2,92	0,00	0,00	0,00	0,00	0,00
ULS2, 16	B1 / End	-0,79	0,00	0,70	0,00	0,00	0,00
	B2 / End	-5,28	0,00	-0,96	0,00	-0,05	0,00
	B4 / End	-5,28	0,00	0,26	0,00	-0,05	0,00
	M5 / End	-0,79	0,00	0,00	0,00	0,00	0,00

Summary

Name	Value	Check status
Analysis	100,0%	OK
Plates	0,0 < 5,0%	OK
Bolts	17,7 < 100%	OK
Welds	7,8 < 100%	OK
Buckling	Not calculated	
GMNA	Calculated	

b, c (orange)

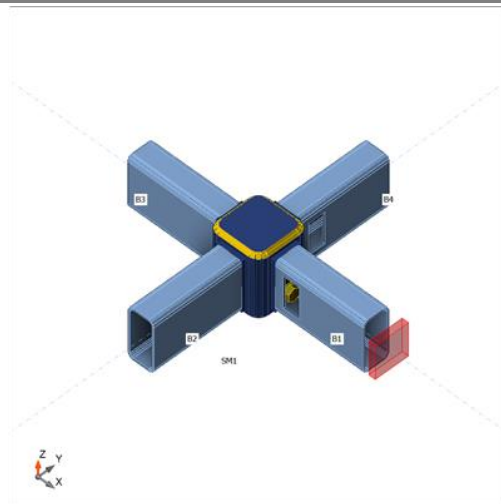
Analysis: Stress, strain/ loads in equilibrium

Members

Geometry

Name	Cross-section	β - Direction [°]	γ - Pitch [°]	α - Rotation [°]	Offset ex [mm]	Offset ey [mm]	Offset ez [mm]
B1	1 - RHS80/40/3.0	0,0	0,0	0,0	0	0	0
B2	1 - RHS80/40/3.0	-90,0	0,0	0,0	0	0	0
B3	1 - RHS80/40/3.0	180,0	0,0	0,0	0	0	0

B4	1 - RHS80/40/3.0	90,0	0,0	0,0	0	0	0
----	------------------	------	-----	-----	---	---	---



Material

Steel	S 355 (EN)
Bolts	M12 8.8

Load effects (forces in equilibrium)

Name	Member	N [kN]	Vy [kN]	Vz [kN]	Mx [kNm]	My [kNm]	Mz [kNm]
ULS1	B1 / End	-5,84	0,00	-0,92	0,00	0,15	0,00
	B2 / End	-5,84	0,00	-0,92	0,00	0,15	0,00
	B3 / End	-5,84	0,00	0,92	0,00	0,15	0,00
	B4 / End	-5,84	0,00	0,92	0,00	0,15	0,00
ULS2a	B1 / End	-2,55	0,00	-0,32	0,00	0,06	0,00
	B2 / End	-0,41	0,00	-0,39	0,00	-0,26	0,00
	B3 / End	-2,55	0,00	0,85	0,00	0,06	0,00
	B4 / End	-0,41	0,00	-0,14	0,00	-0,26	0,00

Summary

Name	Value	Check status
Analysis	100,0%	OK
Plates	0,0 < 5,0%	OK
Bolts	12,0 < 100%	OK
Welds	6,2 < 100%	OK
Buckling	Not calculated	
GMNA	Calculated	

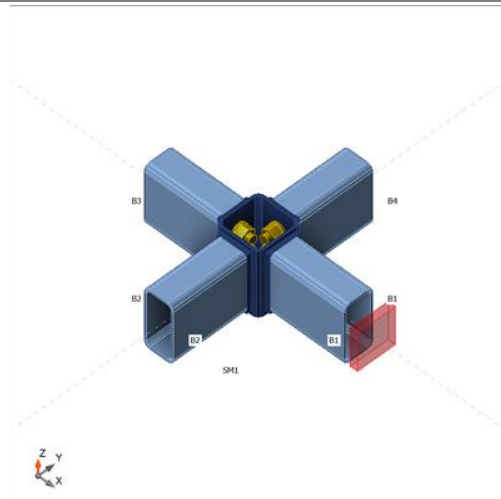
d, f, g, h (blue)

Analysis: Stress, strain/ loads in equilibrium

Members

Geometry

Name	Cross-section	β - Direction [°]	γ - Pitch [°]	α - Rotation [°]	Offset ex [mm]	Offset ey [mm]	Offset ez [mm]
B1	1 - RHS80/40/3.0	0,0	0,0	0,0	0	0	0
B2	1 - RHS80/40/3.0	-90,0	0,0	0,0	0	0	0
B3	1 - RHS80/40/3.0	180,0	0,0	0,0	0	0	0
B4	1 - RHS80/40/3.0	90,0	0,0	0,0	0	0	0



Material

Steel	S 355 (EN)
Bolts	M12 8.8

Load effects (forces in equilibrium)

Name	Member	N [kN]	Vy [kN]	Vz [kN]	Mx [kNm]	My [kNm]	Mz [kNm]
ULS1	B1 / End	-5,58	0,00	-0,79	0,00	0,09	0,00
	B2 / End	-4,90	0,00	-0,91	0,00	0,11	0,00
	B3 / End	-5,58	0,00	0,83	0,00	0,09	0,00
	B4 / End	-4,90	0,00	0,87	0,00	0,11	0,00
ULS2	B1 / End	-2,43	0,00	-0,23	0,00	-0,01	0,00
	B2 / End	-0,45	0,00	-0,49	0,00	-0,11	0,00
	B3 / End	-2,43	0,00	0,79	0,00	-0,01	0,00
	B4 / End	-0,45	0,00	-0,07	0,00	-0,11	0,00

Summary

Name	Value	Check status
------	-------	--------------

Analysis	100,0%	OK
Plates	0,0 < 5,0%	OK
Bolts	13,4 < 100%	OK
Welds	0,0 < 100%	OK
Buckling	Not calculated	
GMNA	Calculated	

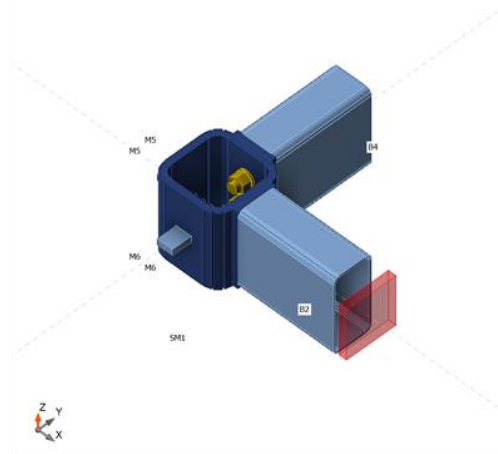
i (black)

Analysis: Stress, strain/ loads in equilibrium

Members

Geometry

Name	Cross-section	β - Direction [°]	γ - Pitch [°]	α - Rotation [°]	Offset ex [mm]	Offset ey [mm]	Offset ez [mm]
B2	6 - RHS100/50/3.0	0,0	0,0	0,0	0	0	0
B4	6 - RHS100/50/3.0	90,0	0,0	0,0	0	0	0
M5	7 - FLA20/8	180,0	0,0	0,0	0	0	0
M6	7 - FLA20/8	-90,0	0,0	0,0	0	0	0



Material

Steel	S 355 (EN)
Bolts	M12 8.8

Load effects (forces in equilibrium)

Name	Member	N [kN]	Vy [kN]	Vz [kN]	Mx [kNm]	My [kNm]	Mz [kNm]
ULS1	B2 / End	-14,91	0,00	-0,46	0,00	0,00	0,00
	B4 / End	-14,91	0,00	-0,46	0,00	0,00	0,00
	M5 / End	-14,91	0,00	0,46	0,00	0,00	0,00
	M6 / End	-14,91	0,00	0,46	0,00	0,00	0,00
ULS2	B2 / End	-5,50	0,00	-0,39	0,00	0,00	0,00
	B4 / End	-3,35	0,00	-0,66	0,00	0,00	0,00

	M5 / End	-5,50	0,00	0,39	0,00	0,00	0,00
	M6 / End	-3,35	0,00	0,66	0,00	0,00	0,00

Summary

Name	Value	Check status
Analysis	100,0%	OK
Plates	0,0 < 5,0%	OK
Bolts	1,1 < 100%	OK
Welds	0,0 < 100%	OK
Buckling	Not calculated	
GMNA	Calculated	

Code settings

Item	Value	Unit	Reference
Safety factor γ_{M0}	1,00	-	EN 1993-1-1: 6.1
Safety factor γ_{M1}	1,00	-	EN 1993-1-1: 6.1
Safety factor γ_{M2}	1,25	-	EN 1993-1-1: 6.1
Safety factor γ_{M3}	1,25	-	EN 1993-1-8: 2.2
Safety factor γ_c	1,50	-	EN 1992-1-1: 2.4.2.4
Safety factor γ_{Inst}	1,20	-	EN 1992-4: Table 4.1
Joint coefficient β_j	0,67	-	EN 1993-1-8: 6.2.5
Effective area - influence of mesh size	0,10	-	
Friction coefficient - concrete	0,25	-	EN 1993-1-8
Friction coefficient in slip-resistance	0,30	-	EN 1993-1-8 tab 3.7
Limit plastic strain	0,05	-	EN 1993-1-5
Detailing	No		
Distance between bolts [d]	2,20	-	EN 1993-1-8: tab 3.3
Distance between bolts and edge [d]	1,20	-	EN 1993-1-8: tab 3.3
Concrete breakout resistance check	Both		EN 1992-4: 7.2.1.4 and 7.2.2.5
Use calculated a_b in bearing check.	Yes		EN 1993-1-8: tab 3.4
Cracked concrete	Yes		EN 1992-4
Local deformation check	No		CIDECT DG 1, 3 - 1.1
Local deformation limit	0,03	-	CIDECT DG 1, 3 - 1.1
Geometrical nonlinearity (GMNA)	Yes		Analysis with large deformations for hollow section joints
Braced system	No		EN 1993-1-8: 5.2.2.5